UQAR
Université du Québec
à Rimouski

Traitement superficiel au laser appliqué aux aciers outils H13 forgé et imprimé par fabrication additive

Analyse expérimentale de la microstructure et des performances mécaniques

Mémoire présenté

dans le cadre du programme de maîtrise en ingénierie

en vue de l'obtention du grade de maître ès sciences appliquées (M.Sc.A.)

PAR

© LAMYA BAALI

Octobre 2023

Composition du jury :

Abderrazak El Ouafi, président du jury, Université du Québec à Rimouski

Noureddine Barka, directeur de recherche, Université du Québec à Rimouski

Véronique Dassylva-Raymond, codirectrice de recherche, Université du Québec à Rimouski /Rio Tinto

Sasan Sattarpanah Karganroudi, examinateur externe, Université du Québec à Trois-Rivières

Dépôt initial le 26 juillet 2023 Dépôt final le 23 octobre 2023

À mes chers parents.

REMERCIEMENTS

Je tiens tout d'abord à remercier mon directeur de recherche Monsieur Noureddine Barka, professeur chercheur à l'université du Québec à Rimouski, pour la confiance qu'il m'a accordée en me confiant ce projet avec une grande autonomie, pour la transmission de ses savoirs faire, et pour sa disponibilité tout au long de mon parcours de recherche.

Je tiens à exprimer ma gratitude et ma reconnaissance envers ma co-directrice de recherche Véronique Dassylva-Raymond ancienne professeure à Université du Québec à Rimouski, pour son soutien moral, ses conseils enrichissants et ses remarques pertinentes qui ont été pour moi une aide précieuse.

Je tiens aussi à remercier les membres du jury d'avoir accepté d'évaluer mon projet de recherche. Votre expertise, votre temps précieux et vos remarques pertinentes ont contribué à enrichir mon mémoire

Je désire exprimer ma sincère reconnaissance envers mes collègues de laboratoire à l'Université de Québec à Rimouski, plus particulièrement Asim Iltaf, Anas Kerbout et Narges Omidi, pour leur précieuse collaboration dans la réalisation des travaux expérimentaux et l'élaboration de ce travail.

Je remercie le personnel du département de mathématiques, informatique et de génie de l'UQAR pour leurs assistances et leur soutien précieux tout au long de mon parcours académique. Votre expertise et votre dévouement ont joué un rôle essentiel dans ma réussite.

RÉSUMÉ

Le traitement surfacique au laser est une méthode thermique largement adoptée dans l'industrie pour améliorer la résistance et les caractéristiques des aciers à outils. Cette technique repose sur l'application précise et localisée d'un faisceau laser à haute puissance. Cette étude s'inscrit dans le cadre de l'amélioration de la microstructure et des caractéristiques mécaniques de l'acier à outils H13, fabriqué à la fois par forgeage classique et par fabrication additive, Ces deux matériaux sont fréquemment utilisés dans l'industrie pour la fabrication de moules et d'outils nécessitant des performances élevées. Le choix d'explorer la fabrication additive s'est révélé pertinent, car elle incarne une technologie innovante qui offre des perspectives inédites en matière de conception et de fabrication de moules complexes. En particulier, la capacité de la fabrication additive à créer des canaux de refroidissement sur mesure, parfaitement adaptés aux géométries complexes des cavités des moules, représente une tendance émergente offrant un potentiel significatif pour l'optimisation de l'efficacité et des performances des outils industriels. Une analyse approfondie des défauts constatés sur les moules a clairement identifié la surface du matériau comme la zone la plus vulnérable, exposée à une variété de contraintes thermiques et mécaniques. Dans cette optique, ce projet vise à remédier à cette problématique en appliquant un traitement surfacique au laser, utilisant des d'unités bioniques sous forme de lignes, sur les deux types d'acier H13.

Une étude expérimentale et statistique a été entreprise pour améliorer la qualité de la surface des deux variantes d'acier H13. Cette étude a intégré un plan d'expérience méthodique, comprenant une gamme variée de paramètres laser, notamment la puissance, la vitesse et la distance de déplacement du faisceau laser. Ces paramètres ont été soumis à une évaluation rigoureuse, prenant en compte leur influence sur des aspects essentiels tels que la microstructure, le profil de dureté, la résistance à la traction ultime, l'élongation à la rupture, ainsi que les modes de fractures. Le microscope électronique à balayage a été utilisé pour étudier le développement et les changements de la structure cristalline résultant des différents traitements au laser. L'outil statistique ANOVA a été déployé pour analyser la contribution et l'effet des paramètres sur la longueur et la largeur de la zone traitée, afin de mieux contrôler les dimensions de la partie affectée. Cette approche a également permis de trouver la corrélation entre les paramètres laser et les propriétés mécaniques statiques suivantes : la résistance ultime à la traction et l'élongation à la fracture. Les résultats ont apporté une démonstration concluante de l'influence significative des paramètres laser sur la microstructure et sur les propriétés mécaniques de l'acier H13, notamment la puissance qui a été identifiée comme ayant la plus grande contribution selon les analyses statistiques. De plus, ces résultats ont confirmé l'efficacité du traitement surfacique au laser à la fois sur l'acier à outils conventionnel et sur celui conçu par fusion sélective au laser.

Mots clés: AISI H13, Propriétés mécaniques; Traitement thermique, Laser, fusion sélective au laser, Fabrication additive, canal de refroidissement conforme, Moulage par injection, Analyse de variance ANOVA, Taguchi.

ABSTRACT

Laser surface treatment is a thermal method widely adopted in industry to improve the strength and characteristics of tool steels. This technique relies on the precise and localized application of a high-power laser beam. This study is aimed at improving the microstructure and mechanical properties of H13 tool steel, manufactured both by conventional forging and additive manufacturing methods. These two materials are frequently used in the industry to produce molds and tools requiring high performance. The choice to explore additive manufacturing has proven to be relevant as it embodies an innovative technology that offers unprecedented prospects in the design and production of complex molds. In particular, the ability of additive manufacturing to create conformal cooling channels that perfectly match to the intricate geometries of mold cavities represents an emerging trend that holds significant potential for optimizing the efficiency and performance of industrial tools. A thorough analysis of mold defects has distinctly identified the material's surface as the most vulnerable area, exposed to various thermal and mechanical stresses. This project seeks to address this issue by applying a laser surface treatment, utilizing bionic units in the form of lines, on both types of H13 steel.

An experimental and statistical study was conducted to enhance the surface quality of the two H13 steel variants. This study incorporated a systematic experimental plan encompassing a diverse range of laser parameters, including power, scanning speed, and laser defocus distance. These parameters underwent rigorous assessment, considering their influence on crucial aspects such as microstructure, hardness profile, ultimate tensile strength, elongation at fracture, and fracture modes. Scanning electron microscopy was utilized to investigate the development and changes in the crystalline structure resulting from the different laser treatments. The statistical tool ANOVA was employed to analyze the contribution and effect of parameters on the length and width of the treated area, with the aim of better controlling the dimensions of the affected region. This approach also facilitated the identification of correlations between laser parameters and static mechanical properties, including ultimate tensile strength and elongation at fracture. The results have provided conclusive evidence of the significant influence of laser parameters on the microstructure and mechanical properties of H13 steel, with power being identified as the parameter contributing most significantly, according to statistical analyses. Furthermore, these results have affirmed the effectiveness of laser surface treatment on both conventional tool steel and that manufactured through selective laser melting.

Keywords: AISI H13, Additive Manufacturing, Conformal Cooling Channel, Selective Laser Melting, Laser, Injection Molding, Heat Treatment, Analysis of Variance ANOVA, Taguchi, mechanical properties.

TABLE DES MATIÈRES

LISTE DES TABLEAUX

LISTE DES FIGURES

LISTE DES ABRÉVIATIONS, DES SIGLES ET DES ACRONYMES

UQAR	Université du Québec à Rimouski
AISI	American Iron and Steel Institute
ANOVA	Analyse de variance
Laser	Light amplification by stimulated emission of radiation
HRC	Dureté Rockwell-C
SLM	Fusion laser sélective
PBF	Fusion sur lit de poudre
L-PBF	Fusion sur lit de poudre laser
Ac1	Température de début de formation de l'austénite
Ac3	Température de fin de formation de l'austénite
RSM	Méthode des surfaces de réponses (Response surface methodology)
DOE	Plan d'expériences (Design of experiments)
SS	Somme des carrés
SEM	Microscopie électronique à balayage
EDS	Spectroscopie à rayons X à dispersion d'énergie
UTS	Résistance à la traction ultime

LISTE DES SYMBOLES

Wt %	Pourcentage de masse
µm	Micromètre
W	Watt
°C	Degré Celsius
J	Joule
mm	Millimètre
s	Seconde
mm/s	Millimètre par seconde
C	Carbone
Cr	Chrome
Mn	Manganèse
Mo	Molybdène
Si	Silicium
V	Vanadium
Fe	Fer

INTRODUCTION GÉNÉRALE

1. CONTEXTE

Le processus de moulage par injection est largement utilisé pour la fabrication en masse des pièces en plastiques avec des taux de production élevés comparativement à d'autres processus de mise en forme des polymères telle que le moulage par soufflage, le moulage par extrusion et le moulage par compression. Ce procédé consiste à injecter et compresser le plastique fondu ou ramolli dans des moules puis à le refroidir pour le solidifier afin de créer la forme désignée [1]. Le moule est l'élément principal le plus couteux de ce procédé sa qualité affecte directement l'efficacité de la production. L'amélioration de ses performances et sa durée de vie joue un rôle significatif.

Les aciers à outils pour travail à chaud sont les plus employés pour la fabrication des moules en raison de leurs excellentes propriétés. Ces derniers peuvent être conçus par des méthodes conventionnelles, et par la fabrication additive qui permet l'exploration de nouvelles approches et de repousser les limites de la conception traditionnelle des moules.

Les moules sont assujettis à des contraintes mécaniques importantes et des frottements, qui se créent aux cours de la compression et les contacts entre la surface des moules et le matériau éjecté. La dureté élevée et la haute résistance à l'usure de ces aciers permettent aux moules de bien résister à ces contraintes. Les moules sont aussi soumis à des contraintes thermiques issues des cycles de chauffages et de refroidissement qui s'appliquent d'une façon consécutive et rapide. Les aciers à outils sont capables de préserver leurs propriétés à des hautes températures et à résister aux ramollissements thermiques. Cette combinaison de caractéristiques des aciers à outils permet de préserver les moules en évitant les sources de leurs défaillances majeures telles que les fissurations et les déformations.

Étant donné que la source fondamentale des défauts est la surface des moules, il s'avère important de traiter la surface pour une meilleure résistance à l'érosion, et pour limiter l'apparition des fissures.

Cette étude s'intéresse à l'amélioration des performances de l'acier AISI H13 acier à outils conventionnel et imprimé en appliquant un traitement thermique suivi d'une trempe au laser qui cible l'amélioration des fonctionnalités de la surface d'une manière localisée et sélective incluant la dureté, la contrainte résiduelle et la microstructure [2].

2. REVUE DE LITTERATURE

2.1 Moulage par injection

Le moulage par injection est un procédé clé qui fait partie des processus de transformation du plastique. Ce procédé permet la production en masse des matières en plastiques avec une cadence de production élevée à moindre coût et à une meilleure qualité [3]. Le moulage par injection est un processus cyclique qui peut être dissocié en trois étapes primordiales comme mentionnée à la Figure 0- 1. La première phase de ce processus implique la fusion et l'homogénéisation de la matière en plastique, qui est ensuite injecter dans le moule jusqu'à ce qu'il soit rempli. La deuxième partie consiste à maintenir la matière fondue en appliquant une pression pour former le produit final souhaité avec précision. Enfin, la dernière étape consiste à refroidir la matière jusqu'à sa solidification à l'intérieur du moule, permettant ainsi à la pièce de devenir rigide et prête à être éjecter [4, 5].

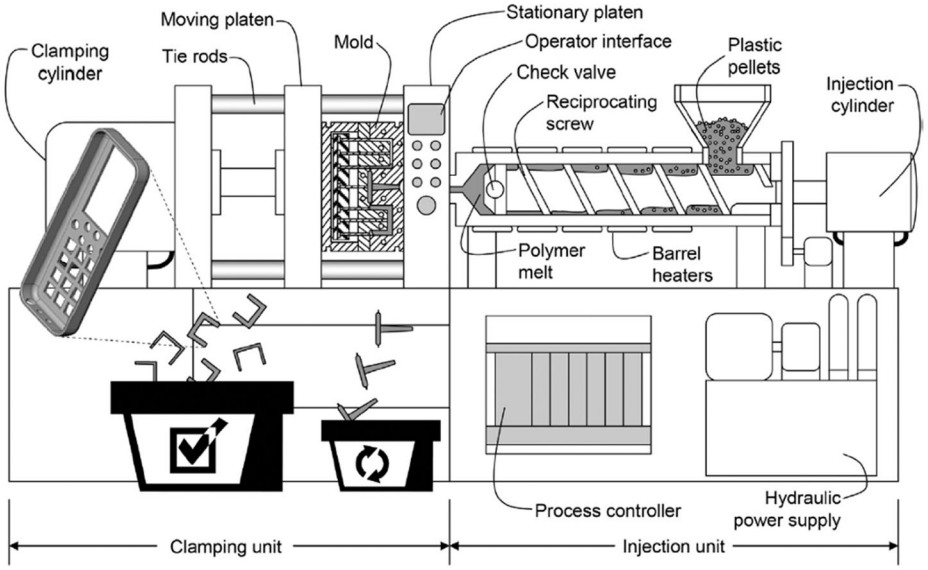

Figure 0- 1: Schéma représentatif du processus du moulage par injection [6]

Le processus de moulage par injection présente de nombreux défis, commençant par le choix du matériau du moule. Ce matériau doit répondre à des exigences spécifiques en termes de résistance à l'usure, à la fatigue, de ténacité et de ductilité à haute température, ainsi que d'une grande conductivité thermique.

La complexité du design des moules peut entraîner une longue durée de développement du prototype, ce qui engendre des coûts plus élevés. Pour optimiser le temps de cycle, il est essentiel de prendre en compte que le refroidissement constitue la partie la plus longue du cycle total de moulage par injection et a un impact direct sur la qualité du produit final. Par conséquent, il est nécessaire d'assurer un refroidissement efficace et rapide.

Un autre aspect crucial est le traitement adéquat du matériau, car les moules subissent d'importantes contraintes mécaniques et thermiques pendant le processus de moulage par injection. Ces contraintes peuvent générer des défauts, initialement sous forme de petites fissures, qui peuvent progressivement devenir plus profondes, nuisant ainsi à la durée de vie du moule [7].

2.2 Aciers à outils

L'acier à outils est un acier au carbone combiné aux éléments d'alliages qui sont responsables des propriétés spécifiques des aciers à outils. Ce groupe peut contenir une grande variété de composition chimique, mais ce qui l'identifie est la capacité du matériau à améliorer ces propriétés en utilisant un traitement thermique.

Conformément aux normes ASTM (American Society for Testing and Materials) les aciers à outils se composent de différentes classes caractérisées par une lettre suivi d'un nombre, la lettre est une désignation sur une caractéristique de l'acier comme mentionné au niveau du Tableau 0- 1[8].

Tableau 0- 1: Classification ASTM de l'acier à outils [8]

Classification ASTM	**Symbole**
Aciers à outils trempés à l'eau	W
Aciers à outils résistants aux chocs	S
Aciers à outils pour travail à froid trempés à l'huile	O
Aciers à outils pour travail à froid moyennement alliés et trempés à l'air	A
Aciers à outils pour travail à froid à haute teneur en carbone et à haute teneur en chrome pour matrices	D
Aciers pour moules en plastique	P
Aciers à outils pour travail à chaud, chrome, tungstène	H
Aciers à outils rapides au tungstène	T
Aciers à outils rapides au molybdène	M

Les principaux éléments d'alliages dans les aciers à outils sont silicium, chrome, molybdène, tungstène et vanadium, ils réagissent avec le carbone pour former un acier à outils aves des propriétés spécifiques. Chaque élément affecte la métallurgie et les propriétés de ce dernier d'une façon unique. Le carbone joue un rôle primordial dans la composition de l'acier à outils, car il permet d'augmenter considérablement la dureté et la résistance à l'usure de ce matériau. Cependant, cette augmentation de la dureté et de la résistance s'accompagne d'un compromis, car elle diminue la ductilité et la ténacité de l'acier [9].

2.2.1 Les aciers à outils pour travail à chaud :

Les aciers à outils pour travail à chaud appartiennent au groupe H qui réfère à leurs applications qui est le moulage à haute températures. Au cours de ce type d'applications le matériau est soumis à des nombreux cycles thermiques et à des forces importantes qui engendrent par la suite des dégradations et des endommagements qui affectent directement la durée de vie de l'acier. L'acier AISI H13 (X40CrMoV5-1 ou Z40CDV5) est le plus utilisé de ce groupe pour le travail à chaud. Il est caractérisé par une teneur en carbone entre 0.32% et 0.45% et un dosage spécifique d'autres éléments en balance avec le fer.

Les aciers d'outillage de travail à chaud ont une excellente combination de propriétés métallurgiques et mécaniques, incluant une bonne résistance à l'usure, résistance aux fissures sous des contraintes de fatigues thermiques, une bonne conductivité thermique, une dureté élevée et une excellente résistance aux contraintes et déformation tout en gardant la ductilité du matériau [8].

2.3 Traitement thermique

Les facteurs qui affectent le plus les moules utilisées dans l'industrie de moulage par injection est le design, le traitement thermique, la bonne utilisation de l'outil et son entretien. En effet, le traitement thermique revête d'une importance cruciale pour achever des propriétés optimales de l'acier à outils et pour répondre aux exigences de l'industrie de

moulage par injection. En tenant compte des statistiques de performances des moules, l'une des causes majeures de leur défaillance prématurée est un traitement thermique inapproprié [9]. Généralement le traitement thermique des aciers à outils consiste à chauffer l'acier jusqu'à la région austénitique où l'austénite est formée, ensuite à le refroidir rapidement pour assurer la transformation d'austénite en martensite, et finalement un revenu pour éliminer l'austénites revenues et former des carbures dans la structure.

2.3.1 Durcissement

Le durcissement de l'acier implique deux étapes importantes une austénitisation suivi d'une trempe. L'austénitisation est le processus de chauffage de l'acier à des températures qui varient entre 780 et 1250 °C, cela dépend de la composition chimique de chaque acier et sa température de formation d'austénite (AC3). Pendant cette température il se provoque une transformation de la phase cubique centré à une phase métallique cubique à faces centrées en raison de la diffusion des atomes de carbones et d'autres éléments d'alliages dans la structure cristalline du matériau. Après le maintien de l'acier à des hautes températures pour permettre aux carbures à se dissoudre et aux atomes de carbones à se diffuser dans la matrice du fer, le matériau est refroidi rapidement soit dans des milieux liquides y compris des bains d'huiles minérales, des bains de sels fondus, et des solutions aqueuses ou bien dans des milieux gazeux. Au cours du refroidissement brutale les éléments d'alliages sont piégé dans le réseau cristallin et enchaine la transformation d'une structure cubique à faces centrées à un tétragonal à corps centré qui est la martensite. Étant donné que la température de finition de la martensite est inférieure à la température ambiante, toute l'austénite n'est pas transformée en martensite, l'austénite restante après trempe est appelée austénite résiduelle. Le but ultime du processus de durcissement est l'amélioration de la dureté et la résistance de l'acier ce qui entraine une bonne résistance à l'usure et aux déformations. Cependant cette opération n'est pas suffisante puisque l'acier est fragile dans cet état.

2.3.2 Revenu

Le revenu est une étape importante du traitement thermique qui vient après la trempe où la structure résultante de l'acier est un mélange hétérogène d'austénite résiduelle, de martensite, et de carbures. Le revenu implique un réchauffage de l'acier à des températures intermédiaires inférieures à celle du durcissement et ensuite refroidi à l'air libre. Le revenu a pour objectif le soulagement des contraintes résiduelles ainsi que la diffusion du carbone hors de la martensite et la formation des carbures pour améliorer la ténacité du matériau. Tout en assurant un équilibre entre les propriétés mécaniques de l'acier à outils [10].

2.3.3 Durcissement en surface des aciers à outils

Le processus de durcissement superficiel est adopté pour des raisons d'améliorations de la surface du matériau en termes de résistance à l'usure et la dureté sans autant affecter l'intérieur plus doux et résistant de l'acier. Cette combinaison de propriétés permet au matériau d'avoir une surface très dure et résistante aux contraintes mécaniques, à l'usure et à l'abrasion, tout en gardant un intérieur robuste résistant aux propagations des fissures et ruptures.

Tableau 0- 2 illustre les différentes méthodes de durcissement en surface qui peuvent se catégoriser en trois approches principales, incluant les méthodes de diffusion thermochimique qui engendre une modification de la composition chimique de la surface en ajoutant des éléments d'alliages durcissantes telles que le carbone, l'azote et le bore, et les méthodes énergétiques ou thermiques appliquées qui ne modifient pas la composition chimique de la partie traité mais plutôt appliquent une source d'énergie pour traiter thermiquement les zones souhaités en modifiant la métallurgie pour achever les propriétés mécaniques désirés, ainsi que les méthodes de revêtements de surface qui entraîne une implantation d'une nouvelle couche différente du substrat pour lui conférer des nouvelles propriétés [11].

Tableau 0- 2: Méthodes de Durcissement en surface [11]

Méthodes de diffusion
Carburation
Nitruration
Carbonitruration
Nitrocarburation
Boruration
Processus de diffusion thermique
Méthodes énergétiques appliquées
Durcissement à la flamme
Trempe par induction
Durcissement par faisceau laser
Durcissement par faisceau d'électrons
Revêtement et modification de surface
Chromage dur
Nickelage autocatalytique
Projection thermique
Rechargement par soudage
Dépôt chimique en phase vapeur
Dépôt physique en phase vapeur
Implantation ionique
Traitement de surface au laser

a) Traitement de surface au laser

Le traitement de surface au laser est un processus thermique basé sur un faisceau laser précis et localisé qui génère des intensités élevées et permet à la surface d'absorber l'énergie transmise et atteindre des températures élevées idéales pour un refroidissement rapide et une bonne qualité de durcissement sans autant fondre le matériau, cet apport de chaleur à la surface est responsable de la formation d'une structure dure et à grain fin au niveau de la

surface. Les régions de températures du durcissement conventionnel et au laser au niveau du diagramme fer-carbone sont montrés sur la Figure 0- 2.

Les avantages de l'utilisation du laser pour le traitement surfacique résultent de sa nature hautement directionnelle et sa capacité à fournir des quantités contrôlées d'énergie aux régions souhaitées avec un cycle thermique très rapide, une régularisation de la profondeur traitée en surveillant les paramètres du procédé. et une application sans contact et sans rejet environnemental. Le traitement de surface au laser comprend différentes méthodes y compris le durcissement au laser, la fusion au laser, revêtement au laser, et l'alliage de surface au laser [12].

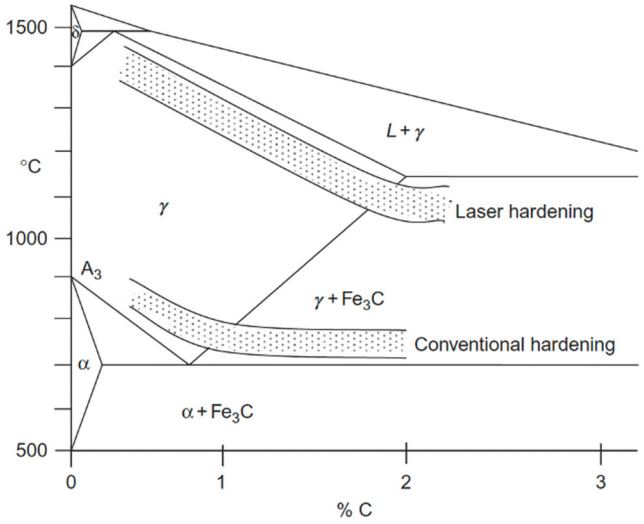

Figure 0- 2: Les régions de températures du durcissement conventionnel et au laser au niveau du diagramme fer-carbone [13]

Pour produire un durcissement par transformation thermique, il faut que l'acier soit soumis à trois cycles de température subséquents : une chauffe, un maintien et un refroidissement. L'acier doit être chauffé jusqu'à une température permettant la formation de l'austénite. Après avoir maintenu cette température, principalement dans le but d'uniformiser la distribution du carbone dans l'austénite, l'acier est rapidement refroidi (trempé) pour former la martensite, une forme cristalline métastable très dure de l'acier. La dureté atteinte dépend principalement du contenu en carbone de l'acier et des cycles thermiques. En effet, il

est possible de produire différentes structures métallurgiques en contrôlant la vitesse de refroidissement. À l'équilibre, la formation de l'austénite débute à la température délimitée par la courbe Ac1 que l'on retrouve sur le diagramme de phase fer-carbone. À partir de ce point, le carbone contenu dans les grains de perlite devient en solution solide, s'homogénéise dans la perlite avant de migrer vers les grains de ferrite, lesquels contient très peu de carbone. Lorsque l'acier est refroidi rapidement, seules les régions d'austénite contenant suffisamment de carbone seront transformées en martensite. Toutefois, il est bien connu que le taux de chauffe affecte largement la formation de l'austénite et son homogénéisation [14].

b) Les paramètres d'opération du traitement au laser:

Les paramètres d'opération du traitement au laser sont nombreux et demandent d'être ajustés en cours de processus pour chacune des composantes mécaniques traitées. Fondamentalement, tout revient à contrôler la durée et l'intensité de l'énergie transférée à la surface en interaction avec le laser, ainsi que le facteur de la vitesse de refroidissement qui agit principalement sur la profondeur durcie et l'état métallurgique de la zone thermiquement affectée. Les facteurs principaux qui ont plus d'influence sont la puissance du faisceau laser, la vitesse de déplacement et la distance de mise au point [13-15] . La Figure 0- 3 est une illustration du processus du durcissement au laser.

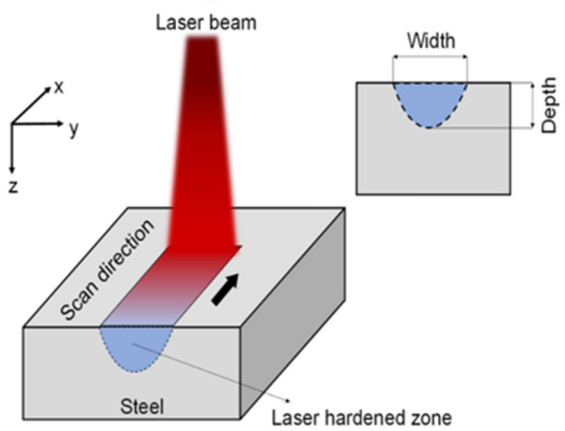

Figure 0- 3: Schéma du processus du traitement au laser [2]

2.4 Fabrication additive

La fabrication additive a été développée dans un premier lieu en tant qu'une technologie de prototypage rapide car elle est majoritairement utilisée pour construire des pièces prototypes à partir des conceptions numériques. Cependant, au fur et à mesure que la technologie progressait et devenait capable de produire des composants fonctionnels et opérationnels, le terme "fabrication additive" est entré en usage pour décrire le processus de manière plus précise [16]. Figure 0- 4 montre les étapes clés du processus du fabrication additive.

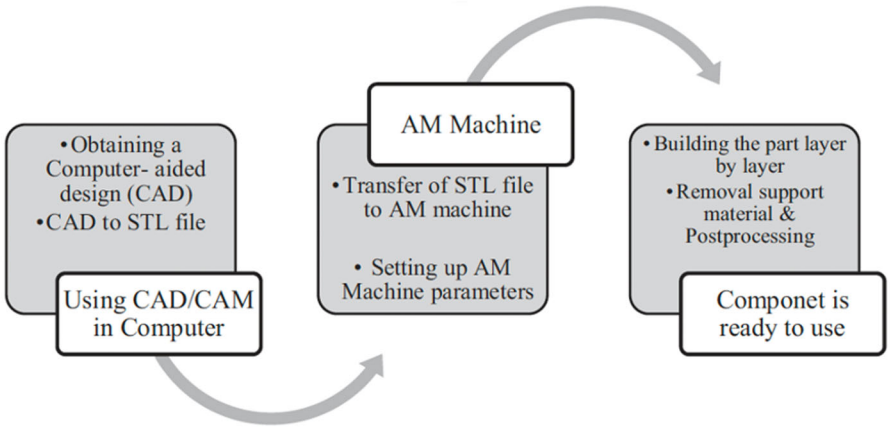

Figure 0- 4: Étapes de base de la fabrication additive [17].

Au cours de la dernière décennie, la technologie de fabrication additive (FA) a fait évoluer l'industrie manufacturière sous de nombreux aspects. Cette technique a démontré un fort potentiel d'innovation en termes de développement de produits, en raison de sa grande flexibilité au niveau du design en réalisant des structures dotées d'une géométrie complexe et ce avec une meilleure précision en une seule opération, par ajout de matière couche par couche, en supprimant presque la partie lié e aux assemblages. La FA peut être une alternative à une méthode conventionnelle ou peut être intégrée à une méthode conventionnelle afin d'utiliser les avantages des deux méthodes[18]. Le côté durable de la fabrication additive lui offre un avantage distincts d'autres méthodes de fabrication, car il offre un potentiel de réduction des déchets en n'utilisant que la quantité exacte de matériau nécessaire pour créer

un produit. Cela peut également entraîner des économies d'énergie, car moins de matériaux doivent être transportés et traités, ce qui réduit les émissions mondiales de gaz à effet de serre [19]. La fabrication additive a connu une croissance exponentielle au cours des dernières années, elle participe dans des nombreux domaines de la science et de l'industrie y compris l'ingénierie, le moulage et outillage la biomédical [20], l'aérospatial [21], la construction [22], et l'automobile [23, 24]. La FA fait partie aussi des éléments majeurs de la quatrième révolution industrielle, à savoir industrie 4.0 qui est un mouvement basé sur des technologies d'automatisation intelligente [25-27] .

2.4.1 Les procédés de fabrication additive

L'American Society for Testing and Materials (ASTM) [29] a spécifié sept majeures catégories de fabrication additive à savoir extrusion métallique, jet de matière, dépôt direct d'énergie, feuille de laminage, polymérisation en cuve, jet de liant et fusion dur lit de poudre. Le principe et les technologies de chaque catégorie est mentionnée au niveau du Tableau 0-3.

Tableau 0- 3: Types de fabrication additive selon ASTM [29]

S. no.	*AM types*	*Technologies*	*Principle*
1	Metal extrusion	Fused deposition modelling Contour crafting	Melted material is deposited through a nozzle. Its typical resolution is 100 μm to 1 cm.
2	Material jetting	Inkjet printing	Using piezo printing heads, droplets of photopolymers in liquid form are deposited and UV lamps are used to cure them. Its typical resolution is 10–25 μm.
3	Direct energy deposition	Laser Engineered NetShaping (LENS) Electronic BeamWelding (EBW)	Material is melted with the help of laser and deposition in a pool of melted material. Its typical resolution is 100 μm to 1 cm.
4	Sheet lamination	Laminated object manufacturing (LOM)	In this method, layers of material are fused together, with the required form carved into each form. Its typical resolution is 200–300 μm.
5	Mat polymerisation	Stereolithography	Focused energy is deposited on the surface of a liquid photopolymer. Its typical resolution is 0.1–100 μm.
6	Binder jetting	Indirect inkjet printing	Combining components in the form of powder with liquid or solid binder. Its typical resolution is 100 μm.
7	Powder bed fusion	Direct metal laser sintering Selective laser melting (SLM) Electron beam melting	Layer wise fusion of powder particles using infrared energy. Its typical resolution is 50–100 μm.

2.4.2 Fabrication additive métallique

Le progrès des technologies de lasers et les faisceaux électroniques a joué un rôle fondamental niveau de la maturation des procédés 3D à base de poudre pour la production des pièces métalliques. Les principaux procédés de FA métalliques sont disposés suivant trois catégories incluant les procédés sans fusion, avec fusion et dépôt direct de matière, et avec fusion et sur lit de poudre. La Figure 0- 5 représente un bilan des méthodes de fabrication additive métalliques. La fusion sur lit de poudre consiste à étaler une fine couche de poudre sur une platform de fabrication, ensuite à fondre sélectivement la poudre en utilisant un laser ou un faisceau d'électrons pour créer une couche solide. Le process se répète jusqu'à l'obtention de la pièce finale. Le dépôt direct d'énergie utilise une source d'énergie laser ou faisceau d'électrons pour fondre initialement la poudre métallique et par la suite la déposer couche par couche pour finalement construire l'objet final [30].

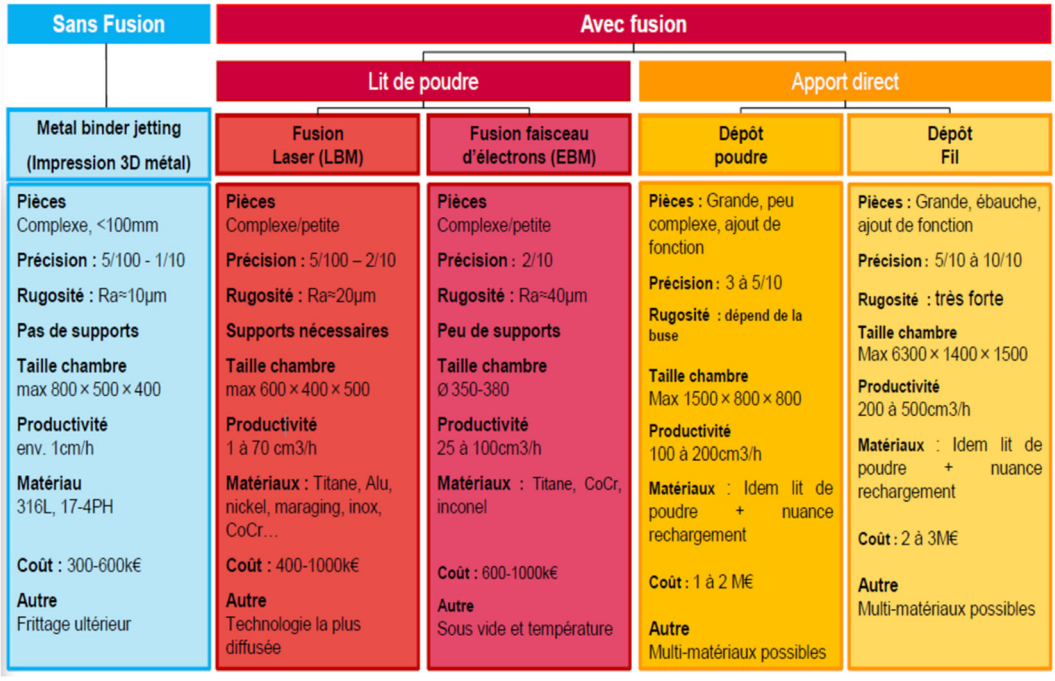

Figure 0- 5: Procédé de fabrication additive métallique [31]

a) Fusion laser sélective sur lit de poudre (SLM)

La fusion laser sélective sur lit de poudre, aussi connu sous le nom de Laser Beam Melting (LBM), ou Selective laser Melting (SLM), est une technologie de fabrication avancée la plus courante des méthodes de FA métallique [32]. Cette technique commence tout d'abord par préparer le modèle numérique CA0 (Conception Assistée par Ordinateur) de la pièce à imprimer, ensuite vient la partie de fabrication qui consiste à étaler une couche fine de poudre métallique sur la plateforme de construction qui est fondu sélectivement par la suite en utilisant un laser à haute puissance selon le modèle CAO. SLM peut fabriquer des composants homogènes avec une densité presque totale, ce qui est dû à sa capacité à fondre complètement la poudre en phase liquide, plutôt que de chauffer les poudres à une température spécifique où les particules de poudre sont partiellement fondues et fusionnées comme la méthode SLS fait [33]. Figure 0- 6 résume les étapes cruciales du processus de SLM.

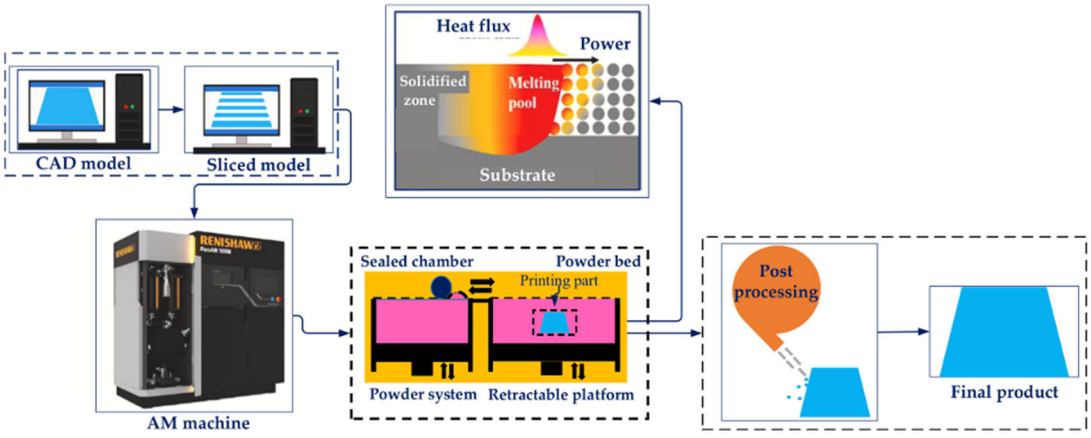

Figure 0- 6 : Principe de fonctionnement du SLM [34].

Les paramètres du processus SLM ont un impact significatif sur les propriétés du matériau résultant, selon la Figure 0- 7, les quatre paramètres clés du SLM processus sont ceux qui sont liés à la machine, au laser, au balayage, et au matériau utilisé qui est sous forme d'une poudre, ils ont un impact direct sur la qualité de l'impression incluant la densité relative

du composant, les contraintes résiduelles, la microstructure, les propriétés mécaniques, et la rugosité de la surface.

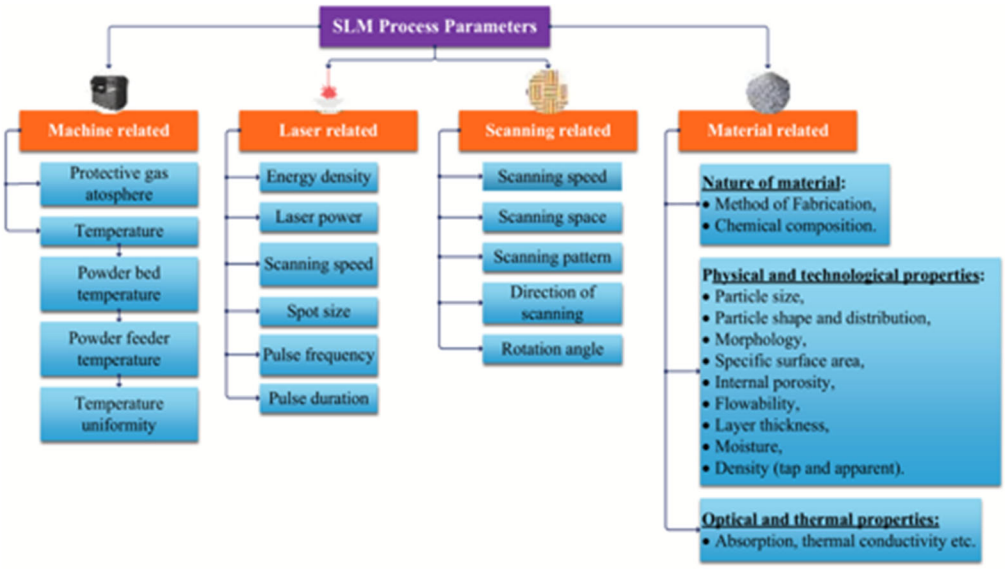

Figure 0- 7: : Principaux paramètres du processus SLM [34].

En effet une utilisation contrôlée et appropriée des paramètres peut minimiser les défauts tels que la porosité, les trous de fusion incomplets et les fissures. En référence à la littérature [35], la surveillance des paramètres qui font partie de l'équation de la densité d'énergie volumétrique peuvent efficacement éviter les défauts du processus SLM. Cette énergie fait démontre l'énergie du faisceau laser transmise à une unité volumétrique de matériau, elle est composée de quatre paramètres illustrés dans Figure 0- 8, et qui sont contrôlés indépendamment :

- La puissance laser (W) est un paramètre critique qui affecte significativement la taille du bain de fusion, la profondeur de pénétration, vitesse de refroidissement et l'évaporation des éléments d'alliage, plus la puissance augmente plus la chaleur est absorbée et assure une fusion suffisante de la poudre, résultant densité meilleure. Ainsi qu'une puissance élevée diminuera la vitesse de refroidissement et par conséquent la contrainte thermique pendant la solidification, minimisant la

tendance à la fissuration. Cependant, une puissance trop élevée devrait être évité, car il augmente la température du bain de fonte, accélérant la vaporisation de éléments d'alliage.

- La vitesse de balayage (mm/s) est inversement proportionnelle à la puissance, une vitesse élevée provoque le manque de fusion et une vitesse de refroidissement très importante ce qu'initie la formation des fissures.
- La distance des hachures (mm)
- L'épaisseur de la couche (mm)

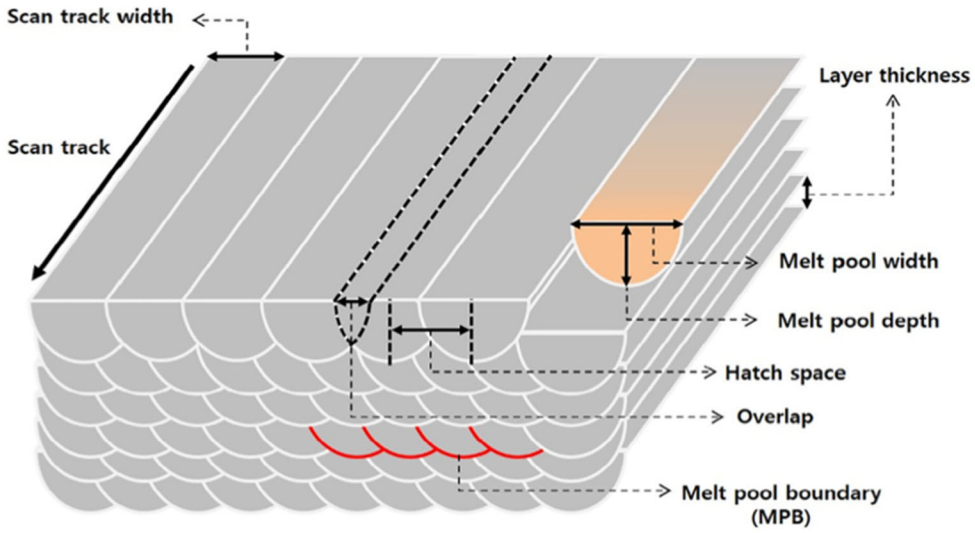

Figure 0- 8 : Diagramme schématique de la stratégie du processus de SLM [36].

Les défauts résultant d'une mauvaise gestion des paramètres du SLM process nuit à la qualité et à la durée de vie des pièces imprimées ce qui nécessite la compréhension de l'impact de chaque facteur sur les propriétés de la pièce, chose qui est expliqué au niveau de la Figure 0- 9.

Figure 0- 9: Effet des paramètres de processus fusion sélective au laser [35].

La poudre métallique est la matière première du SLM processus. Ses caractéristiques en termes de la microstructure des particules, la composition chimique des particules, et leurs morphologies influencent la qualité de la pièce imprimée. Des formes d'irrégularités de la morphologie des particules de poudre est montré dans la Figure 0- 10, qui ont causés par le processus de production. La minimisation des irrégularités de la morphologie de la poudre est une étape primordiale essentiel pour déterminer la fluidité, la densité de tassement, la conductivité thermique et la profondeur de pénétration optique du lit de poudre, ce qui affectera finalement les propriétés des composants fabriqués [37].

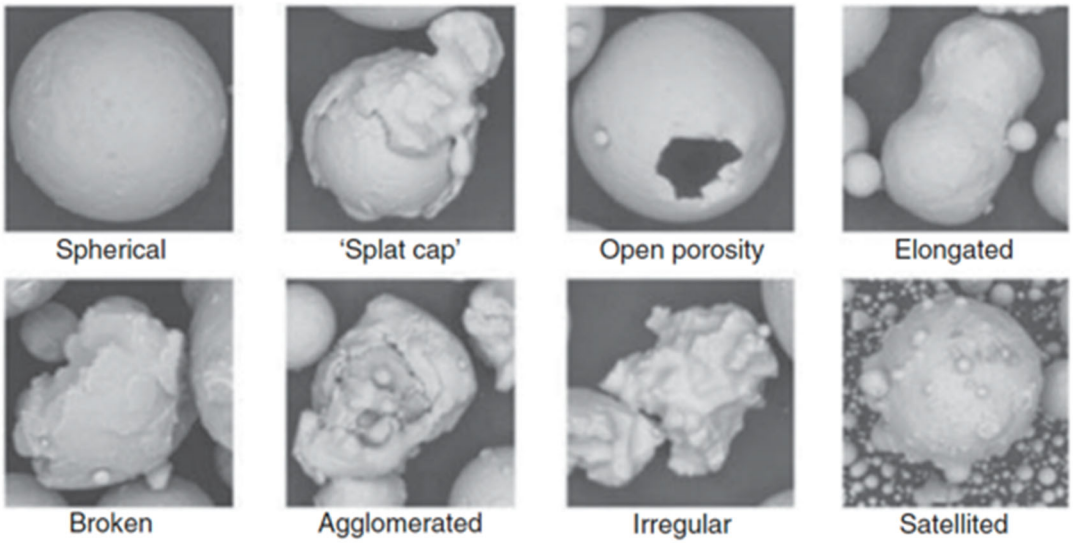

Figure 0- 10: Micrographies de particules de poudre présentant différentes caractéristiques de surface et défauts [38].

Malgré tous les avantages que la fabrication additive métallique peut offrir, il y a néanmoins des problèmes et des défis associés à ce processus, tels que le craquage et contraintes résiduelles, porosité, et le fini de surface comme mentionné au niveau de la Figure 0- 11 qui regroupe les diffèrent défaut associé à la FA métallique au laser avec des mesures pour remédier à chaque issue. Les contraintes résiduelles se développent à cause des hauts gradients thermiques au cours de la construction qui créent par la suite un stress résiduel qui endure des fissures et des craquages dans les cas où ces contraintes dépassent la limite d'élasticité du matériau. La porosité est aussi un défaut courant de la FA, elle est due à une fusion insuffisante du matériau en poudre, ce défaut doit être minimisé en raison de son effet néfaste sur les propriétés mécaniques [39, 40].

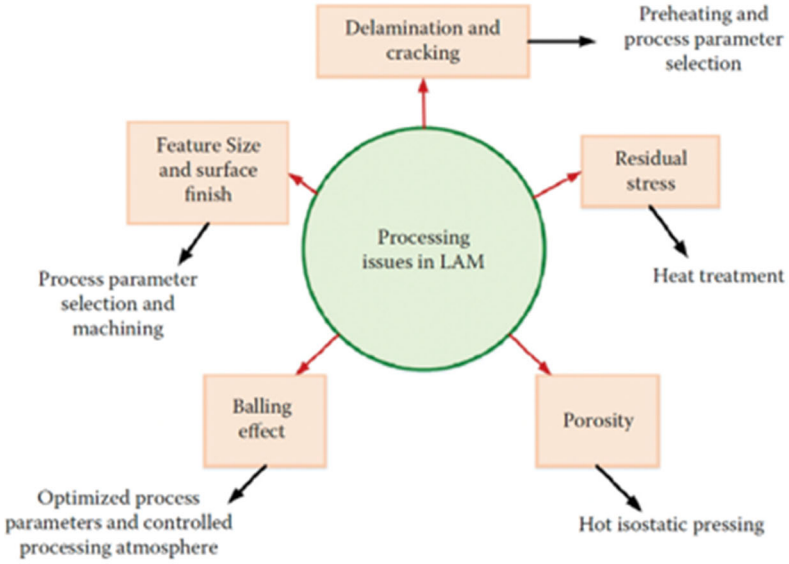

Figure 0- 11 : Problèmes de traitement et leurs mesures correctives dans la fabrication additive laser [41].

2.5 Post-traitement techniques

Les pièces métalliques imprimées font faces à des insuffisances en termes de propriétés mécaniques et de finis de surface, et n'arrivent toujours pas à conquérir celles qui sont fabriqué d'une manière conventionnelle. Étant donné la complexité du procédé , il est difficile de maîtriser des phénomènes métallurgiques et thermo physique qui occurrent durant la fusion et les interactions entre le lit de poudre et le bain de fusion, et entre la poudre et le faisceau laser, il est nécessaire de faire appel à des traitements après l'impression afin d'améliorer les propriétés mécaniques et la qualité de surface qui sont résumé au niveau du Tableau 0- 4[42, 43].

Tableau 0- 4: Procédés de post-traitement pour la fabrication additive à base de poudre métallique [30]

Categories	Representative techniques
Surface quality improvement	Manual grinding
	Machining
	Sandblasting
	Shot peening
	Mechanical polishing
	Chemical polishing
	Chemical etching
	Laser shock peening
	Laser polishing
Residual stress relief and defect reduction	Stress relief annealing
	Hot isostatic pressing
Aesthetic improvement	Spray painting
	Electroplating

2.5.1 Méthodes de post-traitement thermique

Le traitement thermique fait généralement référence à une procédure de chauffage et de refroidissement contrôlée pour des raisons de modification et homogénéisation de microstructure du matériau qui résultent une amélioration considérable des propriétés mécaniques[44, 45]. L'interaction du matériau imprimé avec le traitement thermique varie dépendamment du système d'alliage, de la microstructure initiale, les températures utilisées, ainsi la vitesse et le mode de refroidissement adopté. Le traitement thermique peut induire à des changements majeurs, y compris le changement de la structure cristalline, l'homogénéisation de la microstructure; la dissolution des phases indésirables, précipitation des phases secondaires, et le soulagement des contraintes résiduelles. Tous ces changements

sont à la faveur du matériau en leurs accordant une combinaison des propriétés mécaniques équilibrée. Le traitement thermique est adapté à chaque matériau et aux propriétés désirées. Ils existent trois catégories majeures :

- La relaxation des contraintes a par objectif l'atténuation des contraintes résiduelles et le stress accumuler durant le processus de fabrication additive. Elle demande un contrôle du refroidissement pour éviter les gradients thermiques.

- Le traitement en solution est conçu pour l'homogénéisation de la microstructure à des hautes températures suivi d'une trempe.

- Le pressage isostatique à chaud (HIP) applique des températures élevées et des pressions isostatiques simultanément sur les pièces traitées dans un milieu de transfert, ce traitement est souvent utilisé pour remédier aux défauts de porosité et les pores à l'intérieur du matériau.

Les traitements thermiques utilisé pour les aciers à outils sont présentés sur le Tableau 0- 5 ainsi la microstructure, les propriétés mécaniques, et les propriétés de corrosion.

Tableau 0- 5: Propriétés de l'acier à outils fabriqué par fabrication additive [44]

Alloy	*Common heat treatment*	*Microstructure of AM material before heat treatment*	*Microstructure of AM material after heat treatment*	*Mechanical properties*	*Corrosion properties*	*Considerations*	*ASTM guidance*
					developed in the as-built state.		
Tool steels	Austenitizing followed by several tempering steps	AM tool steels are often featured with non-equilibrium microstructure. In the equilibrium conditions, it is expected to have a martensitic microstructure containing carbide precipitates. However, because of high solidification rates associated with AM, a considerable amount of austenite is retained in the microstructure.	Austenitizing (~1010 °C) homogenizes the heterogeneous microstructure of the as-built tool steels and removes the cellular structure. Austenite transforms into martensite during the quenching step. After austenitizing, quenching and tempering, the microstructure of the AM tool steel is quite similar to that of the CM material but the grain size is smaller. Tempering (~550 °C) makes the newly formed martensite less brittle to improve toughness. Multiple tempering cycles are sometimes applied to ensure that improvement in toughness is attained after microstructural changes induced by the 1st tempering.	Austenitizing followed by double tempering results in comparable and in some cases superior mechanical strength but lower elongation compared to the CM material.		The austenitizing step has been reported to be skipped in some studies because rapid solidification associated with AM results in a martensitic structure during AM and post-AM heat treatment has little influence on mechanical properties. Such microstructure was achieved either by changing AM processing parameters or pre-heating the building plate. However, this should be done with care because the layer-wise approach in AM might lead to microstructural heterogeneities in the as-built AM tool steels, which require solution annealing to overcome.	NA

2.6 Moules avec canaux de refroidissement conformes

Les canaux de refroidissement conforme (CC) Figure 0- 12, constituent une série de canaux de refroidissement qui sont conçues en adéquation avec les cavités des moules appliqué dans le moulage par injection, c'est un système de refroidissement au potentiel prometteur qui peut remplacer les systèmes conventionnels qui sont souvent droit et ne peuvent pas fournir un rechange thermique homogène entre le moule et la pièce plastique ce qui engendre des temps de refroidissement lent et affecte aussi la qualité de surface des produits finaux.

Grâce au développement de la technologie de fabrication additive, des canaux de refroidissement avec formes complexes peuvent être concevoir facilement, chose qui n'était pas faisable avec les méthodes conventionnelles. La FA par fusion laser sélective (SLM) est considéré pour fabriquer des moules équipés avec des CC qui arrivent à suivre les formes et les cavités d e la géométrie des moules, ce qui assurent des meilleures performances de refroidissements dans une courte période, tout en améliorant considérablement la qualité et l'efficacité de la production [46-54]. Figure 0- 13 montre un modèle conçu par FA.

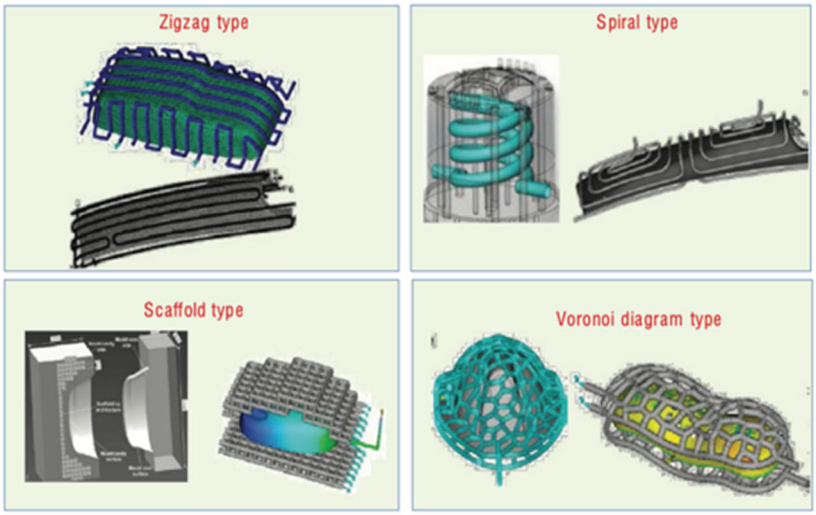

Figure 0- 12 : Type courant de canal de refroidissement conforme [55].

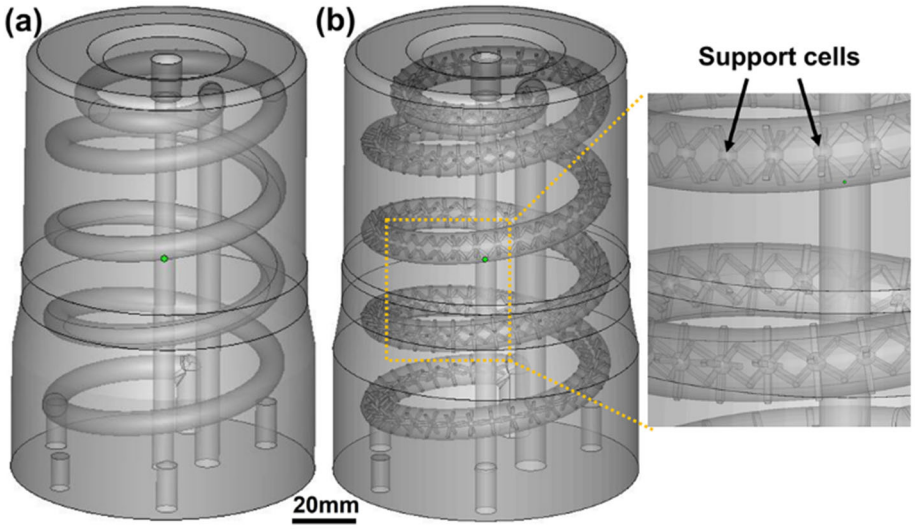

Figure 0- 13 : Modèle CAO 3D du canal de refroidissement conforme [56].

2.7 SLM H13 acier à outils

La FA a apporté des avantages significatifs au domaine de moulage par injection, cette technologie a prouvé sa capacité à créer des moules personnalisées avec des canaux de refroidissement conformes, qui offre des nouvelles possibilités de conception et d'amélioration des performances des moules. Les aciers à outils pour travail à chaud sont les métaux de base les plus utilisé pour les moules, ces aciers doivent prouver des propriétés spécifiques pour résister aux conditions sévères du processus du moulage par injection.

Cette étude s'intéresse principalement à l'acier outils H13, plusieurs recherches approfondies ont été menée pour évaluer et comprendre les propriétés et les caractéristiques du H13 imprimé par la SLM méthode [57, 58] . Dans le procédé SLM, les propriétés mécaniques des pièces métalliques imprimées dépendent fortement des paramètres d'impression. Par conséquent, le control de ces paramètres et la compréhension de leurs effets, représentent une étape nécessaire pour la fabrication de l'acier à outils H13 36

Le Tableau 0- 6 montre les propriétés mécaniques du H13 en termes de dureté, résistance à la traction et l'allongement à la resuture en fonction des paramètres utilisé durant le procédé de fusion laser sélective.

Tableau 0- 6: Les paramètres du procédé de fusion au laser sélective, et les propriétés du H13 [59]

Process parameters	Hardness (HV)	Tensile strength (MPa)	Elongation at break (%)	Reference
P = 300 W, v = 400 mm/s, hatch spacing = 50 µm preheating of 200 °C,	706 ± 147	835 ± 23	4.1 ± 2.3	[24]
P = 300 W, v = 400 mm/s, hatch spacing = 50 µm without preheating	894 ± 48	1236 ± 178	4.1 ± 1.2	[24]
P = 400 W, v = 725 mm/s, hatch spacing = 100 µm, layer thickness = 30 µm, preheating of 200 °C	715	1025	1.7	[1]
P = 280 W, v = 980 mm/s, hatch spacing = 120 µm, layer thickness = 40 µm	575	1026 ± 5	12.9 ± 0.96	[41]
P = 170 W, v = 400 mm, hatch spacing = 100 µm, layer thickness = 40 µm	561	1909	12.4	[15]
P = 90 W, v = 200 mm/s, hatch spacing = 80 µm, layer thickness = 25 µm	-	1700	1.6	[14]
P = 100 W, v = 200 mm/s, hatch spacing = 100 µm, layer thickness = 30 µm	506	-	-	[65]
P = 100 W, v = 250 mm/s, hatch spacing = 120 µm, layer thickness = 50 µm	748.04 ± 27.61	-	-	[33]
P = 175 W, v = 750 mm/s, hatch spacing = 120 µm, layer thickness = 30 µm	-	1550–1650	2–2.25	[67]
P = 175 W, v = 600 mm/s, hatch spacing = 120 µm, layer thickness = 30 µm, preheating of 200 °C	-	1003 ± 9	1.7 ± 0.6	[49]

2.7.1 La microstructure du H13 fabriqué par fusion laser sélective

La poudre métallique subit des cycles thermiques consécutives au cours du processus de fusion laser sélective, au début la poudre est chauffée rapidement à des températures élevées en raison de l'absorption de l'énergie laser, ensuite la région fondue est solidifiée rapidement après le déplacement du faisceau laser. Cette couche construite subis des chauffages et des refroidissements répétés en raison des couches adjacentes. Le processus du SLM entraine des cycles thermiques multiples avec des gradients de température élevé, ce qui résulte des morphologies de microstructures non équilibrées différentes de celle de l'acier à outils conventionnelle.

La Figure 0- 14 est une microscopie électronique à balayage de la microstructure du H13 sélectif fondu au laser, qui représente une combinaison de fine structure cellulaire et colonnaire [59, 60].

La présence d'austénite résiduelle dans le H13 produit par fusion laser sélective (SLM) peut être attribuée à deux facteurs principaux : la teneur élevée en carbone (0,4 % en poids) et le processus de solidification rapide. Lorsque la phase austénitique ne parvient pas à se transformer complètement en martensite, l'austénite retenue se forme à température ambiante, cette phase est thermodynamiquement instable et affecte négativement les propriétés du matériau [61, 62].

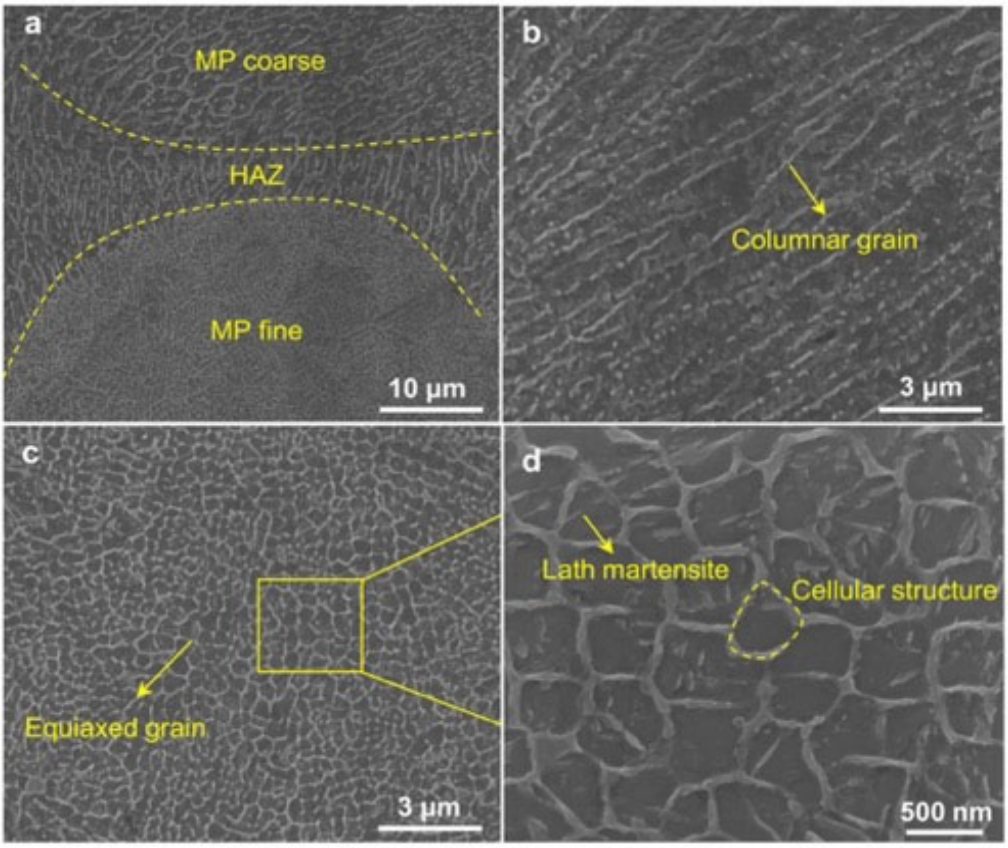

Figure 0- 14: Microscopie électronique à balayage de la microstructure du H13 sélectif fondu au laser [63]

3. PROBLÉMATIQUE

Les aciers de travail à chaud sont utilisés pour des applications de moulages par injection et ils sont soumis à des cycles de températures élevées, et à des contraintes de compressions ce qui endures des défaillances et des défauts de la moule connu par l'usure abrasive et adhésive de la surface, la fatigue thermique, la fissuration, et la déformation plastique. Par conséquent, ces aciers doivent achever des propriétés spécifiques dans le but d'améliorer la durée de vie des outils et l'efficacité du procédé de moulage par injection.

Afin de répondre à ces exigences les aciers à outils doivent disposer d'une excellente combinaison de propriétés mécaniques y compris une grande résistance à haute température, une bonne ténacité, et une meilleure résistance à l'usure t à la fatigue, et surtout une surface durable et résistante aux forces extérieurs, pour ce faire l'acier à outil est susceptible à plusieurs traitements afin d'atteindre une meilleure performance.

Cette étude à adopter l'acier à outils H13 en raison de ses propriétés mécaniques convenable aux critères des matériaux utilisé pour les moules. Le AISI H13 est fabriqué par deux voie différentes conventionnelles, et par la fabrication additive. En effet, la fabrication additive est une technologie qui offre plusieurs avantages à l'industrie du moulage par injection en termes de conception, productivité et efficacité. Les deux formes d'aciers à outils H13 ont la même composition chimique mais complétement différents en ce qui concerne la microstructure et les propriétés mécaniques.

La surface des moules est la source fondamentale des défaillances, à cet égard plusieurs traitements de surface ont été menés pour améliorer la résistance à l'usure par des revêtements, mais ils n'ont pas prouvé une amélioration considérable et ont remarqué plusieurs inconvénients en termes de liaison faible, l'épaisseur de revêtement insuffisante.

L'une des méthodes les plus efficaces est le traitement de la surface au laser, qui permet de traiter sélectivement la partie concernée avec un faisceau laser de haute puissance avec des grandes précisions, la particularité de ce traitement est sa rapidité et flexibilité, par

rapport aux autres méthodes conventionnelles telles que la trempe par induction et à la flamme, traitements thermochimiques, et les méthodes de revêtements, la trempe au laser peut être facilement automatisé et traité des géométrie complexe avec une grande précision. Les températures générées au cours de ce processus peuvent atteindre des températures élevées à l'odore de température d'austenitization, avoir même plus, suivi d'un refroidissement rapide résultant une couche traitée avec des propriétés et microstructure différente du substrat. Le changement de phase de la surface de l'acier à outils H13 permet d'avoir une couche extérieure enrichie avec des éléments d'alliages et une répartition fine des carbures entrainent l'amélioration de la dureté et la résistance à l'usure de la couche extérieure sans autant affecter les propriétés de masse souhaitables telles que la ténacité et la ductilité entraînant un prolongement de la durée de vie du moule.

Un autre point relevé par cette étude est l'exploitation des surfaces non lisses composé es de structure dure et molle, qui ne demande pas le traitement complet de la surface, ces traitements sont inspirés de la nature qui sont connu sous le nom d'unité biomimétiques, où la zone affectée par le laser sert de couche dure, et le substrat sert de couche molle. Plusieurs recherches ont prouvé l'efficacité de ce mode de traitement au laser pour l'amélioration de la fatigue et d'autres propriétés mécaniques [64, 65]. D'ailleurs les propriétés du matériau sont très sensibles aux paramètres du processus traitement au laser, et la compréhension de l'effet de chaque paramètre demande une longue expérimentation, ce qui nécessite à faire appel à un plan d'expérience et des mécanismes statiques pour optimiser les paramètres du processus de traitement au laser.

4. OBJECTIFS

Le projet de ce mémoire a pour objectif l'amélioration des performances de l'acier à outils H13 conventionnel et imprimé. Cet objectif est réalisé en appliquant dans un premier lieu un traitement thermique conventionnel, et dans un second lieu un traitement surfacique au laser par des unité biomimétiques sous formes de lignes, par le biais d'une gamme de paramètres spécifiques. Finalement les pièces traitées au laser sont investiguées en termes de

microstructure et de propriétés mécaniques. Les résultats sont analysés en utilisant des outils d'analyse de variance (ANOVA) pour trouver les paramètres optimaux du traitement au laser.

Le premier objectif consiste à étudier les effets des paramètres laser y compris la puissance, la vitesse, et la distance de dé-focalisation sur la microstructure et le profil de dureté de l'acier à outils H13 conventionnel. Le deuxième objectif est l'investigation des effets des paramètres laser sur les propriétés mécaniques du H13 conventionnel à savoir la résistance ultime à la traction, et l'élongation à la fracture. Ainsi l'analyse des modes de fractures. Le troisième objectif est l'exploration de la microstructure de l'acier outils H13 fabriqué par fusion la sélective dans trois états différents incluant, tel construit, traité thermiquement (soulagement des contraintes résiduelle et trempe et revenu) et traité en surface au laser. En plus l'étude des effets des paramètres laser sur le profil de dureté de la partie traité au laser. Le quatrième et dernier objectif consiste à déterminer la relation entre les paramètres laser et les propriétés mécaniques englobant l'élongation et la résistance ultime à la traction de l'acier H13 fabriqué par SLM, et à examiner les modes de fractures des pièces après les essais de tractions.

5. MÉTHODOLOGIE

La présente méthodologie est la même utilisée pour l'acier à outils H13 conventionnel et fabriqué par fusion au laser sélective. La première étape est la préparation des échantillons de l'acier pour l'expérimentation, le matériau est usiné selon la norme ASTM 8, les pièces usinées sont ensuite traitées thermiquement pour achever une dureté de 44HRC. Le traitement au laser est réalisé par une cellule laser disponible à l'UQAR, avec une puissance maximale de 3000 W. Ce traitement est régi par plusieurs paramètres qui affectent la zone traitée individuellement et d'une façon interactive, selon la littérature les facteurs qui ont plus d'influences sont la puissance laser, la vitesse et la distance de dé-focalisation. Après la définition des paramètres à contrôler durant le processus, un ensemble de tests préliminaires ont été réalisés afin de spécifier les intervalles de chaque facteurs.

La méthode Taguchi est exploitée pour déterminer le plan d'expérience vu les avantages offerts par cette dernière y compris, un nombre minimum d'essais, l'étude de l'effet de plusieurs paramètres simultanément. Un tableau orthogonal L9 est conçu avec trois facteurs et trois niveaux pour chaque paramètre. Les échantillons sont préparés pour répondre au premier et au troisième objectif qui est l'étude de la microstructure et le profil de dureté de la partie pour l'acier à outils H13 conventionnel et imprimé , au niveau des laboratoires du département de mathématiques, informatique et génie à l'UQAR, neuf pièces en été traité avec les sets de paramètres précisés par le plan d'expérience, une fois les pièces sont traitées au laser, un protocole métallographique standard est suivi, commençant par la coupe transversale de la partie traitée, qui est enrobée par la suite. La surface des échantillons subi un polissage et une attaque chimique convenable à chaque acier pour visualiser la microstructure à l'aide d'un microscope électronique à balayage. Les tests de micro-dureté ont été effectués sur les mêmes échantillons à l'aide d'un testeur de micro-dureté automatisé Vickers (CLEMEX CTM) disponible à l'UQAR, avec une charge d'indentation de 200 gf. Une étude statistique (ANOVA) est exécutée pour analyser l'impact de chaque facteur sur la profondeur et la largeur de la zone traitée au laser, ainsi la quantification de la contribution de chaque paramètre à la variation des résultats.

Dans le cadre de cette étude visant aussi à analyser le comportement mécanique statique de l'acier à outils conventionnel et de l'acier à outils imprimé en 3D, une méthodologie a été soigneusement élaborée pour répondre au deuxième et quatrième objectif de la recherche. Tout d'abord les échantillons sont minutieusement préparés pour les deux types d'aciers qui ont ensuite été soumis à un traitement au laser, affectant leurs deux surfaces. De plus, afin de garantir la robustesse des résultats, les paramètres de traitement au laser, tels que la puissance, la vitesse, et d'autres variables pertinentes, ont été systématiquement variés. Pour chaque combinaison de paramètres, trois répétitions indépendantes du processus de traitement au laser ont été effectuées, garantissant ainsi la fiabilité des résultats. À la suite de la préparation des échantillons et de la variation des paramètres de traitement, des essais de traction ont été réalisés pour extraire des données essentielles sur les propriétés mécaniques des aciers à outils. Ces essais ont permis de

déterminer la résistance ultime à la traction et l'élongation à la rupture, deux caractéristiques fondamentales pour évaluer la performance de ces matériaux en conditions statiques. Enfin, pour analyser en profondeur les résultats expérimentaux, le logiciel Matlab a été utilisé. Ce logiciel s'est révélé essentiel pour effectuer des analyses statistiques avancées, notamment l'analyse de variance (ANOVA), la modélisation des relations entre les paramètres de traitement et les propriétés mécaniques à l'aide de surfaces de réponse (RSM), ainsi que la création d'équations de régression linéaire pour quantifier ces relations. L'ensemble de cette méthodologie permet à cette étude d'évaluer l'importance et l'impact des paramètres de traitement au laser sur les performances de l'acier à outils H13, répondant ainsi de manière approfondie aux objectifs de recherche relatifs à l'acier conventionnel et à l'acier imprimé en 3D.

6. STRUCTURE DU MÉMOIRE

Le premier chapitre du mémoire consiste à traiter l'influence du traitement en surface au laser de l'acier à outils H13 conventionnel sur la microstructure et le profil de dureté. Les longueurs et les largeurs de la zone traitée sont ensuite analysées par l'outils statistique ANOVA, pour déterminer un modèle de prédiction et les contributions de chaque facteurs. Le second chapitre est une deuxième partie du premier travail, au niveau de cette partie les propriétés mécaniques statiques de l'acier à outils H13 conventionnel traité au laser sont investigués ainsi les modes de fractures (fractographie). Des essais de tractions sont menés sur des éprouvettes traité sur les deux surfaces au laser. Les résultats sont aussi analysés par ANOVA afin d'établir les effets des paramètres laser sur la résistance ultime à la traction et l'élongation à la fracture. Le troisième chapitre est dédié à l'amélioration de la surface de l'acier à outils H13 fabriqué en 3D par la méthode fusion sélective laser. La microstructure et le profil de dureté de la zone traité en surface au laser sont étudiés. La largeur et la longueur de la partie traitée est aussi examiné à l'aide de l'outil statistique ANOVA. Le quatrième chapitre est aussi une deuxième partie complémentaire du troisième chapitre, où les propriétés mécaniques statiques de l'acier H13 sont analysées et les modes de fractures. Des essais de traction sont appliqués sur des éprouvettes usinés selon la norme ASTM. Les

résultats en termes de la résistance ultime à la traction et l'élongation à la fracture sont examiné par la méthode ANOVA. Finalement une dernière partie est consacrée à une conclusion générale qui présente une synthèse des résultats obtenus de ce travail et des perspectives pour les prochains travaux.

CHAPITRE 1
ANALYSE ÉPERIMENTALE DE L'EFFET DES PARAMÈTRES DU PROCDÉDÉ LASER SUR LA MICROSTRUCTURE ET LE PROFIL DE MICRODURETÉ DE L'ACIER À OUTILS H13 BRUTE

Lamya Baali[1], Narges Omidi[1], Noureddine Barka[1], Véronique Dassylva-Raymond[1]

[1]Mathematics, Computer Science and Engineering Department, Université du Québec à Rimouski (UQAR), 300 Allée des Ursulines, Rimouski, QC G5L 3A1, Québec, Canada

Cet article a été soumis dans Materials and Manufacturing Processes portant le numéro de référence 238062340

1.1 RESUME EN FRANÇAIS DU PREMIER ARTICLE

L'amélioration de la durée de vie et des performances des moules utilisés dans le moulage par injection est réalisé par l'application des lignes au laser sur la surface de l'acier à outils H13 dans l'état trempé et revenu avec une dureté de 40-44 HRC. L'effet des paramètres laser est soigneusement analysé à travers un plan d'expérience basé sur la méthode Taguchi, avec trois niveaux pour trois paramètres laser, incluant la puissance laser, la vitesse et le diamètre de dé-focalisation. La zone traitée se divise en trois parties distinctes pour chacun des neuf ensembles de paramètres : la zone fondue, la zone durcie et la zone affectée thermiquement. Chacune de ces zones fait l'objet d'une investigation approfondie de sa microstructure. Les résultats démontrent une amélioration de la dureté de la couche créée

à la surface par le laser, à l'exception de la zone affectée thermiquement qui affiche une légère diminution par rapport au substrat. L'influence des paramètres laser sur la largeur et la longueur de la zone traitée au laser est soumise à une analyse statistique à l'aide de l'ANOVA, qui révèle que la puissance laser est le facteur ayant la plus grande incidence sur la surface de la partie traitée au laser.

1.2 CONTRIBUTIONS

Ce premier article, intitulé « Study of the Effect of Laser Surface Hardening Process on the Microstructure and Microhardness of H13 Tool Steel » a principalement été rédigé par Lamya Baali, son premier auteur. Noureddine Barka, le troisième auteur, occupe la fonction de directeur de recherche et a joué un rôle clé dans la définition du projet et de la méthodologie adoptée. Le troisième auteur, Narges Omidi, a apporté une contribution à l'amélioration de l'article. Enfin, Véronique Dassylva-Raymond a supervisé le travail et a également contribué à améliorer la rédaction globale.

1.3 TITRE DU PREMIER ARTICLE

Study of the Effect of Laser Surface Hardening Process on the Microstructure and Microhardness of H13 Tool Steel

1.4 ABSTRACT

This article aims to improve the service life and the performances of molds used in injection molding by applying laser lines on the surface of H13 tool steel which widely used for such application. The substrate is quenched and tempered with a hardness of 40-44 HR. The effect of laser parameters is analyzed through a design of experiment using Taguchi method, with three levels of three laser parameters including laser power, speed, and defocus diameter. The laser treated area is distinguished by three zones a melted zone, hardened zone and heat affected zone. The microstructure of each zone is investigated. The results

demonstrated that the hardness of the layer created on top of the surface using laser treatment is improved, except for the heat affected part which had a slight drop of the micro-hardness value compared to the substrate. The effect of laser parameters on the width and length of the lasered part is statistically analyzed using ANOVA, this analysis concluded that the power is the most contributing factor.

1.5 INTRODUCTION

AISI H13 tool steel is a carbon and iron alloy that contains chromium (Cr), molybdenum (Mo), silicon (Si), magnesium (Mn), and vanadium (V), which is widely used for hot work applications. This hot work steel is characterized by good resistance to thermal softening, high hardenability, strength, toughness, and wear resistance at high temperatures. These properties make it an excellent material for making many types of hot work dies, extrusion mandrels, plastic molds, cores, die holder blocks and hot work punches [1]. One of the standard applications of H13 is the hot forming, where dies are subject to a critical static/cyclic load at a very high temperature. This type of applications can lead to thermal fatigue, erosion, and abrasive wear of the die surface, which reduces the useful life of molds and directly impact the industry's production and efficiency [2] . The conventional method treatment of H13 can't meet the industry's evolving expectations and needs. In order to respond to the different requirements of the industry, surface modification is the most effective solution since the most mold failures start from the surface [3]. Surface hardening is one of the heat treatment processes that involves two main methods: a physical one, such as induction hardening, flame hardening, and physical vapor deposition, and a chemical method, such as chemical vapor deposition, carburizing and metallic cementation [4]. Among other surface hardening treatments, laser surface hardening is selected for this study because it has inherent advantages, such as the ability of highly precise focus of the laser beam on the selected area with no contact, and rapid heating and cooling by self-quenching [5] that improves the microstructure and the mechanical properties of the heat affected zone, with a minimal substrate deformation and without scarifying the internal toughness [6]. It also increases abrasion and corrosion resistance due to the homogenous and dense part formed on

the hardened surface [7].The hardening process of hot working tool steels consists of three consecutive temperature cycles, explained in the following paragraph. The first step consists of heating the surface by laser above the austenitization temperature AC3 without reaching the melting point, which allows the formation of the austenite phase, which begins at a temperature limited by the AC1 curve found in the iron-carbon phase diagram. Then the second step is about maintaining a heated surface layer above the austenitic temperature Ac3 for sufficient time for a complete transformation of proeutectoid ferrite to austenite, dissolution of cementite (Fe3C), and uniform diffusion of carbon into the austenite phase. Therefore, for maximum hardness and cure depth, the surface temperature should be as high as possible and limited by the melting point. The final step is the self-quenching, which is a rapid cooling through heat conduction in the rest of the bulk material, in which face-centred cubic FCC austenite phase is transformed into tetragonal body-centered martensite which is a very hard metastable crystalline form of steel [8].

The operating parameters of laser treatment are numerous and require adjustment during the process for each of the mechanical components treated. It all comes down to controlling the duration and intensity of the energy transferred to the surface interacting with the laser, as well as the factor of the cooling rate, which mainly acts on the hardened depth and the metallurgical state of the zone thermally affected. In 2009, Lee *et al* [7] tried to improve the surface hardening and wear properties of AISI H13 using a 200W fiber laser. The controlled parameter is the scan rate in the range of 33.6-336 mm/s, and the results showed that the hardness after laser surface treatment increased from 240 HV to 480-510 HV. The hardening depth and width are increased with the decrease in scan rate. The study of Karmakar *et al* investigates the impact of laser parameters on surface hardened AISI H13 microstructural properties of the melted zone of AISI H13 for laser treatment. They used a Yb-fiber laser in an argon environment with a range of 400-600 W for power, 200-1600 mm/s for scan speed, and a fixed spot diameter at 3 mm tool steel by laser remelting process using a Yb-fiber laser. They realized a significant increase in the melted zone with the increase of the heat input, otherwise for the hardness increased from 250 to 760 HV; the maximum hardness was practically the same for the different process parameters; the difference is about

the depth of the hardened zone which increases with more laser power and less scanning speed. In the research of Babu *et al* [9] a systematic investigation of the laser transformation hardening (LTH) process is carried out on high-strength low-alloy medium carbon steel. The effect of input process parameters like laser power, travel speed over the response hardened width (HW), hardened depth (HD), and hardened area (HA) are analyzed. The analytics results show that the laser power significantly contributes to the hardness profile, followed by scanning speed. The HD and HW increase as the power increases and decrease as the scanning speed decreases. Badkar *et al* [10] attempted to optimize the laser surface hardening parameters through Taguchi methods and variance analysis. Experiments were done on pure titanium using continuous wave 2000 W ND: YAG laser. According to the results scanning speed, laser power, and focal plane position were the most critical parameters that significantly impacted the hardened depth and width. Higher levels of focal plane position, and scanning speed, in combination with a lower level of laser power, were necessary for minimizing hardened depth and maximizing hardened bead width. Oh *et al* [11] developed a predictive model for hardness and thermal deformation for the laser-hardened phase of H13 tool steel based on 48 experiments using a 2000 W fiber laser, which includes six laser power (357, 496, 690, 958, 1331, and 1850 W) and eight laser-scanning speeds (5.0, 6.9, 9.7, 13.4, 18.6, 25.9, 36.0 and 50.0 mm/s). Telasang *et al* [12] reported the effect of laser parameters on the microstructure and hardness profile of the hardened and melted cases by varying the power between 1250 W and 2000 W and constant scan speed settled on 4 mm/s. The microstructure showed that an energy density above 100 J/mm^2 showed melting on the surface, the surface microhardness of the laser treated zone improved from 500 HVN (quenched and tempered substrate) to 610 HVN for the lowest energy density 62,5 J/mm^2, 770 HVN for 100 J/mm^2, and a maximum value 810 HVN for 75 J/mm^2.

Telasang *et al* [13] studied the effect of laser surface hardening and melting on the microstructure of the laser-treated surface; the applied energy varied from 22 J/mm^2 to 130 J/mm^2 with the following laser parameters: power 900 W to 2500 W, linear speed 2 mm/s to 8 mm/s and a spot size of 2 mm. The treatment was carried out with a single pass on the material surface, and the treated samples were subsequently subjected to various tests. The

results showed that the width varied from 12 mm to 19 mm; correspondingly, the depth of the laser-treated region increased from 0.1 mm to 1.8 mm as the energy density of the laser increased for the microstructure applying higher laser energy above 75 J/mm^2 to the apparition of a non-homogenous microstructure of retained austenite, carbides martensite. Zhang *et al* [14] processed a laser surface melting on the annealed H13 tool steel with a laser power varied from 1650 W to 1800 W and a scanning speed of 3 mm/s to 4 mm/s. They carried out three tests of 3 different laser energy densities of 110, 120, and 90 J/mm2, and the microstructure shows different zones with different microstructures that consist of the melted zone, the hardened zone, the heat-affected zone and substrate from the surface to the bottom. For the melted zone, the increasing of the laser energy density comes with more carbides forming within the grains and less lath martensite; moreover, the uniformity of alloying elements is improved, and they are more concentrated at the boundaries between the grains, which refers to precipitated carbides. Jia *et al* [15] conducted a detailed study on the effects of laser parameters on quenched and tempered AISI H13 tool steel using Nd: YAG laser and high-power CO2 through single-factor experiments. The main parameters studied were electric current (80-180 A), pulse duration (5-10 ms), frequency (2-12 Hz), defocus distance (-5 -10 mm), and scanning speed (0.2-2 mm/s). The effect of each parameter was investigated separately by holding the other parameters constant and changing the main parameter.

The study revealed the following results:

- Electric current has a significant impact on the area of the treated zone, which increases with an increase in the current. However, it affects the depth more than the width.
- Pulse duration has a significant effect on the shape of the laser-treated zone, with both the depth and width increasing with an increase in the pulse duration.

- Frequency affects the shape of the treated zone, changing it from a lean parabola-shaped triangle to a full parabola shape. It only affects the width of the zone, with a slight decrease in depth.
- Defocus distance affects the geometry of the laser zone, changing it from a demi-circle to a concave shape. The width of the zone increases with an increase in |z|, and positive defocusing values have a more significant effect on the area of the treated zone.
- Scanning speed does not have a significant influence on the depth and width of the treated zone.

Barka et al [16] analyzed the effects of laser parameters on the depth of the laser-hardened zone of 4340 steel using Anova. This statistical analysis method provides insights into each factor's contribution and interaction.

The operating parameters of laser treatment are numerous and require adjustment during the functioning. It all comes down to controlling the duration and intensity of the energy transferred to the surface interacting with the laser, as well as the factor of the cooling rate, which mainly acts on the hardened depth and the metallurgical state of the zone thermally affected. According to the literature, the major effective parameters are the power of the laser beam (P), traveling speed (S), and the focus distance (D), which will be the input parameters for these experiment [8]. The common laser hardening process applied on H13 attempts to treat the whole surface, however for this study the surface will be treated by lines and do not treat the whole surface. The main objective of this study is to investigate the effect of this new approach of laser treatment and the input parameters on the microstructure, the microhardness, and the depth-width of the hardened zone, by developing an experimental approach supported with mathematical model based on analysis of the variance (ANOVA).

1.6 EXPERIMENTAL PROCEDURE

1.6.1 Material

The base material used for the experimental tests is H13 Rockwell B95 (depending on the supplier MC-master), which belong to the group H steels by the AISI classification system. Two bars received from the supplier with the followed dimensions: 6.35 mm in thick, 76.2 mm wide, 609.6 mm long. The chemical composition is given in Table 1- 1.

Table 1- 1: Chemical composition of H13 Tool steel

Component	C	Si	Mn	Cr	Mo	V	Ph	S	Fe
Composition (%)	0.32-0.45	0.80-1.25	0.25-0.50	4.75-5.50	1.1-1.75	0.80-1.20	0.30 max	0.3 max	Balance

1.6.2 Laser treatment method

The schematic of the geometry of the samples used for the experimentation after machining is shown in Figure 1- 1.

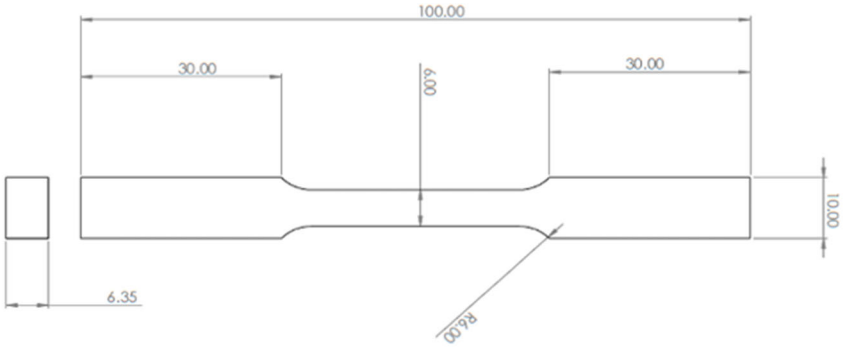

Figure 1- 1: Dimension of specimen after machining (mm)

The H13 samples were subject to a heat treatment of three stages as mentioned Table 1- 2 cracking it [17]. The first one, called austenitization, the material is heated into the austenite region at 1000°C and kept there for 30 minutes, then quenched in oil. The following step is the tempering process, where the material is held at 650°C for 1 hour and then cooled in the air. The most important criterion in selecting a quenching oil is that it provides a cooling rate that will harden the part without cracking it [17].

Table 1- 2: Specifications of heat treatment

	Temperature	**Duration**
Austenitizing	1000 °C	30 minutes
Quenching in the oil	Ambient temperature	3 minutes
Tempering	650 °C	1 hour

After the heat treatment, the samples reached a uniform core hardness of about 40-44 (HRC). The laser surface hardening was carried out by a laser cell which consists of a FANUC M-710iC robot that directs a light beam from a laser head fed through a fiber laser with a maximum power of 3000 and emits continuous waves with a wavelength of 1070 nm. The laser head HIGHYAG BIMO is equipped with both a variable zoom collimator and a fixed focusing lens. The assembly makes it possible to obtain circular focal spots of the order of 0.251 to 0.431 mm in diameter and connected to an optical fiber of 100 mm. Figure 2-1 shows the laser set up used for this experiment.

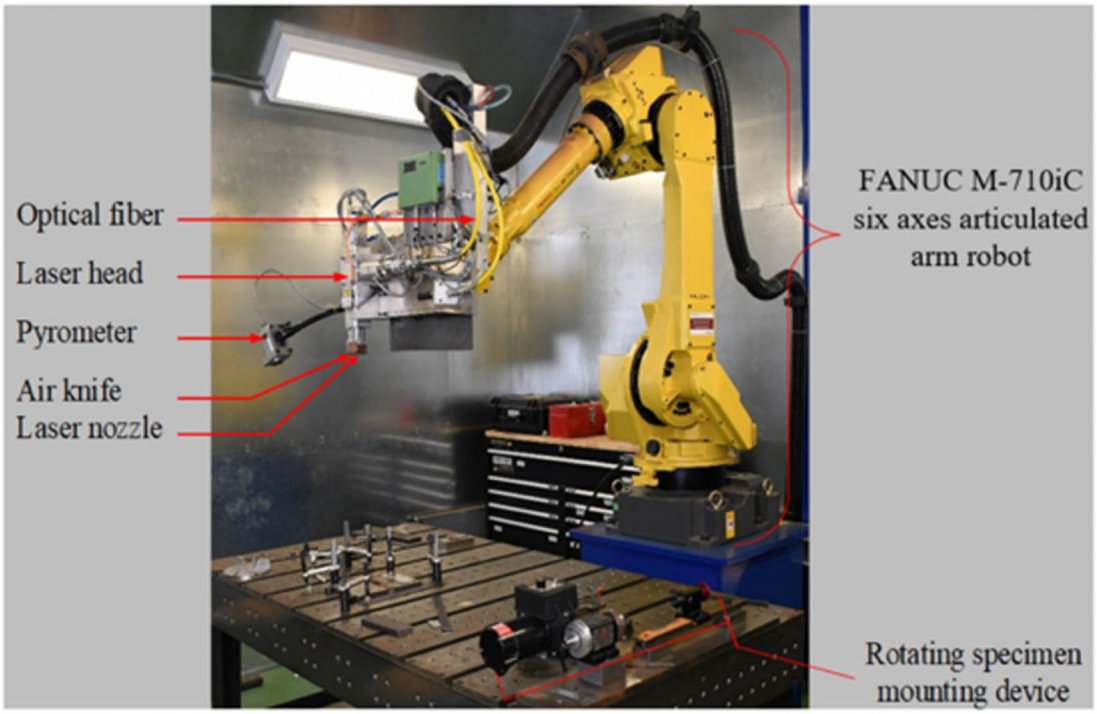

Figure 2-1: Laser cell (3000W: YLS-3000-ST2) mounted on a FANUC robot with 6 axes [18]

This study examines three key factors: laser power, scanning speed, and defocus distance. The focal plane is determined by the focusing lens, and the defocus distance Z represents the gap between the focal plane and the target plane. If the target plane is located above the focal plane, the defocus distance is negative ($Z < 0$), whereas if the target plane is below the focal plane, the defocus distance is positive ($Z > 0$). When the target plane coincides with the focal plane, the defocus distance Z is zero. As the defocus distance $|Z|$ increases, the area of the irradiation surface also increases. In the case of laser hardening processes, it is important to define the experimental margins by allowing for maximal case depth transformation and excessive transformation without cracking the material. Maximal and minimal tuning is necessary before parameter levels can be established. Table 1-3 shows the factors and their variation ranges in these experiments.

Table 1-3: Laser hardening parameters specifications

Factors	Abbreviation	Variation ranges	Unit
Power	P	500, 600 and 700	W
Scanning speed	S	2, 3 and 4	mm/s
Defocus distance	D	8, 12 and 16	mm
Focal diameter	F	0.9, 1.03 and 1.15	mm

Taguchi method is used to determine the experimental plan, to have a minimum number of processed trials and a minimum variation by studying the effect of multiple parameters simultaneously. In contrast, the conventional methods use a very long approach that consists of varying one parameter while keeping the rest constant [19]. For the experimental design three factors are involved with three levels, so the L9 orthogonal Taguchi Table 1- 4 is adopted.

One factor that combines the three laser parameters, laser power, scanning speed, and focal diameter, is laser energy density, calculated by using the equation (1. 1).

$$\text{Laser energy density (j.}mm^{-2}\text{)} = \frac{laser\ power\ (W)}{scanning\ speed(mm/s) \times Focal\ diameter\ (mm)} \qquad (1.\ 1)$$

Laser energy density is a crucial parameter which directly impact the characteristics of the laser treated area, in particular the microstructure, the roughness, the size and shape of the laser transformed area.

Table 1- 4: L9 orthogonal Taguchi table (input parameters)

Test	Defocus distance (mm)	Focal diameter (mm)	Scanning speed (mm/s)	Power (W)	Energy density (J/mm^2)
1	8	0.9	2	500	277.78
2	8	0.9	3	600	222.22
3	8	0.9	4	700	194.44
4	12	1.03	2	600	291.26
5	12	1.03	3	700	226.54
6	12	1.03	4	500	121.36
7	16	1.15	2	700	304.35
8	16	1.15	3	500	144.93
9	16	1.15	4	600	130.43

1.6.3 Mechanical method

Before the microhardness test the sample were cut from the middle of the line, and then mounted and polished properly until the surface was smooth and scratch-free. The microhardness tests were carried out on an automated Vickers microhardness tester (CLEMEX CTM micro hardness testing Figure 1-2 (a)), with an indentation load of 200 gf, and dwell time of 10 s.

Scanning Electron Microscopy (SNE-4500M Plus Tabletop SEM Figure (b)), is used to characterize the different phases of the hardened zone, it has also additional features such as variable spot size control allow for optimal x-ray generation for Energy Dispersive Spectroscopy EDS analysis. The samples with nine set parameters were prepared for SEM by etching the surface after the polishing using the solution Nital 5% which is a solution of acid nitric and alcohol.

CLEMEX CTM micro hardness testing set-up (a) Scanning Electron Microscope (b)

Figure 1-2: Micro-hardness and SEM set-up

1.7 RESULTS AND DISCUSSION

1.7.1 Microstructure of base material

Steel has a several solid phases (ferrite, pearlite, austenite) that change with the temperature and the carbon content variation. The H13 tool steel was subject of a heat treatment of three steps austenitizing, quenching and tempering, which contribute to achieve the microstructure shown in Figure 1-3 [20].The austenitizing consists of transforming ferrite to austenite gamma-phase iron by carbon diffusion from the carbides through the austenite, which increases the grain and the martensitic lath size and produces high secondary carbides. Then come a very rapid cooling with a large thermal gradient, that prevents the carbon diffusion and the rearrangement of the atomic structure into equilibrium positions, also higher saturation of alloying elements in solid solution as well as the precipitation of fine carbides, which results in an appearance of a metastable phase martensite, that leads to tough steel but highly brittle. The third treatment is tempering process that modifies the properties of quenched-tempered H13 to have a good combination of strength, hardness and toughness, by reducing the hardness and increasing the ductility. During the tempering process, two transformations occur:

- The transformation of martensite into tempered and softer martensite.

- Fine carbides precipitation, which can be associated to the hardness drop.

Figure 1-3 shows the microstructure of quenched and tempered H13 in two levels of magnifications, which contain principally tempered martensite and dispersion of carbide precipitate [20]. Carbide is another phase in H13 steel, defined as a round granular structure with different morphologies and sizes that characterize it. The quantity, type, and distribution of this compound have a significant impact on the steel performance; it contributes to the strength of steel in two different ways by providing resistance to wear, which improves the hardenability and contributes to higher yield strengths by impeding the mobility of matrix dislocations [21]. V-rich MC, Mo-rich M_6C, and Cr-rich $M_{23}C_6$ are the most important carbides precipitating in h13 during the tempering process. [22]

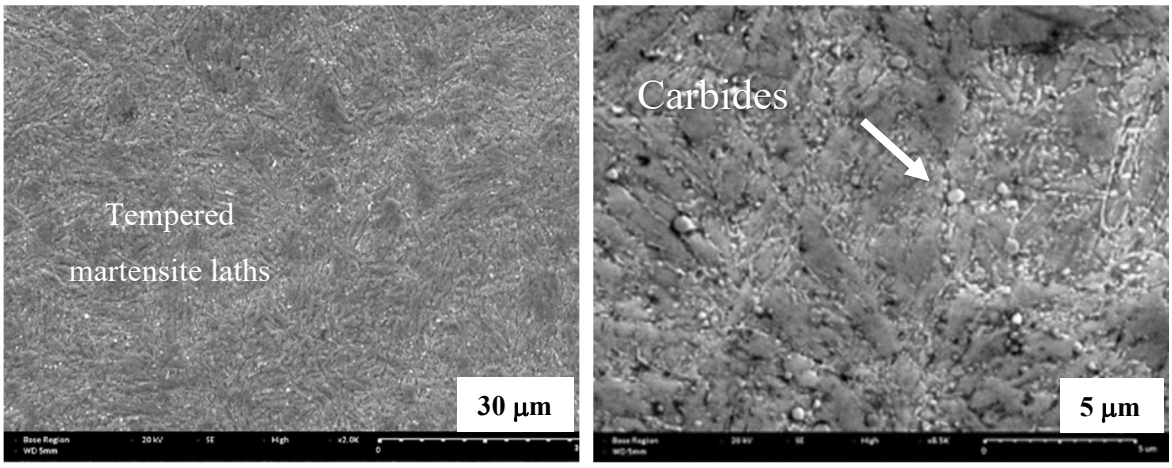

Figure 1-3: SEM of quenched and tempered AISI H13 tool steel

1.7.2 The microstructure of the laser treated zone

Figure 1- 4 shows a cross-sectional view of the laser surface transformation which consists of three zones, melted zone hardened zone – heat affected zone, from the surface towards the depth direction.

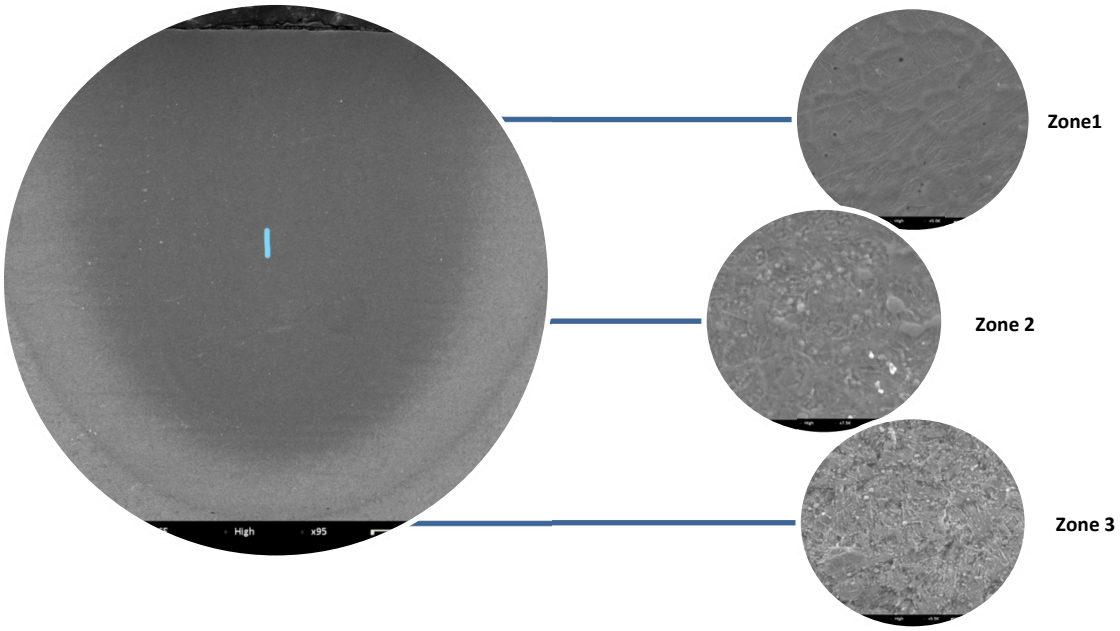

Figure 1- 4: Optical micrographs of the cross-section of laser surface treated AISI H13

H13 tool steel was subject to a laser surface modification, with different process parameters, this causes for the 9 sets a localized melting of the surface layer, followed by a rapid air cooling that leads to the formation of various microstructures, including martensite, retained austenite, and carbides, and each of these components can have different sizes and morphologies. The laser process parameters significantly affect the microstructures, such as the laser power and scanning speed [23]. According to the literature an applied laser energy density above 100 J/mm^2, the surface temperature is presumed to be more than melting point (1450 °C) of AISI H13 tool steel. The observation of the first zone Figure 1- 5 reveals a melted microstructure and rapidly solidified which majorly consists of remelted dendrite cells transformed from martensite, with a non-tempered martensite and inter-dendritic that are enriched with carbides particles [12]. The transition zone as shown in Figure 1- 6 is a hardened zone, the temperature might be above the Ac3 austenitization temperature, the microstructure contains non-tempered martensite with undissolved carbides [24, 25].The third zone mentioned in Figure 1- 7 is over tempered, as the temperature gradually decreases as depth increases due to the reduction in the amount of energy absorbed from the surface,

so the temperature is probably around the Ac1 transformation temperature. Which involves the precipitation of carbides from supersaturated martensite, as a result this zone develops a lower hardness value in comparison to the heat-treated substrate.

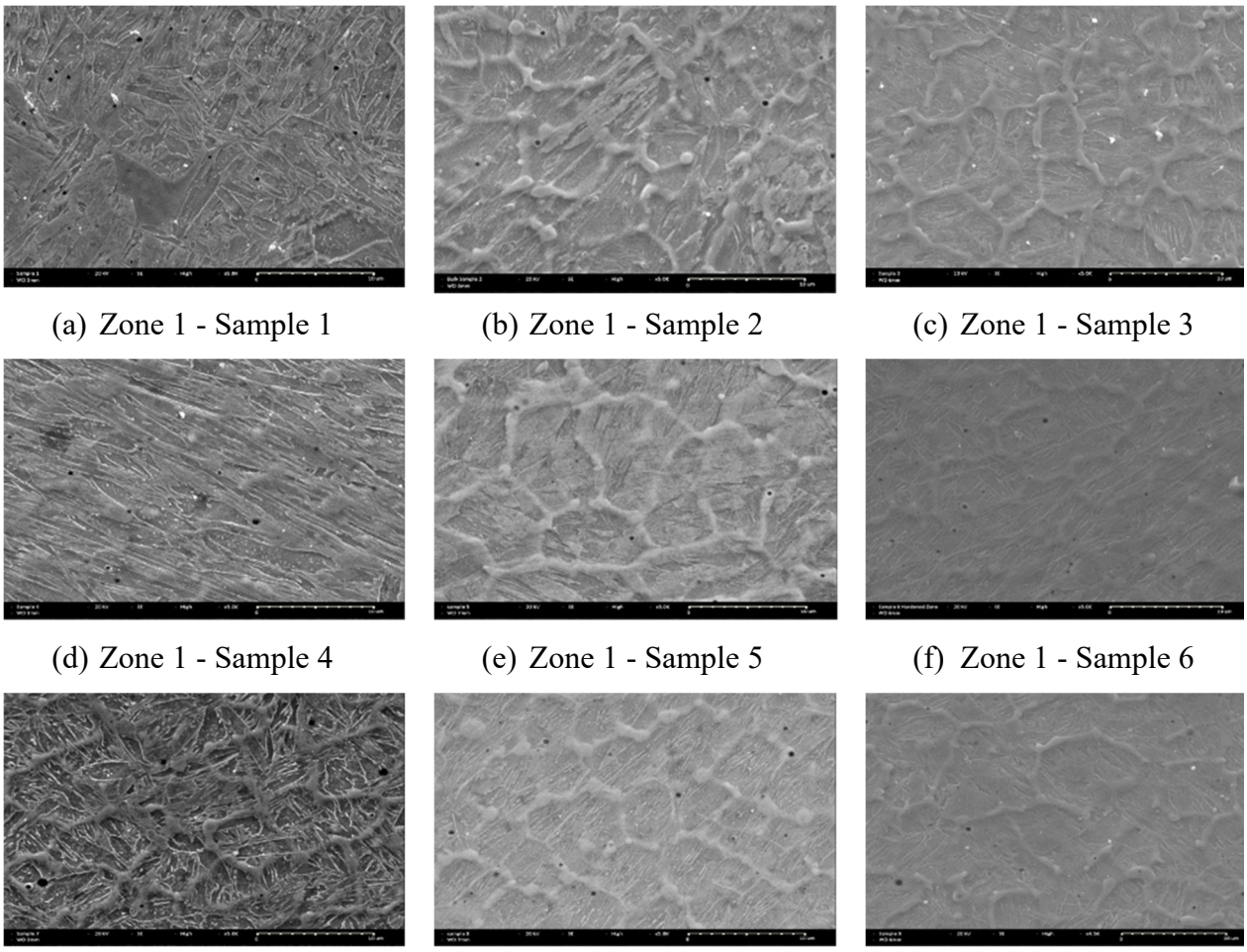

(a) Zone 1 - Sample 1 (b) Zone 1 - Sample 2 (c) Zone 1 - Sample 3

(d) Zone 1 - Sample 4 (e) Zone 1 - Sample 5 (f) Zone 1 - Sample 6

(g) Zone 1- Sample 7 (h) Zone 1- Sample 8 (i) Zone 1 - Sample 9

Figure 1- 5: Scanning electron micrographs of the top surface of different 9 set of parameters

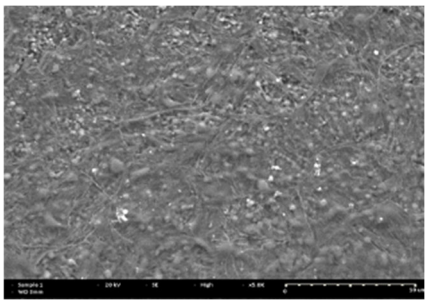

(a) Transition zone - Sample 1

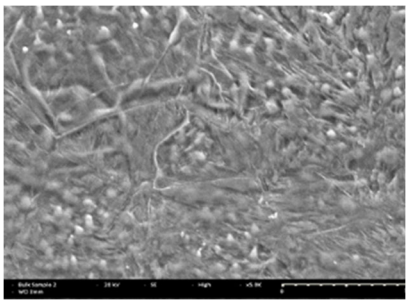

(b) Transition zone - Sample 2

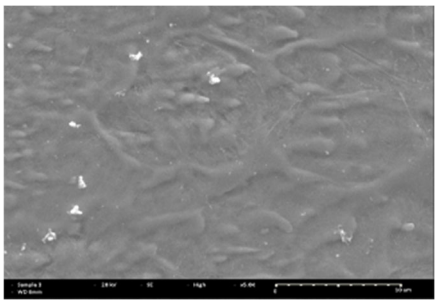

(c) Transition zone - Sample 3

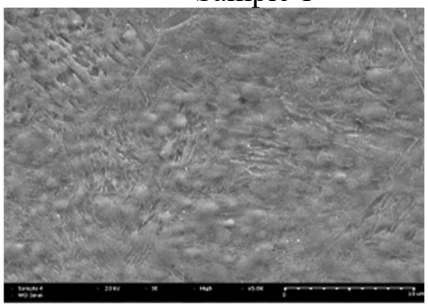

(d) Transition zone - Sample 4

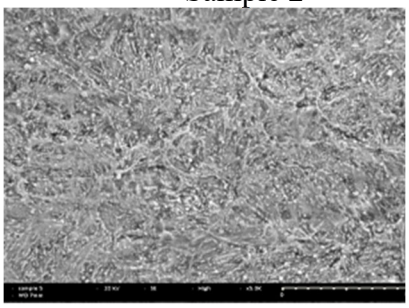

(e) Transition zone - Sample 5

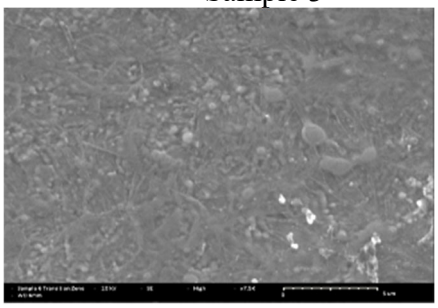

(f) Transition zone - Sample 6

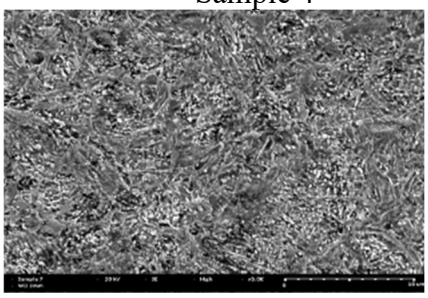

(g) Transition zone - Sample 7

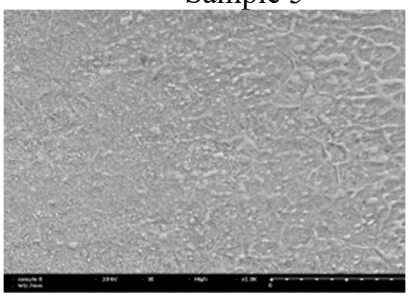

(h) Transition zone - Sample 8

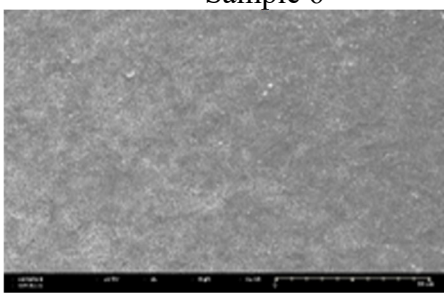

(i) Transition zone - Sample 9

Figure 1- 6:Scanning electron micrographs of the top surface of different 9 set of parameters

According to the Figure 1- 5 the microstructure of the hardened/melted zone tend to vary with the variation of laser energy density. The cells have different sizes and shapes according to the applied laser energy density.

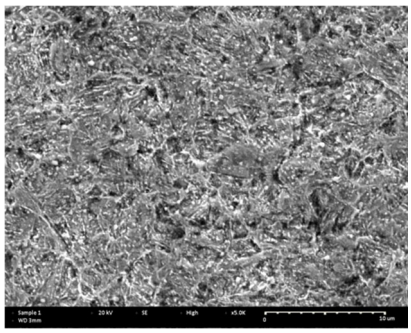

(a) Heat affected zone - Sample 1

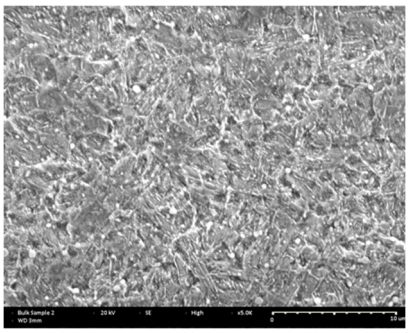

(b) Heat affected zone - Sample 2

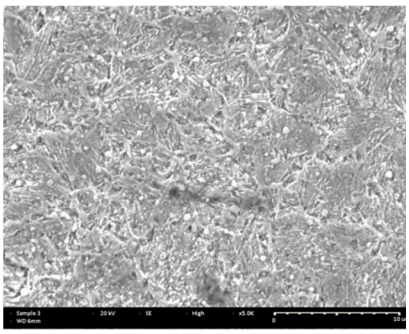

(c) Heat affected zone - Sample 3

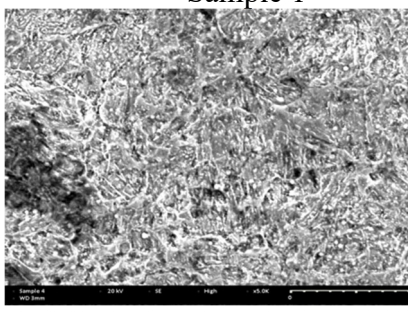

(d) Heat affected zone - Sample 4

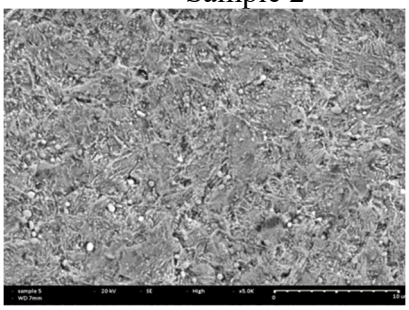

(e) Heat affected zone - Sample 5

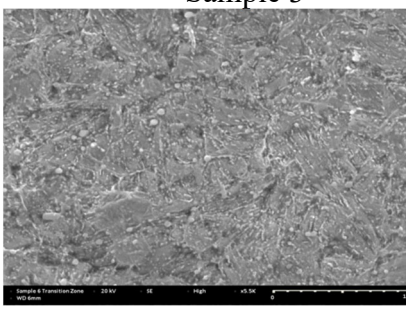

(f) Heat affected zone - Sample 6

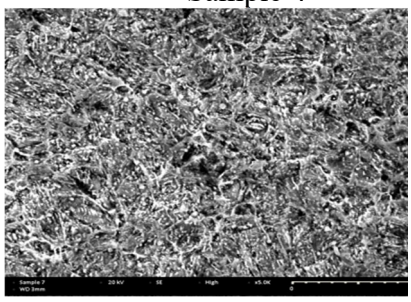

(g) Heat affected zone - Sample 7

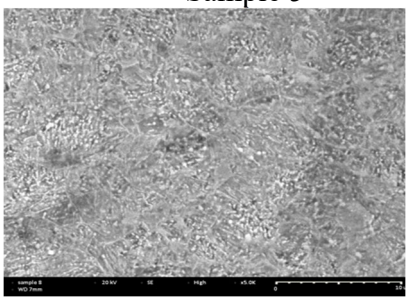

(h) Heat affected zone - Sample 8

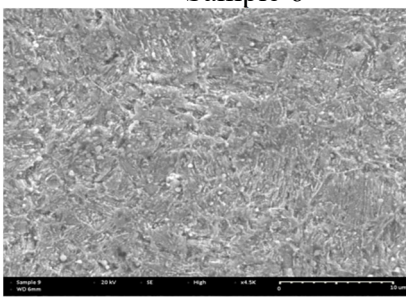

(i) Heat affected zone - Sample 9

Figure 1- 7: Scanning electron micrographs of the heat affected zone of different 9 set of parameters

1.7.3 Microhardness profiles

The mechanical method is based on the analysis of the hardness profile taken from a cross section of the specimen. The total hardened depth is the distance from the surface to where the physical properties of the hardened portion and those of the base material can no

longer be distinguished. The profile of the depth is obtained by creating several measurement points with the distance of 50 μm from the surface and perpendicular to it towards the inside of the specimen. For the width profile the measurement points were taken horizontally with the distance of 50 μm. As reported in the charts above Figure 1- 9, Figure 1- 10, Figure 1- 11, Figure 1- 12 and Figure 1- 13, the nine sets show mostly the same trend in hardness distribution for the width and depth profile, the difference consists on the highest value of hardness and both values of the depth and width of laser transformed zone. The hardness distribution is the most important characteristic of the hardening process. According to the figures, the micro-hardness profile, both in depth and width, is categorized into four regions. The first region is the melted zone, which comprises dendrite cells. The microhardness in this zone is relatively high compared to the substrate. However, the highest value of hardness among the nine samples is observed in the second region hardened zone, which is completely austenitized and transformed into martensite during rapid cooling. The third region is over-tempered and is identified by a drastic reduction in hardness before reaching the initial hardness. Finally, the fourth region is the base material that remains unaffected by the heat flux. The results of the experiment show that increasing the laser power leads to a larger melt zone and higher microhardness values in the melted area. This is because higher laser power causes the laser to diffuse more, resulting in a broader melted region. Additionally, the increased temperature from higher laser power may lead to faster cooling and a greater thermal gradient between the melt area and the surface, resulting in a finer grain size and higher microhardness. Furthermore, there is a clear relationship between laser speed and microhardness value. At a constant laser power of 500W, increasing the laser speed leads to higher microhardness values. This change is attributed to the cooling rate; higher speeds likely result in a faster cooling rate, which in turn leads to a finer grain size and increased microhardness. To gain a more comprehensive understanding of how the processing parameters influence the results, the analysis of variance (ANOVA) technique is employed, and its details will be further discussed.

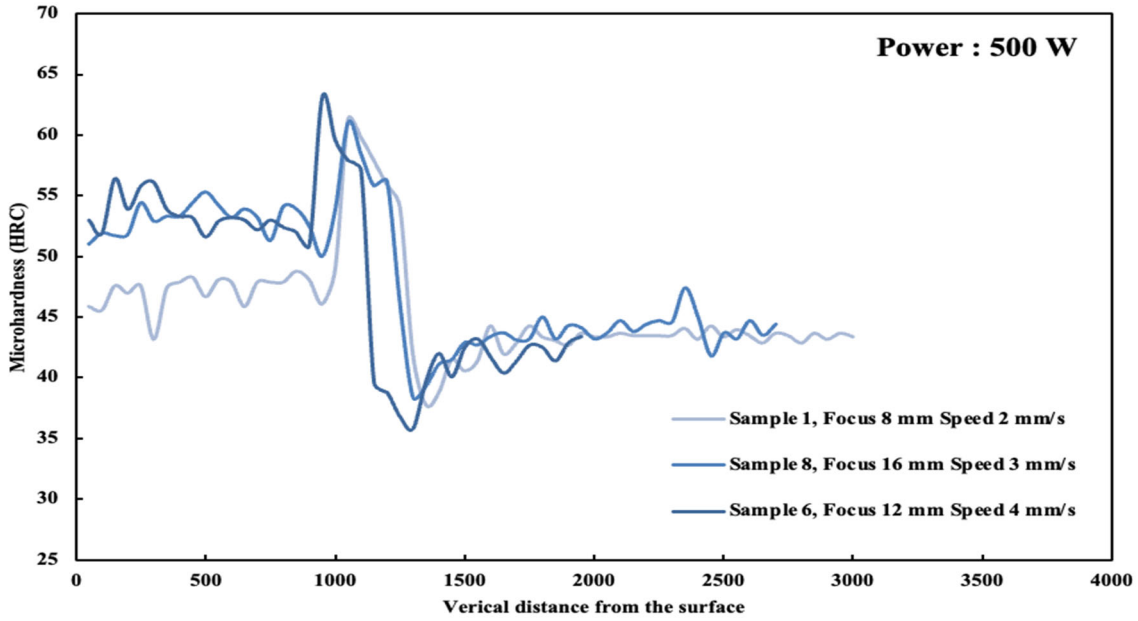

Figure 1- 8: Microhardness profile for the depth (500W)

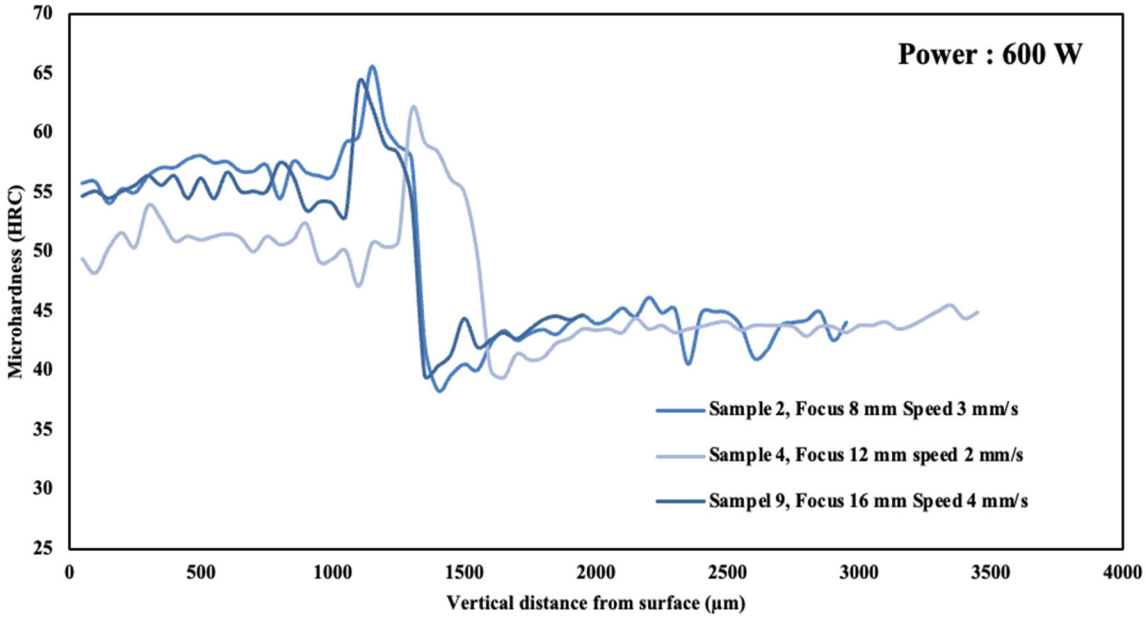

Figure 1- 9: Microhardness profile for the depth (600W)

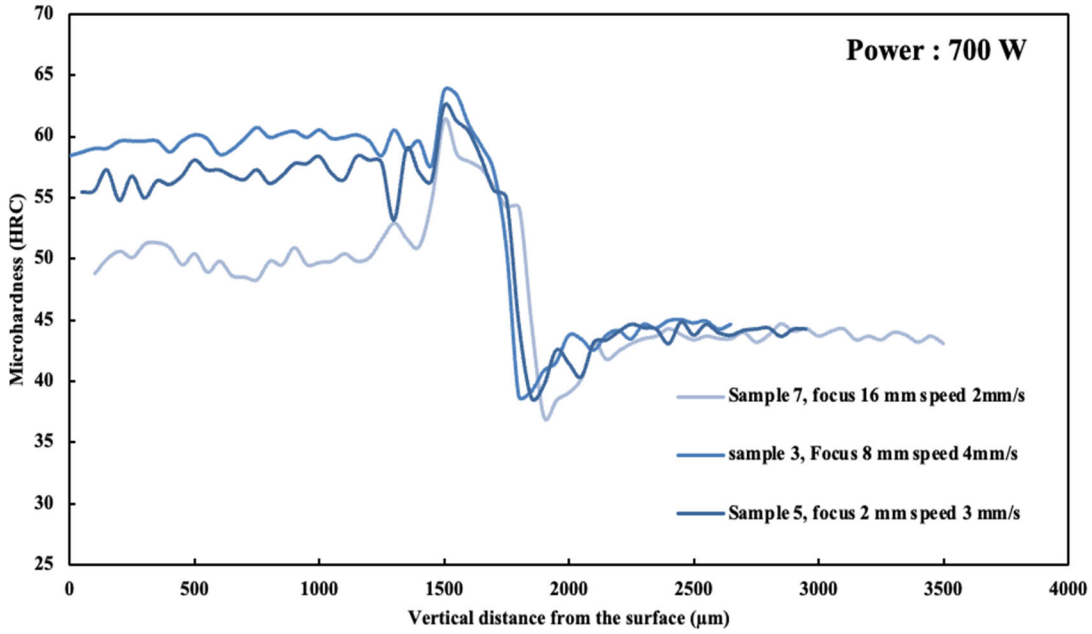

Figure 1- 10: Microhardness profile for the depth (700W)

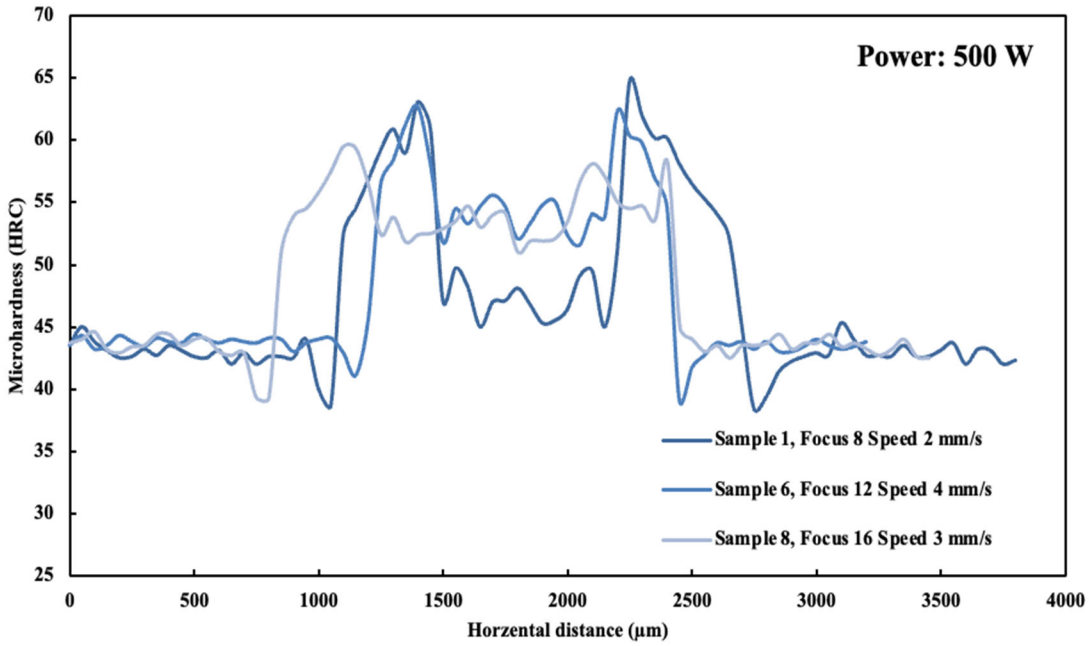

Figure 1- 11: Microhardness profile for the width (500W)

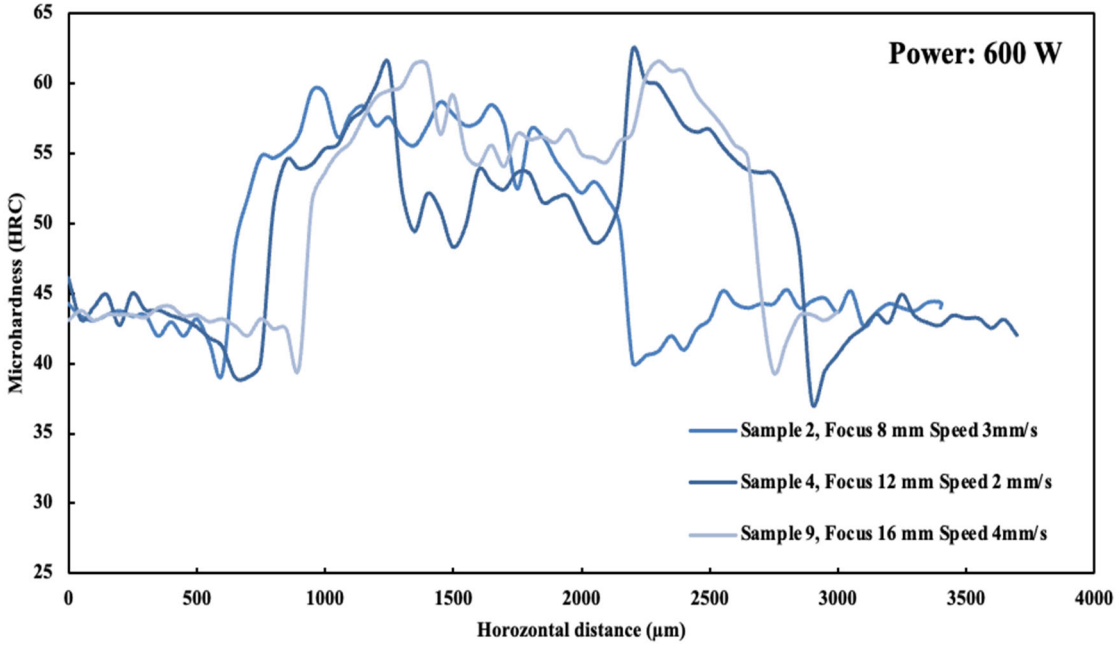

Figure 1- 12: Microhardness profile for the width (600W)

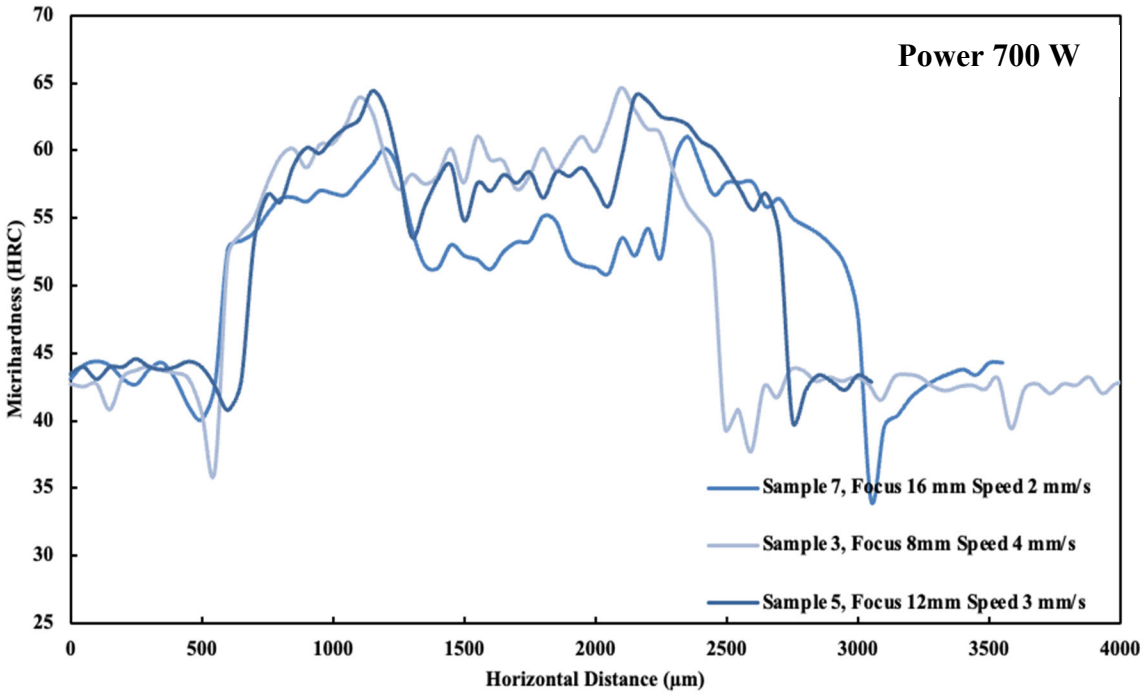

Figure 1- 13: Microhardness profile for the width (700W)

1.7.4 Maximum values of hardness

Table 1- 5 shows the maximum value of the hardness for the width and depth of the laser treated area of each sample, as well as the depth and width values. The microstructure correlate with the hardness profile [8]. The increase of the hardness in the melting/hardened zone surface can be attributed to the precipitation of fine carbides as well as the martensitic transformation upon rapid cooling. When the temperature exceeds the melting point, a cellular microstructure of supersaturated martensite forms, which is relatively soft and ductile phase, resulting in lower hardness compared to the hardened zone that didn't reach the melting point, instead it was heated above Ac3 point, resulting the formation of lath martensite and fine carbides this makes the material hard and brittle. Regarding the depth case, across all nine sets of parameters, the highest hardness values were observed in the hardened zone, which ranged from 65,7 to 61,4 HRC. On the other hand, in terms of width, the maximum hardness varied from 64,3 to 59,5 HRC.

1.7.5 Depth and width of the laser treated zone

The scanning speed influences both the high value of hardness and the dimensions of the Laser transformed zone (LTZ), decreasing the speed, reduces the hardness value, but increases the depth of LTZ, considering that this reduction increases the surface temperature and time of austenite transformation consequently a larger grain size of austenite. According to the Figure 1- 5 the depth varied between 1,30 mm to 1,9 mm, the maximum depths are achieved in three samples (7, 3 and 5), and they share one common laser parameter which is the maximum value of the power (700 W), which indicate that the power of the laser process is an important parameter that affect the depth. In general, this first analyze provides a first insight into the variability of the measurements obtained through the experiments, however a detail analyze of the correlation between laser parameters and the response will be elaborated in the following section.

Table 1- 5: Depth, width and hardness values achieved at different zones for the nine different applied laser density levels

Levels of process parameters					Responses			
Test number	**Defocus distance (mm)**	**Scanning speed (mm/s)**	**Power (W)**	**Energy density (J/mm^2)**	**Width (mm)**	**Depth (mm)**	**Maximum hardness (depth HRC)**	**Maximum hardness (width HRC)**
1	8	2	500	277,78	1,69	1,35	61,3	64,7
2	8	3	600	222,22	1,60	1,40	65,6	59,5
3	8	4	700	194,44	1,94	1,80	63,7	64,6
4	12	2	600	291,26	2,25	1,65	61,9	62,3
5	12	3	700	226,54	2,15	1,85	62,5	64,4
6	12	4	500	121,36	1,40	1,15	63,1	62,7
7	16	2	700	304,35	2,50	1,90	61,3	61
8	16	3	500	144,93	1,65	1,30	61	59,5
9	16	4	600	130,43	1,84	1,35	64,2	61,6

1.8 STATISTICAL ANALYSIS

Previously, a preliminary study was conducted to understand the effects of laser parameters on different outcomes as an initial basic investigation, without getting deeply into details that involves the relationship between the variables of the experiments, or a specific and numerical values of the contribution of each factor, which would require a statistical study. Analysis of Variance (ANOVA) is a statical tool that involves more than two factors used for the forwards purposes:

- Analyzing the impact of each factor on the responses, which helps to determine which factors have more significant effect on the results.
- Quantification of the contribution of each parameter on the overall variation of the data.

- Studying the mean differences that can provide valuable insights into the effect of different parameters on the outcome results [26].

Statistical software (Minitab) is used for this study, it provides an ANOVA table and a regression equation. The table contains the F-statistic, degree of freedom, p-value, and other relevant statistical measures. The most important outcome of ANOVA analysis is P-value which measures the statistical significance of the differences between the means of the groups being compared if the p-value is less than the pre-determined significance level (0,05), it means that the analysis is significant [27].

1.8.1 Effect of laser parameters on the depth:

While running ANOVA using Minitab, the stepwise method is conducted. The process begins with a specified initial model; Minitab then adds or removes factors until all remaining variables have a P-value indicating the variables' significance in the final model. In order to study the effects of laser parameters on the depth, Anova uses the results found in the experiments as an input and gives, as an output, the contribution of each factor, the degrees of freedom (DOF), which is the number of independent factors in the regression model, the sequential sums of squares (Seq SS) are measures of variation for different components of the model, The F-value is the test statistic used to determine whether the term is associated with the response. Furthermore, the p-value is a probability that measures the evidence against the null hypothesis [3].

The results of the variance analysis are presented in the Table 1- 6, which demonstrates that the power and scanning speed are the primary parameters that impact the depth of the laser-treated surface. With a high percentage contribution of 84,29% for the power (P) and only 9,91% for the scanning speed (S), as mentioned in Table 1- 7 The P-value is lower than 0,05, which means that the model is significant, and the error is 0,035170, which is a small value that means most of the variation is due to the parameters, and they mainly affect the depth of the laser-hardened surface. The effect of the three-laser process parameter is shown

Table 1- 6: ANOVA table for the Depth of laser treated surface

Characteristic	Sum of squares	Dof	F-Value	P-value
Scanning Speed	0,06000	1	10,25	0,019
Power	0,51042	1	87,15	0,000
Error	0,03514	6		
Total	0,60556	8		

Table 1- 7: Contributions of laser parameters

Characteristic	Defocus distance	Scanning speed	Power	Error
Contribution (%)	0	9,91	84,29	5,80

Figure 1- 14, it is noticed that the S/N ratio increases with the increase of Laser power (P), and the decreases of scanning speed (S).

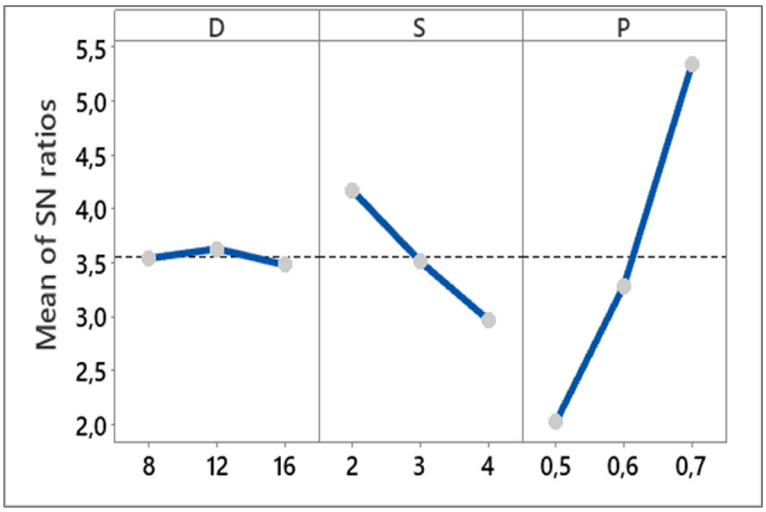

Figure 1- 14: Effect of laser parameters on the depth of laser treated surface (D in mm, S in mm/s and P in kW)

1.8.1.1 Regression equation

$$depth = 0{,}078 - 0{,}1 \times S + 0{,}002917 \times P \quad (1.\ 2)$$

ANOVA can also provide a mathematical equation (1. 2), which is based on linear regression, with the aim of establishing the relationship between the main factors of this study, by calculating an output value from the input factors, and the coefficients attributed to each factor are given by the last mean square method.

Figure 1- 15 indicates the predicted and the experimental values of the depth of the laser treated surface, in order to verify the regression model. As a result, it illustrates that the predicted and measured values are mostly close within the specified parameter ranges:

Power (W): [500−700]; Scanning Speed (mm/s): [2−4]; Defocus distance (mm): [8−12].

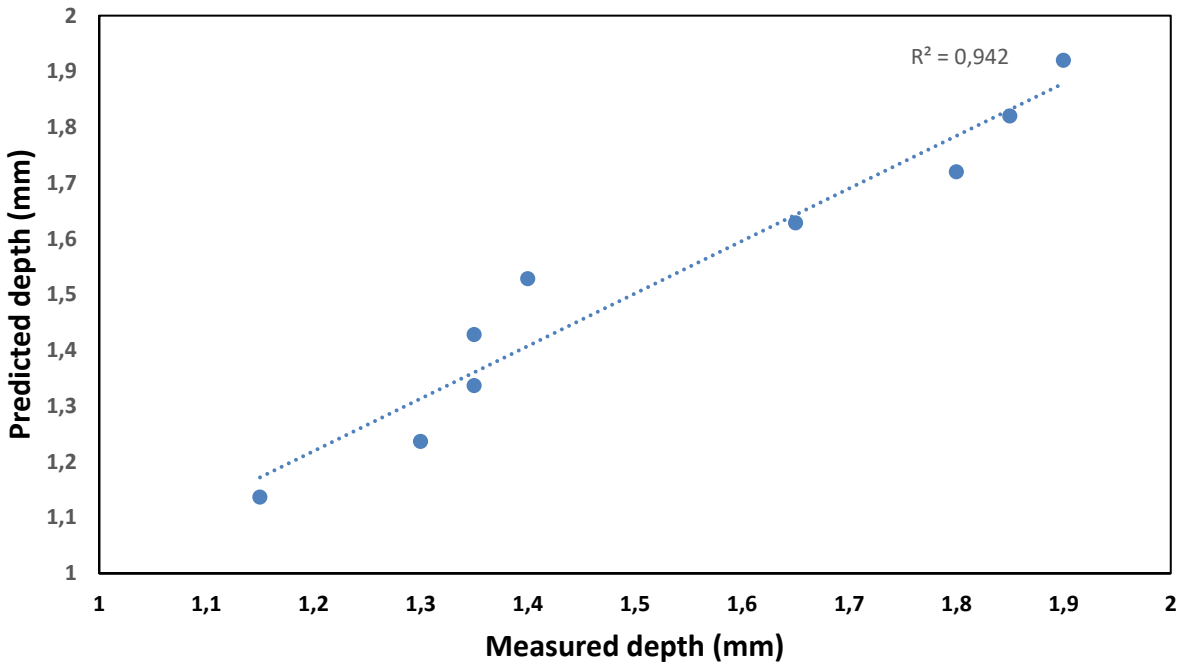

Figure 1- 15: Scatter plot- Measured and predicted Depth of laser treated surface

1.8.2 Effect of laser parameters on the width

In this section the effect of laser parameters on the width of laser treated surface is studied, according to the Table 1- 9, the laser power has the most decisive impact on the width, with a percentage contribution of 57,15 %, followed by the scanning speed that contributes with 26,85%, and then comes finally the defocus distance with only 9,34%. The error contribution is 6,66% which is a small percentage, so variation of the response is mostly due to the inputs.

In the Table 1- 8 the P-values are all less than 0,05 which means the analysis is significant, and all the parameters has a reliable effect on the width in this case.

Table 1- 8: ANOVA table for the width of laser treated surface

Characteristic	Sum of squares	Dof	F-Value	P-value
Defocus distance	0,56700	1	42,91	0,001
Scanning Speed	0,26640	1	20,16	0,006
Power	0,09263	1	7,01	0,046
Error	0,06606	5		
Total	0,99210	8		

Table 1- 9: Contribution of laser parameters

Characteristic	Defocus distance	Scanning speed	Power	Error
Contribution (%)	9,34	26,85	57,15	6,66

Figure 1- 16 shows the main effects plots of factors, it illustrates that the width increases with the increase of laser power and defocus distance, and the decrease of scanning speed.

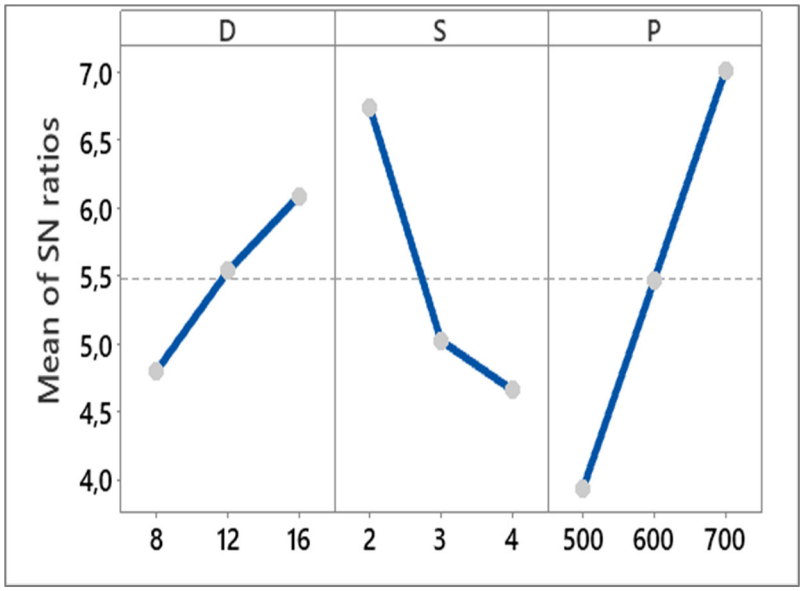

Figure 1- 16: Effect of laser parameters on the width of laser treated surface (D in mm, S in mm/s and P in W)

1.8.2.1 Regression Equation

$$\boldsymbol{Width = 0,308 + 0,0311 \times D - 0,2107 \times S + 0,003074 \times P} \qquad \textbf{(1. 3)}$$

The software Minitab is used to obtain the linear regression equation based on ANOVA method to quantify the relationship between the factors and the width. A mathematical equation is presented below (1. 3), it represents the regression equation for the depth, the three factors adopted in this study, power, scanning speed and defocus distance, seem to affect the width of the laser treated surface.

Figure 1- 17 displays a comparison between the data collected from the experiments and the predicted by the model. Both values show a good compatibility within the specified parameter ranges:

Power (W): [500−700]; Scanning Speed (mm/s): [2−4]; Defocus distance (mm): [8−12].

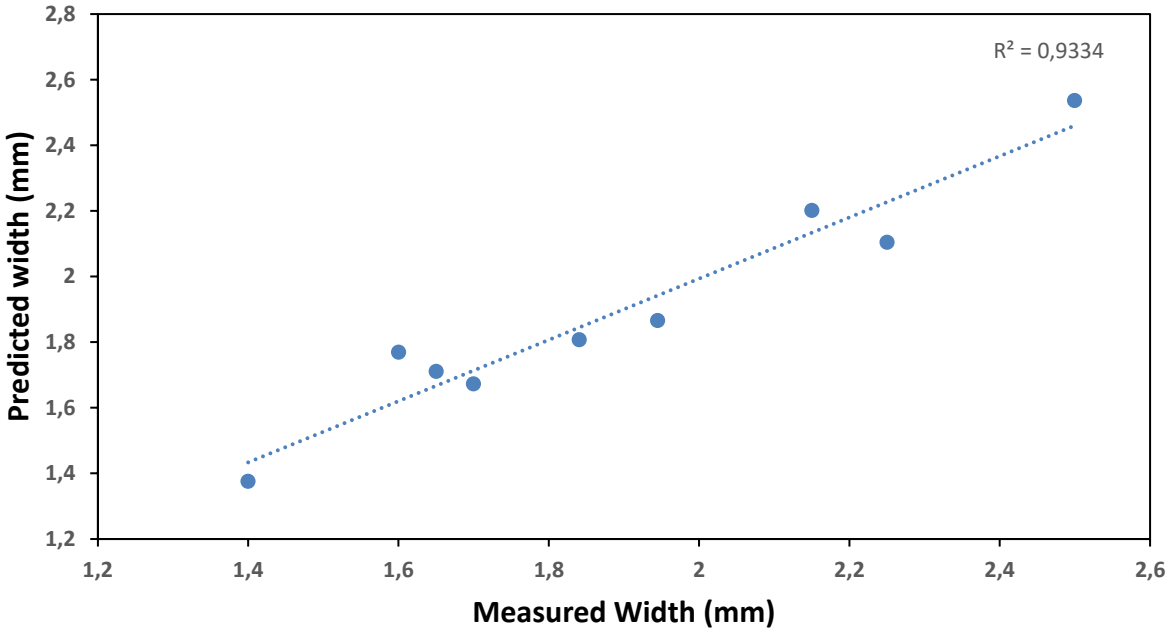

Figure 1- 17: Scatter plot- Measured and predicted width of laser treated surface

1.8.2.2 Response surface method

RSM is a statistical approach for modeling and analyzing cases where multiple variables affect a response. It creates a contour plot that provides a visual representation of how different parameters impact the response and helps to identify optimal settings for achieving the desired outcomes. Firstly, A combined effect of scanning speed and laser power while holding defocus distance at 12 mm is shown in Figure 1- 18, the width increases with increase of power and the decrease of scanning speed. Then, the effect of both power and defocus distance is visualized in the Figure 1- 18, while the scanning speed is fixed at 3 mm/s, the maximum values of width are achieved with high values of power and defocus distance. Finally, the effect of scanning speed and defocus distance is revealed in Figure 1- 18, while fixing the power at 600W, it indicates that the width increases with the increase of defocus distance and the decrease of scanning speed.

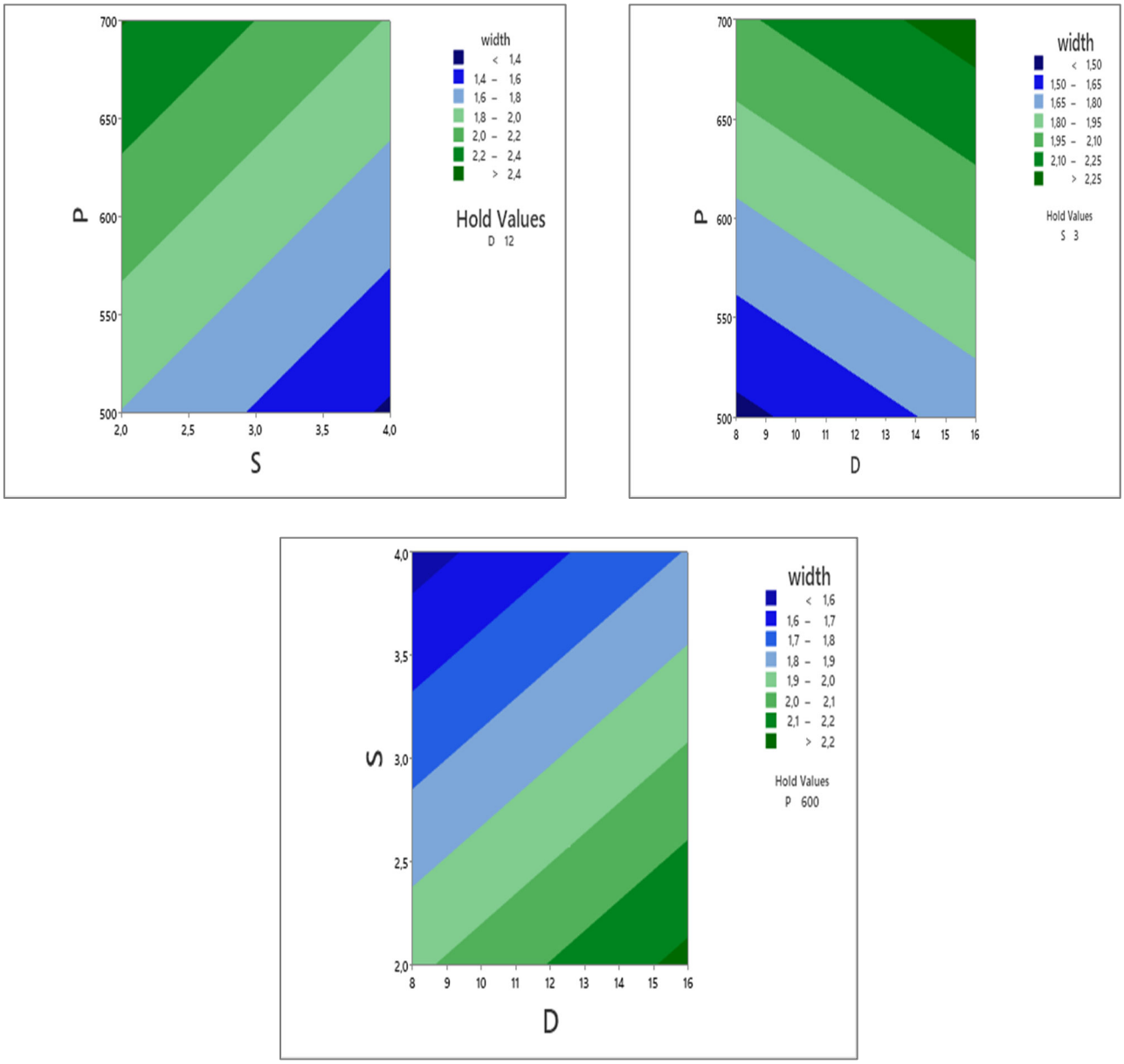

Figure 1- 18: RSM for the width (D in mm, S in mm/s and P in W)

1.9 CONCLUSION

In the present article, a detailed investigation is conducted on the effect of laser process parameters on the microstructure microhardness profile of quenched and tempered H13 tool

steel, the results show a noticeable improvement in material's surface, and opens new prospects for the development of laser surface engineering. Based on the experimentations and the analysis carried out in this study, the following statement may be concluded:

- The quenching and tempering heat treatment of H13 tool steel, achieved a hardness of 40-44 HRC, and the microstructure includes mostly tempered martensite and a dispersion of carbide precipitate.

- The laser surface treatment with the nine sets of parameters, creates three regions: the melted zone, the hardened zone and the heat affected zone.

- The maximum value of hardness for the nine sets was achieved in the hardened zone, and it was significantly improved in a range of 65.7-61.4 HRC for the depth compared to 40-44 HRC for the substrate.

- The depth and the width of laser hardened area changes depending on laser parameters, the depth varied between 1.30 mm to 1.9 mm, and the width changes from 1.4 mm to 2.5 mm.

- According to variance analysis (Anova) the laser power and scanning speed are the main factors that affects the depth of laser treated surface, with a high percentage contribution of 84,29% for the power (P), and only 9,91% for the scanning speed (S).it also shows that the depth increases with the increase of laser power and the decrease of scanning speed.

- Applying the analysis of variance on the width indicates that the laser power has the most decisive impact on the width, with a percentage contribution of 57.15 %, followed by the scanning speed that contributes with 26.85%, and then comes finally the defocus distance with only 9.34%. In addition, the width increases with increase of laser power and defocus distance, and the decrease of scanning speed.

1.10 REFERENCES

1. Wang, J., Z. Xu, and X. Lu, *Effect of the Quenching and Tempering Temperatures on the Microstructure and Mechanical Properties of H13 Steel.* Journal of Materials Engineering and Performance, 2020. **29**(3): p. 1849-1859.
2. Li, S.H., W.C. He, X. Zhang, D.H. Li, and M.G. Xiao, *Research progress on surface treatment technologies of H13 hot work die steel.* Kang T'ieh/Iron and Steel, 2021. **56**(3): p. 13-22 and 40.
3. Jhavar, S., C.P. Paul, and N.K. Jain, *Causes of failure and repairing options for dies and molds: A review.* Engineering Failure Analysis, 2013. **34**: p. 519-535.
4. Dossett, J. and G. Totten, *Introduction to surface hardening of steels.* ASM Handbook, 2013. **4**: p. 389-398.
5. P, D., B. K R, and B.G. Naidu, *Laser surface hardening: A review.* Int. J. of Surface Science and Engineering, 2011. **5**: p. 131-151.
6. Karmakar, D.P., M. Gopinath, and A.K. Nath, *Effect of tempering on laser remelted AISI H13 tool steel.* Surface and Coatings Technology, 2019. **361**: p. 136-149.
7. Jae-Ho, L., J. Jeong-Hwan, J. Byeong-Don, S. Young-Myung, and M. Young-Hoon, *Laser surface hardening of AISI H13 tool steel.* Transactions of nonferrous metals society of China, 2009. **19**(4): p. 917-920.
8. Nath, A.K. and S. Sarkar, *Chapter 11 - Laser Transformation Hardening of Steel*, in *Advances in Laser Materials Processing (Second Edition)*, J. Lawrence, Editor. 2018, Woodhead Publishing. p. 257-298.
9. Dinesh Babu, P., G. Buvanashekaran, and K.R. Balasubramanian, *Experimental investigation of laser transformation hardening of low alloy steel using response surface methodology.* International Journal of Advanced Manufacturing Technology, 2013. **67**(5-8): p. 1883-1897.
10. Badkar, D.S., K.S. Pandey, and G. Buvanashekaran, *Parameter optimization of laser transformation hardening by using Taguchi method and utility concept.* International Journal of Advanced Manufacturing Technology, 2011. **52**(9-12): p. 1067-1077.
11. Oh, S. and H. Ki, *Prediction of hardness and deformation using a 3-D thermal analysis in laser hardening of AISI H13 tool steel.* Applied Thermal Engineering, 2017. **121**: p. 951-962.
12. Telasang, G., J. Dutta Majumdar, G. Padmanabham, and I. Manna, *Wear and corrosion behavior of laser surface engineered AISI H13 hot working tool steel.* Surface and Coatings Technology, 2015. **261**: p. 69-78.
13. Telasang, G., J. Dutta Majumdar, G. Padmanabham, and I. Manna, *Structure-property correlation in laser surface treated AISI H13 tool steel for improved mechanical properties.* Materials Science and Engineering A, 2014. **599**: p. 255-267.
14. Zhang, J., M. Yu, Z. Li, Y. Liu, Q. Zhang, R. Jiang, and S. Sun, *The effect of laser energy density on the microstructure, residual stress and phase composition of H13 steel treated by laser surface melting.* Journal of Alloys and Compounds, 2021. **856**: p. 158168.

15. Jia, Z.-x., J.-q. Li, L.-j. Liu, Y.-w. Liu, Y.-q. Wang, and H.-l. Li, *Influence and application of laser parameters on unit of H13 steel by laser remelting process.* The International Journal of Advanced Manufacturing Technology, 2015. **79**: p. 551-568.
16. Barka, N. and A.E. Ouafi, *Effects of Laser Hardening Process Parameters on Case Depth of 4340 Steel Cylindrical Specimen°™A Statistical Analysis.* Journal of Surface Engineered Materials and Advanced Technology, 2015. **Vol.05No.03**: p. 12.
17. *ASM handbook.* 1991. **Volume 4 heat treatment**.
18. Bensalem, K., N. Barka, S. Sattarpanah Karganroudi, A. Sadeghian, and M. Moradi, *Effects of laser process parameters on the hardness profile of AISI 4340 cylindrical samples: statistical and experimental analyses.* The International Journal of Advanced Manufacturing Technology, 2022. **122**(7-8): p. 2849-2867.
19. Kasman, Ş. and I.E. Saklakoglu, *Determination of process parameters in the laser micromilling application using Taguchi method: A case study for AISI H13 tool steel.* The International Journal of Advanced Manufacturing Technology, 2012. **58**: p. 201-209.
20. Ning, A., Y. Liu, R. Gao, S. Yue, M. Wang, and H. Guo, *Effect of Tempering Condition on Microstructure, Mechanical Properties and Precipitates in AISI H13 Steel.* JOM, 2021. **73**(7): p. 2194-2202.
21. Lin, M., X. Zhao, L. Han, Q. Liu, and J. Gu, *Microstructural Evolution and Carbide Precipitation in a Heat-Treated H13 Hot Work Mold Steel.* Metallography, Microstructure, and Analysis, 2016. **5**(6): p. 520-527.
22. Ning, A., W. Mao, X. Chen, H. Guo, and J. Guo, *Precipitation behavior of carbides in H13 hot work die steel and its strengthening during tempering.* Metals, 2017. **7**(3): p. 70.
23. Aqida, S.N., D. Brabazon, and S. Naher, *An investigation of phase transformation and crystallinity in laser surface modified H13 steel.* Applied Physics A, 2012. **110**(3): p. 673-678.
24. Šebek, M., L. Falat, F. Kováč, I. Petryshynets, P. Horňak, and V. Girman, *The effects of laser surface hardening on microstructural characteristics and wear resistance of AISI H11 hot work tool steel.* Archives of Metallurgy and Materials, 2017. **62**(3): p. 1721-1726.
25. Zhang, J., M. Yu, Z. Li, Y. Liu, Q. Zhang, R. Jiang, and S. Sun, *The effect of laser energy density on the microstructure, residual stress and phase composition of H13 steel treated by laser surface melting.* Journal of Alloys and Compounds, 2021. **856**.
26. Dar, A. and A. N, *Use of orthogonal arrays and design of experiment via Taguchi L9 method in probability of default.* Accounting ISSN 2369-7407, 2017. **4**: p. 113-122.
27. Shanmugam, R., *Applied statistical inference with Minitab: by Sally A. Lesik, 6000 Broken Sound Parkway NW, Suite 300, Boca Raton, FL 33487-2742, CRC Press, 2019, 478+ viix pp., ISBN: 978-1-4987-7998-2*. 2019, Taylor & Francis.

CHAPITRE 2
INVESTIGATION ÉXPERIMENTALE ET STATISTIQUE DE L'IMPACT DES PARAMÈTRES LASER SUR LES PROPRIÉTÉS MÉCANIQUES DE L'ACIER ÀOUTILS H13 BRUTE

Lamya Baali[1], Noureddine Barka[1], Asim Iltaf[1], Véronique Dassylva-Raymond[1]

[1]Mathematics, Computer Science and Engineering Department, Université du Québec à Rimouski (UQAR), 300 Allée des Ursulines, Rimouski, QC G5L 3A1, Québec, Canada

Cet article a été soumis dans Engineering Innovations (EI) portant le numéro de référence 9783035726916

2.1 RESUME EN FRANÇAIS DU DEUXIEME ARTICLE

Cette étude se concentre sur l'impact des paramètres laser sur le comportement en traction de l'acier à outils H13, dans son état trempé et revenu. Un plan d'expérience basé sur la méthode Taguchi, comprenant trois niveaux pour trois paramètres laser (puissance, vitesse de balayage, et distance de focalisation), est adopté pour cette analyse. Le traitement laser est appliqué à la surface de l'acier à l'aide d'une unité bionique équipée de deux lignes parallèles.

L'objectif principal est d'évaluer comment les variations des paramètres laser influent sur deux propriétés mécaniques critiques : la résistance ultime et l'allongement à la rupture. Ces propriétés sont essentielles pour comprendre comment le matériau réagit sous une contrainte de traction. Les données expérimentales sont soumises à une analyse statistique à l'aide de la méthode d'analyse de la variance (ANOVA). Parallèlement, le mode de rupture est examiné

pour chaque ensemble de paramètres laser au moyen d'un microscope électronique à balayage.

Les résultats révèlent que le traitement au laser a entraîné une amélioration de la résistance à la traction ultime des échantillons traités. Cependant, il a également eu un impact négatif sur l'allongement à la rupture. L'analyse fractographique de l'acier à outils H13 traité au laser a mis en lumière une combinaison de caractéristiques ductiles et fragiles. La surface fracturée présentait à la fois des signes de déformation plastique et de rupture, indiquant un comportement principalement ductile avec des zones de fragilité. La zone durcie révélait principalement des caractéristiques fragiles, tandis que la zone fondue présentait une meilleure ductilité, mettant en évidence l'influence des paramètres du procédé laser sur le comportement de rupture du matériau.

2.2 CONTRIBUTIONS

Ce premier article, intitulé « Experimental and Statistical Investigation of the Impact of Laser Process Parameters on the Mechanical Properties of H13 tool steel Bulk » a principalement été rédigé par Lamya Baali, son premier auteur. Noureddine Barka, le deuxième auteur, occupe la fonction de directeur de recherche et a joué un rôle clé dans la définition du projet et de la méthodologie adoptée. Le troisième auteur, Asim Iltaf, a apporté une contribution essentielle à l'amélioration de l'article. Enfin, Véronique Dassylva-Raymond a supervisé le travail et a également contribué à améliorer la rédaction globale.

2.3 TITRE DU DEUXIÈME ARTICLE

Experimental and Statistical Investigation of the Impact of Laser Process Parameters on the Mechanical Properties of H13 tool steel Bulk

2.4 ABSTRACT

This study focuses on the impact of laser parameters on the tensile behavior of H13 tool steel, in its quenched and tempered state. An experimental design based on the Taguchi method, including three levels for three laser parameters (power, scanning speed, and focusing distance), is adopted for this analysis. The laser treatment is applied to the surface of the steel using a bionic unit equipped with two parallel lines.

The main objective is to evaluate how variations in laser parameters influence two critical mechanical properties: ultimate strength and elongation at break. These properties are essential to understanding how the material reacts under tensile stress. The experimental data are subjected to statistical analysis using the analysis of variance (ANOVA) method. At the same time, the failure mode is examined for each set of laser parameters using a scanning electron microscope.

The results reveal that laser treatment resulted in improvement in the ultimate tensile strength of the treated samples. However, it also had a negative impact on elongation at break. Fractographic analysis of laser treated H13 tool steel revealed a combination of ductile and brittle characteristics. The fractured surface showed signs of both plastic deformation and failure, indicating primarily ductile behavior with areas of brittleness. The hardened zone mainly revealed brittle characteristics, while the melted zone showed better ductility, highlighting the influence of laser process parameters on the fracture behavior of the material.

2.5 INTRODUCTION

Hot-work tool steel such as chromium (H1-H19), tungsten (H20-39) and molybdenum (H40-H59) hot work tool steels are commonly used tool materials due to their excellent functional properties and favorable balance between quality and price. Various methods have been employed to enhance the properties of these steel, including heat, mechanical and chemical treatments [1]. H13 tool steel is a type of chromium hot-work steel known for its exceptional toughness and ductility even at elevated temperatures. It boasts excellent wear

resistance, impressive thermal conductivity, and high hardenability. H13 steel is commonly employed in demanding industrial processes such as extrusion dies, hot forging, mold inserts, and die casting dies. These applications necessitate the material to exhibit outstanding resistance against deformation, thermal shock, heat treatment distortion, and high-temperature wear [2]. Molds and dies are extremely an essential tool in industry, during their functioning they're exposed to a high thermal and mechanical stress, concerning thermal stress, it's created due to repeated temperature cycles that are responsible of damaging the structure of the mold material over time, such damage manifest on the surface in the form of small cracks on the surface of the mold, which can gradually grow and expand into deeper fissures [3]. Regarding mechanical stress, it's generally generated by the interactions between the surface of the mols and the particles of the injected material under high pressure and temperature, as a result the erosion wear occurs on the surface. The combination effect of plastic deformation and wear is known to induce a variety of surface defects including surface cracks, dents, scratches, broken edges, and blunt edges [4, 5]. The most die failures are present in the surface, so increasing utile life depends on improving its surface that must resist to tempering and aging while usage [6]. Once the mold is affected it's either replaced with a new one or repaired using different method such as laser remelting, laser cladding [7-9]. In order to prevent all the problems above, limiting surface damage is required by applying a surface modification process before its functioning, such as plasma nitriding [10], liquid carburizing [11], gas nitriding is thermochemical surface modification process [12, 13], powder coating, and laser surface treatment. The selective surface control provided by laser-assisted processes has made laser technology a good candidate for surface modification which made them commonly used for different applications including, laser hardening, laser melting, laser alloying, and laser cladding [14-16]. Laser cladding is a process used to improve surface properties of a substrate by adding a layer material, which is typically in the form of powder in different types of materials, such as metals, ceramics or polymers. This is achieved by melting a powder material using a high-powered laser beam, which fuses with the substrate to create a solid dense layer, to improve the wear resistance, corrosion resistance, hardness and other surface properties [17-20]. However, laser alloying aims to

melt the surface of the substrate and adding alloying elements in the form of powder, to form a new allow layer on the surface, this improves the mechanical properties of the surface and achieve the desirable harness [21, 22].Laser heat treatment includes surface hardening and surface melting, aim to heat the surface of a material using a high-energy laser beam, followed by a controlled cooling process, which modifies the microstructure of the material, resulting in improved properties such as increased hardness, toughness, and wear resistance [23-25]. Laser surface treatment offers several advantages over other traditional methods, as laser process is a non-contact technique, local modifications which allow high precision of the modified surface without mainly affect the surrounded material, and flexible technique that allows for the creation of micro and nano-sized surface structures with high accuracy and repeatability [26]. Biomimetic laser treatment is inspired form nature and biological system, based on non-smooth surface, one of its application is improving molds surface, according to different research, this process has proven to be highly efficient and effective by enhancing the mechanical properties of hot work tool steels, including wear-resistance, tensile strength, and resistance to thermal fatigue [27-31]. The mechanisms of the fatigue wear resistance improvement suggested that bionic texture could not only prominently hinder the propagation of cracks, but also the defects occurring on the bionic texture sample were obviously slight than that of un- treated sample, as the bionic texture played the main supporting to resist the plastic deformation [32].

The heat treatment is one of the conventional processes that aims to improve the mechanical properties of tool steels and achieve a very good combination of hardness, high strength and good corrosion [33, 34]. Ning *et al* [33] identified the effect of tempering temperature and duration on the mechanical properties and microstructure evolution of annealed H13 tool steel. The samples were subjected to austenitization at a temperature of 1029 °C for 20 minutes followed by oil quenching. The tempering temperature range varied from 469°C - 699°C, while the duration range spanned from one hour to 20 hours. The findings of the study showed that the major changes in the hardness values occurs during the first two hours, between 26°C and 500°C the hardness knows a slight decrease, for the temperatures between 500°C and 590°C the hardness increases in a small amount, however

above 600°C the hardness decreases dramatically and achieves 27HRC at 700°C. For the tensile impact, the yield and ultimate strength decreased as tempering temperature raise from 1500MPa to 750 MPa and 2000 MPa to 900 MPa respectively, while elongation increases from 1% to 17% with the temperature. The softening effect observed was explained by the phenomenon of static recrystallization, martensite decomposition, and carbide coarsening. Zhu *et al* [35] Implemented a pre-tempering process during the heat treatment of the AISI H13 tool steel, with the aim of improving its microstructure and mechanical properties. Their findings indicated that applying a temperature of 640°C for 10 minutes led to significant improvements in various mechanical properties. For instance, the tensile strength increased to about 1921 MPa, yield strength to 1534 MPa, impact toughness to 0.138 $J.mm^{-2}$, hardness to 53 HRC, and tensile elongation to 11.8%. This was a notable improvement compared to the traditional process of tempering at 600°C, which only resulted in a tensile strength of 1569 MPa and a hardness of 48.3 HRC. The pre-tempering process contributed to the development of tempered martensite and dispersed carbides, which helped to increase the tensile strength. Meanwhile, the presence of ferrite and lath retained austenite played a role in enhancing the ductility of the steel. Overall, the implementation of the pre-tempering process proved to be a promising technique for improving the properties of AISI H13 tool steel. Telasang *et al* [36] investigated the tensile properties of H13 tool steel after laser surface treatment tool using a 3kN micro-tensile testing machine, their findings revealed that the yield stress increased by approximately from 1230 MPa for the quenched and tempered H13 to 1460 MPa with 1240 W applied laser power. However, the substrate sample (quenched and tempered) exhibited the highest percentage elongation of 6.5%. The highest ultimate strength of 2290 MPa was obtained by applying an energy of 62.5 J/mm^2, which resulted in surface hardening without any melting. This study concluded that the increase in yield strength was correlated with the microstructure of the laser-treated sample, which consisted primarily of martensite and carbides. Telasang *et al* [20] applied laser cladding with 6kW continuous wave diode laser, on hardened (1030°C for 10 minutes) and tempered (620°C for 2h) AISI H13, using H13 tool steel powder. The energy density was approximately 133 J/mm^2, and powder density 13.3×10^{-3} g/mm^2. After the cladding process,

the sample was tempered at 550°C for 2 hours. To evaluate the mechanical properties of the samples, micro-tensile testing was conducted on four types of samples: the as-built sample, the laser-clad sample in both the longitudinal and transverse directions, and the tempered sample after laser cladding. The results showed that the as-clad sample exhibited the highest ultimate strength of around 1757 MPa, and the highest yield strength of 1425 MPa. Additionally, the tempered clad sample displayed the highest elongation of 8%, compared to the quenched and tempered AISI H13 tool steel that showed a yield strength of 1229 MPa, an ultimate strength of 1457 MPa, and an elongation of 7%. The microstructure analysis, which utilized electron backscatter diffraction, indicated that the microstructure primarily consisted of martensite and alloy carbides such as $Cr_{23}C_6$, Cr_7C_3, VC and MO_2C. The chromium carbides were found to be more prominent due to the high percentage of chromium in the chemical composition of H13. Meng *et al* [37] conducted a study on the surface treatment of AISI H13 tool steel using two different techniques, laser surface melting (LSM) and laser surface alloying (LSA). The authors aimed to compare the effectiveness of the two techniques on improving the mechanical properties of the steel. To achieve this, the authors treated the steel samples with a bionic laser process, using different fractions of two powders: titanium carbide (TiC) and H13. The TiC fractions ranged from 10% to 70%. Tensile tests were carried out on the laser surface-treated samples to assess their strength and elongation. The results showed that the strength of the samples increased gradually with increasing TiC fraction, while the elongation decreased. The LSA treated samples showed better results compared to the LSM process. The highest ultimate strength achieved was about 1200 MPa, compared to the untreated sample which achieved only 450 MPa, while the LSM sample achieved 750 MPa. Wang *et al* [38] applied biomimetic coupled laser remelting using peg-shaped units which is different laser point on the sample, with different laser energy input. The investigation of energy input on the tensile properties and the morphology of laser treatment is conducted. The applied energies are 70, 115, 160 and 205 J/cm^2. the main results shows that the optimal energy density is 160 J/cm^2 as it provides an increase in the elongation and strength simultaneously, while more the energy increase for 205 J/cm^2 case the stress-strain gave lower strength and elongation compared to non-treated sample. Zhi *et al* [39]

utilized laser remelting biomimetic technology in order to create different biomimetic coupling models on the mold surface in order to improve their service life. The laser energy varied from 1.53 J/mm^2 to 1.75 J/mm^2.The upcoming results showed that the treated samples manifested an improved hardness, also fatigue and wear resistance, the number of cracks reduced for about 30% on the laser treated samples compared to untreated samples. The most important factors are the shape of the units and the laser energy density applied on the surface.

In this essay laser surface melting process with biomimetic morphology is adopted in order to improve the mechanical properties of AISI H13 tool steel and achieve a good compromise between ductility and strength. The ductility is an important factor in mold materials because it allows the mold to withstand the high stresses and strains that occur during the molding process, a good ductility will make the possibility to the material to deform slightly without cracking or breaking, which helps to prevent damage to the mold. Whereas the strength is also important in mold materials because it helps to prevent deformation or damage to the mold. A strong mold material will be able to resist the stresses and strains that occur during the molding process and will be less likely to warp or deform over time. In addition to study the effect of laser unit, this study aims to optimize the laser treatment parameters for better mechanical properties, using an analysis of variance ANOVA.

2.6 EXPERIMENTAL METHODS

2.6.1 Materials

The material used in the present investigation is AISI H13 tool steel, with the given chemical composition in Table 2- 1. Two bars of dimensions 6.35 x 76.2 x 609.6 mm were received from the supplier (McMaster). In accordance with the ASTM E8M [40] , a total of 40 samples were machined for the study, as illustrated in Figure 2- 2. Tensile tests were performed, with each set consisting of three repetitions. Among the samples, 27 underwent

laser treatment, while three samples were subjected to quenching and tempering for comparison purposes.

Table 2- 1: Chemical composition of H13 tool steel as measured by EDS

Component	C	Si	Mn	Cr	Mo	V	Ph	S	Fe
Composition (%)	0.32-0.45	0.80-1.25	0.25-0.50	4.75-5.50	1.1-1.75	0.80-1.20	0.30 max	0.3 max	Balance

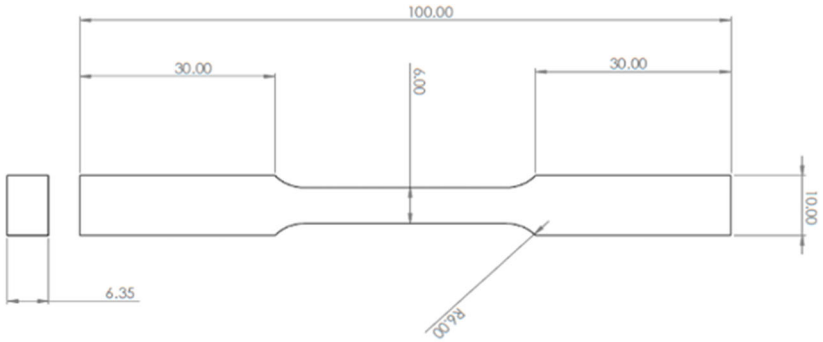

Figure 2- 2: Dimensions of tensile tests specimen (All dimensions are in mm)

The heat treatment of the H13 samples involved a two-stage process. The first stage, known as austenitization, involved heating the material to 1000°C and maintaining it at that temperature for 30 minutes, followed by quenching in oil. The subsequent stage was tempering, where the material was held at 650°C for 1 hour and then cooled in ambient air, as depicted in Figure 2- 3.

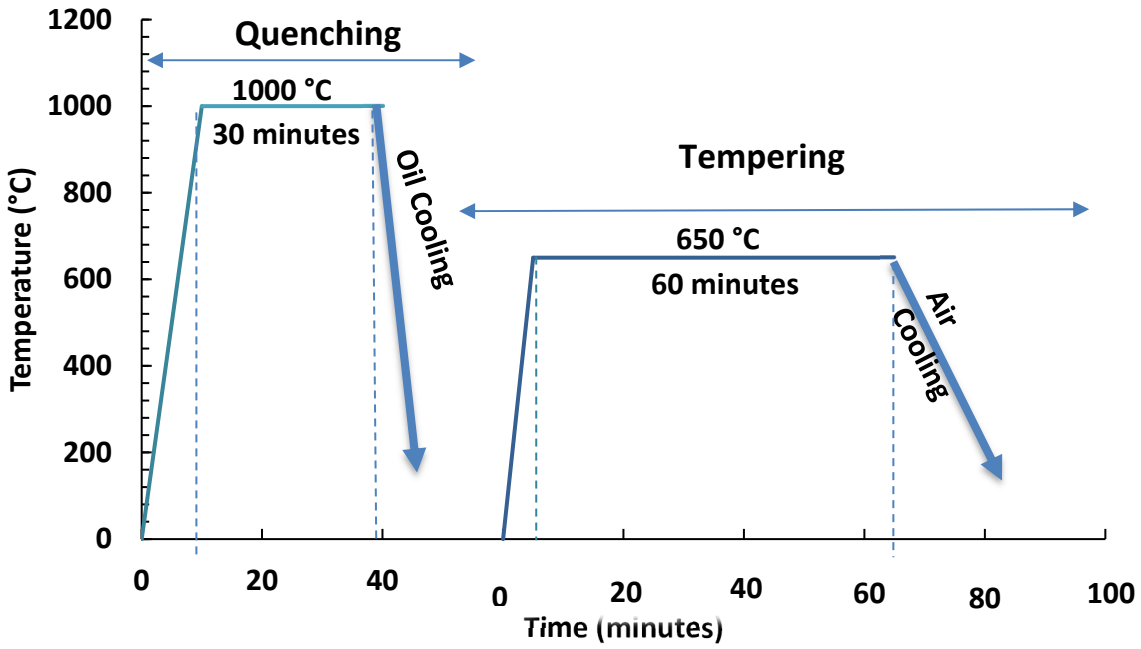

Figure 2- 3: Heat treatment cycle used for the current study

In the laser treatment processes, three factors were chosen as they have the most significant influence. presents the factors along with their respective ranges of variation employed in the experiments.

Table 2- 2 presents the factors along with their respective ranges of variation employed in the experiments.

Table 2- 2: Laser Treatment parameters

Factors	Abbreviation	Variation Ranges	Unit
Power	P	500, 600 and 700	W
Scanning speed	S	2, 3 and 4	mm/s
Defocus distance	D	8, 12 and 16	mm
Focal diameter	F	0.9, 1.03 and 1.15	mm

The Taguchi method is employed to determine the experimental plan, aiming to minimize the number of trials and variation by simultaneously studying the effects of multiple parameters. This approach differs from conventional methods, which involve lengthy processes of varying one parameter while keeping others constant.

For the experimental design, three factors with three levels each are considered, leading to the adoption of the L9 orthogonal Taguchi Table 2- 3. This table facilitates the arrangement of experiments to efficiently analyze the combined effects of the factors.

Table 2- 3: L9 orthogonal Taguchi table (input parameters)

Test	Defocus distance (mm)	Scanning speed (mm/s)	Power (W)
1	8	2	500
2	8	3	600
3	8	4	700
4	12	2	600
5	12	3	700
6	12	4	500
7	16	2	700
8	16	3	500
9	16	4	600

2.6.2 Laser surface treatment

The laser surface hardening process was conducted using a laser cell comprising a FANUC M-710iC robot that directs a light beam. The laser head is connected to a fiber laser with a maximum power of 3000 and emits continuous waves at a wavelength of 1070 nm. The HIGHYAG BIMO laser head is equipped with a variable zoom collimator and a fixed focusing lens. This configuration enables the generation of circular focal spots ranging from

approximately 0.251 to 0.431 mm in diameter, connected to a 100 mm optical fiber. Figure 2- 4 depicts the setup of the laser used in this experiment.

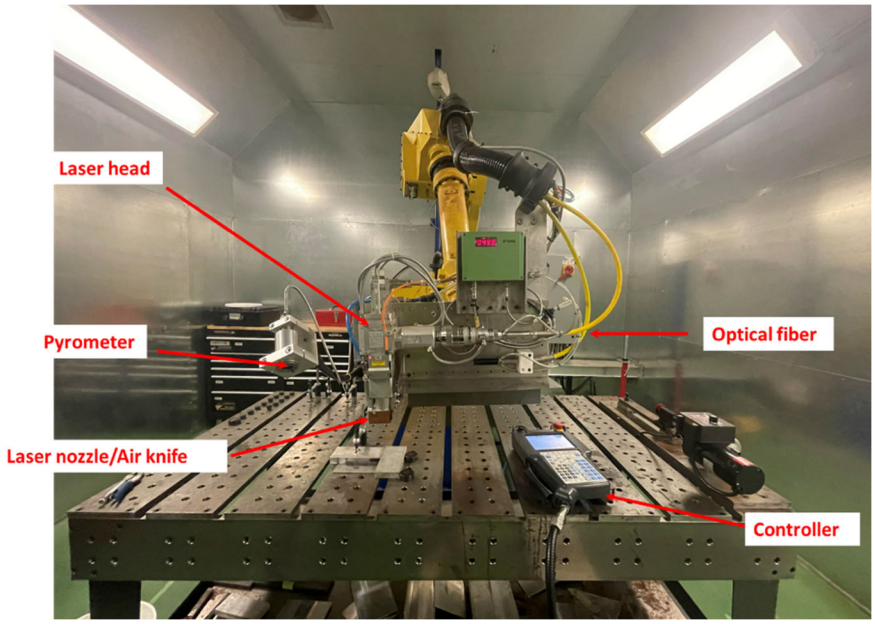

Figure 2- 4: Laser cell (3000W: YLS-3000-ST2) mounted on a FANUC robot with 6 axes

Figure 2- 5 illustrates the non-smooth surface, where the units with superior microhardness and strength are regarded as the hard phase, while the base metal serves as the soft phase. Laser treatment was performed on both surfaces to enhance their properties.

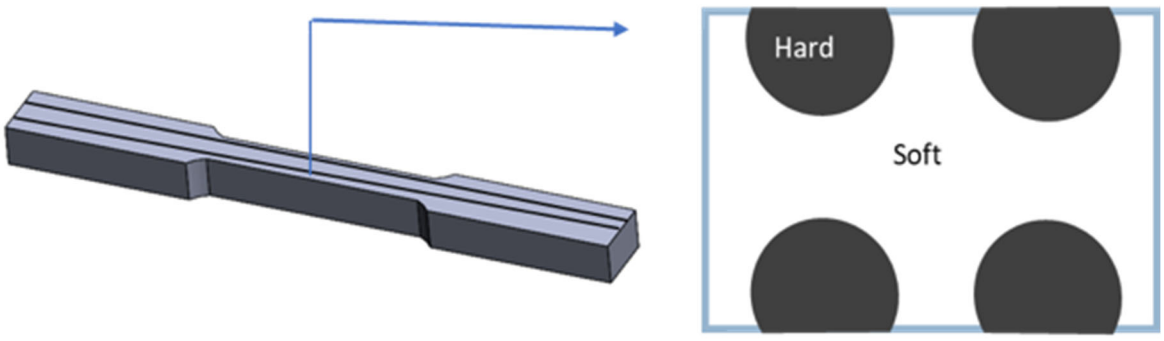

Figure 2- 5: Schematic illustration of laser treatment and cross-section of laser biomimetic units

The SEM images were captured using a high-resolution tabletop scanning electron microscope (SEM) SNE-3000MS, providing detailed information about the material's microstructure. Microhardness tests were conducted using a Vickers indenter with a 200-gf load applied for 10 seconds. These tests enable the determination of the material's hardness and its resistance to indentation.

For the tensile tests, an 810 Material Test System was utilized, which is a uniaxial servo-hydraulic machine equipped with a contact extensometer. Each set of parameters underwent a minimum of three repeated tensile tests to ensure accurate and reliable results. The strain rate during the tests was maintained at 0.2 mm/min, and all mechanical testing was performed at room temperature.

2.7 RESULTS AND DISCUSSION

2.7.1 Morphology of the laser treated zone

The primary objective of laser surface melting is to induce structural and property modifications in the material. This is accomplished by creating a chemically uniform and finely crystalline surface layer while preserving the original chemical composition of the material.

Figure 2- 6 illustrates the usual formation of three distinct zones as a result of laser treatment on the surface of H13 tool steel under different laser process parameters. These zones include the melted zone (MZ), hardened zone (HZ), and heat-affected zone (HAZ). The MZ is the region where the material is fully melted and subsequently solidified. The HZ refers to the region adjacent to the MZ, where the material undergoes a rapid cooling process, leading to increased hardness. The HAZ, on the other hand, experiences localized heating but does not reach the melting point. The thickness of each zone is determined by the specific laser parameters employed during the treatment process.

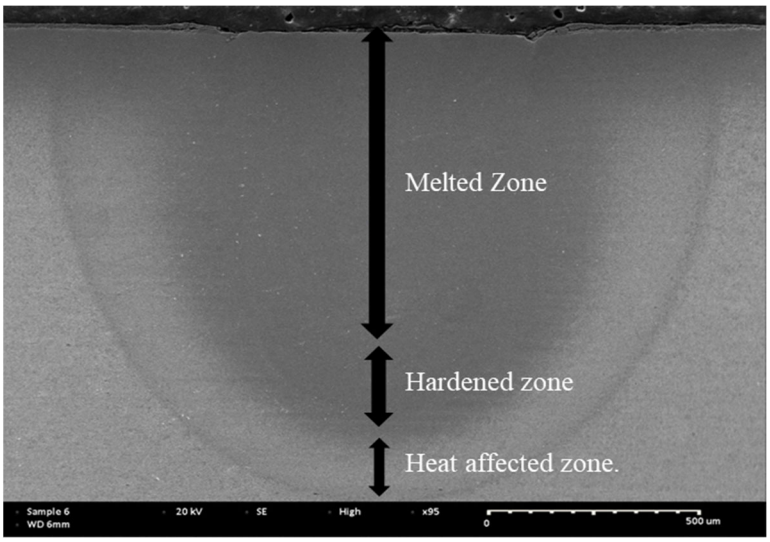

Figure 2- 6: Cross section on the middle of the line of laser treatment

2.7.2 Microstructural analysis of the laser-treated area

According to Figure 2- 7, the laser treatment process leads to the formation of four distinct regions with different microstructural characteristics and hardness values. The first region, known as the melted zone (MZ), is characterized by the complete melting and subsequent solidification of the material. Within this zone, dendrite cells can be observed, which are formed during the solidification process. The microhardness in the melted zone is relatively high compared to the substrate due to the rapid solidification of the molten material. Adjacent to the melted zone is the hardened zone (HZ), which exhibits the highest hardness value among the nine samples. In this region, the material undergoes a process called austenitization, where it is heated above its critical temperature and transformed into austenite. During rapid cooling, the austenite is rapidly quenched, resulting in the formation of martensite. The transformation from austenite to martensite contributes to the high hardness observed in the hardened zone. The third region is known as the over-tempered zone (OTZ), where the material experiences a tempering process. In this zone, the material is heated to a temperature below the austenitization temperature and held for a certain duration, allowing for the diffusion and rearrangement of atoms within the microstructure. As a result, there is a reduction in hardness compared to the hardened zone. The drastic

decrease in hardness in this region indicates that the material has been excessively tempered. The fourth region corresponds to the base material (BM), which remains relatively unaffected by the heat flux during the laser treatment process. The microstructure and hardness of the base material remain similar to the pre-treatment condition.

Therefore, the laser treatment process creates distinct regions with varying microstructures and hardness values, including the melted zone, hardened zone, over-tempered zone, and base material. Each region plays a crucial role in determining the overall mechanical properties and performance of the treated material.

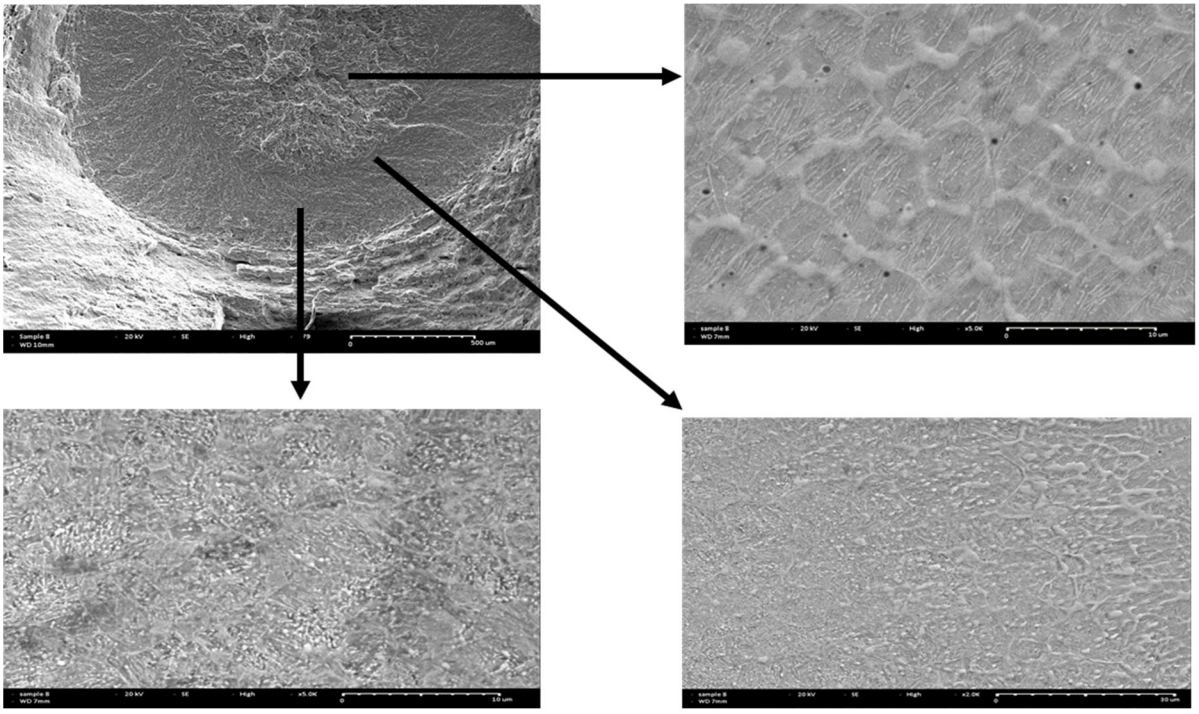

Figure 2- 7: Microstructure of the laser-treated surface for sample 8

2.7.3 Mechanical properties

Figure 2- 8, Figure 2- 9 and Figure 2- 10 illustrate the engineering stress versus engineering strain diagrams for the substrate quenched and tempered AISI H13 tool steel, as well as the laser-treated samples using various sets of laser parameters.

Table 2- 4 provides the measured tensile properties extracted from the engineering stress-strain curves, including ultimate strength and elongation. The non-treated sample exhibited the highest elongation of 14.71%, indicating good ductility compared to the laser-treated samples. However, its ultimate strength was found to be the lowest among all the specimens, measuring at 1247.23 MPa. When analyzing the elongation values of the laser-treated samples, it is observed that the fractured nature is primarily brittle for most of the samples, except for samples 1 and 6. These particular samples were treated with low laser power (500 W), a speed of 2 mm/s, and a defocusing distance of 4 mm/8 mm, resulting in an elongation of over 5%, indicative of a ductile fracture. The laser-treated samples, in general, exhibited lower elongation values, which can be attributed to the presence of high residual stress induced during the laser surface treatment process.

On the other hand, the laser-treated samples demonstrated significantly higher ultimate strength values compared to the substrate. The ultimate strength ranged between 1342.27 MPa and 1497.25 MPa for the laser-treated samples, surpassing the ultimate strength of the non-treated substrate (1247.23 MPa). Additionally, the yield strength of all the laser-treated samples was found to be higher than that of the substrate, indicating a notable improvement. This improvement in yield strength is particularly significant as it positively impacts the service life of the die steel.

Overall, the results highlight the trade-off between elongation and ultimate strength in the laser-treated samples. While there is a reduction in ductility, there is a significant increase in ultimate strength. This trade-off is essential in achieving a desirable compromise between ductility and strength for the application of the die steel.

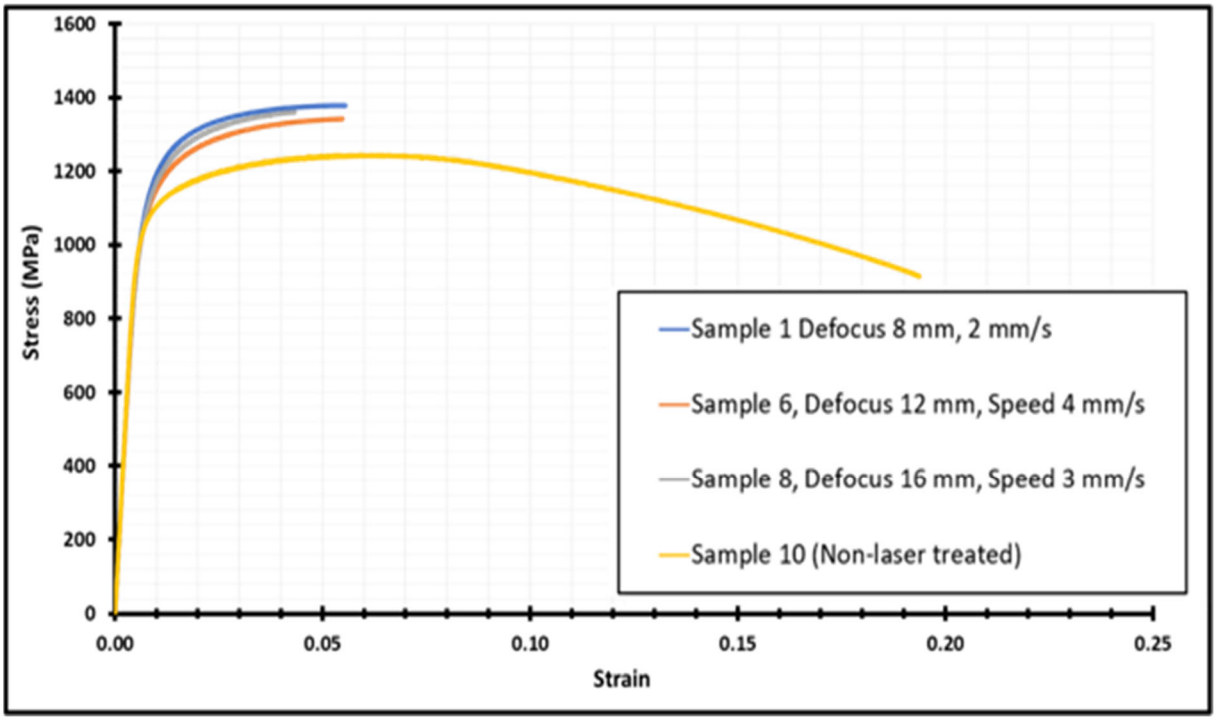

Figure 2- 8: Engineering stress-strain curves (500W)

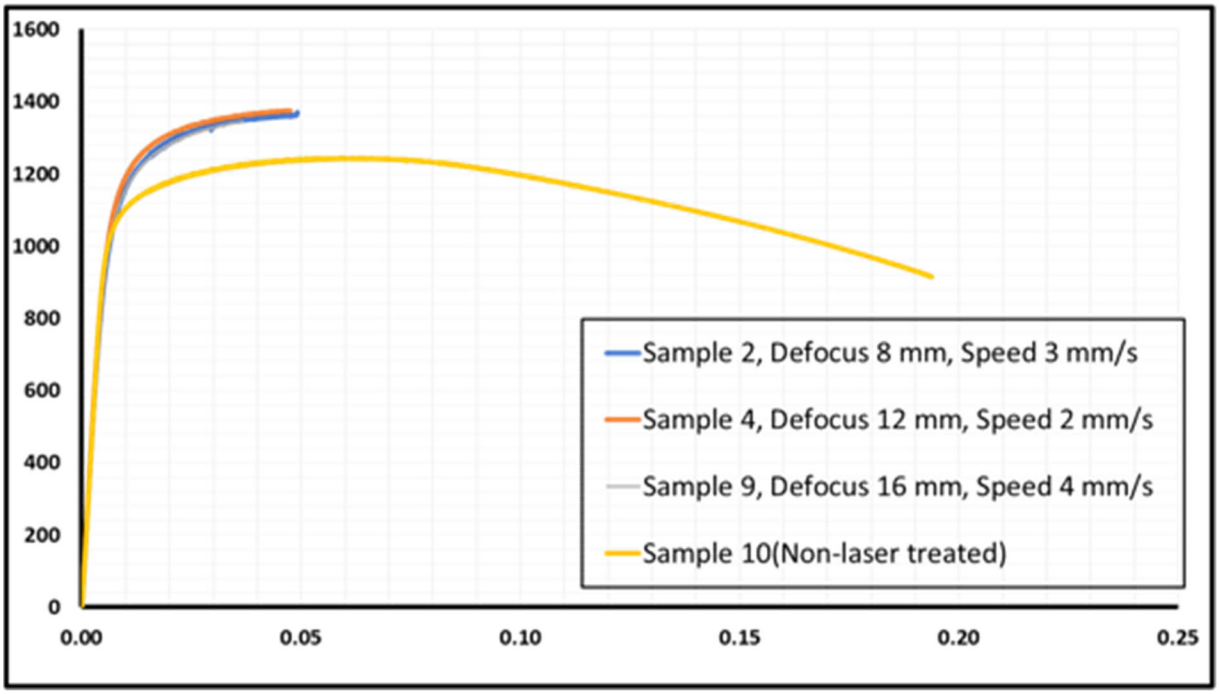

Figure 2- 9: Engineering stress-strain curves (600W)

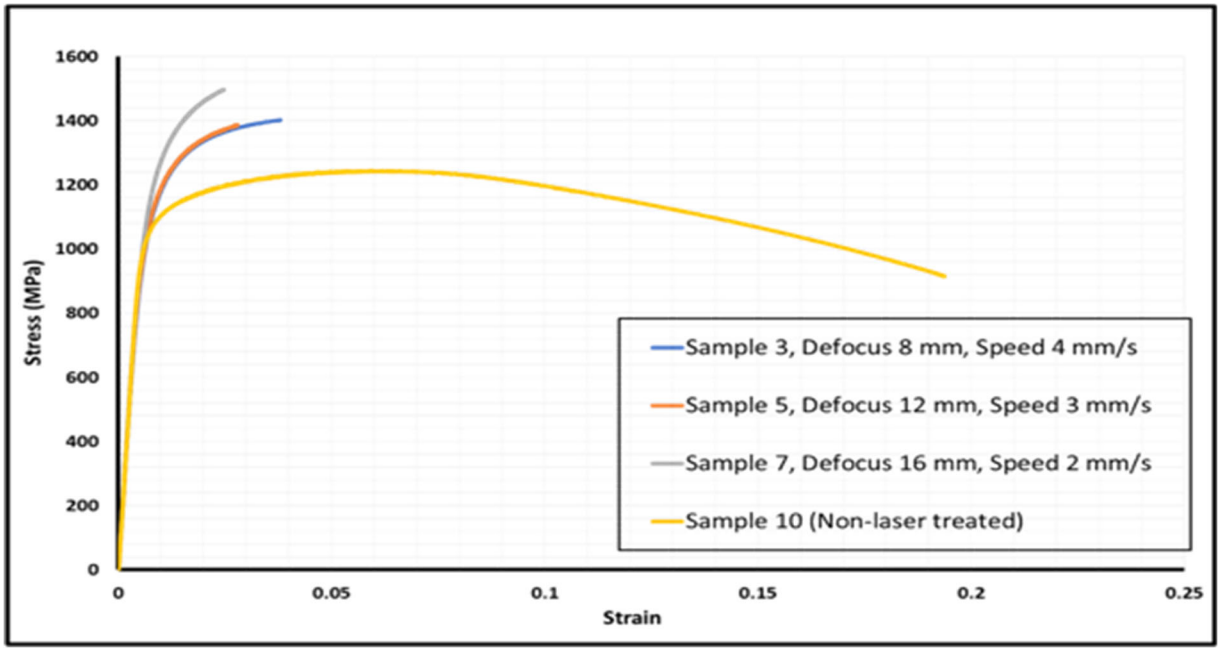

Figure 2- 10: Engineering stress-strain curves (700W)

Table 2- 4: Mechanical properties of the laser-treated samples and substrate (non-treated)

	Parameters and their levels Input			**Tensile test Results**	
Sample No.	**Defocusing (mm)**	**Speed (mm/s)**	**Power (W)**	**UTS (MPa)**	**Elongation (%)**
1	8	2	500	1378,82	5,55
2	8	3	600	1370,56	4,91
3	8	4	700	1402,44	3,80
4	12	2	600	1375,85	4,75
5	12	3	700	1387,03	2,80
6	12	4	500	1342,61	5,48
7	16	2	700	1497,27	2,46
8	16	3	500	1360,40	4,33
9	16	4	600	1344,96	3,67
10 (non-treated)	NT	NT	NT	1247,23	14,71

2.7.4 Fractography

Fractography involves the analysis of a fractured surface to understand its topographic characteristics, identify different types of fractures, determine the factors causing the fractures, and ultimately determine the fracture mechanisms. The fracture surface refers to the newly formed surface that occurs when a solid body is subjected to loads or stresses, resulting in separation [41]. Ductile and brittle fractures are two common types of fractures that can occur in tool steels. Ductile fracture is characterized by significant plastic deformation before failure, with the material undergoing noticeable necking and elongation. On the other hand, brittle fracture occurs with little to no plastic deformation and is characterized by a rapid and sudden separation of the material without any significant necking or deformation. The type of fracture observed depends on various factors such as material properties, loading conditions, and environmental conditions. By studying the fracture surface and its characteristics, such as the presence of dimples in ductile fractures or smooth and flat surfaces in brittle fractures, valuable insights can be gained regarding the failure mechanisms and the behavior of the material under different conditions. Fractography plays a vital role in understanding the causes and prevention of failures in tool steels.

2.7.4.1 Base material fractured surface

Figure 2- 11, the fractography of a quenched and tempered sample that underwent tensile testing is presented, allowing for a detailed analysis of the fracture surface. The fractographic features observed provide insights into the fracture mode and behavior of the material. The analysis of the fractographic features indicates that the mode of fracture is ductile. Ductile fractures are characterized by plastic deformation and the formation of fine dimples and voids on the fracture surface. In this case, the sample exhibits an uneven array of dimpled facets with scattered large voids, which are consistent with typical ductile fracture behavior. The surface of the sample displays a range of dimples with varying sizes. The deepest and narrowest dimples are observed in the base material. This observation aligns

with the stress-strain graph, which indicates significant plastic deformation prior to failure. The plastic deformation causes the material to stretch and elongate, leading to the formation of these dimples. The presence of these dimples suggests that the material absorbed energy during the fracture process, indicating a ductile fracture mode. The scattered large voids observed on the fracture surface further support the ductile fracture behavior. These voids are regions where material separation has occurred, indicating the occurrence of local fracture events within the material. The distribution of these voids throughout the fracture surface is consistent with ductile fractures. By examining the fractographic features in detail, it becomes evident that the quenched and tempered sample experienced a ductile fracture mode characterized by the presence of fine dimples and voids. These features reflect the significant plastic deformation and energy absorption by the material before ultimate failure. The fractographic analysis provides valuable information for understanding the fracture behavior and mechanical properties of the material under tensile loading conditions.

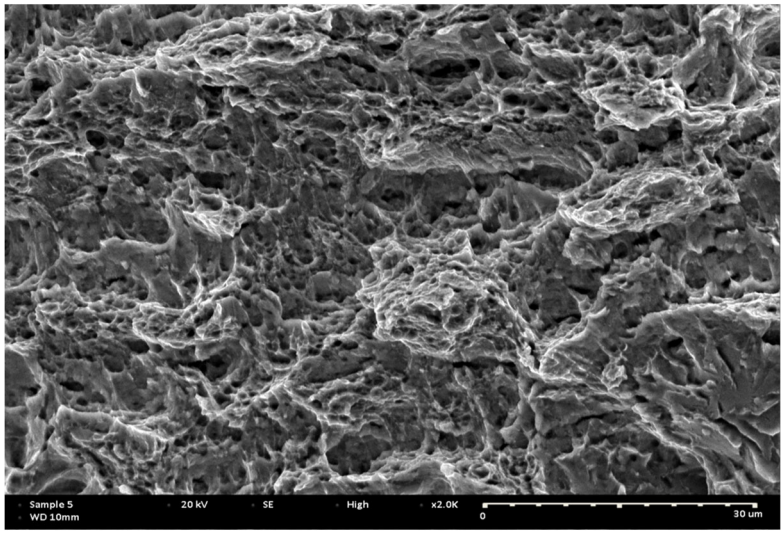

Figure 2- 11: Fractured surface of the tensile testing specimen of quenched and tempered H13 tool steel

2.7.4.2 Fractured surfaces of laser-treated samples

The fracture morphologies of the laser-treated samples after tensile testing are depicted below, with distinct regions including the melted zone, hardened zone, and heat-affected

zone. The fractographic analysis reveals a combination of brittle and ductile fractures at the microscopic scale. In the laser-treated zone, the mode of fracture appears to be predominantly brittle. This is indicated by the presence of cleavage steps, which are characteristic of brittle fractures. Additionally, a small number of circular and oval-shaped dimples can be observed, suggesting some degree of localized ductile behavior in this zone. The presence of both brittle and ductile fracture features indicates a mixed fracture mode within the laser-treated zone. Moving into the heat-affected zone, the dimples become finer in size compared to the laser-treated zone. This suggests a more pronounced ductile behavior in this region, as the finer dimples are indicative of greater plastic deformation before fracture. Overall, the fractographic analysis reveals a combination of brittle and ductile fracture features in the laser-treated samples. The laser-treated zone exhibits predominantly brittle fracture with some localized ductility, while the heat-affected zone displays a greater extent of ductile behavior. This observation highlights the complex fracture mechanisms and the influence of the laser treatment on the material's response to mechanical loading.

The fractured surface of sample 1 exhibits four distinct zones, as depicted in Figure 2-12. Figure 2- 12 (a) shows the overall fractured surface, which includes the base metal, it shows a predominantly clean appearance with few visible signs of plastic deformation or extensive ductile features. This indicates a primarily brittle fracture behavior in this region. The melted zone, as seen in Figure 2- 12 (b), displays a clean and smooth appearance, indicating a brittle fracture mode. The absence of significant plastic deformation or ductile features suggests that the material in this zone underwent limited or no plastic deformation before fracture. In Figure 2- 12 (c), the hardened zone is characterized by a relatively clean and flat surface with minimal evidence of plastic deformation. This zone also exhibits a brittle fracture behavior, similar to the melted zone. The heat-affected zone, as shown in Figure 2-12(d), displays a slightly different fracture morphology compared to the other zones. While still exhibiting a predominantly clean appearance, this zone shows some minor signs of plastic deformation, including small dimples or localized regions of slight roughness. This suggests a limited degree of ductility in the heat-affected zone, although the overall fracture behavior remains predominantly brittle. Overall, the fractured surface of sample 1 reveals a

combination of brittle and limited ductile fracture characteristics across the different zones. The melted and hardened zones display a primarily brittle fracture mode, while the heat-affected zone shows minor indications of ductility but still retains a predominantly brittle nature. These findings highlight the complex fracture behavior resulting from the laser treatment process, with variations observed in the extent of plastic deformation and ductility among the different zones.

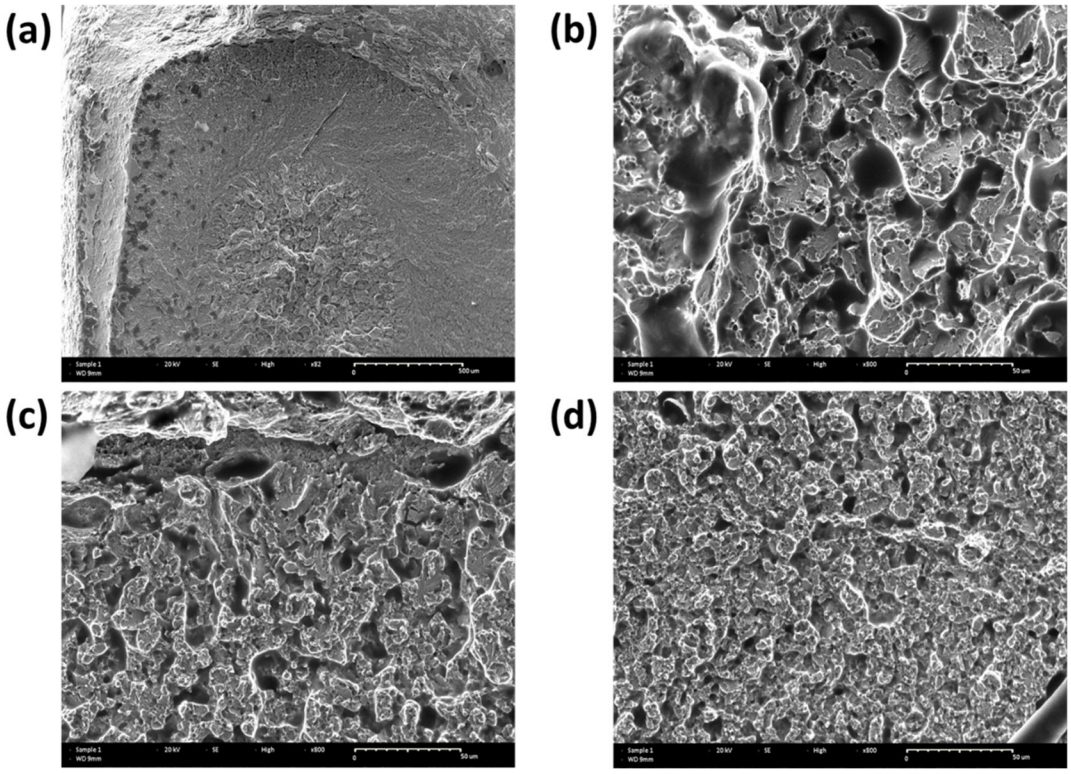

Figure 2- 12: (a) Fractured surface of sample 1 (b) Melt zone (c) Hardened zone (d) Heat affected zone

The fractured surface of sample 2, as shown in Figure 2- 12, exhibits similar zone classifications to sample 1, but with a greater presence of ductile features. However, the fracture behavior remains predominantly brittle overall. Figure 2- 12(a) shows the overall fractured surface, including the base metal, which shows a combination of brittle and ductile features. There are indications of plastic deformation and elongation, suggesting a certain level of ductility, but the presence of clean and smooth regions indicates a brittle fracture

mode prevailing in this zone. In Figure 2- 11(b), the melted zone exhibits a combination of brittle and ductile features. While some clean areas indicate brittle fractures, there are also visible signs of plastic deformation and localized dimples, suggesting some degree of ductility within this zone. The hardened zone, shown in Figure 2- 11 (c), also displays a combination of brittle and ductile characteristics. The presence of cleavage steps and clean regions indicates a brittle fracture mode, while the occurrence of small dimples suggests localized ductility. The heat-affected zone, as seen in Figure 2- 11(d), exhibits a similar pattern to the other zones. It shows a mixture of brittle and ductile features, with some clean areas indicating brittle fracture and localized dimples representing ductile behavior. In summary, the fractured surface of sample 2 demonstrates more prominent ductile features compared to sample 1, although the overall fracture behavior remains predominantly brittle. The melted and hardened zones exhibit a combination of brittle and ductile characteristics, while the heat-affected zone shows a similar pattern with indications of both brittle and ductile fracture modes. These observations highlight the complex fracture behavior resulting

from the laser treatment process, with variations in the extent of plastic deformation and ductility observed among the different zones.

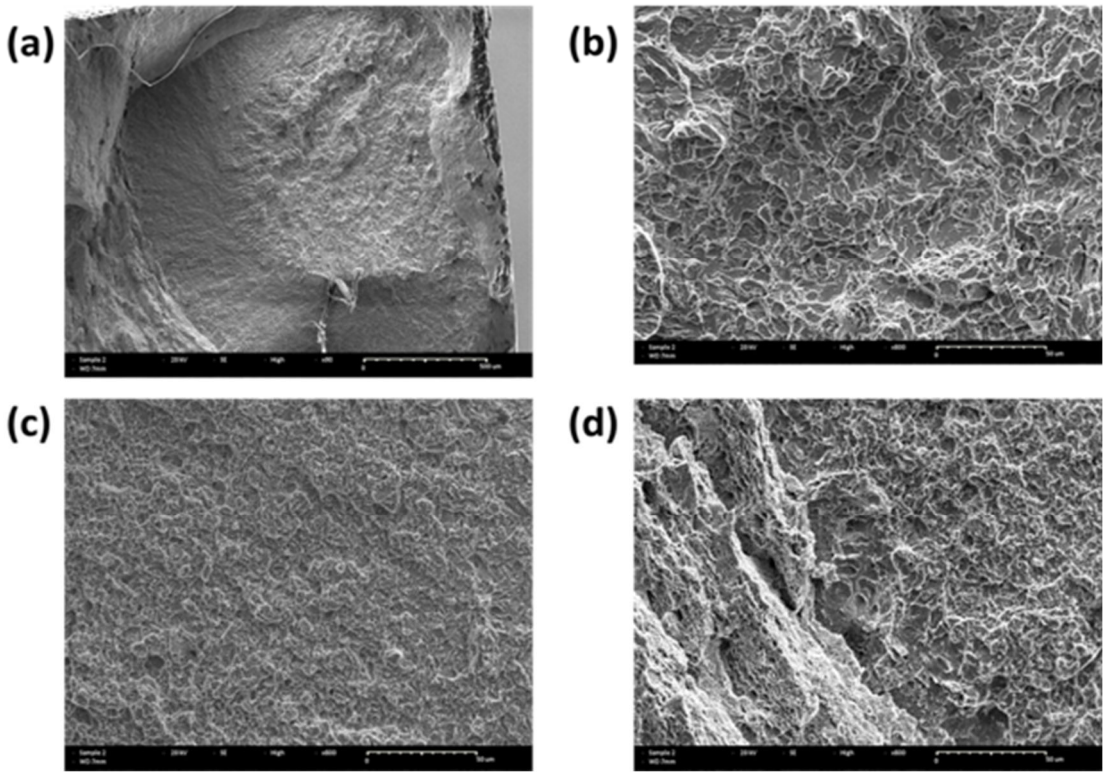

Figure 2- 13: (a) Fractured surface of sample 2 (b) Melt zone (c) Hardened zone (d) Heat affected zone

The fractured surface of sample 3, as depicted in Figure 2- 14, demonstrates a brittle fracture behavior similar to samples 1 and 2. However, it also exhibits some additional features, such as ledges, steps, and indications of porosity. Figure 2- 14 (a) indicates the overall fractured surface, including the base metal, displays a predominantly brittle fracture mode. It shows clean and smooth regions, indicating minimal plastic deformation and brittle fracture behavior. In Figure 2- 14 (b), the melted zone shows similar characteristics to the other samples, with a clean and smooth appearance indicative of brittle fracture. The

hardened zone, as shown in Figure 2- 14 (c), exhibits a combination of brittle fracture features along with the presence of ledges and steps. These ledges and steps are indicative of fracture surfaces intersecting with each other, suggesting multiple fracture paths or planes. This fracture behavior is consistent with a brittle fracture mode, although the presence of ledges and steps indicates some complexity in the fracture process. In Figure 2- 14 (d), the heat-affected zone displays similar characteristics to the other zones, with indications of both brittle and ductile features. However, in addition to the ledges and steps observed in the hardened zone, there are also indications of porosity. These pores are voids within the material that can result from various factors, such as gas entrapment during solidification or localized shrinkage during cooling. The presence of porosity further contributes to the complexity of the fracture behavior observed in this zone. In summary, the fractured surface of sample 3 exhibits a predominantly brittle fracture behavior, similar to the other samples. Additionally, it displays ledges and steps in the hardened zone, suggesting multiple fracture paths or planes. Moreover, the presence of porosity in the heat-affected zone adds another dimension to the fracture characteristics. These observations highlight the complex nature of the fracture behavior resulting from the laser treatment process, with a combination of brittle features, ledges, steps, and porosity observed in different zones of the fractured surface.

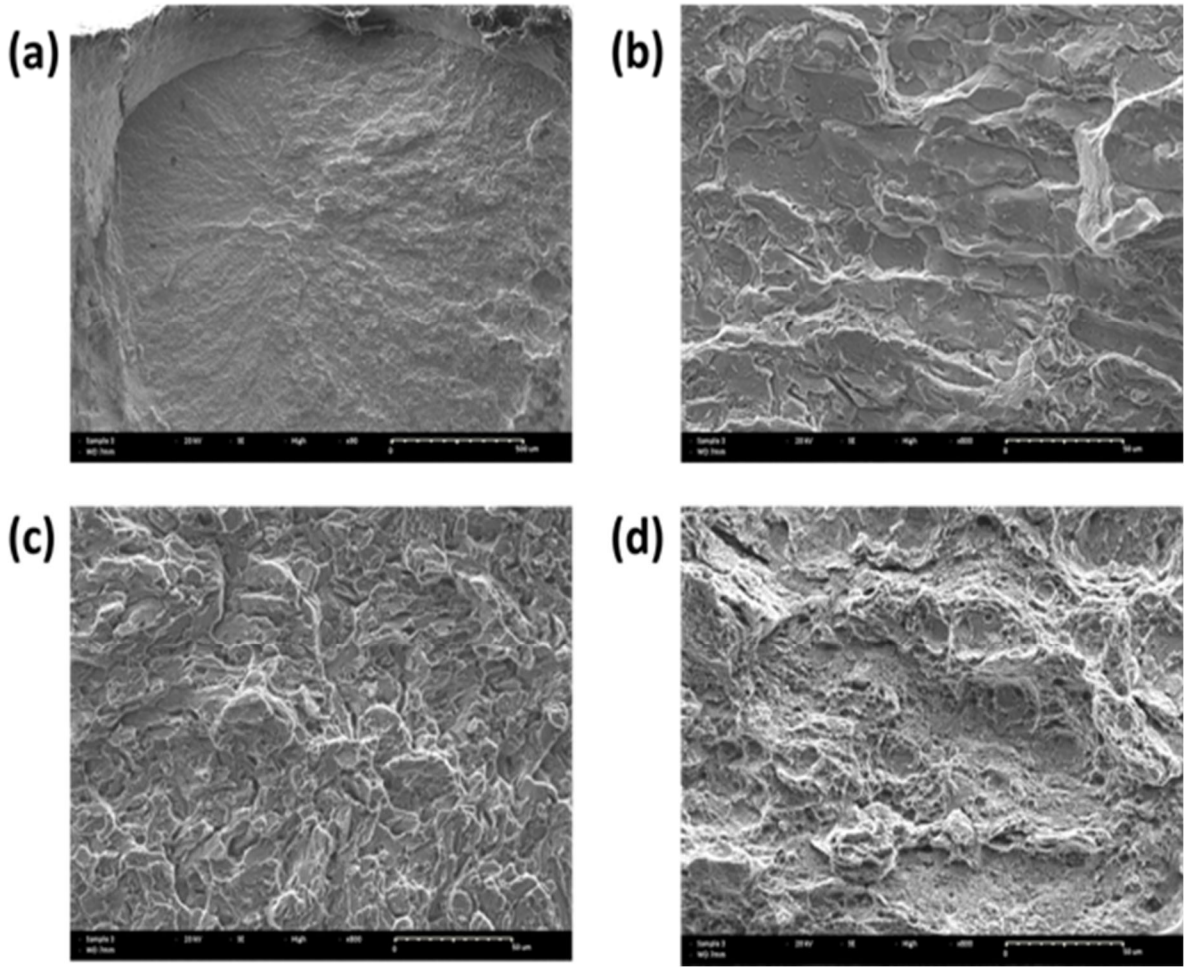

Figure 2- 14: (a) Fractured surface of sample 3 (b) Melt zone (c) Hardened zone (d) Heat affected zone

The fractured surface of sample 4 exhibits similar features to sample 1, indicating a predominantly brittle fracture behavior. Figure 2- 15 (a) exhibits the overall fractured surface, including the base metal, showing a clean appearance with limited signs of plastic deformation or extensive ductile features, confirming a predominantly brittle fracture mode. In Figure 2- 15 (b), the melted zone displays a smooth and clean surface, indicating a brittle fracture behavior. The absence of significant plastic deformation suggests limited or no ductility in this zone. Figure 2- 15 (c) represents the hardened zone, which also exhibits a relatively clean and flat surface with minimal evidence of plastic deformation. Similar to the melted zone, the hardened zone displays a brittle fracture behavior. The heat-affected zone,

shown in Figure 2- 15 (d), reveals a fracture morphology consistent with the other zones. It displays a clean appearance with indications of limited plastic deformation, possibly in the form of small dimples or localized roughness. While there is some minor evidence of ductility in this zone, the overall fracture behavior remains predominantly brittle. In summary, the fractured surface of sample 4 shares similar characteristics with sample 1, indicating a primarily brittle fracture behavior. The melted and hardened zones exhibit a brittle fracture mode with limited signs of ductility. The heat-affected zone shows minor indications of ductility but still retains a predominantly brittle nature. These findings emphasize the consistent nature of the fracture behavior observed across multiple samples and highlight the influence of the laser treatment process on the material's response to mechanical loading.

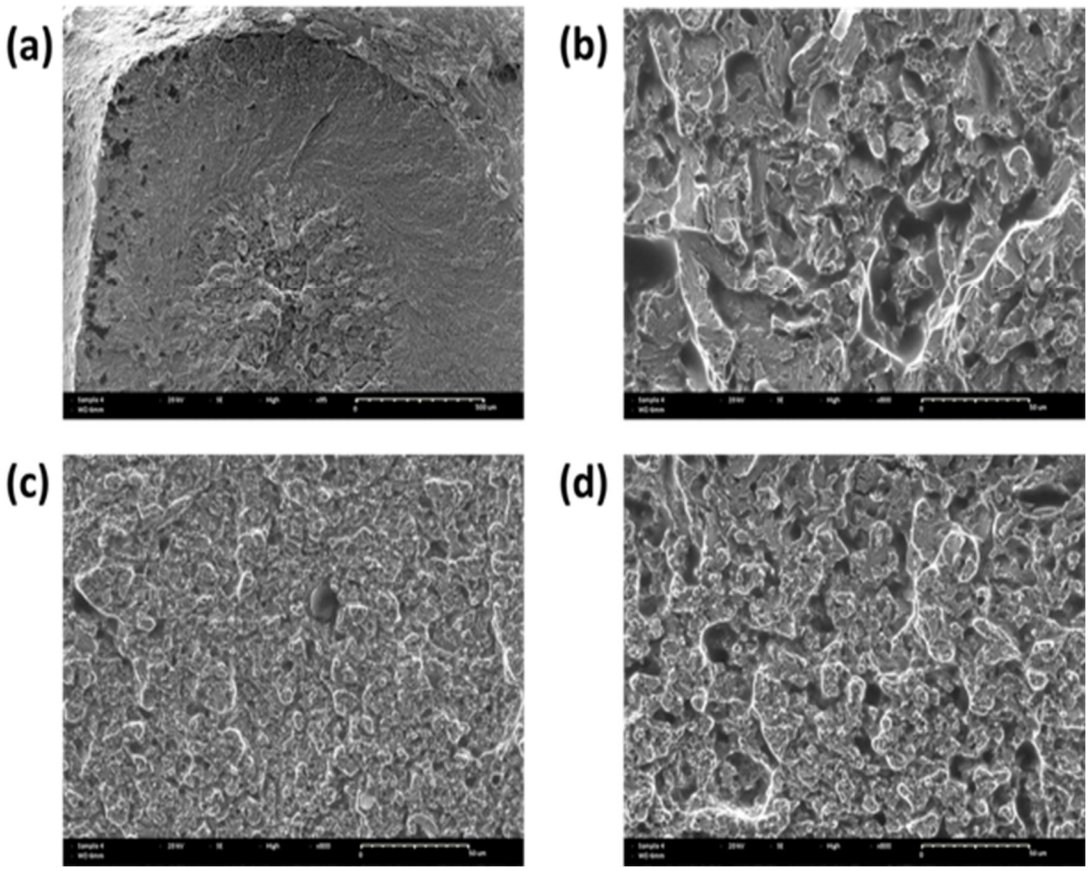

Figure 2- 15: (a) Fractured surface of sample 4 (b) Melt zone (c) Hardened zone (d) Heat affected zone

The fractured surface of sample 5 displays a notable presence of ductile features along with indications of porosity and pores coalescence. We can continue using the same notations to describe the different zones on the fractured surface. Figure 2- 16 (a) depicts the overall fractured surface, including the base metal, which exhibits a combination of brittle and ductile features. While some areas show a clean appearance indicative of brittle fracture, there are also visible signs of plastic deformation and elongation, suggesting a significant degree of ductility. In Figure 2- 16 (b), the melted zone showcases a combination of brittle and ductile characteristics. Alongside the clean regions associated with brittle fracture, there are also signs of plastic deformation and localized dimples, indicating a degree of ductility within this zone. The hardened zone, as depicted in Figure 2- 16 (c), demonstrates a mixed fracture behavior. It displays features consistent with both brittle fracture, such as cleavage steps, and ductile behavior, such as dimples and evidence of plastic deformation. This suggests a combination of brittle and ductile fracture modes within the hardened zone. Figure 2- 16 (d) presents the heat-affected zone, which exhibits similar patterns to the other zones. While there are indications of both brittle and ductile fracture modes, there is also evidence of porosity and pores coalescence. The presence of pores, voids, or gas entrapment within the material can lead to coalescence during fracture, further contributing to the ductile fracture behavior observed in this zone. In summary, the fractured surface of sample 5 showcases a more pronounced presence of ductile features compared to sample 1. It exhibits a combination of brittle and ductile fracture modes across the different zones. Additionally, the presence of porosity and the coalescence of pores further contribute to the ductile fracture behavior observed. These findings underscore the complex nature of the fracture behavior resulting from the laser treatment process, with variations in the extent of plastic deformation, ductility, and the presence of porosity observed among the different zones of the fractured

surface.

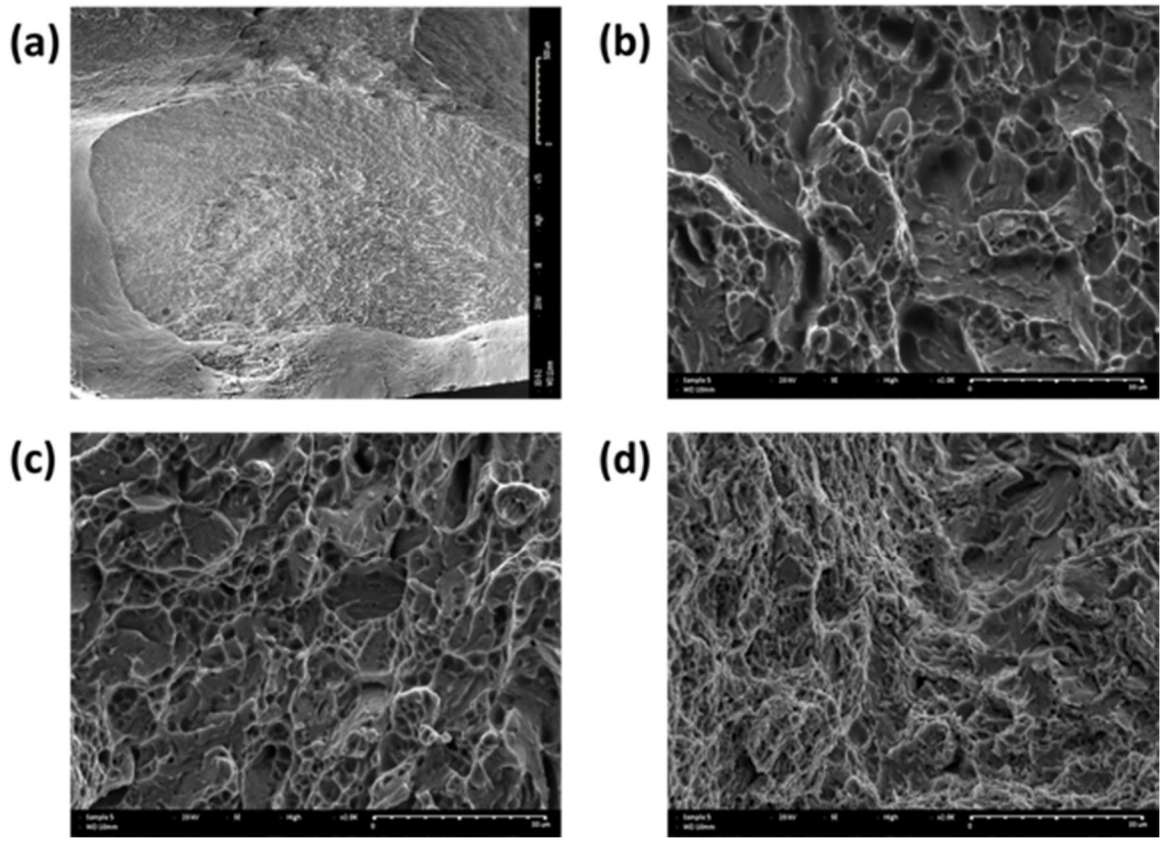

Figure 2- 16: (a) Fractured surface of sample 5 (b) Melt zone (c) Hardened zone (d) Heat affected zone

In sample 6, the fractured surface is represented by Figure 16. We can describe the fracture characteristics of each zone. Figure 2- 17 (a) shows the overall fractured surface, including the base metal, which displays a combination of brittle and ductile features. Clean regions indicate a brittle fracture, while signs of plastic deformation and elongation suggest ductility. In Figure 2- 17 (b), the melted zone exhibits predominantly brittle fracture characteristics. Cleavage steps and a limited number of circular or oval dimples indicate a brittle fracture mode in this zone. Figure 2- 17 (c) represents the hardened zone, which also shows brittle fracture features. Similar to the melted zone, the presence of cleavage steps and a limited number of dimples suggests a predominantly brittle fracture behavior. Figure 2- 17 (d), the heat-affected zone demonstrates a more ductile appearance compared to the other

zones. It exhibits evidence of plastic deformation, such as the presence of fine dimples, indicating a ductile fracture mode. Additionally, porosity is observed in this zone, contributing to the ductile fracture behavior observed. In summary, the fractured surface of sample 6, as depicted in Figure 2- 17 displays different fracture characteristics in each zone. The melted and hardened zones exhibit predominantly brittle fracture features, while the heat-affected zone shows a more ductile appearance with the presence of porosity. These observations emphasize the complex nature of the fracture behavior resulting from the laser treatment process, with distinct fracture modes and the influence of porosity observed in different zones of the fractured surface.

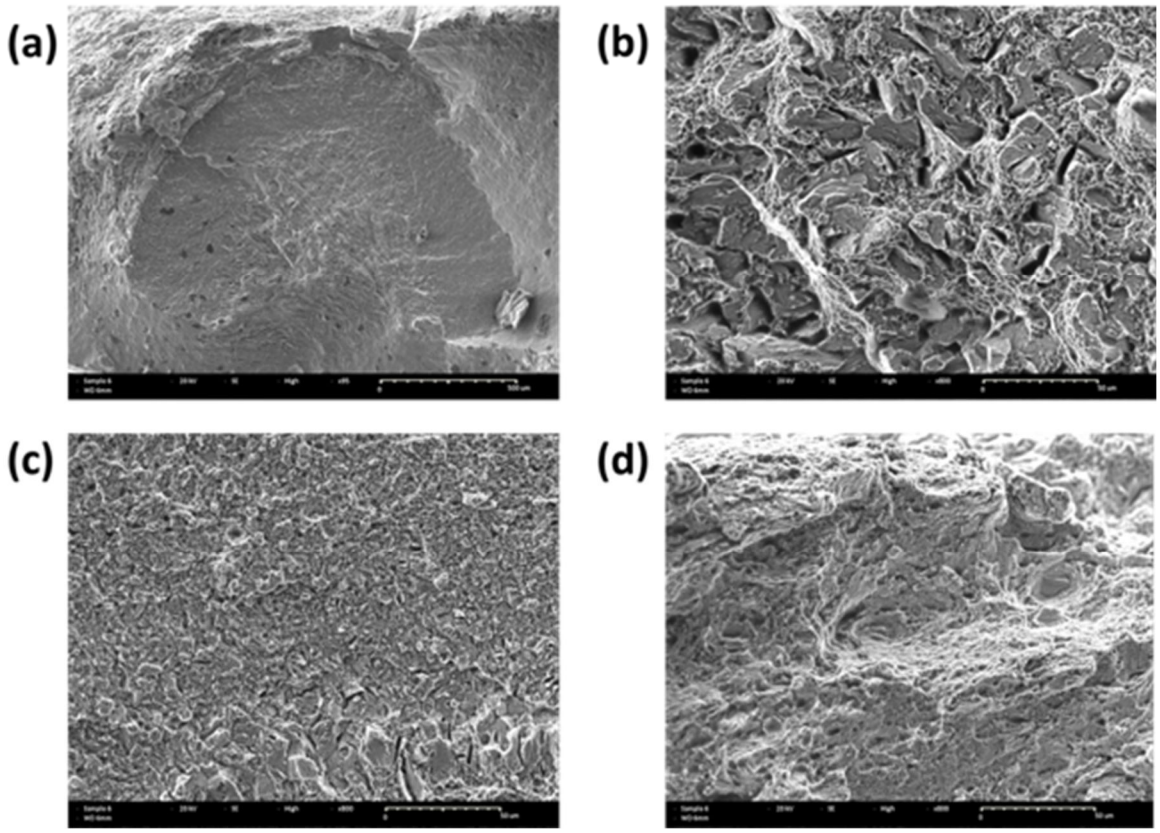

Figure 2- 17: (a) Fractured surface of sample 6 (b) Melt zone (c) Hardened zone (d) Heat affected zone

The fractured surface of sample 7, as depicted Figure 2- 18, displays distinct fracture characteristics in different zones, with patches of brittle features and the presence of pores. Figure 2- 18 (a) shows the overall fractured surface, including the base metal, revealing a combination of brittle and ductile features. While some regions exhibit a clean appearance indicative of brittle fracture, there are also visible signs of plastic deformation and elongation, suggesting a degree of ductility. In Figure 2- 18 (b), the melted zone exhibits both brittle and ductile characteristics. The presence of cleavage steps and areas of clean fracture indicates a brittle fracture mode, while localized dimples and signs of plastic deformation suggest some degree of ductility. Figure 2- 18 (c) represents the hardened zone, which shows a combination of brittle and ductile features. Cleavage steps and areas of clean fracture are indicative of brittle fracture, while the presence of localized dimples suggests some degree of ductility. In the heat-affected zone, depicted in Figure 2- 18 (d), there are patches of brittle fracture along with the presence of pores. The brittle features appear as areas of clean fracture, while the presence of pores adds complexity to the fracture behavior. Furthermore, the coalescence of larger pores can be observed in this zone, contributing to the overall fracture characteristics. In summary, the fractured surface of sample 7 exhibits a variety of fracture characteristics in different zones. The melted and hardened zones show a combination of brittle and ductile features, while the heat-affected zone displays patches of brittle features along with the presence of pores, including the coalescence of larger pores. These findings highlight the complex nature of the fracture behavior resulting from the laser treatment process, with variations in fracture modes and the influence of pore presence observed in different zones of the fractured surface.

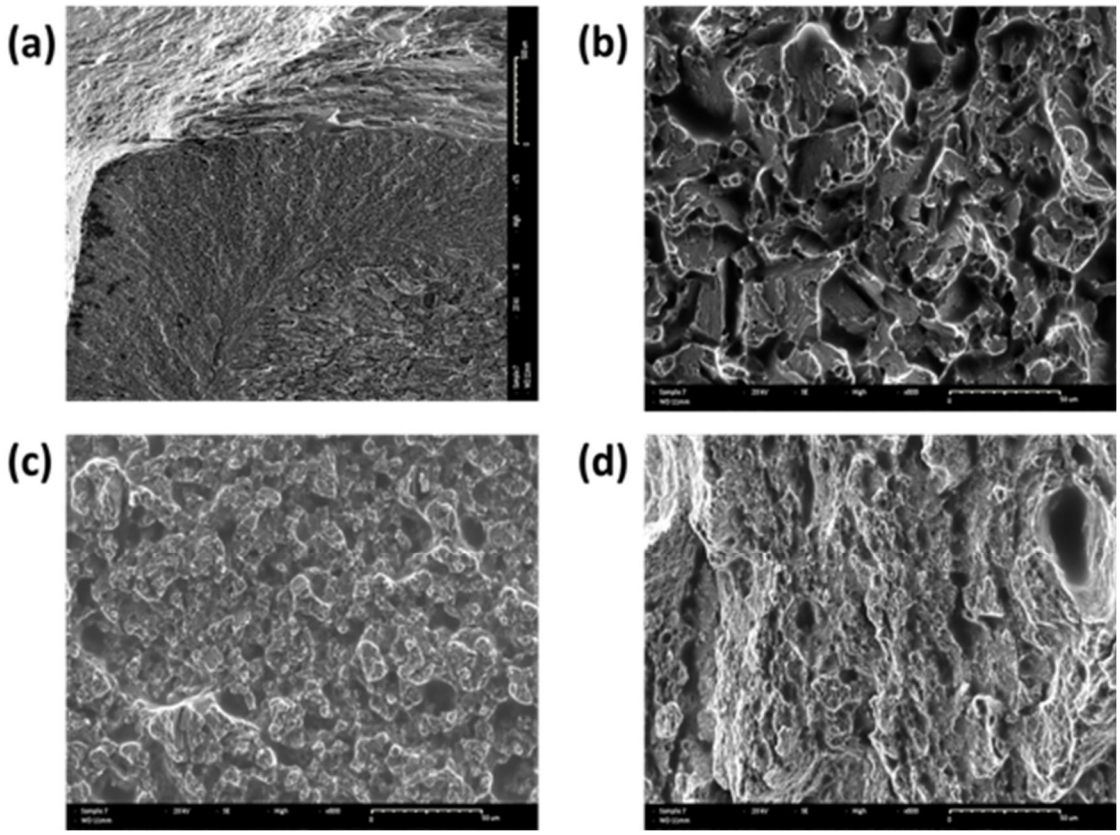

Figure 2- 18: (a) Fractured surface of sample 7 (b) Melt zone (c) Hardened zone (d) Heat affected zone

The fractured surface of sample 8, as depicted in Figure 2- 19, exhibits a predominance of ductile fracture features, characterized by the presence of dimples and pores, particularly in the heat-affected zone. However, there are also indications of brittle features observed in certain areas. In

Figure 2- 20 (a) the overall fractured surface, including the base metal, displays a combination of ductile and brittle features. While the majority of the surface shows signs of plastic deformation and the presence of dimples, there are also regions with a clean appearance, indicating brittle fracture. In

Figure 2- 20 (b), the melted zone predominantly exhibits ductile fracture characteristics. The presence of dimples, which are indicative of plastic deformation, suggests a ductile fracture mode in this zone.

Figure 2- 20 (c) represents the hardened zone, which also displays a predominantly ductile appearance. The presence of dimples and signs of plastic deformation further support a ductile fracture behavior in this zone. In the heat-affected zone, depicted in

Figure 2- 20 (d), there is a predominance of ductile features, particularly the presence of dimples. Additionally, the zone displays larger pores, particularly noticeable in this area. The presence of these pores adds complexity to the fracture behavior. However, some regions within this zone may also exhibit brittle features, indicating a mixed fracture behavior. In summary, the fractured surface of sample 8, as shown in

Figure 2- 20, primarily exhibits ductile fracture features. Dimples and the presence of pores, especially in the heat-affected zone, are indicative of ductile fracture behavior. However, there are also indications of brittle features in certain regions, suggesting a mixed fracture behavior. These findings highlight the complex nature of the fracture behavior resulting from the laser treatment process, with variations in fracture modes and the influence of pore presence observed in different zones of the fractured surface.

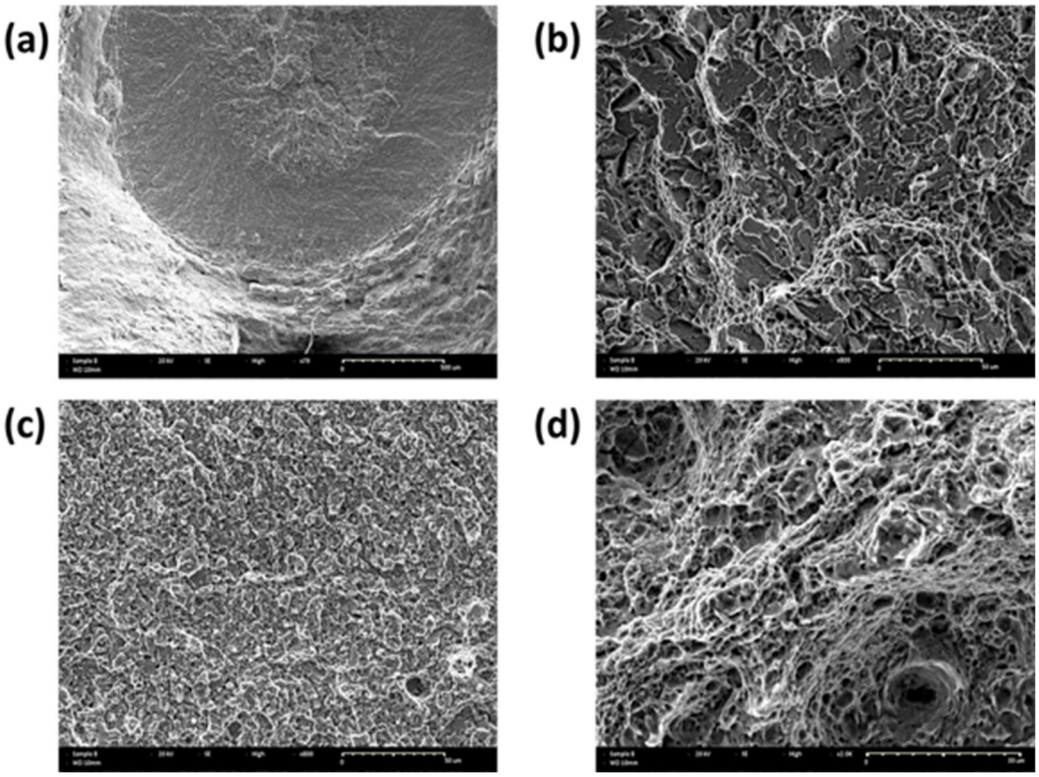

Figure 2- 20: (a) Fractured surface of sample 8 (b) Melt zone (c) Hardened zone (d) Heat affected zone

The fractured surface of sample 9, as depicted in Figure 2- 21, exhibits the highest occurrence of ductile fracture features among all the previous samples, along with some small brittle patches. The heat-affected zone of sample 9 stands out as the most ductile zone observed thus far. Figure 2- 21 (a) shows the overall fractured surface, including the base metal, showcases a combination of ductile and brittle features. The presence of extensive plastic deformation, elongation, and numerous dimples indicates a predominantly ductile fracture behavior. However, there are also small areas with a clean appearance, indicating brittle fractures. In Figure 2- 21 (b), the melted zone displays a predominantly ductile appearance. The surface exhibits a significant number of dimples, indicating substantial plastic deformation and a ductile fracture mode in this zone. Figure 2- 21 (c) represents the hardened zone, which also exhibits a predominantly ductile fracture behavior. The presence

of numerous dimples and evidence of plastic deformation suggests a ductile response in this zone. The heat-affected zone, depicted in Figure 2- 21 (d), stands out as the most ductile heat-affected zone among all the previous samples. It displays an extensive occurrence of dimples and signs of significant plastic deformation, emphasizing the ductile fracture behavior in this region. Although small brittle patches may be present, the overall fracture characteristics of this zone are predominantly ductile. In conclusion, the fractured surface of sample 9, as shown in Figure 2- 21, displays the highest occurrence of ductile fracture features among all the samples examined. Extensive plastic deformation, numerous dimples, and a ductile response dominate the overall fracture behavior. The heat-affected zone stands out as the most ductile zone observed, with a limited presence of small brittle patches. These findings highlight the influence of the laser treatment process on enhancing the ductility of the material, particularly in the heat-affected zone.

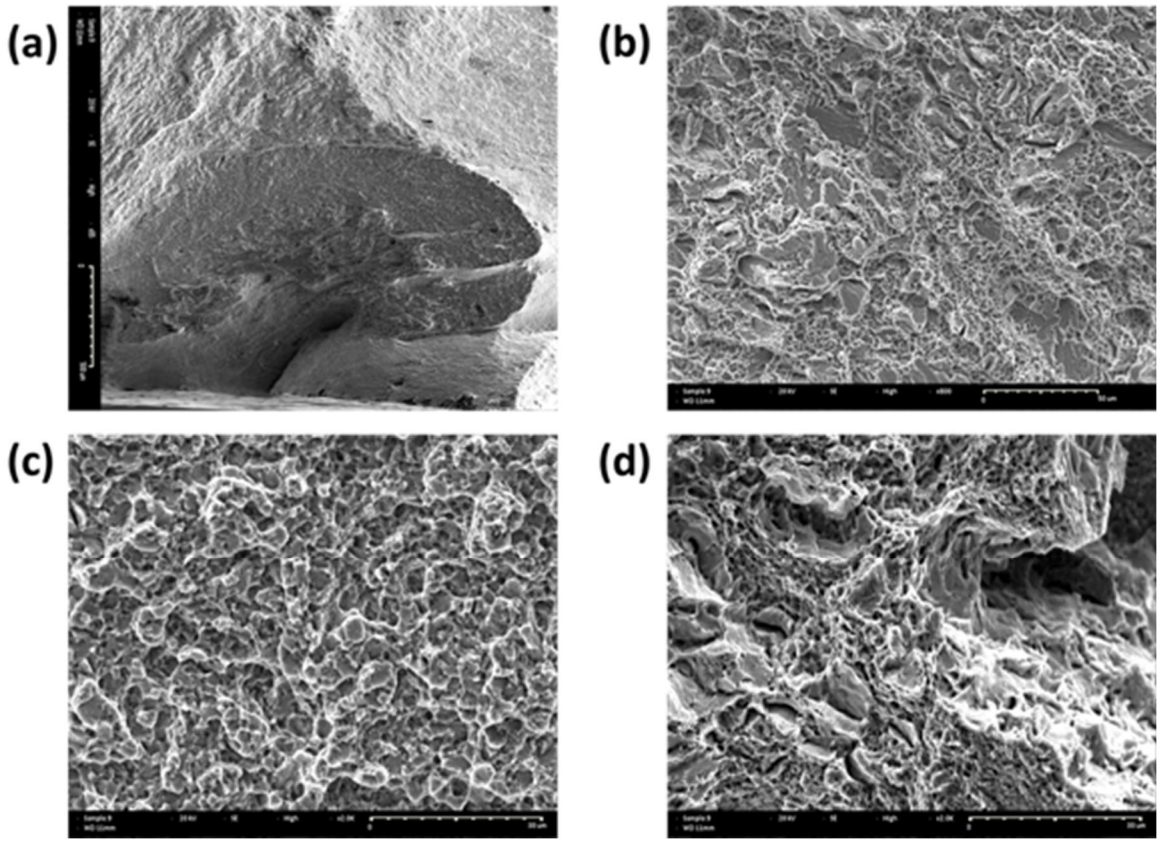

Figure 2- 21: (a) Fractured surface of sample 9 (b) Melt zone (c) Hardened zone (d) Heat affected zone

2.8 STATISTICAL ANALYSIS

In order to assess the impact of specific laser process parameters, namely laser power (P), scanning speed (S), and defocusing distance, on the resulting material properties such as ultimate strength and elongation, a statistical analysis tool called Analysis of Variance (ANOVA) is employed. ANOVA enables the evaluation of multiple factors and their effects on the variability of response variables, thereby identifying the significant factors that influence the outcomes. By conducting ANOVA analysis on the data derived from laser processing experiments, it becomes possible to discern the most influential laser parameters affecting the ultimate strength and elongation of the material. Subsequently, by optimizing

the laser parameters based on ANOVA results, the ultimate strength and elongation of the processed material can be enhanced to fulfill the specific requirements of the intended application.

For this study, statistical software such as Minitab is utilized to perform the ANOVA analysis. This software generates an ANOVA table and a regression equation, enabling a comprehensive understanding of the intricate relationships between laser parameters and material properties. This analytical approach assists in optimizing laser processing techniques, thereby enhancing efficiency and effectiveness in achieving desired material properties. Overall, the utilization of ANOVA in laser processing offers a robust methodology for investigating the impact of laser parameters on material properties, facilitating informed decision-making, and enabling the development of optimized laser processing strategies.

2.8.1 Effect of laser parameters on ultimate tensile strength (UTS)

Table 2- 5, the ANOVA table, provides a concise summary of the sources of variation in the response variable of ultimate tensile strength (UTS). It includes important statistical measures such as the sum of squares (SS), degrees of freedom (Dof), F-statistic, and p-value. The SS column represents the sum of squared deviations from the mean, reflecting the total variability in the UTS data. The Dof column indicates the degrees of freedom associated with each source of variation, representing the number of independent pieces of information available for estimating the respective parameter. The F-statistic compares the mean square of each factor to the mean square error and evaluates the significance of the factors in influencing the UTS. The p-value, associated with each factor, quantifies the statistical significance and represents the probability of obtaining a similar or more extreme result if the null hypothesis of no effect is true.

Table 2- 6 focuses on the effect of each individual factor on the ultimate strength of the material. The results highlight that the scanning speed and laser power significantly impact the ultimate strength. The laser power contributes approximately 40% towards the observed

variation in ultimate strength, while the scanning speed accounts for approximately 25.34%. These findings indicate that precise control and optimization of the laser power and scanning speed parameters during the manufacturing process can yield substantial improvements in the mechanical properties of the material, particularly in terms of ultimate strength.

By examining the ANOVA table and Table 2- 6, it becomes evident that the scanning speed and laser power are key factors influencing the ultimate strength of the material. These findings provide valuable guidance for practitioners, enabling them to make informed decisions regarding parameter settings and thereby enhance the mechanical properties of the material.

Table 2- 5: ANOVA table for ultimate tensile strength

Characteristic	Sum of squares	Dof	F-Value	P-value
Scanning Speed	4370	1	4,46	0,079
Power	6998	1	7,14	0,037
Error	5877	6		
Total	17246	8		

Table 2- 6: Contribution of laser parameters

Characteristic	Scanning speed	Power	Error
Contribution (%)	25,34	40,58	34,08

Figure 2- 22 illustrates the main effects plot for the Signal-to-Noise (SN) ratio, which mentions the effect of each laser parameter on the ultimate strength of the laser-treated samples. The plot indicates that the laser power has a good effect on the ultimate strength, increasing the laser power result in an increase in ultimate strength. On the other hand, the decrease in scanning speed results in an increase in ultimate strength.

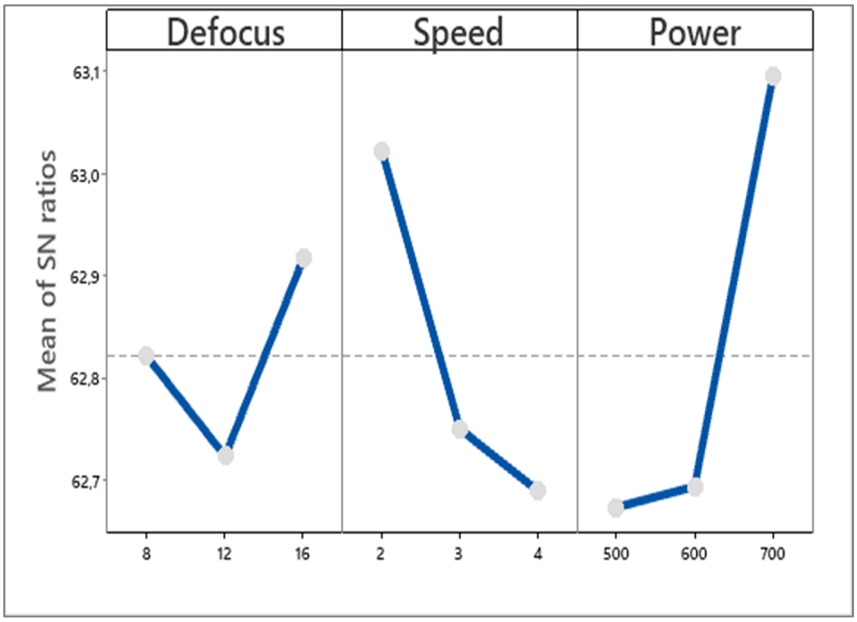

Figure 2- 22: Effect of laser parameters on ultimate tensile strength (D in mm, S in mm/s and P in W)

2.8.1.1 Regression equation

The ANOVA method not only helps in determining the significant factors that affect the response variables, but it also provides a regression equation that models the relationship between these variables, as presented in equation (2. 1), within the specified parameter ranges:

Power (W): [500−700]; Scanning Speed (mm/s): [2−4]; Defocus distance (mm): [8−12].

$$Ultimate\ strength = 1260{,}5 - 27 \times S + 0{,}342 \times P \qquad (2.\ 1)$$

2.8.1.2 Response surface method

RSM, or Response Surface Methodology, is a statistical approach employed for modeling and analyzing situations where multiple variables influence a response. It allows for the creation of a contour plot, which visually represents the impact of various parameters

on the response variable. This plot aids in identifying the optimal parameter settings to achieve the desired outcomes.

Figure 2- 23 presents a contour plot illustrating the influence of laser power and scanning speed on the ultimate strength of the material. The defocus distance is held constant at 12 mm. The contour plot helps visualize the regions within the parameter space where high values of ultimate strength can be attained. Upon examining the contour plot, two options emerge for achieving a high ultimate strength. The first option involves utilizing high values of both laser power and scanning speed. The second option entails employing low values for both parameters. These regions on the contour plot represent the parameter combinations that result in elevated ultimate tensile strength values. By utilizing RSM and analyzing the contour plot, researchers and practitioners can gain insights into the relationship between laser power, scanning speed, and the ultimate strength of the material. This information enables them to identify the optimal parameter settings required to achieve the desired mechanical properties and enhance the performance of the material.

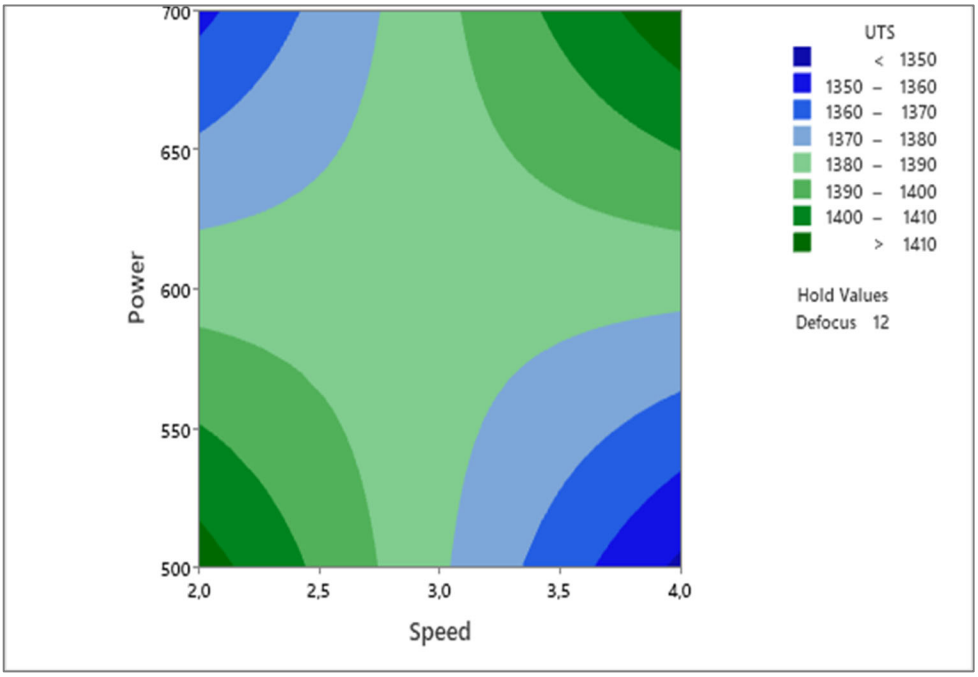

Figure 2- 23: RSM for the ultimate tensile strength (D in mm, S in mm/s and P in W)

2.8.2 Effect of laser parameters on Elongation

Table 2- 7 presents the ANOVA table, providing a summary of the statistical significance of the laser parameters on the elongation of the material. The P-values associated with all factors are below 0,005, indicating that the results are highly statistically significant. Additionally, the table includes the error term, which represents the unexplained variability in the elongation that cannot be attributed to the laser parameters alone. In this case, the error term is approximately 0,6910, suggesting that there is some residual variability in the elongation that is not accounted for by the laser parameters. Table 2- 8 offers insights into the percentage contribution of the defocus distance and laser power to the elongation of the material. The results reveal that laser power plays a significant role, contributing 68,11% to the observed elongation. Similarly, the defocus distance also exhibits a notable impact, contributing 24,78% to the elongation. These findings highlight the significant influence of laser power and defocus distance on the elongation of the material. The high statistical significance and notable percentage contributions underscore the importance of carefully controlling and optimizing these laser parameters to achieve the desired elongation characteristics in the manufactured parts.

Table 2- 7: ANOVA table for elongation

Characteristic	Sum of squares	Dof	F-Value	P-value
Defocus distance	2,4067	1	20,90	0,004
Power	6,6150	1	57,44	0,000
Error	0,6910	6		
Total	9,7126	8		

Table 2- 8:Contribution of laser parameters on the elongation values

Characteristic	Defocus distance	Power	Error
Contribution (%)	24,78	68,11	7,11

Figure 2- 24, illustrates the main effects plot for the Signal-to-Noise ratio on elongation. The graph demonstrates that the elongation decreases as both power and defocus distance increase.

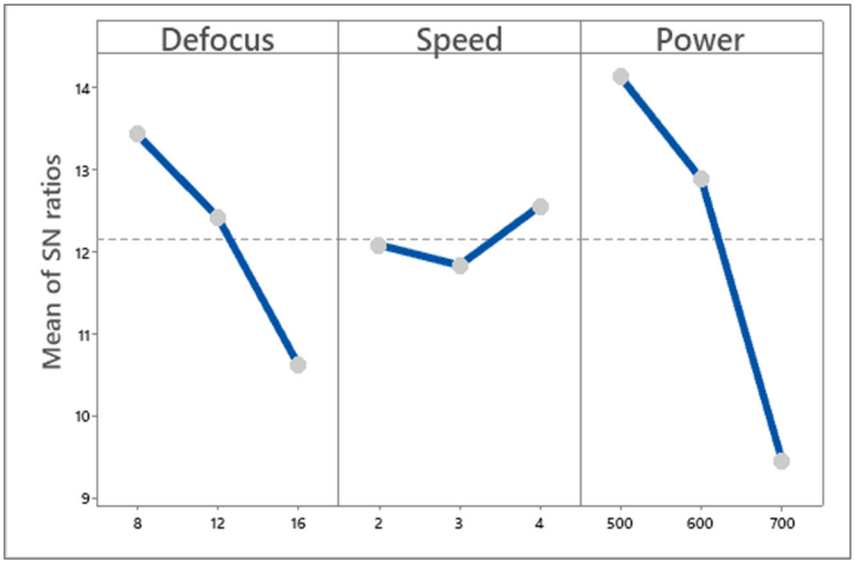

Figure 2- 24: Effect of laser parameters on Elongation (D in mm, S in mm/s and P in W)

2.8.2.1 Regression equation

In addition to identifying significant factors that impact the response variables, the ANOVA method also provides a regression equation that mathematically models the relationship between these variables. (2. 2) demonstrates this empirical relation and can be utilized to predict the response variables based on the values of the factors, within the specified parameter ranges:

Power (W): [500−700]; Scanning Speed (mm/s): [2−4]; Defocus distance (mm): [8−12].

$$Elongation = 12{,}394 - 0{,}1583 \times D - 0{,}0105 \times P \qquad (2.\ 2)$$

2.8.2.2 Response surface method

Figure 2- 25, a contour plot generated using RSM, depicts the influence of laser power and defocus distance on elongation while keeping the scanning speed constant at 3 mm/s. The contour plot visualizes the parameter space and identifies regions where high elongation values can be achieved. From the contour plot, it can be observed that low values of both laser power and defocus distance contribute to higher elongation. The contour lines in the plot represent areas with similar elongation values. The regions with high elongation are typically associated with combinations of low laser power and defocus distance. The contour plot aids in identifying the optimal parameter settings for achieving desired elongation values in the manufactured parts. By selecting appropriate values of laser power and defocus distance within the identified regions, manufacturers can enhance the elongation characteristics of the material and potentially meet specific design requirements. This analysis provides valuable insights into the relationship between laser parameters and elongation, aiding in the optimization of process parameters for improved material performance.

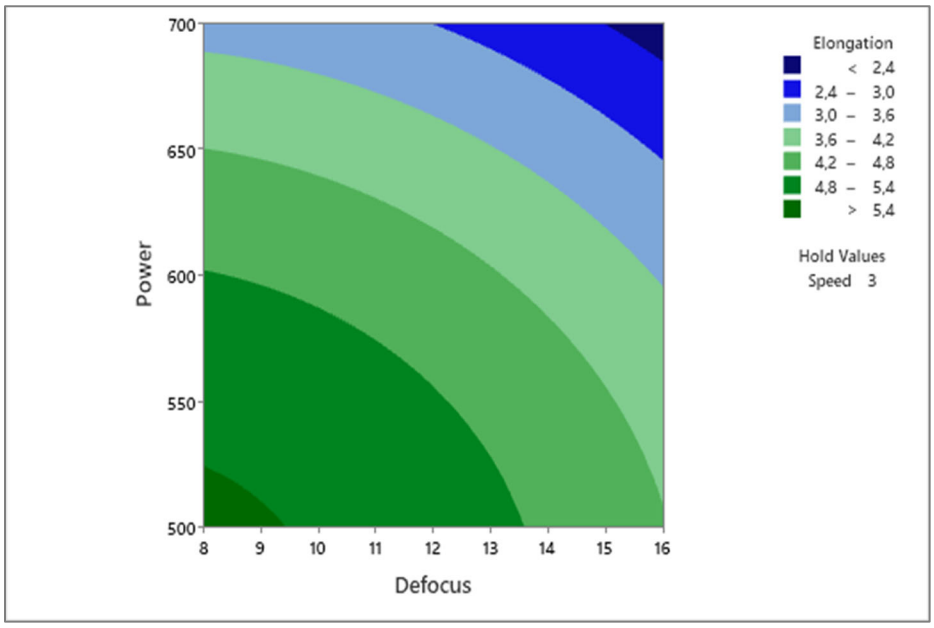

Figure 2- 25:RSM for the Elongation (D in mm, S in mm/s and P in W)

2.9 CONCLUSION

The study demonstrates that the laser surface treatment, specifically using a specific line pattern, effectively enhances the surface quality of quenched and tempered H13 tool steel. The following key findings were observed:

- The untreated sample, which served as the control, exhibited the highest elongation at fracture (15%), indicating good ductility, but the lowest ultimate strength (1247 MPa) compared to the laser-treated samples.

- The elongation and ultimate strength of the laser-treated samples showed an inverse relationship.

- The laser-treated samples displayed a range of ultimate strength values between 1342 to 1497 MPa and elongation values ranging from 2.46% to 5.55%.

- Among the laser-treated samples, sample number 7, treated with specific parameters (16 mm defocus distance, 2 mm speed, and 700 W laser power), showed the highest ultimate strength of 1497 MPa, representing a 20% improvement over the substrate. However, the elongation at fracture for this sample dropped to the lowest value of 2.46%.

- The mode of fracture for most laser-treated samples appeared to be predominantly brittle based on elongation values, except for samples 6 and 1, which were treated with the lowest laser power of 500 W.

- Fractography analysis revealed that at microscopic scales, the mode of fracture for the laser-treated samples was a combination of brittle and ductile fracture.

- The fractography analysis reveals a diverse range of fracture behaviors in the different zones of the material. Throughout the investigation, a combination of ductile and brittle features has been observed on the fractured surfaces, indicating the complexity of the material response under different laser process parameters.

- The analysis of variance (ANOVA) indicated that the laser power and scanning speed were the two primary factors affecting the ultimate tensile strength (UTS) of the laser-treated samples, with respective contribution percentages of 40.58% for the power and 25.34% for the scanning speed.

- An increase in laser power led to higher UTS values, while a decrease in scanning speed also contributed to increased UTS values.

- The analysis of variance on the elongation at fracture indicated that the laser power had the most significant impact, contributing 68.11%, followed by the defocus distance with a contribution of 24.78%. Moreover, a decrease in defocus distance and laser power resulted in increased elongation at fracture.

Overall, the laser surface treatment improved the ultimate tensile strength of the H13 tool steel but negatively affected its ductility, leading to a more brittle mode of fracture in most cases.

2.10 REFERENCES

1. Dobrzański, L.A., T. Tański, A.D. Dobrzańska-Danikiewicz, E. Jonda, M. Bonek, and A. Drygała, *1 - Structures, properties and development trends of laser-surface-treated hot-work steels, light metal alloys and polycrystalline silicon*, in *Laser Surface Engineering*, J. Lawrence and D.G. Waugh, Editors. 2015, Woodhead Publishing. p. 3-32.
2. Outeiro, J.C., *11 - Residual stresses in machining*, in *Mechanics of Materials in Modern Manufacturing Methods and Processing Techniques*, V.V. Silberschmidt, Editor. 2020, Elsevier. p. 297-360.
3. Naimi, S. and S.M. Hosseini, *Tool steels in die-casting utilization and increased mold life.* Advances in Mechanical Engineering, 2015. **7**(1): p. 286071.
4. Jhavar, S., C.P. Paul, and N.K. Jain, *Causes of failure and repairing options for dies and molds: A review.* Engineering Failure Analysis, 2013. **34**: p. 519-535.
5. Papageorgiou, D., C. Medrea, and N. Kyriakou, *Failure analysis of H13 working die used in plastic injection moulding.* Engineering Failure Analysis, 2013. **35**: p. 355-359.
6. Klobčar, D., L. Kosec, B. Kosec, and J. Tušek, *Thermo fatigue cracking of die casting dies.* Engineering Failure Analysis, 2012. **20**: p. 43-53.

7. Cong, D., H. Zhou, M. Yang, Z. Zhang, P. Zhang, C. Meng, and C. Wang, *The mechanical properties of H13 die steel repaired by a biomimetic laser technique.* Optics & Laser Technology, 2013. **53**: p. 1-8.
8. Cong, D., H. Zhou, Z. Ren, Z. Zhang, H. Zhang, C. Meng, and C. Wang, *The thermal fatigue resistance of H13 steel repaired by a biomimetic laser remelting process.* Materials & Design, 2014. **55**: p. 597-604.
9. Ma, S., T. Zhou, H. Zhou, G. Chang, B. Zhi, and S. Wang, *Bionic Repair of Thermal Fatigue Cracks in Ductile Iron by Laser Melting with Different Laser Parameters.* Metals, 2020. **10**(1): p. 101.
10. Tóth, L., T.A. Kovács, Z. Nyikes, and V.-G. Ghica, *Increasing the H13 tool steel wear resistance by plasma nitriding and multilayer PVD coating.* UPB Sci. Bull. Ser. B: Chem. Mater. Sci.(1454–2331), 2021. **83**(2): p. 273-282.
11. Divagar, S., M. Sudhahar, T. Kannan, P. Vijayakumar, and R. Tamizhselvan, *Enhancement of Wear Resistance in AISI h13 Tool Steel by Liquid Carburizing.* J. Emerg. Technol., 2020. **8**(10): p. 156-160.
12. Liu, B., B. Wang, X. Yang, X. Zhao, M. Qin, and J. Gu, *Thermal fatigue evaluation of AISI H13 steels surface modified by gas nitriding with pre-and post-shot peening.* Applied Surface Science, 2019. **483**: p. 45-51.
13. Wang, B., X. Zhao, W. Li, M. Qin, and J. Gu, *Effect of nitrided-layer microstructure control on wear behavior of AISI H13 hot work die steel.* Applied Surface Science, 2018. **431**: p. 39-43.
14. Muthukumaran, G. and P. Dinesh Babu, *Laser transformation hardening of various steel grades using different laser types.* Journal of the Brazilian Society of Mechanical Sciences and Engineering, 2021. **43**: p. 1-29.
15. Zhou, Z.C., J. Du, Y.-J. Yan, and C.-L. Shen. *The recent development of study on H13 hot-work die steel*. in *Solid State Phenomena*. 2018. Trans Tech Publ.
16. Li, L., *2 - The Challenges Ahead for Laser Macro, Micro and Nano Manufacturing☆*, in *Advances in Laser Materials Processing (Second Edition)*, J. Lawrence, Editor. 2018, Woodhead Publishing. p. 23-42.
17. Chen, H., Y. Lu, Y. Sun, Y. Wei, X. Wang, and D. Liu, *Coarse TiC particles reinforced H13 steel matrix composites produced by laser cladding.* Surface and Coatings Technology, 2020. **395**: p. 125867.
18. Lu, J.Z., J. Cao, H.F. Lu, L.Y. Zhang, and K.Y. Luo, *Wear properties and microstructural analyses of Fe-based coatings with various WC contents on H13 die steel by laser cladding.* Surface and Coatings Technology, 2019. **369**: p. 228-237.
19. Norhafzan, B., S. Aqida, E. Chikarakara, and D. Brabazon, *Surface modification of AISI H13 tool steel by laser cladding with NiTi powder.* Applied Physics A, 2016. **122**: p. 1-6.
20. Telasang, G., J. Dutta Majumdar, N. Wasekar, G. Padmanabham, and I. Manna, *Microstructure and Mechanical Properties of Laser Clad and Post-cladding Tempered AISI H13 Tool Steel.* Metallurgical and Materials Transactions A: Physical Metallurgy and Materials Science, 2015. **46**(5): p. 2309-2321.

21. Lee, K.-H., S.-W. Choi, J. Suh, and C.-Y. Kang, *Effect of laser power and powder feeding on the microstructure of laser surface alloying hardened H13 steel using SKH51 powder.* Materials & Design, 2016. **95**: p. 173-182.
22. Gläser, T., S. Bausch, C. Ruset, E. Grigore, T. Craciunescu, and I. Tiseanu, *Combined Laser Alloying/Dispersing and Plasma Nitriding, an Efficient Treatment for Improving the Service Lifetime of the Forging Tools.* Plasma Processes and Polymers, 2009. **6**(S1): p. S291-S296.
23. Jia, Z.-x., Y.-w. Liu, J.-q. Li, L.-J. Liu, and H.-l. Li, *Crack growth behavior at thermal fatigue of H13 tool steel processed by laser surface melting.* International Journal of Fatigue, 2015. **78**: p. 61-71.
24. Brytan, Z., M. Bonek, L.A. Dobrzański, D. Ugues, and M.A. Grande. *The laser surface remelting of austenitic stainless steel*. in *Materials Science Forum*. 2010. Trans Tech Publ.
25. Wang, C., H. Zhou, N. Liang, C. Wang, D. Cong, C. Meng, and L. Ren, *Mechanical properties of several laser remelting processed steels with different unit spacings.* Applied Surface Science, 2014. **313**: p. 333-340.
26. Stratakis, E., J. Bonse, J. Heitz, J. Siegel, G.D. Tsibidis, E. Skoulas, A. Papadopoulos, A. Mimidis, A.C. Joel, P. Comanns, J. Krüger, C. Florian, Y. Fuentes-Edfuf, J. Solis, and W. Baumgartner, *Laser engineering of biomimetic surfaces.* Materials Science and Engineering: R: Reports, 2020. **141**: p. 100562.
27. Zang, C., T. Zhou, H. Zhou, Y. Yuan, P. Zhang, C. Meng, and Z. Zhang, *Effects of substrate microstructure on biomimetic unit properties and wear resistance of H13 steel processed by laser remelting.* Optics & Laser Technology, 2018. **106**: p. 299-310.
28. Zhang, P., H. Zhou, C.-t. Wang, Y. Liu, and L.-q. Ren, *Wear properties of H13 with micron scale and nano scale grains bionic units processed by laser remelting.* Optics & Laser Technology, 2013. **54**: p. 219-224.
29. Li, H., H. Zhou, C.L. Zang, C. Shi, D.P. Zhang, and P. Zhang, *Study on the response and wear property of die steels with varying compositions to laser remelting bionic treatment.* Materials Chemistry and Physics, 2022. **291**: p. 126723.
30. Sui, Q., H. Zhou, L. Yang, H. Zhang, L. Feng, and P. Zhang, *Couple of biomimetic surfaces with different morphologies for remanufacturing nonuniform wear rail surface.* Optics and Laser Technology, 2018. **99**: p. 333-341.
31. Meng, C., H. Zhou, H. Zhang, X. Tong, D. Cong, C. Wang, and L. Ren, *The comparative study of thermal fatigue behavior of H13 die steel with biomimetic non-smooth surface processed by laser surface melting and laser cladding.* Materials & Design, 2013. **51**: p. 886-893.
32. Li, H., H. Zhou, D.P. Zhang, P. Zhang, and T. Zhou, *Influence of varying distribution distance and angle on fatigue wear resistance of 40Cr alloy steel with laser bionic texture.* Materials Chemistry and Physics, 2022. **277**: p. 125515.
33. Ning, A., Y. Liu, R. Gao, S. Yue, M. Wang, and H. Guo, *Effect of Tempering Condition on Microstructure, Mechanical Properties and Precipitates in AISI H13 Steel.* JOM, 2021. **73**(7): p. 2194-2202.

34. Zhang, J.J.J., *A Novel Heat Treatment Strategy Based on Quenching and Carbides Preprecipitation and Subsequent Critical Quenching to Improve the Thermal Fatigue Performance of AISI H13 Tool Steel.* steel research international, 2023.
35. Zhu, J., Z. Zhang, and J. Xie, *Improving strength and ductility of H13 die steel by pre-tempering treatment and its mechanism.* Materials Science and Engineering: A, 2019. **752**: p. 101-114.
36. Telasang, G., J. Dutta Majumdar, G. Padmanabham, and I. Manna, *Structure-property correlation in laser surface treated AISI H13 tool steel for improved mechanical properties.* Materials Science and Engineering A, 2014. **599**: p. 255-267.
37. Meng, C., R. Cao, J. Li, F. Geng, Y. Zhang, C. Wu, X. Wang, and W. Zhuang, *Mechanical properties of TiC-reinforced H13 steel by bionic laser treatment.* Optics & Laser Technology, 2021. **136**: p. 106815.
38. Wang, C., H. Zhou, Z. Zhang, Y. Zhao, P. Zhang, D. Cong, C. Meng, and F. Tan, *Tensile property of a hot work tool steel prepared by biomimetic coupled laser remelting process with different laser input energies.* Applied Surface Science, 2012. **258**(22): p. 8732-8738.
39. Zhi, B., T. Zhou, H. Zhou, P. Zhang, S. Ma, and G. Chang, *Improved localized fatigue wear resistance of large forging tools using a combination of multiple coupled bionic models.* SN Applied Sciences, 2019. **1**(12): p. 1682.
40. Standard, A., *E8. Standard test method for tension testing of metallic materials.* West Conshohocken (USA): ASTM, 2004.
41. González-Velázquez, J.L., *Fractography and failure analysis*. Vol. 24. 2018: Springer.

CHAPITRE 3
ÉTUDE DE L'EFFET DU TRAITEMENT SURFACIQUE AU LASER SUR L'ACIER SUR L'ACIER À OUTILS FABRIQUÉ ADDITIVEMENT SUR LA MICROSTRUCTURE ET LA MICRODURETÉ

Lamya Baali[1], Narges Omidi[1], Noureddine Barka[1], Véronique Dassylva-Raymond[1]

[1]Mathematics, Computer Science and Engineering Department, Université du Québec à Rimouski (UQAR), 300 Allée des Ursulines, Rimouski, QC G5L 3A1, Québec, Canada

Cet article a été soumis dans Advances in Materials and Processing Technologies portant le numéro de référence 233298193

3.1 RESUME EN FRANÇAIS DU PREMIER ARTICLE

La fabrication additive, une technologie émergente, ouvre de nouvelles perspectives pour l'industrie, notamment dans le domaine du moulage par injection. Elle permet d'introduire des canaux de refroidissement conformes dans les moules, ce qui améliore considérablement l'efficacité du refroidissement, un facteur essentiel pour la durée de vie du moule et la productivité du processus. Dans cette étude, l'acier à outils H13 est fabriqué en utilisant la fusion laser sélective (SLM). Cependant, les propriétés du matériau telles qu'elles sont initialement construites ne répondent pas pleinement aux exigences des moules, nécessitant ainsi un post-traitement. Dans cet article, l'acier H13 tel qu'il est construit est soumis à un traitement thermique visant à homogénéiser sa microstructure métastable et à éliminer les contraintes résiduelles générées pendant le processus de SLM. De plus, la surface

est soumise à un traitement au laser sous forme de lignes parallèles. Pour étudier l'impact de ces traitements, un plan d'expérience est mis en place pour contrôler les paramètres du laser. Cette approche permet d'analyser en profondeur la microstructure et le profil de dureté de la zone traitée au laser. Les résultats obtenus révèlent que le traitement thermique a permis d'homogénéiser la microstructure, tandis que le traitement au laser a créé trois zones distinctes : la zone fondue, la zone durcie et la zone affectée par la chaleur. La dureté de la surface traitée au laser s'est améliorée, à l'exception de la zone affectée par la chaleur, qui a montré une légère baisse par rapport au substrat. L'utilisation de l'analyse de variance (ANOVA) a permis de comprendre comment chaque paramètre laser affecte la largeur et la profondeur de la zone traitée au laser.

3.2 CONTRIBUTIONS

Ce premier article, intitulé « A Study of the in Influence of Laser Hardening on Microstructure, Microhardness of Additively Manufactured H13» a principalement été rédigé par Lamya Baali, son premier auteur. Noureddine Barka, le deuxième auteur, occupe la fonction de directeur de recherche et a joué un rôle clé dans la définition du projet et de la méthodologie adoptée. Le troisième auteur, Narges Omidi, a apporté une contribution à l'amélioration de l'article. Enfin, Véronique Dassylva-Raymond a supervisé le travail et a également contribué à améliorer la rédaction globale.

3.3 TITRE DU DEUXIÈME ARTICLE

A Study of the in Influence of Laser Hardening on Microstructure, Microhardness of Additively Manufactured H13.

3.4 ABSTRACT

Additive manufacturing, an emerging technology, opens new perspectives for the industry, particularly in the field of injection molding. It allows conformal cooling channels

to be introduced into molds, significantly improving cooling efficiency, a critical factor in mold life and process productivity. In this study, H13 tool steel is manufactured using selective laser melting (SLM). However, the material properties as-built do not fully meet the requirements of the molds, thus requiring post-processing. In this paper, the as-constructed H13 steel is subjected to heat treatment aimed at homogenizing its metastable microstructure and eliminating residual stresses generated during the SLM process. Additionally, the surface is subjected to laser processing in the form of parallel lines. To study the impact of these treatments, an experimental plan is set up to control the laser parameters. This approach allows for in-depth analysis of the microstructure and hardness profile of the laser-treated area. The results obtained reveal that the heat treatment made it possible to homogenize the microstructure, while the laser treatment created three distinct zones: the molten zone, the hardened zone and the heat-affected zone. The hardness of the laser-treated surface improved, except for the heat-affected zone, which showed a slight decrease compared to the substrate. The use of analysis of variance (ANOVA) provided an understanding of how each laser parameter affects the width and depth of the laser treated area.

3.5 INTRODUCTION

Initially, the term "Rapid Prototyping" was used to describe additive manufacturing (AM), as it was primarily utilized to fabricate prototypes from digital designs. However, as the technology progressed and became capable of producing functional and operational components, the term "Additive Manufacturing" came into use to describe the process more accurately [1]. 3D printing process is a revolutionary technology with a wide range of advantages, it’s able to produce highly customized and personalized products, and can help to reduce waste and material costs by producing objects with the exact amount of material needed, reducing the need for excess material. It can also help with reducing product development cycle, as the 3D printing process allows for the rapid production of prototypes and functional parts. This capability enables engineers and designers to test and refine their designs more quickly, reducing the time and cost of traditional prototyping methods [2].

Additive manufacturing is a technology that enables the creation of complex geometries at a fine resolution from three-dimensional Computer Aided Design (3D CAD) data, by adding material in a very thin layer. This manufacturing process involves different materials including plastics, metals, ceramics and composites, which extends its applications in a multitude of industries such as construction, die production, aerospace, and biomechanical [3-5].The sustainability aspect of additive manufacturing is one of its most advantages, as it offers a potential to reduce waste by only using the exact amount of material needed to create a product. This can also lead to energy savings as less material needs to be transported and processed, also reducing reduce global greenhouse gas emissions [6].There are several main methods of additive manufacturing that depend on various factors, such as required material properties, resolution, applications, economic aspect and cost. Fused Deposition Modeling (FDM) involves filament of a thermoplastic polymer heated and then extruded layer by layer to create a 3D object. Stereolithography (SLA) uses a liquid photopolymer resin that is solidified layer by layer using a UV laser or other light source. Powder bed fusion is a process that uses a laser or electron beam to melt and fuse powder material, such as metal or plastic, layer by layer. The process begins with a thin layer of powder spread over a build platform. The laser or electron beam selectively melts the powder in a specific pattern, fusing the particles together to create a solid layer. This process is repeated layer by layer, building up the part from the bottom up. Direct energy deposition (DED) involves melting a metal powder or wire using a laser or electron beam and depositing it layer by layer to create the final part. Binder Jetting involves selectively depositing a liquid binder onto a powdered material, such as sand or metal, to create a solid object. Material Jetting uses multiple print heads to deposit droplets of material, typically a photopolymer resin, onto a build platform. Laminated Object Manufacturing (LOM) involves the layer-by-layer cutting and bonding of sheet materials, typically paper or plastic, to create a three-dimensional object. In LOM, the material sheets are fed into a printer where a laser or blade cuts the material to the shape of the object being printed. Each layer is then bonded to the previous one using heat, pressure, or an adhesive [7].Metallic additive manufacturing has made a significant progress in recent years, with the developments of modern manufacturing

technologies and information systems. Currently, the commonly used methods for metallic additive manufacturing are typically powder bed additive manufacturing techniques that involves the use of layers of metal powder that are melted by either Selective Laser Melting (SLM) or electron beam melting [8].

H13 is a widely used steel for its excellent combination of strength, toughness and heat resistance. Additive manufacturing has opened a new possibility of applications of additive manufactured H13 tool steel. Among this application there's molds in injection molding manufacturing, additive manufacturing offers an important deign freedom and innovation enabling the creation of bio-inspired inserts, development of internal lattice structures and incorporation of conformal cooling channels in the design of the mold which optimize heat dissipation, achieving uniform cooling and ultimately increases productivity [9-12].

The implementation of metal additive manufacturing (AM) in the injection molding industry indeed offers a new possibility for molds makers in terms of design freedom, but it still requires the achievement of comparable or even better mechanical properties in 3-D printed steel molds compared to the conventionally made ones. The SLM process parameters have a significant impact on the result material properties, according to the literature the key SLM parameters are laser power, scanning speed, hatch spacing and layer thickness, they mainly impact the microstructure, porosity, fatigue, residual stress, surface roughness, and mechanical properties [13, 14]. The relative density increases with the increase of energy density, to reach an optimal level then decreases, because a lower energy density can result in incomplete melting and inadequate fusion, leading to the formation of voids, porosity and weak bonding between layers, however an excessive energy leads to a high thermal gradient, resulting in more residual stress, it can also causes a rapid vaporization of the metal powder and creates voids, porosity and irregularities [15]. A study [16] optimized the SLM process parameters for H13 steel specimens in order to achieve a maximum relative density of 99.2% and best mechanical and microstructure properties, by applying a laser power of 170 W and a scanning speed of 400 mm/. Another study [17] adopted a statistical approach to determine the optimum SLM process parameters of AISI H13 tool steel, with two factors and three

levels- laser power (170, 260, 350 W) and scanning speed(540, 970, 1400 mm/s) a minimal porosity of 0.2% was found for an applied volumetric energy density of 100.3 J/mm3. Lei et al [31] established the correlation between the microstructure and mechanical properties of as selective laser melted H13, the process was conducted with the variation of the power and scanning speed, the volumetric energy density (VED) is 56.7, 76.6, 83.3, 95.8, 111.1 and 127.8 J/mm3 . the maximum value of hardness is 53 HRC and spotted at a VED of 95.8 J/mm3, it also reached 99.6% as relative density. the microstructure analysis shows two zone the melt pool and the transition zone which is heat affected. the martensite is the dominant phase, with a small amount of retained austenite, also a cellular structure is detected.

Compared to the conventional parts, additive manufactured ones have several defects such as pores, lack of fusion, inhomogeneity of the microstructure, residual stresses, surface roughness, cracks generation, anisotropy, and loss of alloying elements[18, 19]. Most of these defects may be controlled during the selective laser melting through a careful process optimization, parameter control, powder quality with a proper particle size distribution and minimal impurities, preheating and effective heat management to reduce the thermal gradients and minimize the residual stress [20].

Despite implementing all the process control mentioned above, the as-built H13 tool steel can still exhibit undesirable defects its mechanical and microstructural properties. As a result, its performance in fulfilling specific applications and meeting the expected conventional H13 properties is compromised [21]. Post processing methods are necessary to meet the desirable performance requirements, the two major post processing techniques include at first thermal post treatment that play a crucial role in homogenizing the microstructure of the material, reducing residual stress, and minimizing chemical segregation. Then comes surface treatments employed to achieve a desirable surface finish and properties. This includes reducing surface roughness to a minimum and imparting a certain level of surface hardening, which enhance the material’s resistance to fatigue and corrosion that affects mainly the durability and service life during various operating conditions [22-24]. In contrast with traditional casting methods, the selective laser melting

utilizes a high localized melting and ultrafast cooling rates, which results a unique and non-equilibrium microstructure. The microstructure of H13 tool steel produced through selective laser melting (SLM) exhibits distinct features. In the as-built condition, SLM H13 typically consists of fine dendritic structures with a refined grain size. The rapid solidification during the SLM process results in a non-equilibrium microstructure with a high density of dislocations and a significant presence of retained austenite [25-28]. To address these issues a heat treatments methods including stress relief, austenitizing, quenching, and series of tempering are required to homogenize the microstructure, relieve residual stresses, and promote the formation of desirable phases. It facilitates the conversion of retained austenite into martensite, leading to improved hardness and mechanical properties [29, 30].

Yuan et al [31] studied the main effect of post treatment on the microstructure and mechanical properties behavior of laser beam powder bed fused H13, the samples were subject to two different treatment, the first one is conventional heat treatment, by heating the as-built to 1020 °C for 30 minutes and quenched in oil, then tempered twice at 580 °C for 2h. The second treatment the samples were directly tempered twice at 625°C for 2h. One of the objectives of this treatments is the stress relief and reducing retained austenite. The microstructure of direct tempered H13 has boundaries but less important than the as built, the quenched and tempered samples have more homogenous microstructure, and the melt pool boundaries disappeared. For the carbides the M_7C_3 and M_3C are the more dominant in the quenched and tempered samples, the hardness improved from 49.17 HRC as built to 50.92 HRC for both quenched/tempered and double tempered. This essay also investigated the softening treatment with two post treatment, the samples were subject to isothermal holding at 550°C and 600°C for 5h, 25h, 50h and 100h. The results shows that the higher the temperature and the longer the duration, the hardness decreases drastically. Yan et al [32] studied the effect of tempering on selective laser melted H13 tool steel, the heat treatment was conducted at 600°C and 700°C for 2h. The microstructure of the as built H13 consists of cellular dendritic structure with a dominant martensite lath, and the coexistence of martensite and retained austenite, and M2C carbides enriched with Mo and Cr. The 600°C tempered H13 is mainly cellular, with the presence of martensite lath and three kinds of

carbides Cr- rich M_7C_3 $M_{23}C_6$ and V-rich V_8C_7 carbides. The 700°C tempered H13 exhibited that the martensite lath is still present; the cellular structure is replaced with homogenous ferrite matrix with dispersing of carbides M_7C_3, $M_{23}C_6$ and V_8C_7. Bae et al [33] investigated the effect of tempering temperatures and times on the selective laser melting manufactured H13 steel. The H13 was subject to a solution treatment at 1000°C for 1h and oil quenched, then tempered at 200, 300, and 500 °C for 2, 3 and 5 hours and cooled in air. The phase analysis shows that all the specimens show a peak of α' martensite and $(Cr, Fe)_7C_3$ (M_7C_3), The retained austenite is observed only in the as built H13 due to rapid cooling during the additive manufacturing process, it indicates that the transformation to austenite didn't complete during the cooling. All the tempered samples the martensite transformed to a lath martensite. Samples tempered under 500°C have bigger and more M_7C_3 precipitates because of the carbon diffusion from lath martensite. The as built shows the highest hardness about 47.5 HRC it's lied to the sub-grain cells and M_7C_3 carbides, the tempering treatment decreases slightly the hardness. Sun et al [28] investigated the thermal conductivity of selective laser melted H13 in both cases as-built and post treated. The study utilized specific parameters, including a laser power of 190W, hatch spacing of 110 μm, and layer thickness of 30 μm. For the scanning speed, a range of values was examined, namely 250 mm/s, 400 mm/s, 550 mm/s, 800 mm/s, 1200 mm/s, 1800 mm/s, and 2400 mm/s In terms of heat treatment, the process involved an initial austenitizing stage at 1020 °C for 70 minutes, followed by quenching and double tempering at 585 °C for 2.5 hours. The microstructure of the as-built material exhibited a cellular structure in the bottom of the melted pools due to the high temperature gradient during solidification. In the upper parts of the melt pools, a columnar structure was observed, characterized by a lower temperature gradient compared to the bottom region. The study also reported that the quenching treatment effectively eliminated the cellular structure of the selectively laser melted H13 material, resulting in a martensite microstructure. Both the quenching and tempering treatments exhibited a lath martensite structure with the precipitation of V-rich and MC types of carbides. The heat treatment led to a reduction in retained austenite. It was observed that the thermal conductivity of the selectively laser melted H13 material was lower than that of conventional

H13 due to factors such as porosity, the cellular-columnar microstructure, and a high-volume fraction of carbon area known as retained austenite. However, the heat treatment was found to improve the thermal conductivity of the selectively laser melted H13 material by approximately 9% to 22%. Zanni et al [34] studied the effects of heat treatment parameters on the mechanical properties of H13 manufactured by LPBF method. the first treatment was the stress relief at 690 °C for 2 hours. The samples were subject to two main heat treatments. Austenitizing at 1050°C in vacuum, quenching in nitrogen gas, and a triple tempering at 540-550°C. Austenitizing at 1070°C in vacuum, quenching in nitrogen gas, double tempering at 510-520°C, a sub-zero treatment at -80°C, and finally a tempering at 520°C-530°C.

The as built H13 showed the same hierarchical microstructure which is cellular. For the both heat treatment the **α**-ferrite is the dominant phase and alloying carbides M6C and M23C6 which is proven by EDS analysis, for the microstructure it's totally homogenous, and exhibited tempered martensite. The second heat treatment achieved 665HV, and the first one 636 HV. Jung et al [35] tried a pre-post processing in order to ameliorate the density of SLM parts, which is laser re-melting with a dual scanning speed during the selective laser melting. This method closes proses in each layer which highly improve the density. The selective laser melting parameters are 90W for the power, 80 mm for the hatch space, 25 mm for the layer thickness. The first and second scanning speed ranged from 100 mm/s to 1000 mm/s. The highest relative density of 99.94% and hardness value of 53.5 HRC are achieved with a first scanning speed of 400 mm/s and then a second one of 600 mm/s. Kumar et al [36] manufactured a SLM H13 with 99% for the relative density and a minimum porosity, which is obtained with a volumetric energy density of 733.3 J/mm^3 , the adopted parameters are 203 W for the power, 92.3 m/s scanning speed, 50 μm for the layer thickness, and 60 μm for hatch spacing. The SLM samples were subjected to a tempering heat treatment at 550°C for two hours and then air cooled, and then TiAlN coated to improve the surface quality. The surface characteristics of the as-built SLM sample exhibited a presence of austenite and lath martensite. On the other hand, the tempered-SLM sample displayed a considerable amount of tempered austenite, along with the presence of ferrite and carbides, which improved the wear and mechanical properties. additionally, the atomic force microscopy (AFM) analysis

revealed enhanced surface quality following the deposition of a TiAlN coating. The microhardness of the as-SLM sample was significantly improved, exhibiting an increase of 1.5 times after tempering and times after the deposition of the TiAlN coating.

Despite the promising developments of selective laser melting in terms of design freedom, the as built sample can't be directly implemented in its application such as molds for injection molding, according to the literature H13 tool steel manufactured by SLM knows a common defect that arise during the process. To ameliorate the main concerns linked to the heterogeneous microstructure of the as-built H13, the pronounced brittleness, the presence of residual stress, and the surface characteristics, two post-treatment methods have been implemented in this essay. The first method involves heat treatment, which includes stress relief, followed by conventional heat treatment techniques such as quenching and tempering. The primary objective of this approach is to homogenize the microstructure, which directly impacts the mechanical properties. The second treatment method involves surface bionic laser treatment, specifically targeting the material's surface to achieve the stringent requirements of mold injection molding because any imperfection on the mold surface is directly transferred to the final product, also the most die failures present in the surface [37-40].

In this study, the effect of laser surface treatment on the microstructure, microhardness profile, and geometrical characteristics of additively manufactured H13 is investigated. A statistical approach is planned in two stages to optimize the laser surface treatment and enhance the properties of the surface. The first stage involves determining the optimal number of tests for three laser parameters (laser power, scanning speed, and defocus distance) with three levels using the Taguchi method. The second stage involves analyzing the experimental results using ANOVA (Analysis of Variance) to understand the effects of each laser parameter on the final parts and to identify the best combination. The ANOVA analysis, known for its predictive capabilities, is chosen for this study. Additionally, Response Surface Methodology (RSM) is employed to establish the relationship between the parameters and the outcomes.

3.6 MATERIAL AND METHODS

3.6.1 Materials

Table 3- 1 shows the chemical composition of the H13 powder used during the selective laser melting process provided by the supplier. the powder shape and size are spherical and in the range of 15-53 µm.

Figure 3- 1 shows the scanning electron microscopy images of the powder at different magnifications.

Table 3- 1: Chemical composition of the H13 powder

Element	Cr	Mn	Mo	Si	V	C	Fe	Others
Min-Max (wt.%)	5.0-6.0	0-0.6	1.0-2.0	0.5-1.0	0.5-2.0	0.3-0.5	Balance	0-0.05

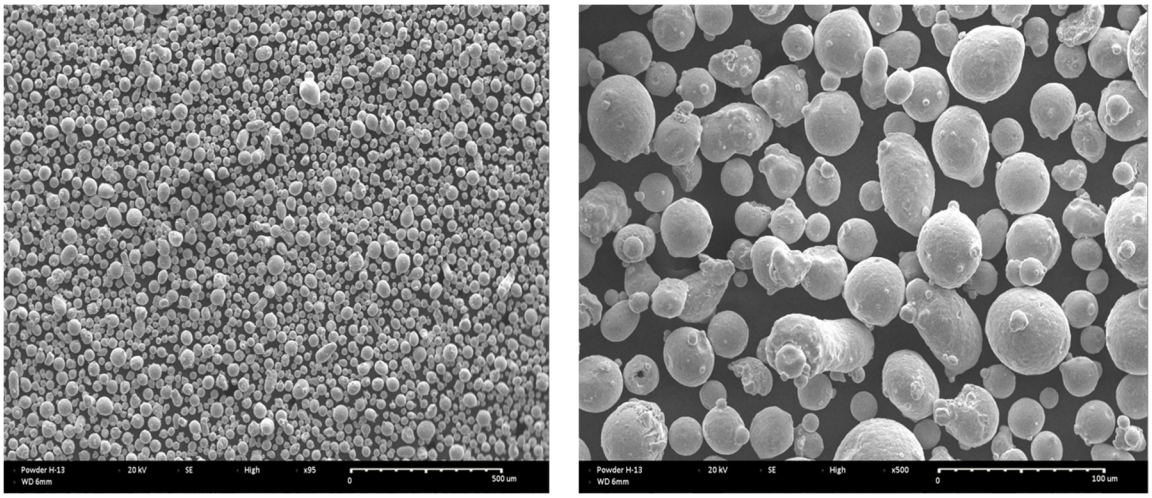

Figure 3- 1: SEM images of the particle's distribution of the used H13 powder

3.6.2 Methods

SLM machine of M290 is used for manufacturing. The printing process was performed with the printing strategy 67º of rotation in each layer, layer thickness equal to 40 µm, the hatch distance was set at 0.12 mm, laser power of 275 W, and a scanning speed of 800 mm/s. The heat treatment temperatures and duration are presented in Table 3- 2

Table 3- 2: Heat treatment characterization

	Temperature	**Duration**
Stress relief	650°C	8 Hours
Austenitizing	1000°C	30 minutes
Quenching in the oil	Ambient temperature	3 minutes
Tempering	650°C	1 Hour

The laser surface hardening was carried out by a laser cell which consists of a FANUC M-710iC robot that directs a light beam from a laser head fed through a fiber laser with a maximum power of 3000 emits continuous waves with a wavelength of 1070 nm. The laser head HIGHYAG BIMO is equipped with both a variable zoom collimator and a fixed focusing lens. The assembly makes it possible to obtain circular focal spots of the order of 0.251 to 0.431 mm in diameter and connected to an optical fiber of 100 mm. The Figure 3-2 shows the laser set up used for this experiment. In the case of laser hardening processes, it is important to define the experimental margins by allowing for maximal case depth transformation and excessive transformation without cracking the material. Maximal and minimal tuning is necessary before parameter levels can be established. Table 3- 3 shows the factors and their variation ranges in these experiments.

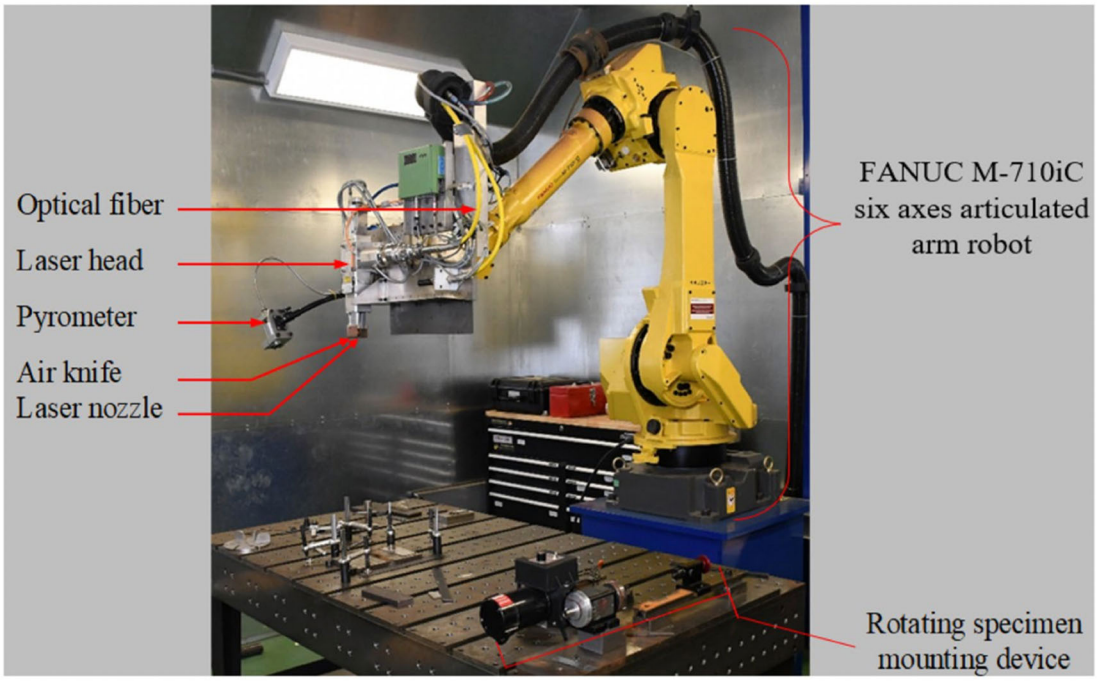

Figure 3- 2: Laser cell (3000W: YLS-3000-ST2) mounted on a FANUC robot with 6 axes [41]

Table 3- 3: Laser hardening parameters specifications

Factors	Abbreviation	Variation Ranges	Unit
Power	P	400, 500 and 600	W
Scanning speed	S	2, 3 and 4	mm/s
Defocus distance	D	8, 12 and 16	mm
Focal diameter	F	0.9, 1.03 and 1.15	mm

Taguchi method is used to determine the experimental plan, to have a minimum number of processed trials, and a minimum variation by studying the effect of multiple parameters simultaneously, while the conventional methods use a very long approach that consists of varying one parameter while keeping the rest constant [42]. For the experimental design three factors are involved with three levels, so the L9 orthogonal Taguchi Table 3- 4 is adopted.

Table 3- 4: L9 orthogonal Taguchi table (input parameters)

Test	Defocus distance (mm)	Scanning speed (mm/s)	Power (W)
1	8	2	400
2	8	3	500
3	8	4	600
4	12	2	500
5	12	3	600
6	12	4	400
7	16	2	600
8	16	3	400
9	16	4	500

Before the microhardness test the sample was cut from the middle of the line, and then mounted and polished properly until the surface was smooth and scratch-free. The microhardness tests were carried out on an automated Vickers microhardness tester (CLEMEX CTM micro hardness testing, Figure 3- 3(a)), with an indentation load of 200 gf, and dwell time of 10 s. To obtain the depth profile, multiple measurement points were taken at intervals of 50 μm from the surface and perpendicular to it towards the inside of the specimen. Similarly, for the width profile, measurements were taken horizontally at intervals of 50 μm. Microstructure observation at high magnifications were performed on the cross section of the laser treated using scanning electron microscopy (SEM) Scanning Electron Microscopy (SNE-4500M Plus Tabletop SEM, Figure 3- 3(b)), it has also additional features such as variable spot size control allow for optimal x-ray generation for Energy Dispersive Spectroscopy EDS analysis. The samples with nine set parameters were prepared for SEM by etching the surface after the polishing using the solution Nital 8% which is a solution of acid nitric and alcohol (8% nitric and 92% ethanol).

(a) CLEMEX CTM micro hardness testing set-up *(b) Scanning Electron Microscope*

Figure 3- 3: Micro-hardness and SEM set-up

3.7 RESULTS

3.7.1 Properties of the as-built H13

Figure 3- 4 (a) shows the unique non equilibrium microstructure attributed to the selective laser melted H13, which is a combination of fine cellular/ columnar structure. It has been determined that the rapid cooling rate during SLM effectively suppress the diffusion and precipitation of carbides throughout the process, which exists in conventionally forged H13.In the process of selective laser melting (SLM) for H13, the rapid melting and cooling of the powder particles give rise to the formation of certain undesired and unpredictable phases, which can have an impact on the mechanical properties. The resulting SLM-ed H13 material consists of both the martensite phase and retained austenite that remains after the SLM process. The presence of retained austenite in H13 produced through selective laser melting (SLM) can be attributed to two main factors: the high carbon content (0.4 wt%) and the rapid solidification process. When the austenite phase fails to fully transform into martensite, retained austenite forms at room temperature, this phase id thermodynamically unstable and negatively affects the material's properties [43, 44].

Figure 3- 4 (b) illustrates the microstructure of H13 tool steel after three heat treatment including stress relief, quenching, and finally tempering. The austenitizing heat treatment dissolve the heterogenous microstructure attributed to the as- built H13, it promotes the homogenization of the chemical composition throughout the material, and induces recrystallization, resulting in the formation of new austenite grains with a uniform composition and equiaxed morphology. The tempering process plays a crucial role in several aspects. Firstly, it facilitates the tempering and softening of the martensitic structure. Additionally, it promotes the transformation of any remaining retained austenite. Ultimately, it leads to the even distribution of secondary carbides within the martensite matrix [47].

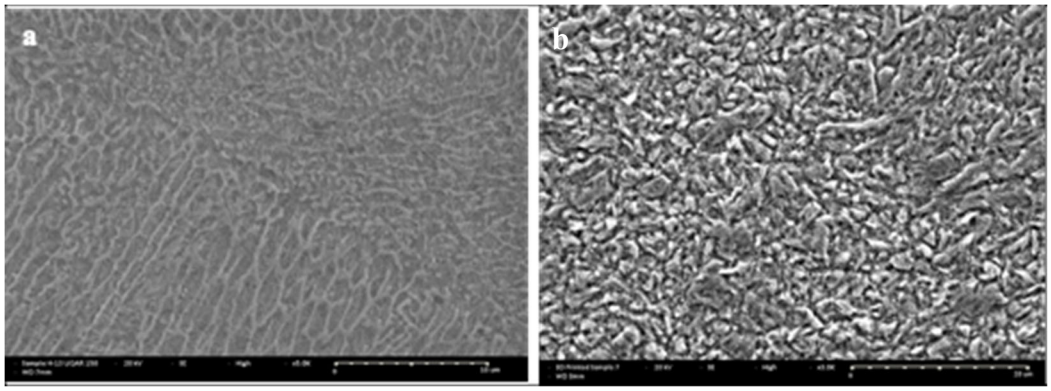

Figure 3- 4: SEM micrographs of: (a) as built H13 tool steel, and (b) heat treated H13 tool steel

3.7.2 Microstructure of the laser treated H13

Figure 3- 5 indicates the morphology of the laser surface treated zone, three zones can be observed:

- Melted zone in this region the laser energy is focused, resulting in complete melting of the surface layer and then undergoes rapid solidification.
- Hardened zone refers to the area adjacent to the melted zone, the temperature reaches a level that allows for significant transformation and rearrangement of the

microstructure. The cooling rates in the hardened zone are slower compared to the melted zone, resulting in a coarser microstructure with larger grain size.

- Heat affected zone is the region surrounding the melted and hardened zones where the material is subjected to high temperatures but does not experience melting or a significant phase transformation.

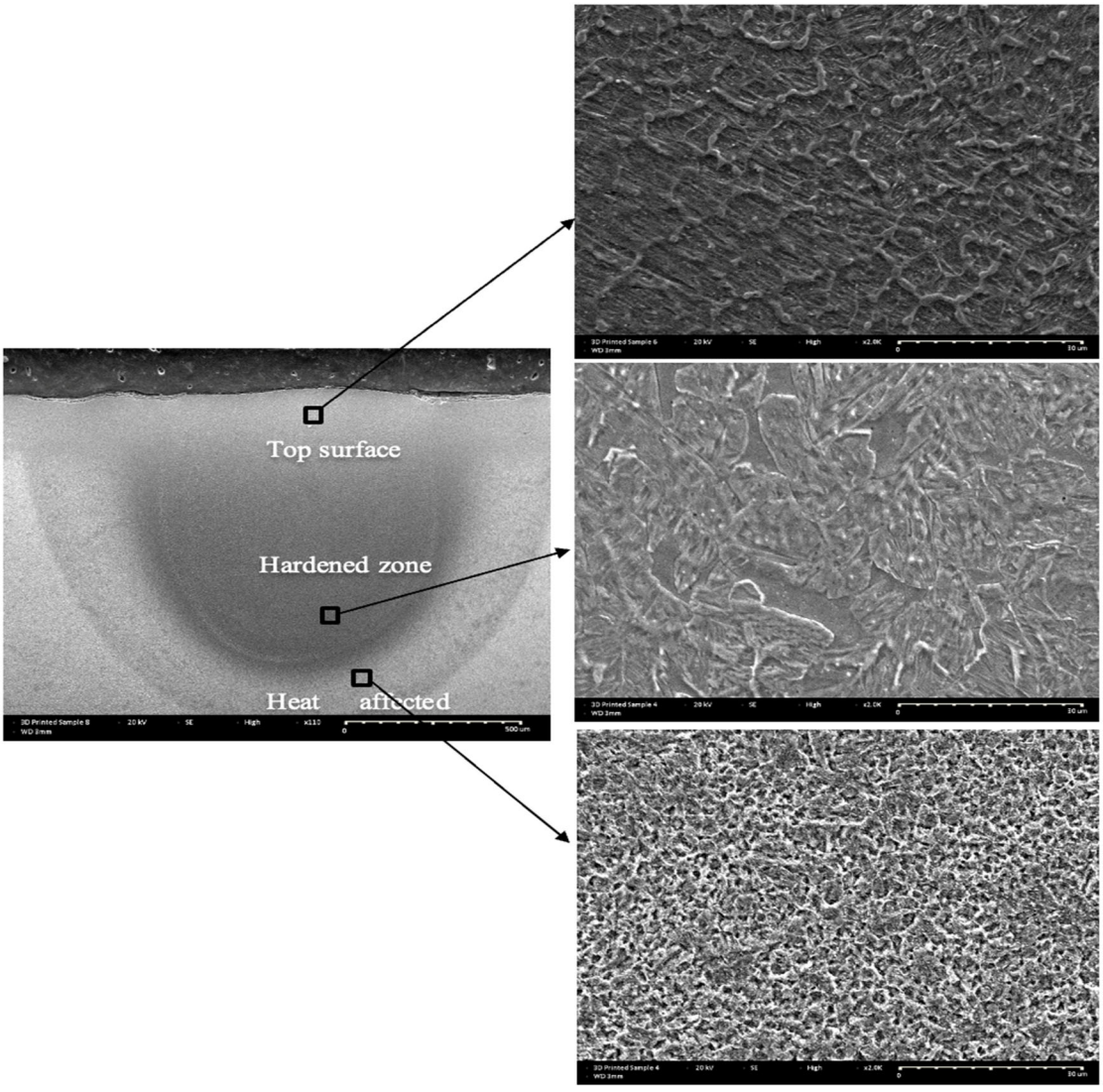

Figure 3- 5: SEM image of a) cross-section of the laser treated zone, b) top surface, c) hardened area, and c) heat affected zone

The microstructure of all the samples as shown in Figure 3- 6 in the three regions appeared to be quite similar, with only slight differences observed in grain size and morphology. These subtle variations can be attributed to differences in the processing parameters employed during fabrication. Interestingly, the microstructure of the heat-affected zone remained relatively unchanged, indicating that the processing parameters had minimal impact on this region. This zone represents an over-tempered region where the temperature gradually decreases with increasing depth. This temperature reduction occurs due to a decrease in the amount of energy absorbed from the surface. The temperature in this zone is likely around the transformation temperature (Ac1). Here, carbides precipitate from the supersaturated martensite, resulting in a lower hardness value compared to the heat-treated substrate.

Similarly, the hardened area exhibited little variation in its microstructure, suggesting that the processing parameters were not a significant influencing factor in this zone either. This area, which is hardened corresponds to an overheated region of the quenched and tempered base material, the temperature likely exceeds the austenitization temperature (Ac3). The microstructure in this zone consists of non-tempered martensite containing undissolved carbides. However, in contrast to the other regions, the microstructure of the surface area displayed noticeable changes across the nine sample sets. Generally, this area undergoes rapid solidification, resulting in the formation of remelted dendrite cells that originate from martensite. This zone consists predominantly of non-tempered martensite and inter-dendritic regions enriched with carbide particles. However, at a laser power of 400W, the microstructure revealed a combination of thin cellular structures along with small carbides and tiny martensite laths. Upon increasing the laser power to 500W, the number and width of martensite laths increased slightly, and the carbides became slightly larger. Subsequently, at a laser power of 600W, the carbides showed further enlargement, accompanied by smaller martensite laths and larger cellular structures. These observations can likely be attributed to the higher temperature and cooling rate at higher laser power levels, facilitating carbide diffusion and coarsening. In summary, the results highlight the significance of processing

parameters in influencing the microstructure of the surface area, while the heat-affected zone and hardened area remain relatively unaffected by these parameters.

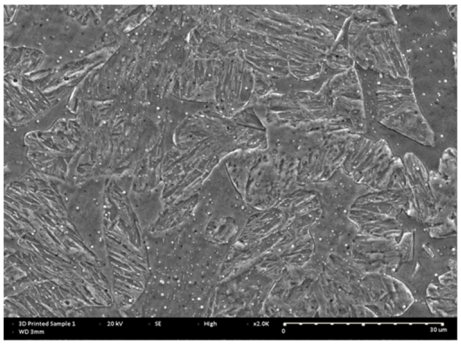

(a) Top surface - Sample 1

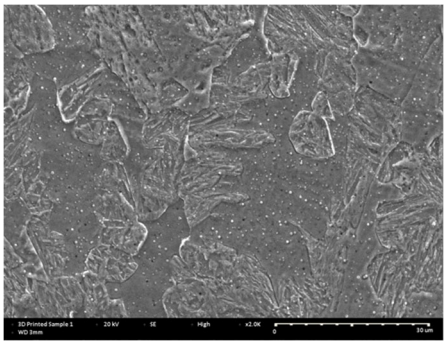

(b) Hardened zone - Sample 1

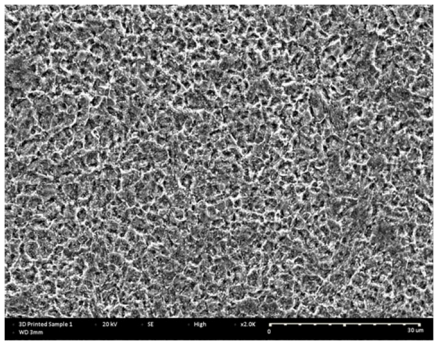

(c) Heat affected zone - Sample 1

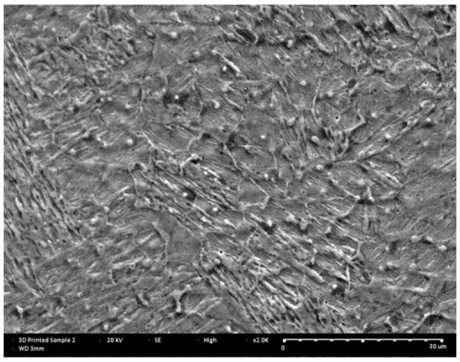

(a) Top surface - Sample 2

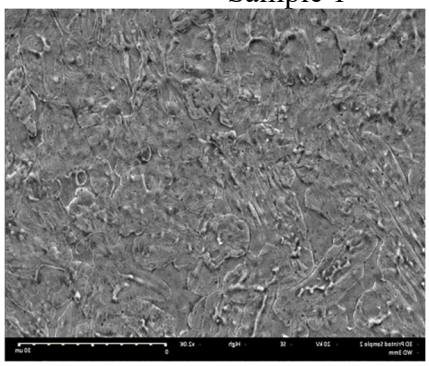

(b) Hardened zone - Sample 2

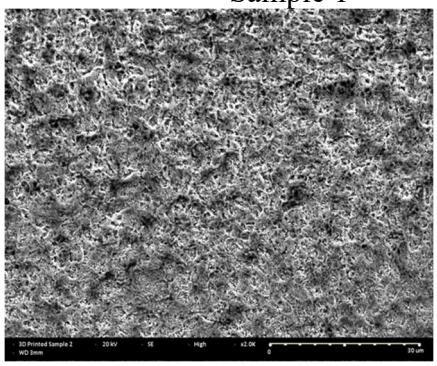

(c) Heat affected zone - Sample 2

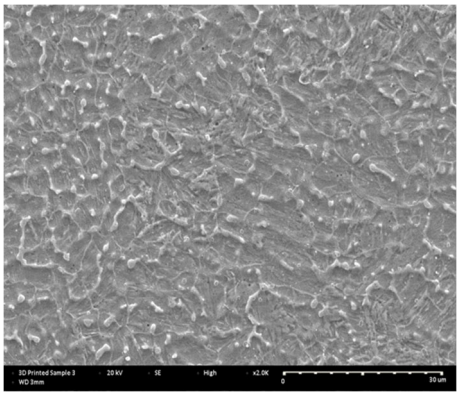

(a) Top surface - Sample 3

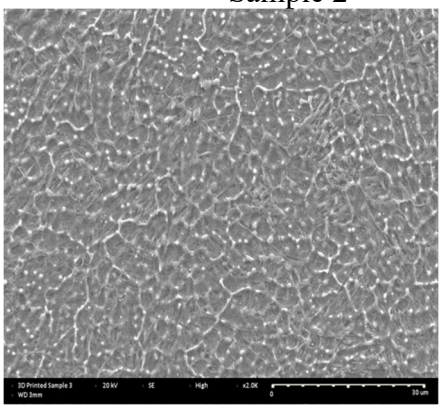

(b) Hardened zone - Sample 3

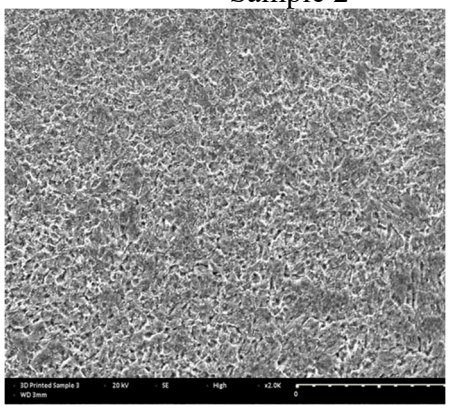

(c) Heat affected zone - Sample 3

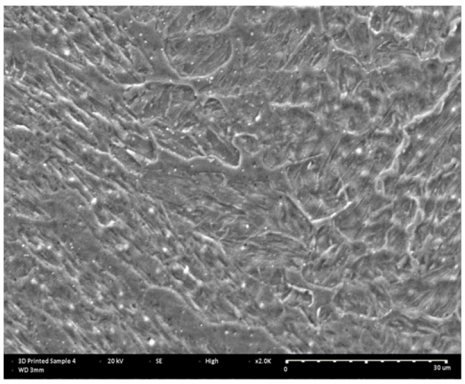

(a) Top surface - Sample 4

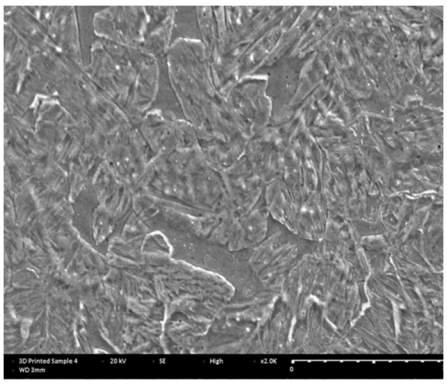

(b) Sample 4- Hardened zone

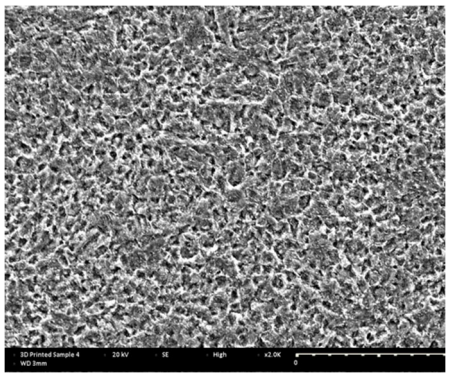

(c) Sample 4- Heat affected zone

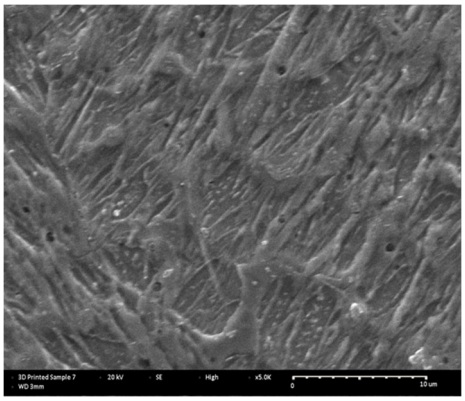

(a) Top surface - Sample 5

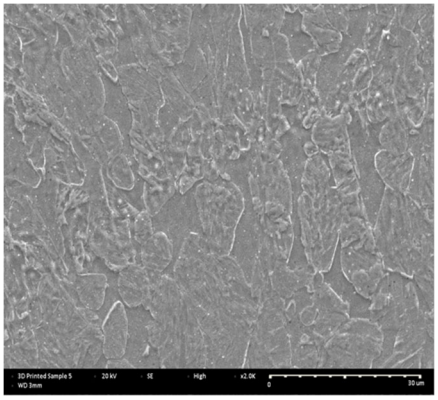

(b) Hardened zone - Sample 5

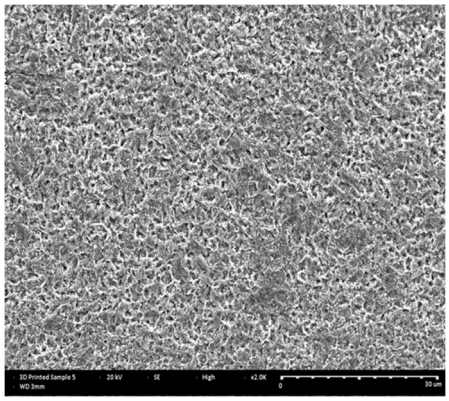

(c) Heat affected zone - Sample 5

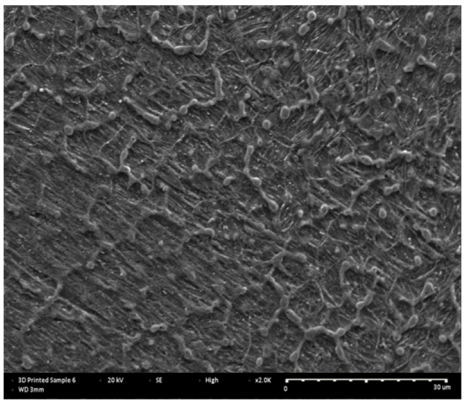

(a) Top surface - Sample 6

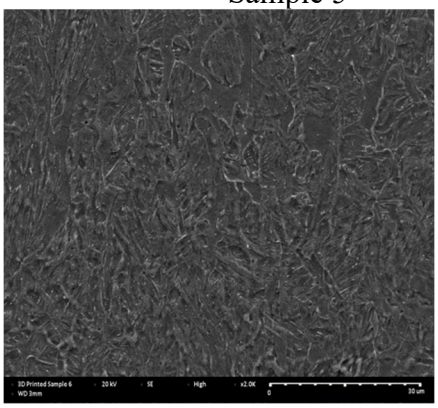

(b) Hardened zone - Sample 6

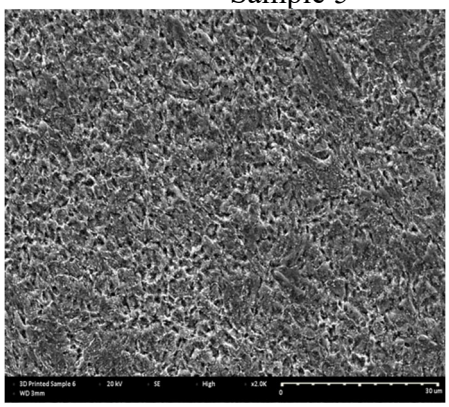

(c) Heat affected zone - Sample 6

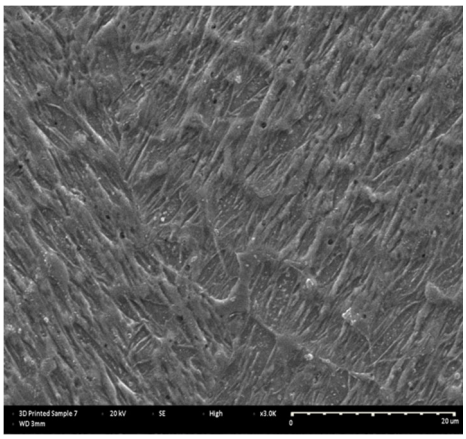

(a) Top surface - Sample 7

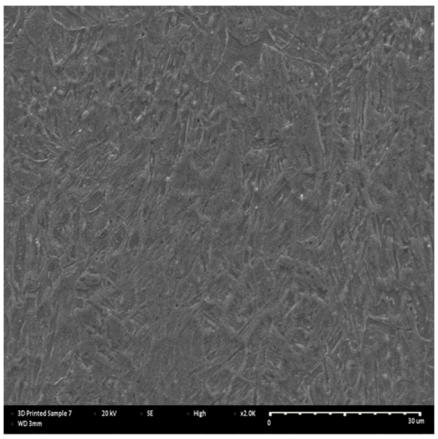

(b) Hardened zone - Sample 7

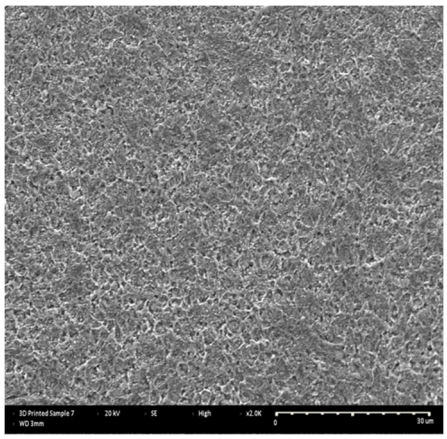

(c) Heat affected zone - Sample 7

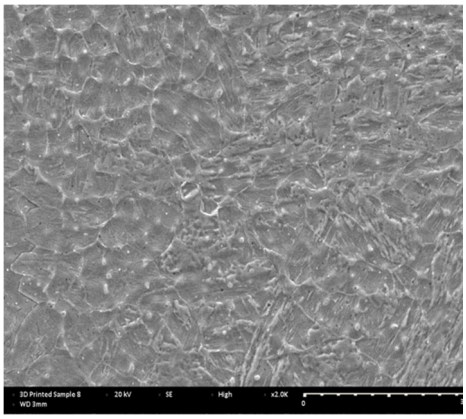

(a) Top surface - Sample 8

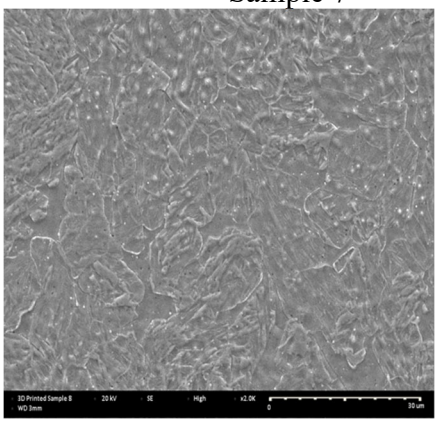

(b) Hardened zone - Sample 8

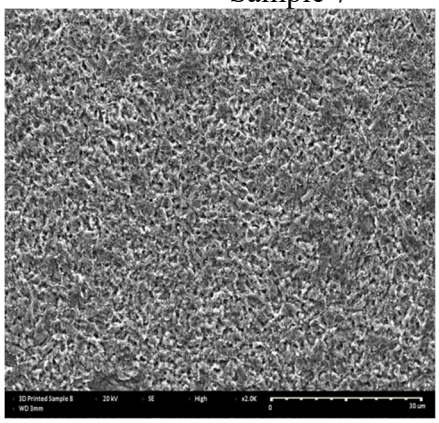

(c) Heat affected zone - Sample 8

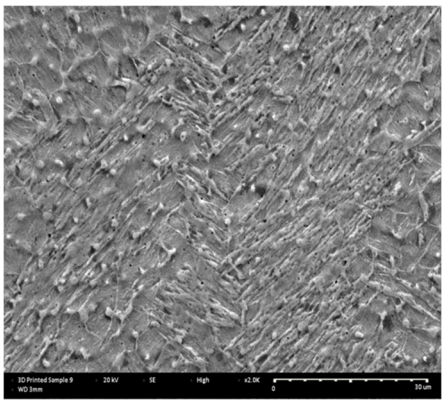

(a) Top surface - Sample 9

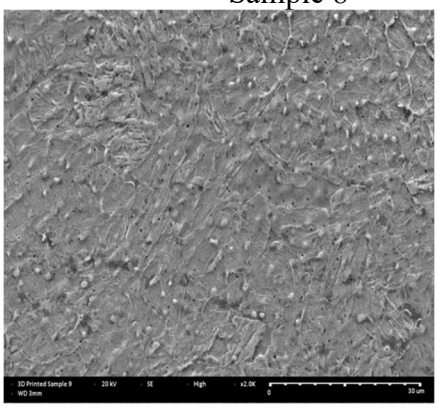

(b) Hardened zone - Sample 9

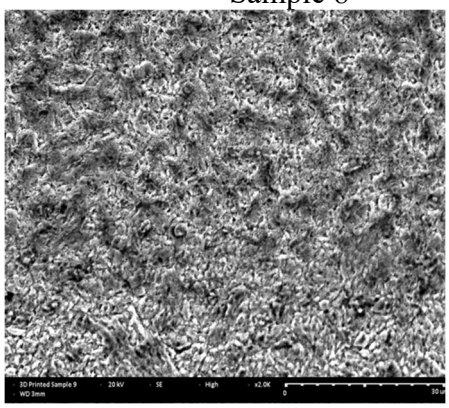

(c) Heat affected zone - Sample 9

Figure 3- 6: SEM of laser surface affected H13 tool steel

3.7.3 Microhardness profiles

The hardness is an important factor, a high hardness value increases resistance to friction and erosion wear. To obtain the depth profile, multiple measurement points were taken at intervals of 50 μm from the surface and perpendicular to it towards the inside of the specimen. Similarly, for the width profile, measurements were taken horizontally at intervals of 50 μm. The microhardness of the as built H13 tool steel is 56,35 HRC, the stress relief, quenching and tempering heat treatment reduced the microhardness to 42-44 HRC. Based on the data presented in the provided charts below Figure 3- 7, Figure 3- 8, Figure 3- 9, Figure 3- 10, Figure 3- 11 and Figure 3- 12, the nine parameter sets demonstrate a consistent trend in hardness distribution for both the width and depth profiles. The main difference lies in the highest recorded hardness value and the dimensions of the laser-transformed zone. The micro hardness profile of a laser-treated surface typically exhibits variations across different regions. These variations can be attributed to the specific parameters used during the laser melting process and the resulting microstructural changes. As depicted in the figures, the micro-hardness profile can be categorized into four distinct regions. The first region corresponds to the melted zone, characterized by the presence of dendrite cells. In this zone, the microhardness is relatively higher compared to the substrate material. The second region, known as the hardened zone, exhibits the highest hardness value among the nine samples. This zone experiences complete austenitization and subsequent transformation into martensite during rapid cooling. The third region is the over-tempered zone, which demonstrates a significant reduction in hardness compared to the initial hardness the hardness value undergoes to 38 HRC. This decrease in hardness can be attributed to the tempering process. Finally, the fourth region represents the base material, which remains unaffected by the heat flux and maintains its original hardness.

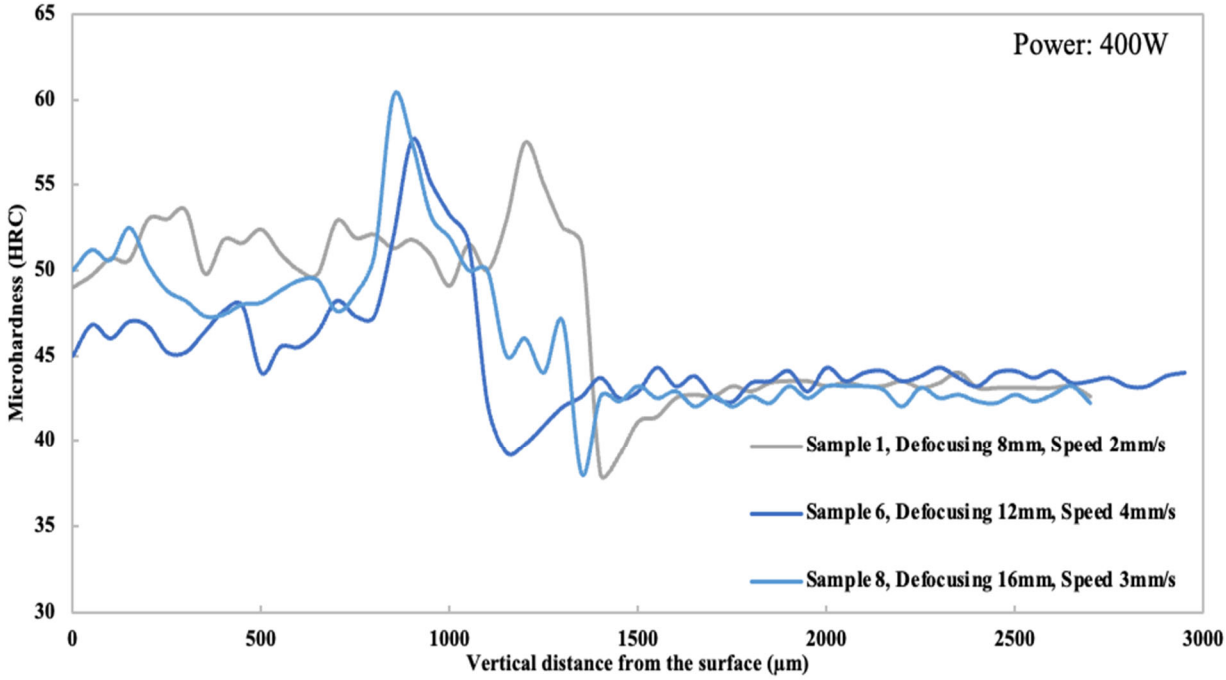

Figure 3- 7: Microhardness profile of the depth (400W)

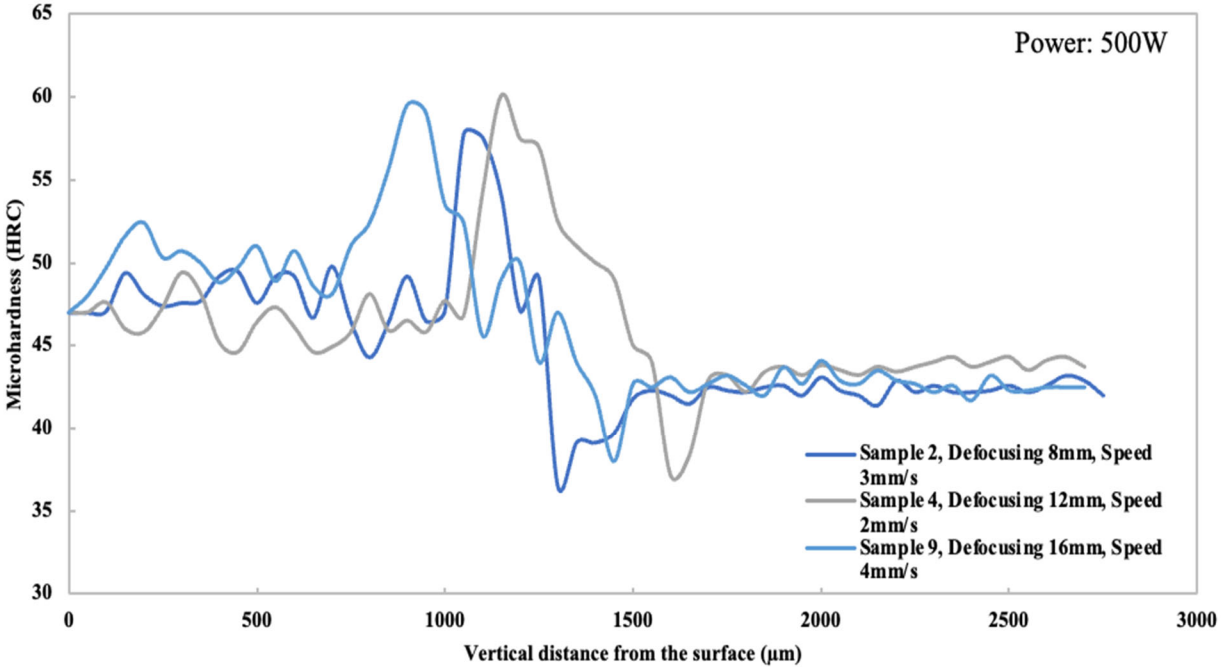

Figure 3- 8: Microhardness profile of the depth (500W)

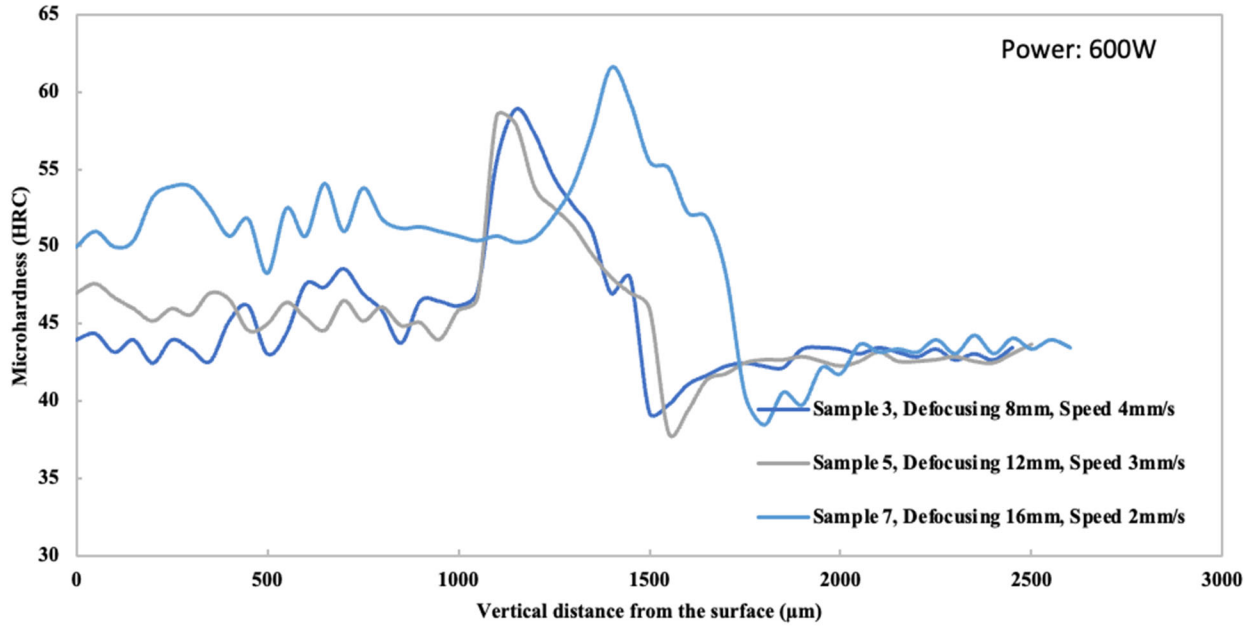

Figure 3- 9: Microhardness profile of the depth (600W)

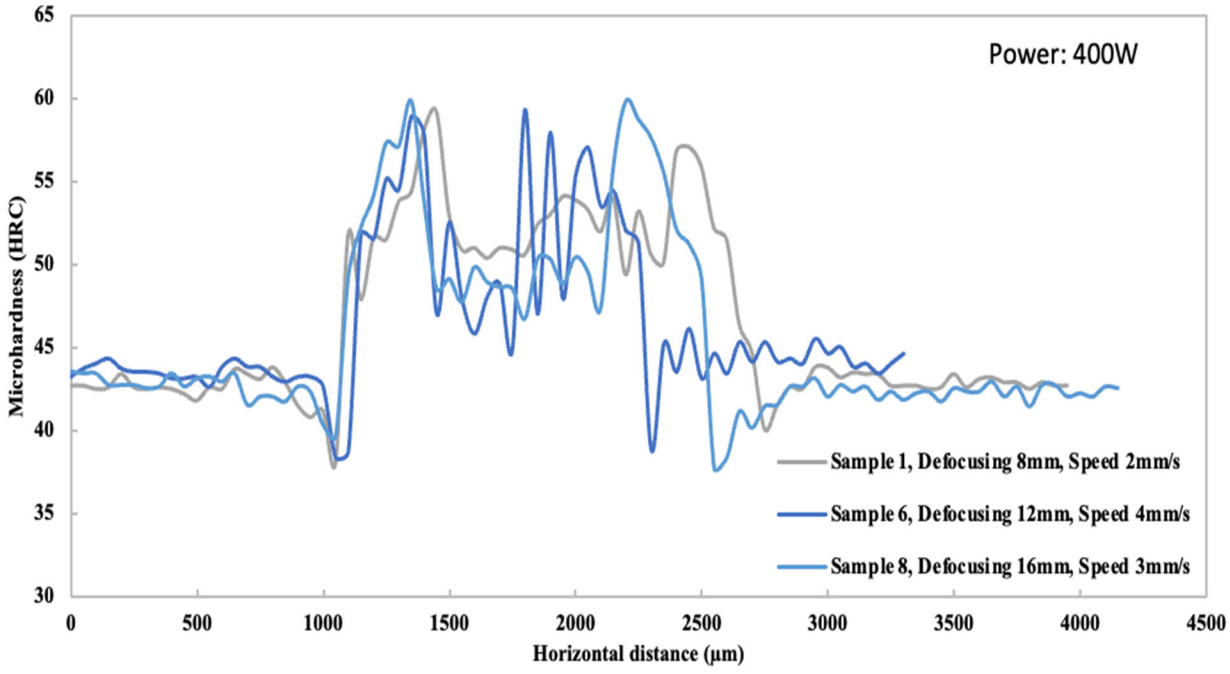

Figure 3- 10: Microhardness profile of the width (400W)

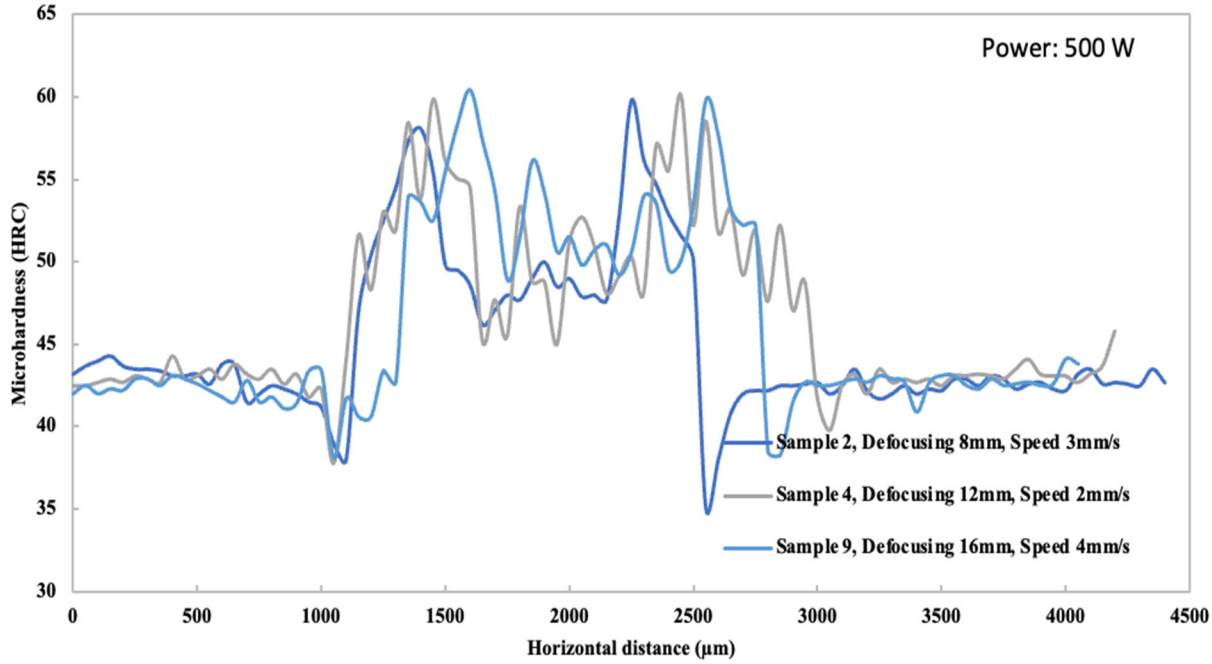

Figure 3- 11: Microhardness profile of the width (500W)

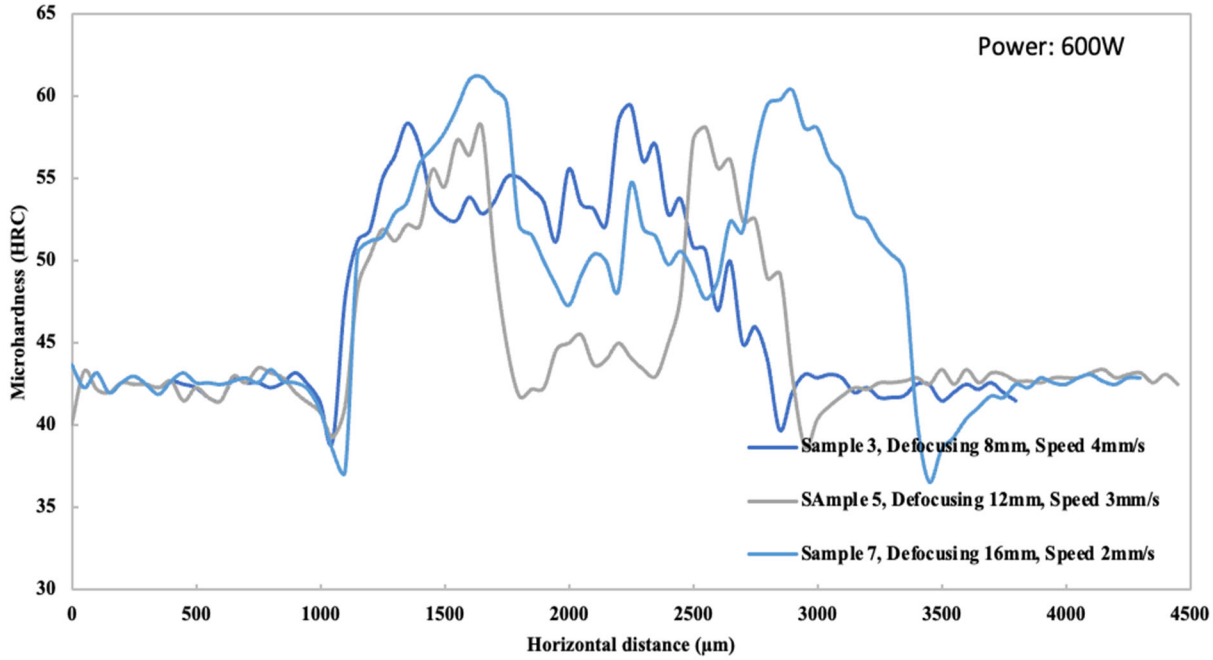

Figure 3- 12: Microhardness profile of the width (600W)

3.7.4 The maximum values of hardness

Table 3- 5 displays the maximum microhardness values observed throughout the depth and width profiles of the laser-treated surface for each specific set of laser parameters. Additionally, the corresponding depth and width values are provided.

The microstructure plays a significant role in determining the hardness profile. The increase in hardness observed in the melting/hardened zone of the surface can be attributed to the precipitation of fine carbides and the martensitic transformation that occurs during rapid cooling. When the temperature exceeds the melting point, a cellular microstructure composed of supersaturated martensite forms. This phase is relatively soft and ductile, resulting in a lower hardness compared to the hardened zone, where the material did not reach the melting point. Instead, it was heated above the Ac3 point, leading to the formation of lath martensite and fine carbides. This combination makes the material hard and brittle. Regarding the depth profile, across all nine parameter sets, the highest hardness values were consistently observed in the hardened zone, ranging from 61.6 to 57.5 HRC. On the other hand, in terms of the width profile, the maximum hardness varied from 61.2 to 58.1 HRC. These findings highlight the influence of both microstructure and processing parameters on the resulting hardness distribution across the treated surface.

The depth and width of the laser-treated surface of H13 tool steel refers to the measurement of how far below the surface and extended the laser treatment has penetrated and affected the material where changes in microstructure hardness, and other material properties occur. The depth value varied depending on the specific laser parameters employed during the surface treatment. The range of depth values observed in the laser-treated surface of H13 can be described as falling between 1.30 mm and 1.8 mm. For the width value varied from 1.26 mm to 2.4 mm. The maximum values of microhardness, depth and width values are attributed to the simple 7 with high laser power of 600W and lower scanning speed of 2mm/s and higher defocusing distance of 16mm.

Table 3- 5: Depth, width, and maximum microhardness values for the nine sets of laser parameters

	Levels of process parameters			Responses			
Test	Defocus distance (mm)	**Scanning speed (mm/s)**	**Power (W)**	**Width**	**Depth**	**Maximum hardness (depth)**	**Maximum hardness (width)**
1	8	2	400	1,70	1,40	57,7	59,2
2	8	3	500	1,45	1,30	57,8	59,8
3	8	4	600	1,80	1,50	58,9	59,3
4	12	2	500	2,00	1,60	60,1	60,1
5	12	3	600	1,90	1,55	58,4	58,1
6	12	4	400	1,26	1,15	57,6	59,3
7	16	2	600	2,40	1,80	61,6	61,2
8	16	3	400	1,60	1,35	60,2	59,8
9	16	4	500	1,75	1,45	59,5	60,4

3.8 STATISTICAL ANALYSIS:

In the initial phase of the study, a preliminary investigation was conducted to explore the effects of laser parameters on various outcomes. However, this exploration did not delve into the intricate details concerning the relationship between the experimental variables or provide specific numerical values for each factor's contribution. To achieve a more comprehensive understanding, a statistical analysis is required. ANOVA, or analysis of variance, encompasses a range of statistical techniques used to compare variances. Its primary application involves comparing differences in means by utilizing variance estimates [45].

ANOVA, a statistical tool that accommodates more than two factors, is employed in this study for several purposes. Firstly, it allows for the analysis of each factor's impact on the responses, aiding in the identification of the factors that exert a significant influence on the results. Secondly, ANOVA facilitates the quantification of each parameter's contribution to the overall variation observed in the data. Lastly, it enables the examination of mean differences, which can provide valuable insights into how different factors affect the outcome results. The ANOVA table includes essential statistical measures such as the F-statistic, degree of freedom, p-value, and more. The primary focus of ANOVA analysis is the p-value, which determines the statistical significance of the mean differences between the compared groups. A p-value lower than the predetermined significance level (0,05) indicates the significance of the analysis.

3.8.1 Effect of laser parameters on the depth of the laser treated zone

ANOVA takes the experimental results as input and provides valuable output, including the contribution of each factor, the degrees of freedom (dof) representing the independent factors in the regression model, the sequential sums of squares (Seq SS) that quantify variation in different components of the model. The F-value serves as a test statistic to determine the association between the term and the response. Additionally, the p-value signifies the probability that measures the level of proof opposing the idea of no significant difference. Table 3- 6, presents the ANOVA table which examines the impact of laser parameters on the depth, Notably, the error value is quite small, measuring 0,02347. This indicates that the variation observed in the output results primarily stems from the input parameters. Therefore, the input parameters play a crucial role in determining the depth of the affected area because de p values are less than 0,05 but for the defocusing distance.

Table 3- 6: ANOVA table for the depth of laser treated surface

Characteristic	Sum of squares	Dof	F-Value	P-value
Defocusing distance	0,02667	1	5,68	0,063
Scanning Speed	0,08167	1	17,40	0,009
Power	0,15042	1	32,04	0,002
Error	0,02347	5		
Total	0,28222	8		

Table 3- 7 provides insights into the specific contributions of each parameter on the depth. It reveals that the scanning speed and laser power have the most significant effects. The laser power contributes 53,30% to the outcome results, while the scanning speed contributes 28,94%. On the other hand, the defocusing distance has a comparatively lower contribution of only 9,45%. For both the scanning speed and laser power, the p-values are less than the significance level of 0,05. This signifies that the statistical results are considered significant and reliable, providing strong evidence against the null hypothesis.

Table 3- 7: Contribution of laser parameters on the Depth value

Characteristic	Defocus distance	Scanning speed	Power	Error
Contribution (%)	9,45	28,94	53,30	8,32

Figure 3- 13 visually illustrates the behavior of the depth in relation to the laser parameters. It clearly demonstrates that the depth increases with higher laser power and defocusing distance, while it decreases with a higher scanning speed. This graphical representation further reinforces the observed relationships between the laser parameters and the resulting depth.

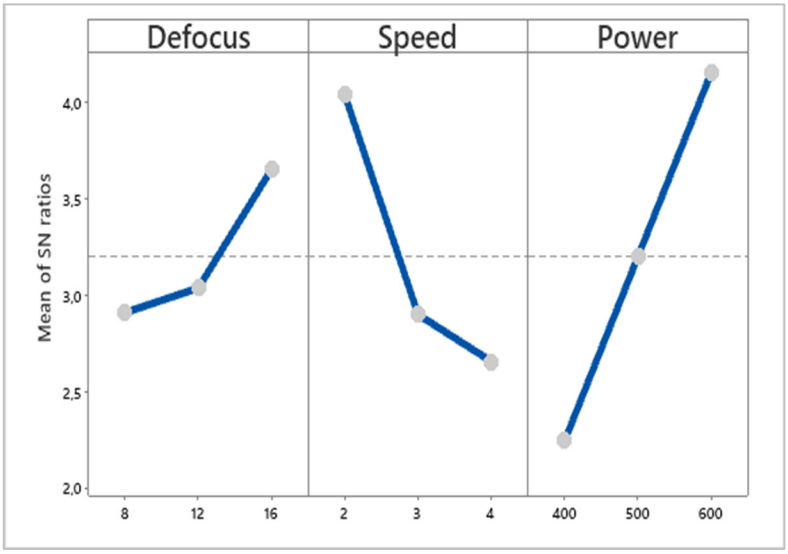

Figure 3- 13: Effect of laser parameters on the Depth of laser treated surface (D in mm, S in mm/s and P in W)

3.8.1.1 Regression equation:

The ANOVA analysis not only provides an ANOVA table but also yields a linear regression equation. In the case of multiple linear regression, the equation comprises an output variable that is computed based on the input parameters, with coefficients determined using the method of least squares.

Equation (3. 1) presents the regression equation for the obtained model in the following range of parameters:

Power (W): $[400 - 600]$; Scanning Speed (mm/s): $[2 - 4]$; Defocus distance (mm): $[8 - 12]$.

$$depth = 0{,}814 + 0{,}01667D - 0{,}1167S + 0{,}001583P \quad (3.\ 1)$$

The regression equation enables predictions of the results based on the specified levels of parameters used in the previous design of experiments (DOE) Figure 3- 14 illustrates the comparison between the predictions and the actual experimental outcomes. As shown in the

chart both predicted and experimental outcomes display one axis and the test numbers on the other. Based on the analysis, it can be inferred that the predicted model demonstrates reliability and agreement with the experimental results.

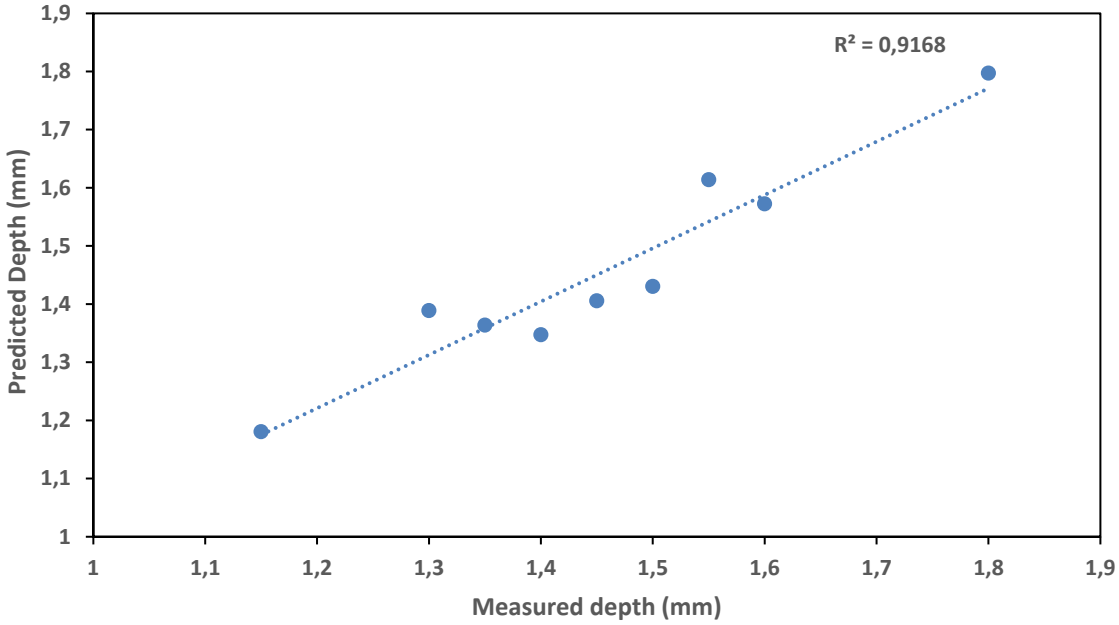

Figure 3- 14: Predicted value VS Experimental data for the depth

3.8.1.2 Response surface method

The purpose of the response surface method is to model and optimize complex relationships between input variables (factors) and the response variable of interest. The process includes creating various experiments, gathering information, and applying statistical methods to create a mathematical model that estimates how the input variables and response are related. This model can then be analyzed and used to make predictions, understand the influence of the input variables, and identify optimal settings or conditions for the response variable. The response surface method is particularly useful when there are multiple factors that interact with each other, and it helps in efficiently exploring the design space to achieve the desired response.

The findings in Figure 3- 15 indicate that under constant power at 500W, higher depth values are obtained by employing a larger defocusing distance and reducing the scanning speed. On the other hand, when maintaining the scanning speed at 3 mm/s, elevated depth values can be achieved by using both high laser power and a larger defocusing distance. Notably, when the defocusing distance is set to 12 mm, higher depth values can be attained by utilizing high power while simultaneously decreasing the scanning speed. These relationships highlight the importance of carefully controlling the laser power, scanning speed, and defocusing distance to optimize depth outcomes in the studied process.

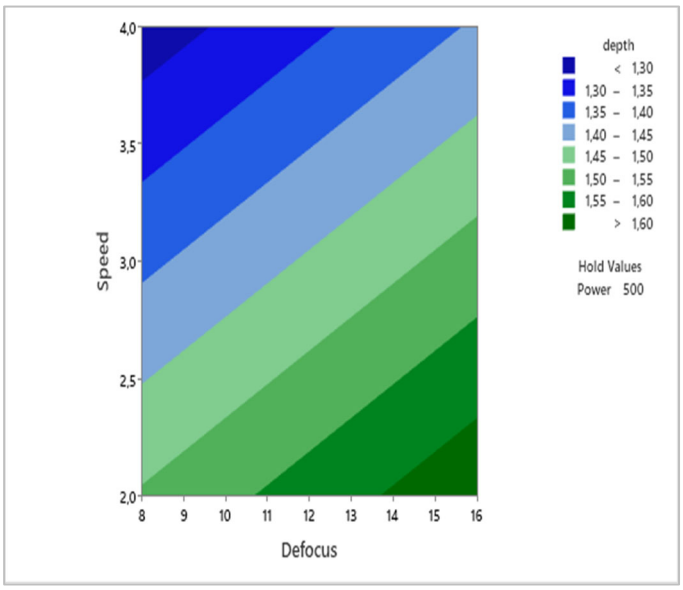

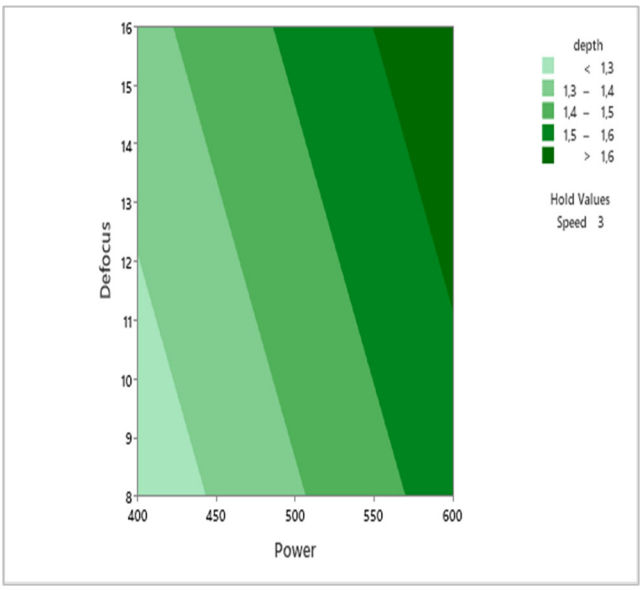

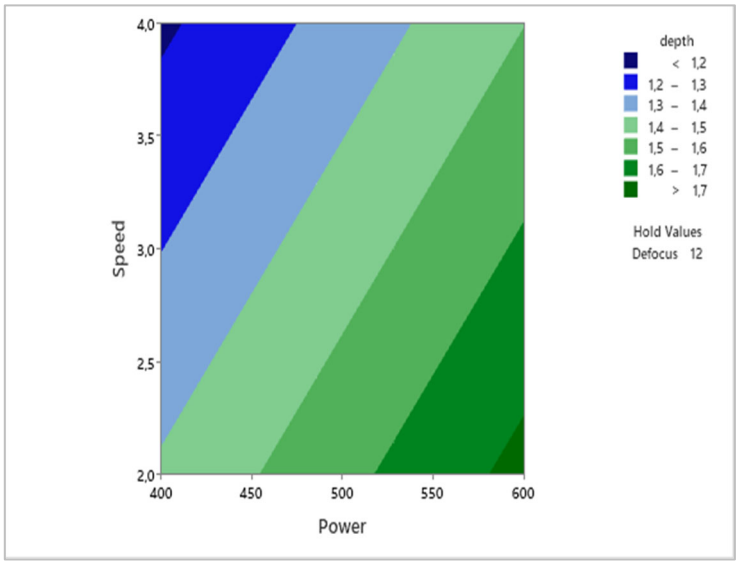

Figure 3- 15: RSM for the Depth (D in mm, S in mm/s and P in W)

3.8.2 Effect of laser parameters on the width of the laser treated zone

3.8.2.1 ANOVA table

The analysis of both Table 3- 8 and Table 3- 9, clearly indicates that the laser power significantly influences the width of laser treated zone, In fact, it demonstrates the highest contribution of 54,76% among all the parameters considered. The low P-value (0,005) associated with the power reinforces the reliability of the study. Additionally, the scanning speed contributes to the outcome with 32,11%, and its P-value satisfies the requirement to reject the null hypothesis. Although the defocusing distance has a slightly lower contribution 12,35% and a P-value of 0,054, it is still considered in the model as this is an initial and exploratory.

Table 3- 8: ANOVA table for the width of laser treated surface

Characteristic	Sum of squares	Dof	F-Value	P-value
Defocus distance	0,10667	1	6,31	0,054
Scanning Speed	0,27735	1	16,42	0,010
Power	0,39527	1	23,40	0,005
Error	0,08447	5		
Total	0,86376	8		

Table 3- 9: Contribution of laser parameters on the width value

Characteristic	Defocus distance	Scanning speed	Power	Error
Contribution (%)	12,35	32,11	45,76	9,78

Figure 3- 16, provides a visual representation of the width's behavior in relation to the laser parameters. it shows that increasing the laser power and defocusing distance leads to an increase in the width. Conversely, a higher scanning speed is associated with a decrease in the width. This graphical depiction solidifies the observed correlations between the laser parameters and the resulting width.

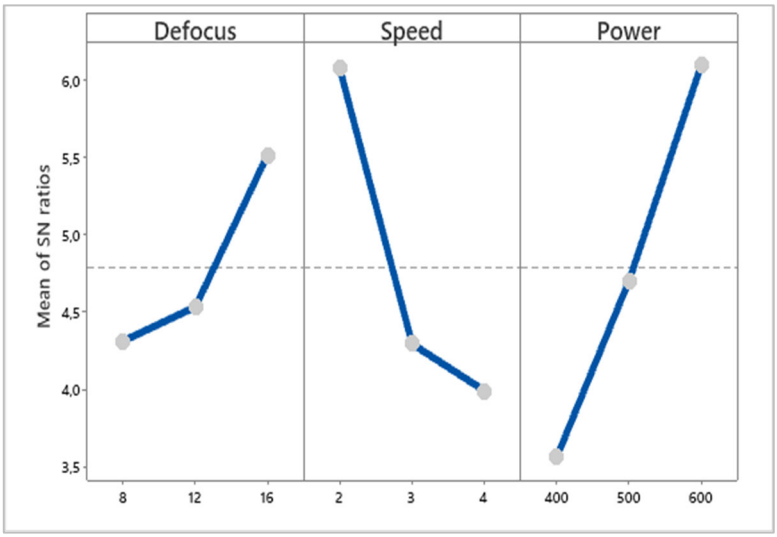

Figure 3- 16: Effect of laser parameters on the width of laser treated surface (D in mm, S in mm/s and P in W)

3.8.2.2 Regression Equation

The ANOVA analysis, a robust statistical method for data analysis, not only allows us to examine the data but also provides regression equations for the width. These equations are utilized to determine whether there is a relationship between different data sets. The equation presented below (3. 2) demonstrates an empirical relationship between the width and various laser process parameters, such as laser power, scanning speed, and defocusing distance in the following range of parameters:

Power (W): $[400 - 600]$; Scanning Speed (mm/s): $[2 - 4]$; Defocus distance (mm): $[8 - 12]$

$$Width = 0{,}724 + 0{,}0333D - 0{,}2150S + 0{,}002567P \quad (3.\ 2)$$

Figure 3- 17, provides a detailed comparison between the predicted and experimental data, enabling a thorough assessment of the accuracy and reliability of the predictive model. This analysis allows us to evaluate how closely the predicted values align with the actual

measurements obtained through experimentation. By analysing the level of agreement between the predicted and experimental data points, the model is accurate and reliable.

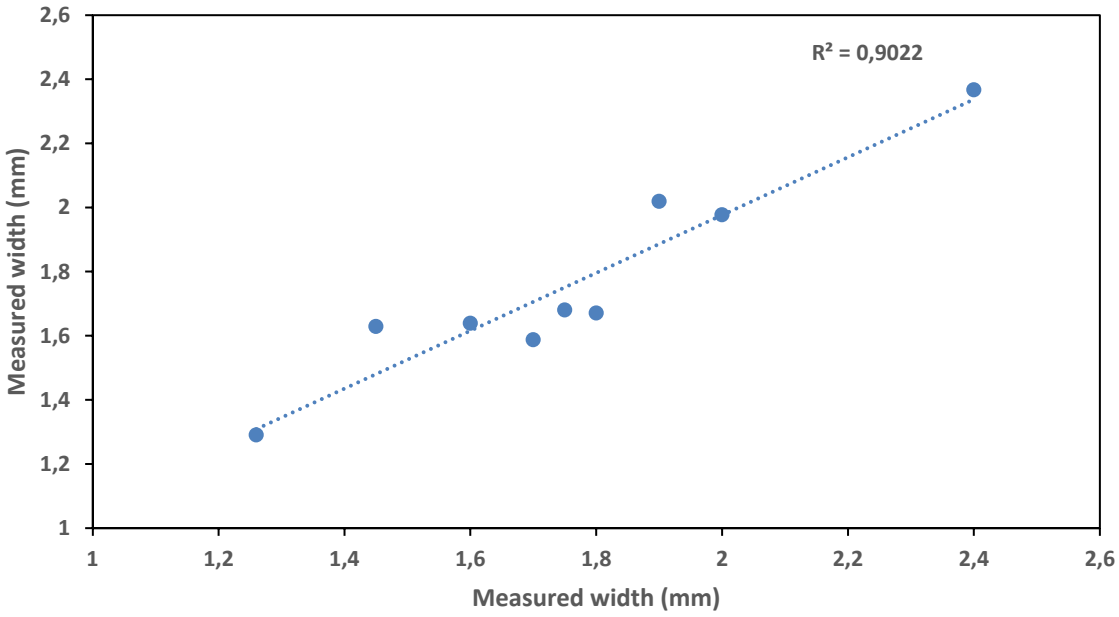

Figure 3- 17: Predicted value VS experimental data for the width

3.8.2.3 Response surface method

The results presented in Figure 3- 18 provide valuable insights into the relationship between various laser parameters and width values. When the laser power is held constant at 500W, it is observed that increasing the defocusing distance and reducing the scanning speed lead to higher width values. Conversely, when the scanning speed is maintained at 3 mm/s, achieving elevated width values can be accomplished by employing both high laser power and a larger defocusing distance. Notably, when the defocusing distance is set to 12 mm, higher width values can be obtained by utilizing high power while simultaneously decreasing the scanning speed.

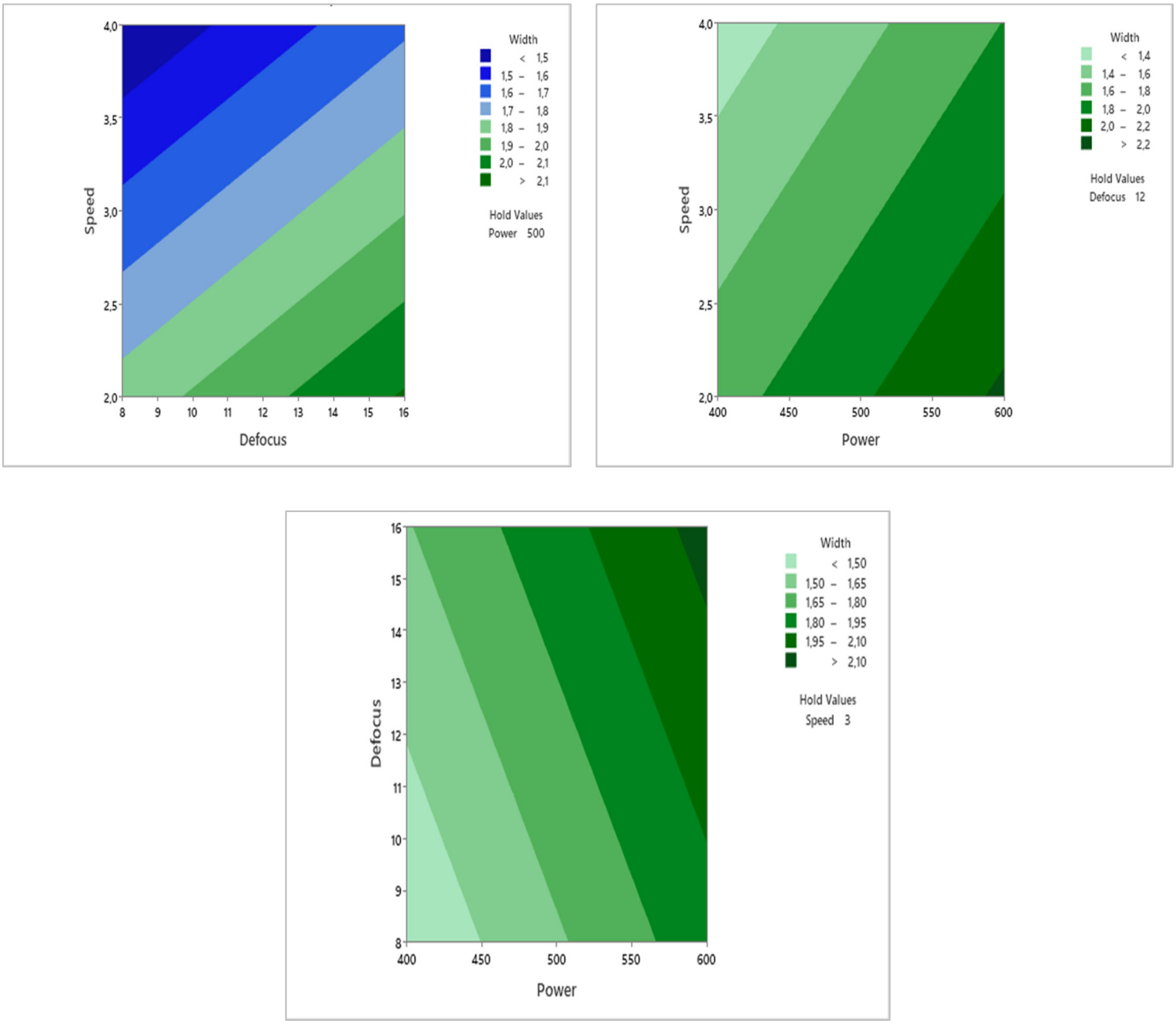

Figure 3- 18: RSM for the Width (D in mm, S in mm/s and P in W)

3.9 CONCLUSION

The following statement are concluded from this essay:

- The microstructure of the as built H13 tool steel is analyzed using SEM, it reveals that the microstructure is heterogenous and combines a fine cellular and columnar structure which mainly due to the high thermal gradient during the SLM process.
- The microstructure of stress relieved, quenched and tempered SLM H13 is also examined, the heterogenous microstructure is dissolved, and any retained austenite is transformed.
- The laser surface treatment displayed three distinct regions, a melted, hardened and heat affected zone.
- According to the microhardness measurements the base material achieved 42-44 HRC after the heat treatment procedure.
- The microhardness profile of the depth and width of the nine sets of the laser parameters has the same pace, the remaining difference is the highest values of the hardness and the depth and width values of the laser treated area.
- The highest values of the microhardness are detected in the hardened zones of the depth and width among the nine sets, the maximum values for the depth range from 61.6-57.5 HRC, and for the width the values varied from 61.2-58.1 HRC.
- For the nine sets the depth varied from 1.3-1.8 mm, and the width from 1.26-2.4 mm.
- The statistical analysis using ANOVA of the effect of laser parameters on the depth value of the treated zone revealed that the laser power contributes 53.30% to the outcome results, while the scanning speed contributes 28.94% and the defocusing distance has a comparatively lower contribution of only 9.45%.

- For the width, the ANOVA analysis mentioned that the highest contribution of 54.76% is attributed to the laser power, the scanning speed contributes to the outcome with 32.11%, Although the defocusing distance has a slightly lower contribution 12.35%.

3.10 REFERENCES:

1. Gibson, I., D. Rosen, B. Stucker, M. Khorasani, D. Rosen, B. Stucker, and M. Khorasani, *Additive manufacturing technologies*. Vol. 17. 2021: Springer.
2. Pérez, M., D. Carou, E.M. Rubio, and R. Teti, *Current advances in additive manufacturing.* Procedia CIRP, 2020. **88**: p. 439-444.
3. Liu, J., V. Nguyen-Van, B. Panda, K. Fox, A. du Plessis, and P. Tran, *Additive manufacturing of sustainable construction materials and form-finding structures: a review on recent progresses.* 3D Printing and Additive Manufacturing, 2022. **9**(1): p. 12-34.
4. Oter, Z.C., M. Coskun, Y. Akca, Ö. Sürmen, M.S. Yılmaz, G. Özer, G. Tarakçı, and E. Koc, *Benefits of laser beam based additive manufacturing in die production.* Optik, 2019. **176**: p. 175-184.
5. Mohd Yusuf, S., S. Cutler, and N. Gao, *The impact of metal additive manufacturing on the aerospace industry.* Metals, 2019. **9**(12): p. 1286.
6. Ahn, D.-G., *Direct metal additive manufacturing processes and their sustainable applications for green technology: A review.* International Journal of Precision Engineering and Manufacturing-Green Technology, 2016. **3**: p. 381-395.
7. Ngo, T.D., A. Kashani, G. Imbalzano, K.T.Q. Nguyen, and D. Hui, *Additive manufacturing (3D printing): A review of materials, methods, applications and challenges.* Composites Part B: Engineering, 2018. **143**: p. 172-196.
8. Oros Daraban, A.E., C.S. Negrea, F.G. Artimon, D. Angelescu, G. Popan, S.I. Gheorghe, and M. Gheorghe, *A deep look at metal additive manufacturing recycling and use tools for sustainability performance.* Sustainability, 2019. **11**(19): p. 5494.
9. Omidi, N., P. Farhadipour, L. Baali, K. Bensalem, N. Barka, and M. Jahazi, *A Comprehensive Review of Additively Manufactured H13 Tool Steel Applicable in the Injection Mold Industry: Applications, Designs, Microstructure, Mechanical Properties.* JOM, 2023.
10. Mazur, M., P. Brincat, M. Leary, and M. Brandt, *Numerical and experimental evaluation of a conformally cooled H13 steel injection mould manufactured with selective laser melting.* The International Journal of Advanced Manufacturing Technology, 2017. **93**: p. 881-900.

11. Mazur, M., M. Leary, M. McMillan, J. Elambasseril, and M. Brandt, *SLM additive manufacture of H13 tool steel with conformal cooling and structural lattices.* Rapid Prototyping Journal, 2016. **22**(3): p. 504-518.
12. Klocke, F., K. Arntz, M. Teli, K. Winands, M. Wegener, and S. Oliari, *State-of-the-art laser additive manufacturing for hot-work tool steels.* Procedia Cirp, 2017. **63**: p. 58-63.
13. Nandhakumar, R. and K. Venkatesan, *A process parameters review on selective laser melting-based additive manufacturing of single and multi-material: Microstructure, physical properties, tribological, and surface roughness.* Materials Today Communications, 2023. **35**: p. 105538.
14. Savrai, R.A., D.V. Toporova, and T.M. Bykova, *Improving the quality of AISI H13 tool steel produced by selective laser melting.* Optics & Laser Technology, 2022. **152**: p. 108128.
15. Cottam, R., J. Wang, and V. Luzin, *Characterization of microstructure and residual stress in a 3D H13 tool steel component produced by additive manufacturing.* Journal of Materials Research, 2014. **29**(17): p. 1978-1986.
16. Ren, B., D. Lu, R. Zhou, Z. Li, and J. Guan, *Preparation and mechanical properties of selective laser melted H13 steel.* Journal of Materials Research, 2019. **34**(8): p. 1415-1425.
17. Véle, F., M. Ackermann, V. Bittner, and J. Šafka, *Influence of selective laser melting technology process parameters on porosity and hardness of AISI H13 tool steel: statistical approach.* Materials, 2021. **14**(20): p. 6052.
18. DebRoy, T., H.L. Wei, J.S. Zuback, T. Mukherjee, J.W. Elmer, J.O. Milewski, A.M. Beese, A. Wilson-Heid, A. De, and W. Zhang, *Additive manufacturing of metallic components – Process, structure and properties.* Progress in Materials Science, 2018. **92**: p. 112-224.
19. Bidare, P., A. Jiménez, H. Hassanin, and K. Essa, *Porosity, cracks, and mechanical properties of additively manufactured tooling alloys: a review.* Advances in Manufacturing, 2022. **10**(2): p. 175-204.
20. Tan, Q., Y. Yin, F. Wang, H. Chang, S. Liu, G. Liang, T. Wu, and M.-X. Zhang, *Rationalization of brittleness and anisotropic mechanical properties of H13 steel fabricated by selective laser melting.* Scripta Materialia, 2022. **214**: p. 114645.
21. Mahmood, M.A., D. Chioibasu, A. Ur Rehman, S. Mihai, and A.C. Popescu, *Post-Processing Techniques to Enhance the Quality of Metallic Parts Produced by Additive Manufacturing.* Metals, 2022. **12**(1): p. 77.
22. Ge, J., S. Pillay, and H. Ning, *Post-Process Treatments for Additive-Manufactured Metallic Structures: A Comprehensive Review.* Journal of Materials Engineering and Performance, 2023.
23. Peng, X., L. Kong, J.Y.H. Fuh, and H. Wang, *A Review of Post-Processing Technologies in Additive Manufacturing.* Journal of Manufacturing and Materials Processing, 2021. **5**(2): p. 38.
24. Maleki, E., S. Bagherifard, M. Bandini, and M. Guagliano, *Surface post-treatments for metal additive manufacturing: Progress, challenges, and opportunities.* Additive Manufacturing, 2021. **37**: p. 101619.

25. Narvan, M., K.S. Al-Rubaie, and M. Elbestawi, *Process-structure-property relationships of AISI H13 tool steel processed with selective laser melting.* Materials, 2019. **12**(14): p. 2284.
26. Bajaj, P., A. Hariharan, A. Kini, P. Kürnsteiner, D. Raabe, and E.A. Jägle, *Steels in additive manufacturing: A review of their microstructure and properties.* Materials Science and Engineering: A, 2020. **772**: p. 138633.
27. Wen, T., F. Yang, J. Wang, H. Yang, J. Fu, and S. Ji, *Ultrastrong and ductile synergy of additively manufactured H13 steel by tuning cellular structure and nano-carbides through tempering treatment.* Journal of Materials Research and Technology, 2023. **22**: p. 157-168.
28. Sun, Y., J. Wang, M. Li, Y. Wang, C. Li, T. Dai, M. Hao, and H. Ding, *Thermal and mechanical properties of selective laser melted and heat treated H13 hot work tool steel.* Materials and Design, 2022. **224**.
29. Laleh, M., E. Sadeghi, R.I. Revilla, Q. Chao, N. Haghdadi, A.E. Hughes, W. Xu, I. De Graeve, M. Qian, I. Gibson, and M.Y. Tan, *Heat treatment for metal additive manufacturing.* Progress in Materials Science, 2023. **133**: p. 101051.
30. Wang, J., S. Liu, Y. Fang, and Z. He, *A short review on selective laser melting of H13 steel.* The International Journal of Advanced Manufacturing Technology, 2020. **108**: p. 2453-2466.
31. Yuan, M., Y. Cao, S. Karamchedu, S. Hosseini, Y. Yao, J. Berglund, L. Liu, and L. Nyborg, *Characteristics of a modified H13 hot-work tool steel fabricated by means of laser beam powder bed fusion.* Materials Science and Engineering A, 2022. **831**.
32. Yan, J., H. Song, Y. Dong, W.-M. Quach, and M. Yan, *High strength (~2000 MPa) or highly ductile (~11%) additively manufactured H13 by tempering at different conditions.* Materials Science and Engineering: A, 2020. **773**: p. 138845.
33. Bae, K., H.S. Moon, Y. Park, I. Jo, and J. Lee, *Influence of Tempering Temperature and Time on Microstructure and Mechanical Properties of Additively Manufactured H13 Tool Steel.* Materials, 2022. **15**(23).
34. Zanni, M., F. Berto, P.E. Vullum, L. Tonelli, A. Morri, and L. Ceschini, *Effect of heat treatment and defects on the tensile behavior of a hot work tool steel manufactured by laser powder bed fusion.* Fatigue and Fracture of Engineering Materials and Structures, 2023.
35. Jung, I.D., J. Choe, J. Yun, S. Yang, D.-Y. Yang, Y.-J. Kim, and J.-H. Yu, *Dual speed laser re-melting for high densification in H13 tool steel metal 3D printing.* Archives of Metallurgy and Materials, 2019: p. 571-578-571-578.
36. Kumar, S., S.R. Maity, and L. Patnaik, *Mechanical and Scratch behaviour of TiAlN Coated and 3D Printed H13 Tool Steel.* Advances in Materials and Processing Technologies, 2022. **8**(sup2): p. 337-351.
37. Deirmina, F., N. Peghini, B. AlMangour, D. Grzesiak, and M. Pellizzari, *Heat treatment and properties of a hot work tool steel fabricated by additive manufacturing.* Materials Science and Engineering: A, 2019. **753**: p. 109-121.
38. Fonseca, E.B., J.D. Escobar, A.H.G. Gabriel, G.G. Ribamar, T. Boll, and É.S.N. Lopes, *Tempering of an additively manufactured microsegregated hot-work tool*

steel: A high-temperature synchrotron X-ray diffraction study. Additive Manufacturing, 2022. **55**: p. 102812.
39. Law, W.K., K.-C. Wong, H. Wang, Z. Sun, and C.S. Lim, *Microstructure evolution in additively manufactured steel molds: a review.* Journal of Materials Engineering and Performance, 2021. **30**(9): p. 6389-6405.
40. Meng, C., C. Wu, X. Wang, J. Li, and R. Cao, *Effect of thermal fatigue on microstructure and mechanical properties of H13 tool steel processed by selective laser surface melting.* Metals, 2019. **9**(7): p. 773.
41. Bensalem, K., N. Barka, S. Sattarpanah Karganroudi, A. Sadeghian, and M. Moradi, *Effects of laser process parameters on the hardness profile of AISI 4340 cylindrical samples: statistical and experimental analyses.* The International Journal of Advanced Manufacturing Technology, 2022. **122**(7-8): p. 2849-2867.
42. Kasman, Ş. and I.E. Saklakoglu, *Determination of process parameters in the laser micromilling application using Taguchi method: A case study for AISI H13 tool steel.* The International Journal of Advanced Manufacturing Technology, 2012. **58**: p. 201-209.
43. Katancik, M., S. Mirzababaei, M. Ghayoor, and S. Pasebani, *Selective laser melting and tempering of H13 tool steel for rapid tooling applications.* Journal of Alloys and Compounds, 2020. **849**.
44. Krell, J., A. Röttger, K. Geenen, and W. Theisen, *General investigations on processing tool steel X40CrMoV5-1 with selective laser melting.* Journal of Materials Processing Technology, 2018. **255**: p. 679-688.
45. Allen, T.T. and T.T. Allen, *Software overview and methods review: Minitab.* Introduction to Engineering Statistics and Lean Six Sigma: Statistical Quality Control and Design of Experiments and Systems, 2019: p. 575-600.

CHAPITRE 4
ÉTUDE EXPÉRIMENTALEET STATISTIQUE DU COMPORTEMENT MÉCANIQUE DE L'ACIER À OUTILS H13 FABRIQUÉ ADDITIVEMENT ET TRAITÉ AU NIVEAU DE LA SURFACE AU LASER

Lamya Baali[1], Noureddine Barka[1], Asim Iltaf[1], Véronique Dassylva-Raymond[1]

[1]Mathematics, Computer Science and Engineering Department, Université du Québec à Rimouski (UQAR), 300 Allée des Ursulines, Rimouski, QC G5L 3A1, Québec, Canada

Cet article a été soumis dans Bioceramics, Biocomposites, biomaterials : engineering application and applied research portant le numéro de référence 9783036402451`

4.1 RESUME EN FRANÇAIS DU PREMIER ARTICLE

L'acier à outils H13 est couramment utilisé pour les applications d'outillage de travail à chaud, ce qui nécessite des propriétés mécaniques spécifiques et une bonne qualité de surface Dans cette étude, l'acier à outils H13 a été fabriqué en utilisant les paramètres de fusion laser sélective (SLM) suivants : puissance laser de 125 W, vitesse de balayage de 800 mm/s, épaisseur de couche de 40 mm, et un espacement de 0,12 mm entre les couches. Après le processus de SLM, le matériau H13 a été soumis à un traitement thermique spécifique. Ce traitement a débuté par la réduction des contraintes résiduelles à 650 °C pendant huit heures, suivi d'une austénitisation à 1000 °C pendant 30 minutes, puis d'une trempe à l'huile. Enfin, il s'est conclu par un revenu à 650 °C pendant une heure afin d'éliminer toutes les contraintes résiduelles potentielles. Étant donné que la surface est une source majeure de défauts pour

les moules, un traitement thermique de surface au laser a été appliqué selon un plan expérimental contrôlant la puissance du laser, la vitesse de balayage, et la distance de défocalisation. Les résultats ont montré que le traitement au laser a eu un impact positif sur la résistance ultime à la traction (UTS), l'améliorant de manière significative par rapport aux échantillons ayant subi uniquement un traitement thermique. Cependant, il a été observé que l'allongement à la rupture diminuait. L'analyse du mode de fracture a également été effectuée à l'aide d'un microscope électronique à balayage (MEB).

4.2 CONTRIBUTIONS

Ce premier article, intitulé « Experimental and Statistical Study of the Mechanical Behavior of H13 Tool Steel Additively Manufactured and Laser Surface Treated » a principalement été rédigé par Lamya Baali, son premier auteur. Noureddine Barka, le deuxième auteur, occupe la fonction de directeur de recherche et a joué un rôle clé dans la définition du projet et de la méthodologie adoptée. Le troisième auteur, Asim Iltaf, a apporté une contribution essentielle à l'amélioration de l'article. Enfin, Véronique Dassylva-Raymond a supervisé le travail et a également contribué à améliorer la rédaction globale.

4.3 TITRE DU PREMIER ARTICLE

Experimental and Statistical Study of the Mechanical Behavior of H13 Tool Steel Additively Manufactured and Laser Surface Treated.

4.4 ABSTRACT

H13 tool steel is commonly used for hot work tooling applications, which requires specific mechanical properties and good surface quality. In this study, H13 tool steel was manufactured using the parameters selective laser melting (SLM) systems: laser power of 125 W, scanning speed of 800 mm/s, layer thickness of 40 mm, and spacing of 0.12 mm between layers. After the SLM process, the H13 material was subjected to a specific heat

treatment. This treatment began with residual stress reduction at 650°C for eight hours, followed by austenitization at 1000°C for 30 minutes, then oil quenching. Finally, it concluded with tempering at 650°C for one hour in order to eliminate any potential residual stresses. Since the surface is a major source of defects for molds, laser surface heat treatment was applied according to an experimental design controlling laser power, scanning speed, and de-focusing distance. The results showed that the laser treatment had a positive impact on the ultimate tensile strength (UTS), improving it significantly compared to samples that underwent only heat treatment. However, it was observed that the elongation at break decreased. Fracture mode analysis was also carried out using a scanning electron microscope (SEM).

4.5 INTRODUCTION

ASI H13 tool steel, a chromium-molybdenum (Cr-Mo) hot work tool steel, is recognized for its good thermal fatigue stability, wear resistance along high temperatures, a high hardenability because of elevated carbon content and alloy elements that also aims to enhance the resistance to tempering and develop finely dispersed carbides. Additionally, H13 has an excellent combination of strength and ductility [1]. The great combination of the characteristics mentioned above, makes H13 tool steel on of the most utilized material in hot working applications that require withstanding rapid and repeated temperature changes, resisting to deformation and abrasive forces, enduring pressures without failure, and preventing cracking and fractures. This applications includes die casting, molds for plastic injection molding , forging and extrusion dies [2].

Conventional H13 tool steel is used in his optimal properties by applying a heat treatment process, generally involving quenching and tempering at specific conditions of temperatures and durations, depending on the desirable characteristics and properties of the material based on the intended application [3]. However, the conventional manufacturing methods of H13 dies are restricted and time consuming especially when it comes to a complex designs, and creating cooling systems that ensure heat uniformity and distribution

that improve cooling efficiency and extend the service life of the mold [4]. Which require advanced manufacturing techniques with a high precision and flexibility [5]. Additive manufacturing is a developing technology that enables the manufacturing of three-dimensional complex geometries with high efficiently, by adding material layer by layer. It is widely used in different domains such as injection molding, automobile, construction and bio-medical[6]. It is a competitive technique, because it offers design freedom to create complex geometries, which accelerates the production of prototypes and makes it less challenging and lowers the expenses, also the ability of creating unique and customized products to a specific needs [7]. The main principal categories of metallic additive manufacturing are direct energy deposition (DED) and powder bed fusion (PDF). DED methods use the energy source to melt and fuses the powder then deposit it on the previous built layers. In contrast for the PBD a thin layer of the powder, generally metal or ceramic, is spreader over the build platform, then a high thermal energy, either laser or electron beam, comes to selectively melt the powder conforming to the desirable design [8, 9]. Extensive research has been conducted over the past years to improve the metallic additive manufacturing through exploring various aspects, printing H13 tool steel using selective laser melting gained a lot of interests lately, numerous studies have successfully manufactured H13 and examined its microstructure and mechanical properties [10, 11]. Therefore, the application of selective laser melting to process H13 tool steel is quite challenging, because of its high carbon content and alloying elements causing the high hardenability, and the high thermal gradient during the process results cellular-columnar dendritic structure which is a non-uniform microstructure, which creates high residual stress that promote the propagation of cracking and distortion [12, 13]. Selective laser melted H13 tool steel is very sensitive to the process conditions starting with the powder material quality and properties, laser and scanning parameters, build environment parameters, and finishing with powder bed properties and recoat parameters [14]. The behavior of H13 is so complex and sensitive to the variation of the process parameters, a study [15] concluded that the most influencing parameters are the laser power, scanning speed, layer thickness, and hatch spacing. The increase in both laser power and scanning speed results improvements of the relative density

which is a very important indicator that helps to gain insights into the final's part uniformity, porosity, and quality. The layer thickness and hatch space impact surface roughness and have less impact on the density. The preheating was found to be an effective method to manage the defects along the process [16]. SLM of H13 tool steel exhibits a distinctive microstructure compared to the conventional one, it has a unique cellular-columnar dendritic, which consists mainly of a combination of martensite and varying amount of retained austenite depending on the process parameters. A study [17] mentioned that a higher volumetric energy density applied during SLM process lea to a higher fraction of Retained austenite. Furthermore, Deirmina [18]. Reported that an X-ray diffraction (XRD) analysis revealing up to 19 vol% of RA in SLM H13 tool steel. In the other hand, for the mechanical properties of as-built H13 in the selective laser melting (SLM) process are significantly influenced by the chosen parameters. A comprehensive review [19] on SLM-printed H13 reported that the tensile strength can vary between 835 MPa to 1909 MPa, depending on the specific SLM process parameters and conditions. Similarly, the elongation of the material was found to vary from 1,6% to 12,9%. Another essay[20] provided an overview of the published mechanical properties of H13 tool steel printed using different additive manufacturing methods. The ultimate tensile strength (UTS) of as-produced additive manufactured H13 tool steel was observed to range from 1000 MPa to 2064 MPa, while the elongation ranged from 0,8% to 6%. The significant variation in mechanical properties of SLM H13 tool steel can be attributed to the presence of residual stress and defects [21], it's also important to mention that the SLM H13 has superior strengths compared to the traditionally manufactured H13. However, the elongation to failures of the as built H13 samples is so low compared to the conventional H13, indicating reduced ductility and toughness for the as-SLMed H13[9, 22]. The H13 tool steel in the as built condition showed unsatisfactory properties, in terms of tensile properties especially the elongation fracture that doesn't answer the requirements of molds for injection moulding. Additionally, the inhomogeneous microstructure and the significant volume fraction of retained austenite impact negatively the tool life. So, understanding the behavior of SLM H13 under varying

post processing treatment is crucial for improving and ameliorating the service life and the productivity of injection molding.

Asberg *et al* [23] studied the effect of the following post treatments: stress relieve, standard hardening and tempering, and hot isostatic pressing, on the microstructure and mechanical properties of additive manufactured H13. the selective laser melting parameters are the following, layer thickness of 30 μm, argon gas during the building process, laser power of 175 W, laser scanning speed of 720 mm/s, and hatch distance of 0,12 mm. First post treatment is an isothermal heat treatment at 650°C for 8h to make sure all the residual stresses is removed. Second treatments consist of a stress relieve followed by the conventional hardening at 1020°C for 70-75 min quenching in nitrogen and tempering twice at 585°C for 2,25-3h heat treatment. Third one contains a stress relive, HIP for 6h at 1130°C and 100 MPa pressure and a conventional heat treatment. The maximum hardness of 562 HV attributed to the third treatment, the conventional heat treatment achieved 511 HV, and after the stress relieve the hardness is about 428 HV. The ultimate tensile strength also increased as the heat treatments were applied. The stress relieves specimens had an ultimate tensile strength of 1297MPa, which increased to 1640 MPa after SR + HT treatment. The highest values of 1743 MPa were observed after SR + HIP + HT. Elongation at fracture was 4,2% in the SR specimen. Hardening and tempering treatment of the SR specimens lead to a drop of elongation at fracture down to 3,3%, which is not a surprise as material after SR is softer than after SR + HT. Application of SR + HIP + HT post treatment, lead to an increase in elongation at fracture to 6,6%. Remarkably, is that SR + HIP + HT post treatment led to an increase in both, elongation at fracture and hardness. Yan *et al* [24] opted tempering heat treatment, to optimize the mechanical properties of selective laser melted H13 with the following process parameters that reached 99,6% relative density: 175 W laser power, hatch distance of 100 μm, layer thickness of 30 μm, and scanning speed equal to 725 mm/s. Tempering is conducted with two temperatures of 600°C and 700°C for 2h. The as-built sample exhibited the lowest elongation of 2,42%, which is mainly affected by high residual stresses and 1430 MPa for UTS, the tempering at 600°C improved the elongation at 5,8% and exhibited the highest ultimate strength of 1938 MPa. The tempered samples at 700°C had the highest

elongation of 11% and lowest UTS of 1076 MPa. Lee *et al* [25] aims to investigate the effect of the selective laser melting process especially the scanning speed on the tensile tests properties and fracture behavior. The study utilized specific printing parameters, including a laser power of 900W, hatch spacing of 80 μm, layer thickness of 25 μm, and varying scanning speeds of 200, 400, and 800 mm/s. The findings revealed that an increase in the scanning speed led to a decrease in both the ultimate strength and elongation. The corresponding values for ultimate strength and elongation at a scanning speed of 200 mm/s were determined as 1704 MPa and 1,55%, respectively. At a scanning speed of 400 mm/s, the ultimate strength was measured at 1332 MPa with an elongation of 0,35%. Finally, at a scanning speed of 800 mm/s, the ultimate strength was recorded as 1227 MPa, while the elongation was 0,30%. Ren *et al* [26] conducted a comparative study between selectively laser melted H13 and conventional H13 after undergoing forging, spheroidized annealing, and thermal refining, which involved water quenching and double tempering at temperatures of 610°C and 580°C for 2 hours. The results revealed that the selectively laser melted H13, with optimal process parameters consisting of a laser power of 170 W, scanning speed of 400 mm/s, hatch spacing of 100 μm, and layer thickness of 40 μm, achieved significantly improved mechanical properties. Specifically, the selectively laser melted H13 exhibited an ultimate tensile strength of 1909 MPa, which was three times better than that of the conventional H13. Furthermore, it demonstrated an elongation of 12,4%, indicating enhanced ductility. On the other hand, the conventional H13 showcased a higher tensile strength of 1962 MPa but had a lower elongation of 4.4%. Mazur *et al* [27] The mechanical properties of selectively laser melted (SLM) H13 tool steel in the as-built condition were compared to those of conventional H13 tool steel. The SLM parameters used were a laser power of 175W, laser speed of 607,64 mm/s, hatch spacing of 0,12 mm, and layer thickness of 0,30 mm. The SLM H13 underwent a heat treatment process involving stress relief in a vacuum at 600°C for 2 hours, followed by furnace cooling. The conventional H13 was heat treated to achieve a hardness of 50 HRC. The conventional heat-treated H13 exhibited an ultimate tensile strength (UTS) of 1930 MPa and an elongation of 12%. In contrast, the as-built SLM H13 showed a UTS of 1370 MPa, an elongation of 1,7%, and a hardness of 59 HRC. The lower strength of the as-built

specimens can be attributed to the accumulation of residual and externally imposed stresses during the SLM process. After undergoing stress relief, the SLM H13 demonstrated a UTS of 1860 MPa, an elongation of 2,2%, and a hardness of 51 HRC. These results closely resembled the mechanical properties of the reference conventional material. However, the stress relieved SLM samples exhibited reduced ductility compared to the conventional material.

The previous findings from the literature represents a significant comprehending and understanding of the different properties of selective laser melted H13 tool steel in the as-built state and after different post treatments. This essay is dedicated to ameliorating the performances of molds processed by SLM H13 tool steel, by applying in a first stage a stress relieve is applied to reduce the maximum possible of retained austenite, then a The H13 samples are subject to a conventional heat treatment consisting of quenching and tempering to secure the microstructure homogeneity and removing all the left retained austenite. A second treatment is a biomimetic laser treatment applied on the surface of the quenched and tempered H13 samples, because the most die failures are present in the surface, so increasing utile life depends on improving its surface that must resist to tempering and aging while usage [28]. The biological systems and nature are the source of inspiration of biomimetic laser treatment, it allows the treatment of the surface with different shapes and designs to enhance the mold's surface properties. Various studies applied on the conventional H13 have demonstrated the remarkable efficiency and effectiveness of this process in improving the mechanical properties of hot work tool steels. These improvements include enhanced wear-resistance, increased tensile strength, and improved resistance to thermal fatigue [29-32]. The investigation of the effects of laser surface treatment including laser power, scanning speed, and defocus distance on the mechanical properties of post treated H13, is one of the main objectives of this work, using statistical tools, starting with a design of experiment using Taguchi method, followed by an analyze of the gathered data (ultimate strength and elongation) from the experiments using Analysis of Variance tool (ANOVA).

4.6 MATERIALS AND METHODS

4.6.1 Materials

Table 4- 1 shows the chemical composition of the H13 powder used during the selective laser melting process provided by the supplier. The powder shape and size are spherical and in the range of 15-53 µm. Furthermore, Figure 4- 1 shows the scanning electron microscopy images of the powder at different magnifications.

Table 4- 1:Chemical composition of H13 powder

Element	Cr	Mn	Mo	Si	V	C	Fe	Others
Min-Max (wt.%)	5.0-6.0	0-0.6	1.0-2.0	0.5-1.0	0.5-2.0	0.3-0.5	Balance	0-0.05

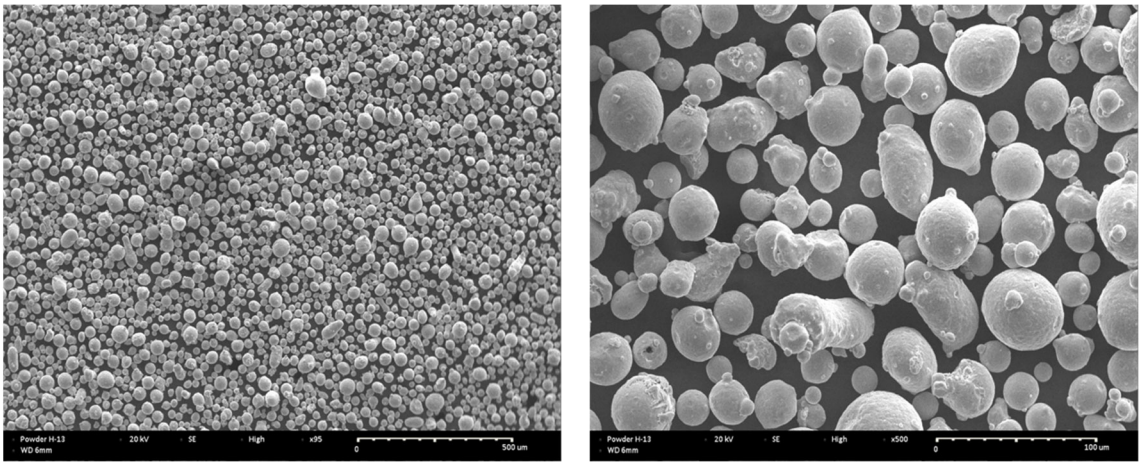

Figure 4- 1: SEM of the used H13 powder

4.6.2 Selective laser melting process

Selective laser melting (SLM) is categorized under powder bed fusion additive manufacturing technique, it employs a high powder density laser to selectively fuse metallic

powder. The selected parameters of additive manufacturing process are mentioned in Table 4- 2.

Table 4- 2: Selective laser melting process parameters

Laser power (W)	Scanning speed (mm/s)	Hatch distance (mm)	Layer thickness (mm)
275	800	0.12	40

4.6.3 Heat treatment

As-built selective laser melted H13 tool steel often exhibits significant residual stress, primarily resulting from the high temperature gradient experienced during the process. Rapid and intense heating followed by quick cooling and simultaneous remelting creates elevated residual stress levels that may lead to distortion and compromise the final product's functionality. Stress relief heat treatment is the most effective post-treatment to address this issue, typically applied before hardening and finish machining. The gradual cooling process during stress relief helps prevent the introduction of additional internal stress, resulting in improved structural integrity and performance of the final product [33, 34]. The non-equilibrium microstructure of the as-built H13 in selective laser melting (SLM) can lead to various issues due to the elevated solidification rate, directly impacting the mechanical properties of the final SLM parts. To optimize the microstructure and mechanical properties, a conventional heat treatment is recommended. According to ASM guidelines, the suggested hardening treatment temperature is between 995°C and 1040°C, followed by tempering at temperatures between 540°C and 650°C. This process results in a hardness range of 38-53 HRC [35]. The heat treatment process for the samples in this article involved austenitization at 1000°C for 30 minutes in a furnace, followed by oil cooling to form the martensite phase and homogenize the microstructure. Subsequently, tempering treatment was performed at 650°C for 1 hour. This heat treatment aims to reduce the brittleness of the newly formed

martensite and achieve an ideal balance of high microhardness and favorable toughness. The detailed summary of the conducted heat treatment on as-built H13, is shown in Table 4- 3.

Table 4- 3: Heat treatment characterizations

	Temperature	**Duration**
Stress relief	650°C	8 Hours
Austenitizing	1000°C	30 minutes
Quenching in the oil	Ambient temperature	3 minutes
Tempering	650°C	1 Hour

4.6.4 Surface treatment

The laser surface hardening process was performed using a FANUC M-710iC robot integrated with a laser cell. The laser cell utilized a fiber laser with a maximum power of 3000 watts, emitting continuous waves at a wavelength of 1070 nm. The laser head used was HIGHYAG BIMO, which had both a variable zoom collimator and a fixed focusing lens. This assembly enabled circular focal spots ranging from approximately 0.251 to 0.431 mm in diameter and was connected to an optical fiber of 100 mm length. Figure 4- 2 illustrates the laser setup used in this experiment.

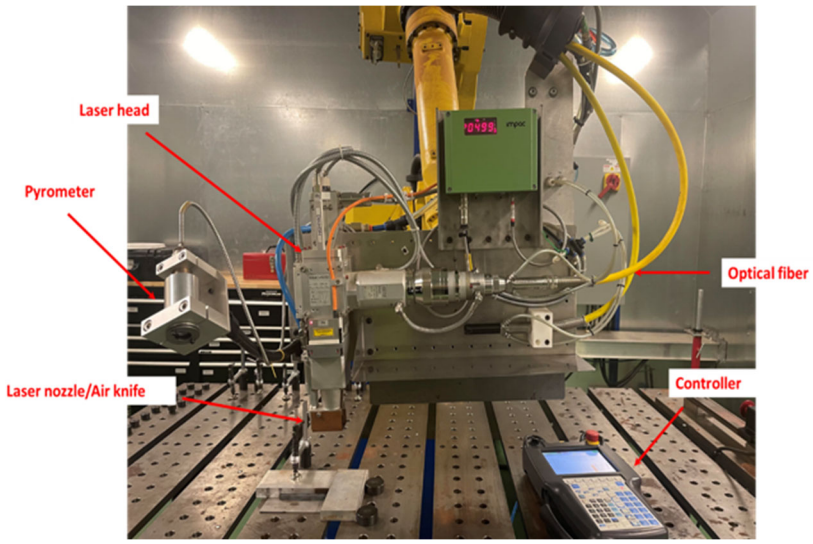

Figure 4- 2: Laser cell (3000W: YLS-3000-ST2) mounted on a FANUC robot with 6 axes

In laser hardening processes, defining experimental margins is crucial to ensure optimal case depth transformation without risking material cracking. It is essential to find the balance between achieving maximal case depth transformation and avoiding excessive transformation. This requires careful tuning to determine the appropriate parameter levels before conducting the actual laser hardening treatment. Table 4- 4 shows the factors and their variation ranges in these experiments.

Table 4- 4: Laser hardening parameters specifications

Factors	Abbreviation	Variation Ranges	Unit
Power	P	400, 500 and 600	W
Scanning speed	S	2, 3 and 4	mm/s
Defocus distance	D	8, 12 and 16	mm
Focal diameter	F	0.9, 1.03 and 1.15	mm

The Taguchi method is employed to design an efficient experimental plan with minimal trials and reduced variation. It allows the simultaneous study of multiple parameters, aiming to optimize the process. In contrast, conventional methods typically involve a lengthier

approach, where one parameter is varied at a time while keeping the rest constant. The Taguchi method's advantage lies in its ability to efficiently analyze the effects of multiple parameters simultaneously, leading to better optimization and understanding of the process [36]. For the experimental design three factors are involved with three levels, so the L9 orthogonal Taguchi Table 4- 5 is adopted.

Table 4- 5: L9 orthogonal Taguchi table (input parameters)

Test	Defocus distance (mm)	Scanning speed (mm/s)	Power (W)
1	8	2	400
2	8	3	500
3	8	4	600
4	12	2	500
5	12	3	600
6	12	4	400
7	16	2	600
8	16	3	400
9	16	4	500

The Figure 4- 3 shows the non-smooth surface, in which these units with superior microhardness and strength are considered to play the role of a hard phase, while base metal plays the part of the soft phase. The laser treatment was conducted on both surfaces.

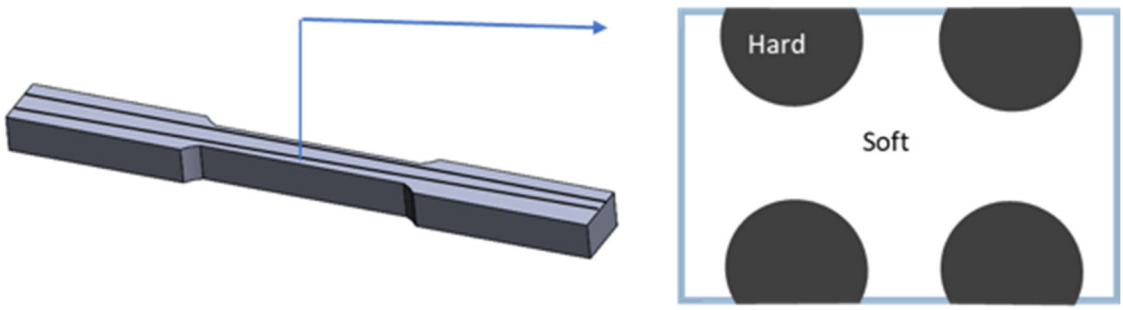

Figure 4- 3: Schematic illustration of laser treatment and cross-section of laser biomimetic units

4.6.5 Tensile tests

Tensile tests test carried out using 810 Material Test System which is a uniaxial servo-hydraulic machine, equipped with a contact extensometer. Each set of parameters underwent a minimum of three repeated tensile tests. The strain rate was maintained at 0.2 mm/min and all mechanical tests were carried out at room temperature. A total of 40 samples were machined according to ASTM standard E8/E8M [37] as shown in Figure 4- 4.

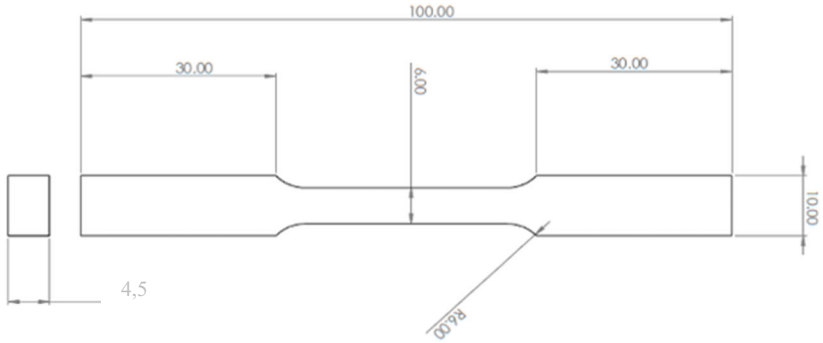

Figure 4- 4: Dimensions of tensile tests specimen (All dimensions are in mm)

SEM images of the middle part were acquired using a high-resolution scanning electron microscope, while microhardness tests were conducted using a Vickers indenter with a load of 200 gf for 10 seconds. These analyses provide valuable data to understand the material's microstructural features and its behavior under mechanical loading conditions.

4.7 RESULTS AND DISCUSSION

4.7.1 Morphology of the laser treated zone

The nine sets of laser parameters exhibited the same parabolic morphology as shown in

Figure 4- 5, however the difference is the surface characteristic of the laser surface treated area. The SEM images revealed three distinct phases generated during the laser surface treatment including melted zone(MZ), hardened zone 5HZ), and finally heat affected zone (HAZ).The laser treatment parameters applied on the surface play an important role on the shape, size, microstructure and the microhardness of the treated zone [38]. The depth values measurements showed a variation from 1.30 mm to 1.8 mm, the same for the width values displayed notable deviation range from 1.6 mm to 2.4 mm.

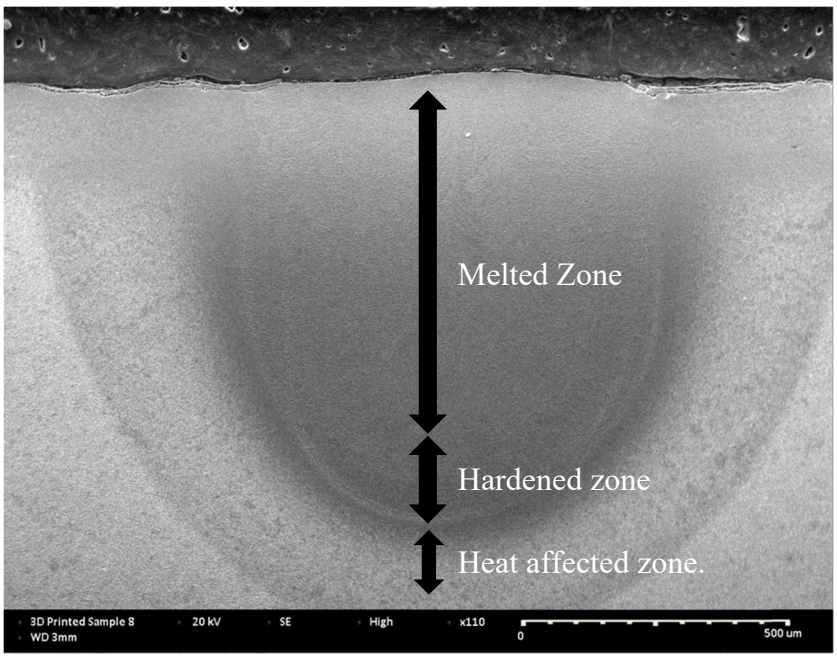

Figure 4- 5: Cross section SEM of the middle of the line of laser treatment

4.7.2 Microstructure

During the laser surface treatment of quenched and tempered H13 tool steel with a high thermal gradient, the surface experiences rapid heating above the melting point, followed by rapid cooling. The resulting microstructure characteristics, as shown in Figure 4- 6, it indicates three distinct regions. The top region exhibits a microstructure similar to the as-built H13, with cellular-columnar dendrite cells [17, 39], and notably high microhardness, reaching a maximum of 54 HRC, surpassing the substrate's hardness. The hardened zone, located below the upper region, undergoes complete austenitization but does not reach the melting point, displaying the highest microhardness among the nine sets. The third region, known as over-tempered, demonstrates lower microhardness than the substrate, with a value of 38 HRC [40].

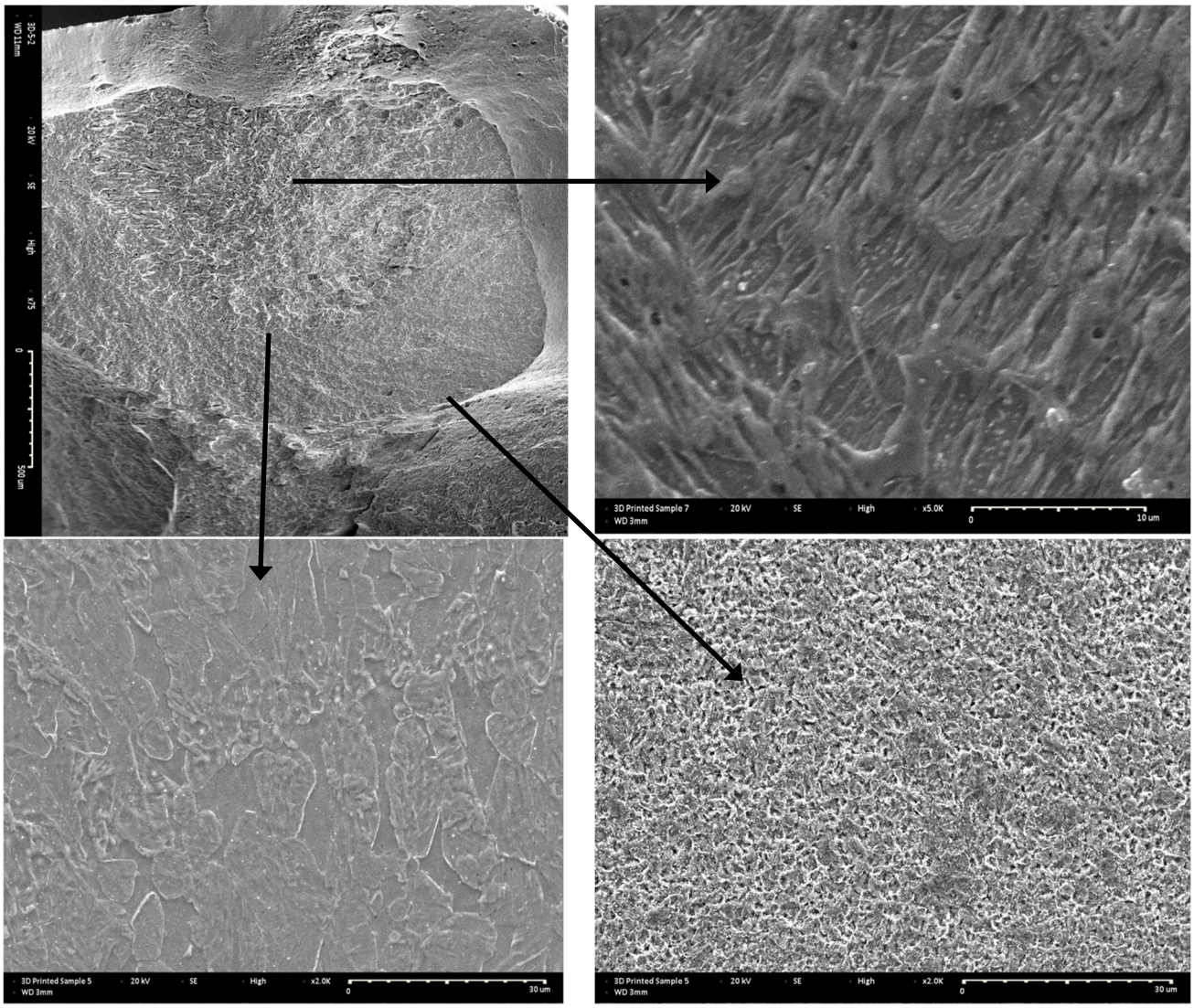

Figure 4- 6: Microstructure of laser surface treated for sample 5

4.7.3 Tensile properties

The tensile properties of laser surface treated H13 tool steel are presented in Figure 4-7, Figure 4- 8 and Figure 4- 9 and compared to the substrate material, SLM H13 in quenched and tempered conditions. The main purpose is to gain insights into the influence of laser parameters on the tensile properties. To facilitate analysis, the charts are categorized based on the laser power, as it is observed to have a significant impact. Figure 4- 7 represents the

sets with a fixed power of 400W, Figure 4- 8 displays the results obtained at a laser power of 500W, and Figure 4- 9 showcases the behavior at a laser power of 600W.

Engineering stress was obtained from the experimental data and calculated employing a conventional formula $\sigma = \frac{F}{S_0}$ where S_0 represents the initial cross-sectional area of the specimen. For the strain it's measured using an extensometer device attached to the samples during the experimental tests.

The Quenched and tempered H13 tool steel exhibited the lowest tensile strength around 1233,28 MPa compared to the laser surface treated samples, and a higher elongation of 12,80% which is due to the conventional hardening and tempering heat treatment that soften the material [41], this values align approximatively with the documented standard strength levels of conventionally hardened and tempered AISI H13 tool steel as indicated in the available literature [32, 42].

The laser process parameters including laser power, scanning speed and defocus had a notable impact on the resulting values of ultimate strength and elongation. The samples treated with the lowest power of 400W showed a relatively minor improvement in ultimate strength. For instance, in the case of sample 8 treated with a defocus distance of 16mm and scanning speed of 3 mm/s, the ultimate strength increased from 1233.28 MPa to 1253.56 MPa, this corresponded to the highest improvement of 9.75% in ultimate strength. On the other hand, the other parameter sets resulted in a 1.65% increase in ultimate strength for a defocus distance of 12 mm and a high scanning speed of 4mm/s, and a 9.41% improvement for a defocus distance of 8mm and a scanning speed of 2mm/. for the second level of laser power at 500W, the ultimate strength showed moderate improvements, the maximum improvement of 19.05% was observed in sample 4, where the ultimate strength increased from 1233.28 MPa to 1468.40 MPa using a defocus distance of 12mm and scanning speed of 2mm/s. The other parameter sets achieved improvements of 10.87% and 6.95%. In the case of the highest laser power level of 600W, the ultimate strength reached its peak values. The sample with the highest ultimate strength among the nine parameter sets was sample 7,

where the ultimate strength improved from 1233.28 MPa to 1567.04 MPa, indicating a significant 27.05% improvement. The other samples achieved improvements of 13.13% and 18.32%.

In conclusion, the study demonstrates that the laser process parameters had a notable positive impact on the ultimate strength of the laser-treated samples. However, it was observed that the elongation at fracture was generally reduced in the laser-treated samples. These findings highlight the importance of carefully selecting and optimizing laser parameters to achieve the desired mechanical properties while considering potential trade-offs in material ductility.

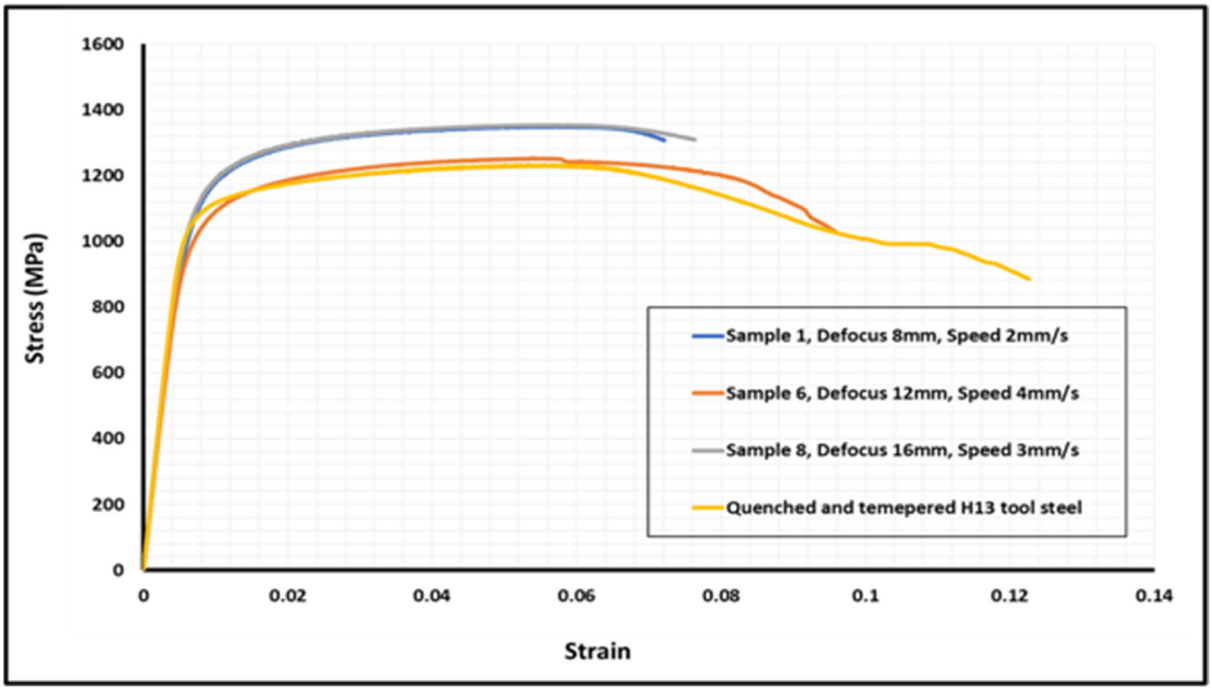

Figure 4- 7: Engineering stress-strain curves (400W)

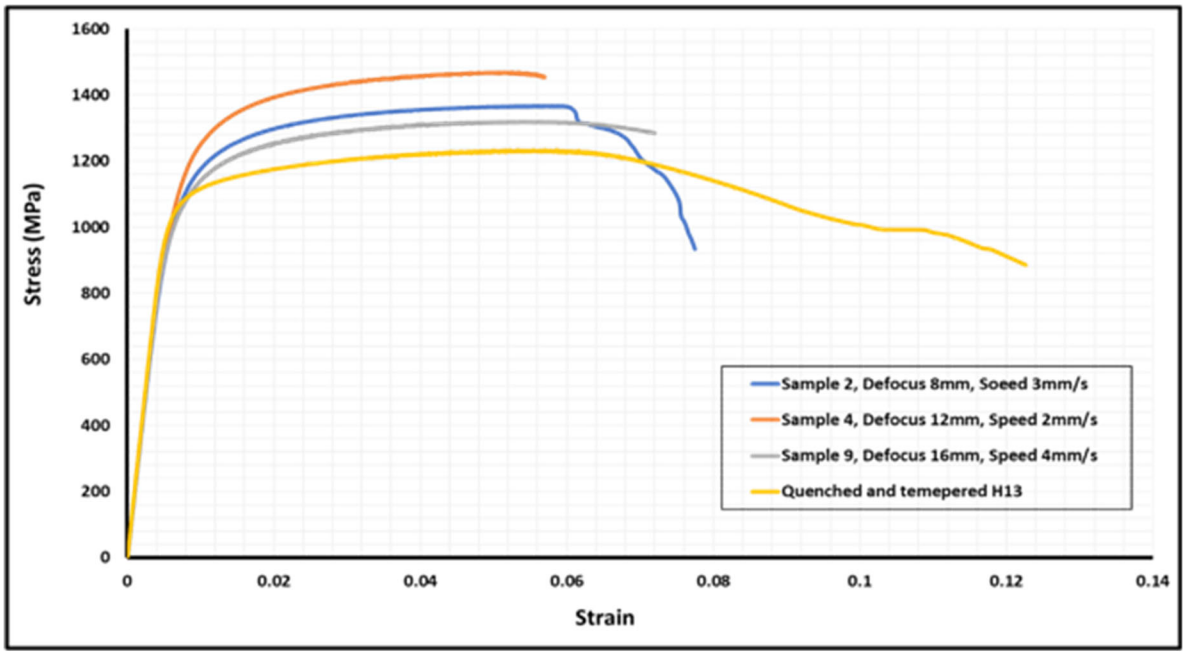

Figure 4- 8: Engineering stress-strain curves (500W)

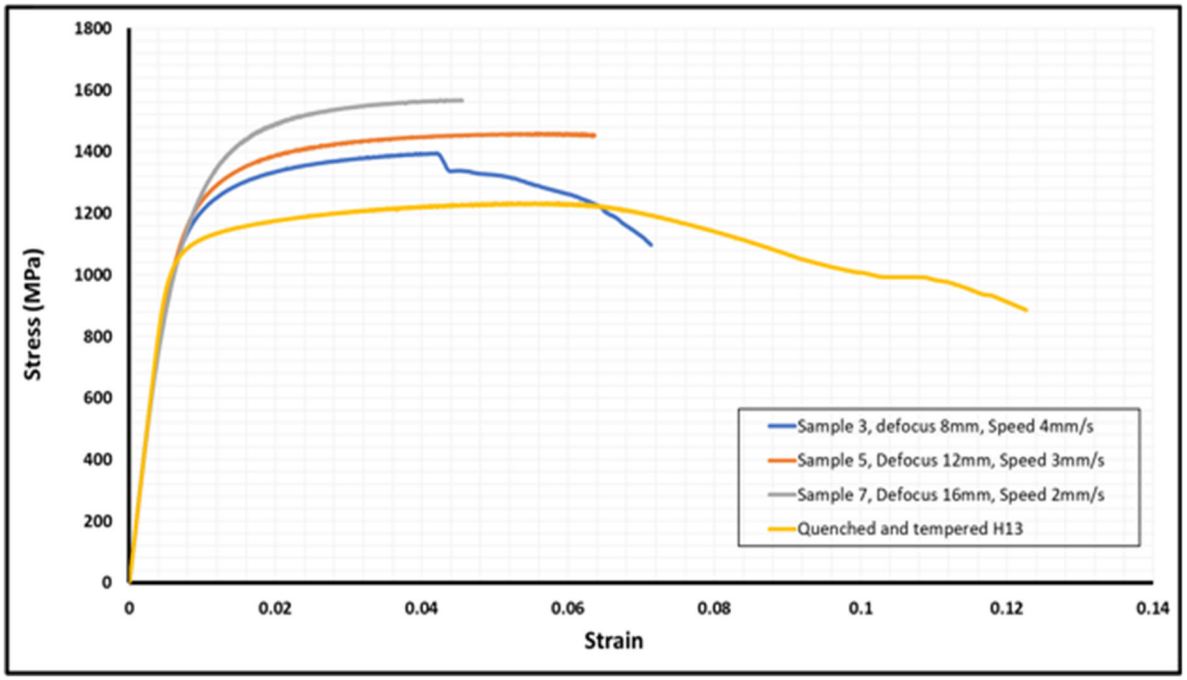

Figure 4- 9: Engineering stress-strain curves (600W)

4.7.4 Fractography

4.7.4.1 Base material

Figure 4- 10, the SEM fractography of the as-quenched and tempered H13 tool steel is displayed, revealing the morphology and characteristics of the different surfaces after tensile tests, aimed at understanding the mode of failure. For the quenched and tempered H13, the fractured surface exhibits numerous dimples distributed throughout, indicating a ductile fracture behavior. This correlation is evident when considering the stress-strain curve, which demonstrates significant plastic deformation and energy absorption by the sample before reaching failure. These observations suggest that the quenched and tempered H13 tool steel underwent substantial plastic deformation, providing ductile behavior and energy dissipation before ultimate failure occurred.

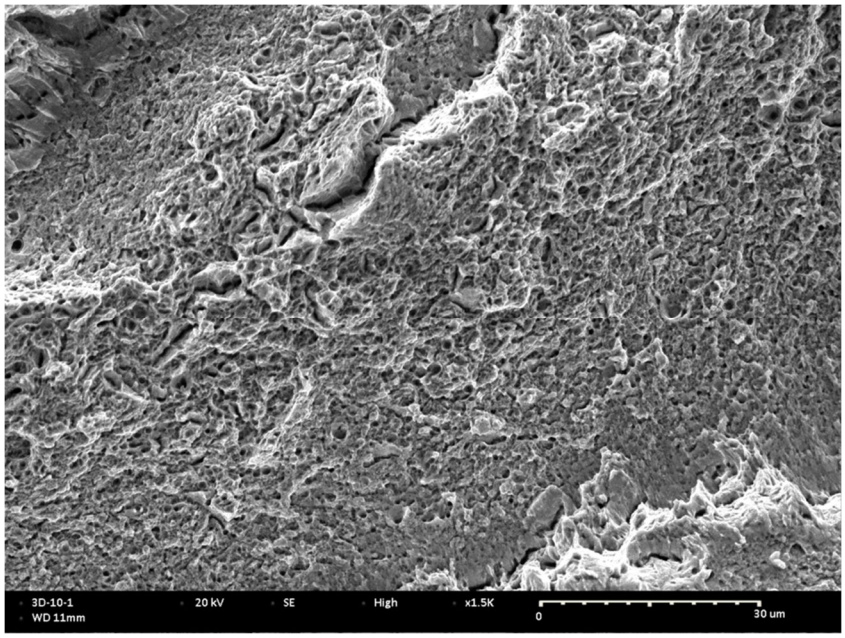

Figure 4- 10: SEM fractography of Quenched and tempered SLM H13

4.7.4.2 Laser treated samples

Figure 4- 11 is a presentation of the laser surface treated sample 1. The fractured surface exhibits a combination of ductile and brittle features. On the laser-treated surface, there is a presence of cleavage and equiaxed dimples, which indicate a predominantly brittle nature with some certain level of ductility. Therese's also a presence of porosity in different surfaces of the selective laser melted H13 tool steel, which may influence the material's mechanical properties.

To provide a more detailed description of the different zones on the fractured surface of sample 1: Figure 4- 11(a) The overall fractured surface, including the base metal, showcases a combination of ductile and brittle features. The presence of extensive plastic deformation, elongation, and numerous dimples indicates a predominantly ductile fracture behavior. However, there are also small areas with a clean appearance, indicating brittle fracture. Figure 4- 11(b), the base region displays a predominantly ductile appearance. The surface exhibits a significant number of dimples, indicating substantial plastic deformation and a ductile fracture mode in this zone. Figure 4- 11(c), the hardened zone exhibits a mixed behavior with both ductile and brittle features. While there are some dimples suggesting ductile characteristics, the presence of cleavage steps indicates a certain level of brittleness in this zone. Overall, the fractured surface of sample 1 demonstrates a complex combination of ductile and brittle features in different zones. The presence of porosity further adds to the intricacies of the material's fracture behavior. These observations provide valuable insights into the fracture behavior of the laser-treated H13 tool steel and may guide further improvements in the laser surface treatment process to optimize the material’s mechanical properties.

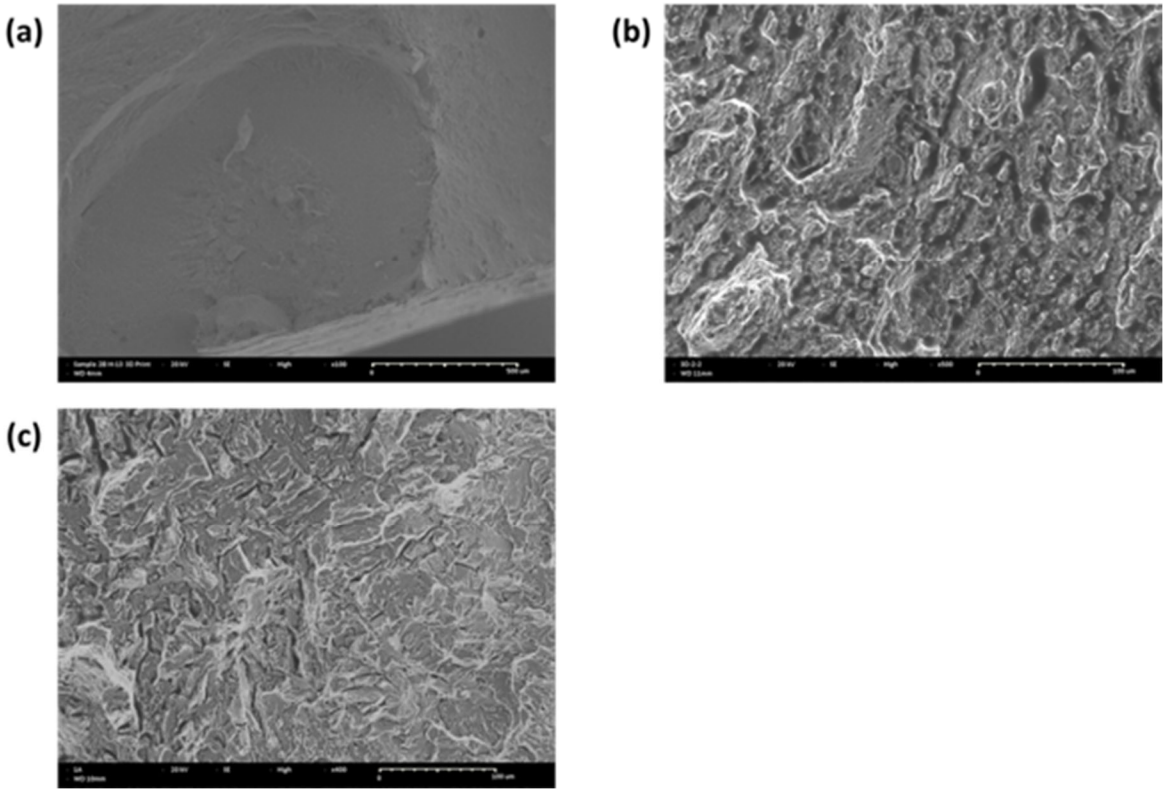

Figure 4- 11: (a) Fractured surface of sample 1 (b) Base region (c) Hardened zone

Now for sample 2, Figure 4- 12 is showing the fractured surface. (a) The overall fractured surface, including the base material, showcases a combination of ductile and brittle features. The presence of extensive plastic deformation, elongation, and numerous dimples indicates a predominantly ductile fracture behavior. However, there are also small areas with a clean appearance, indicating brittle fracture. Figure 4- 12(b) represents the base region, where the fractured surface exhibits a mixed behavior with both ductile and brittle features. Some areas display dimples, suggesting ductile characteristics, while other areas reveal a clean appearance, indicating brittle fracture.

In Figure 4- 12 (c), the hardened zone exhibits a more ductile appearance compared to other zones. The surface exhibits some dimples and less cleavage, indicating a relatively more ductile fracture mode in this zone. Finally, Figure 4- 12 (d) presents the melt zone,

which predominantly displays a ductile appearance. The surface reveals a significant number of dimples, indicating substantial plastic deformation and a predominantly ductile fracture mode in this zone. Overall, the fractured surface of sample 2 demonstrates a complex combination of ductile and brittle features in different zones. The presence of ductile dimples in the melt zone contrasts with the relatively more ductile characteristics observed in the hardened zone, as well as some areas of the base region. These observations provide valuable insights into the fracture behavior of the laser-treated H13 tool steel and may guide further improvements in the laser surface treatment process to optimize the material's mechanical properties.

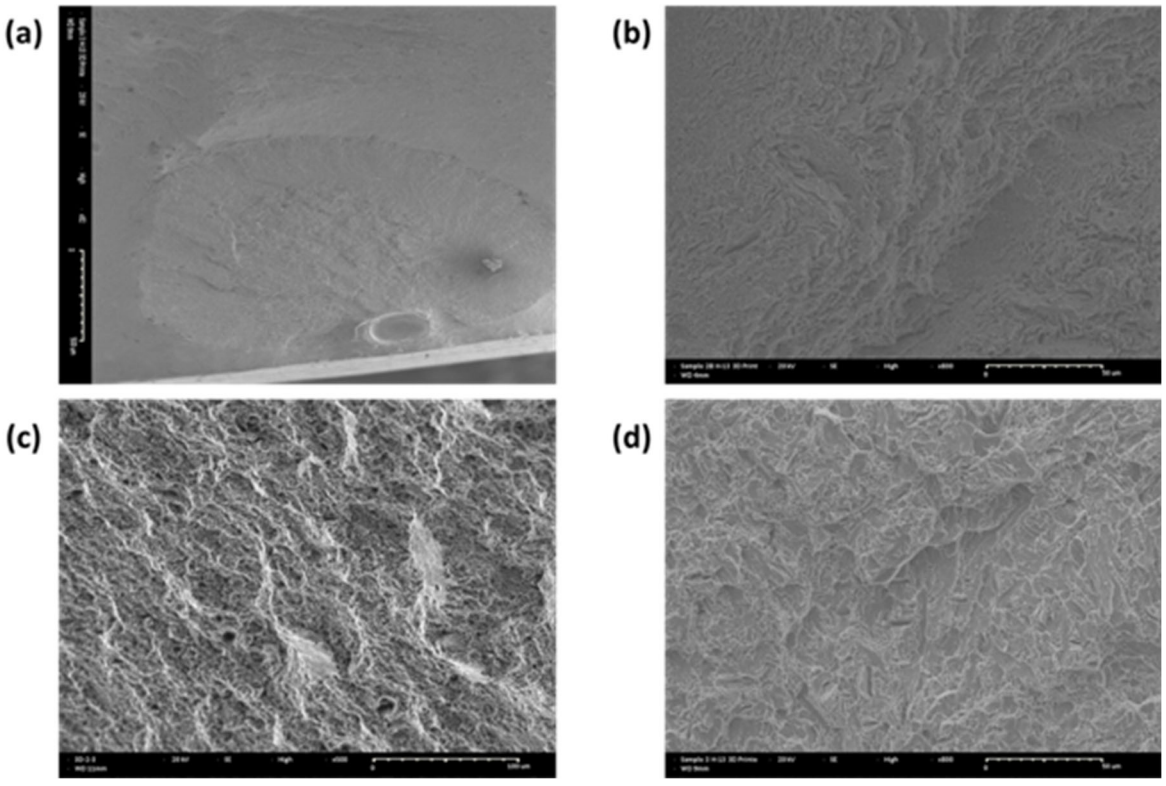

Figure 4- 12: (a) Fractured surface of sample 2 (b) Base region (c) Hardened zone (d) Melt zone

Figure 4- 13 provides a description of fractured images for sample 3. Figure 4- 13(a) The overall fractured surface, including the base material, showcases a combination of ductile and brittle features. The presence of extensive plastic deformation, elongation, and numerous dimples indicates a predominantly ductile fracture behavior, along with some areas of clean appearance indicating brittle fracture. Figure 4- 13Figure 4- 13 (b) displays the base region, which exhibits a predominantly ductile appearance. The surface reveals a significant number of dimples, suggesting substantial plastic deformation and a predominantly ductile fracture mode in this zone. Moving to Figure 4- 13 (c), the hardened zone exhibits a more brittle appearance compared to other zones. The surface shows cleavage steps and fewer dimples, indicating a relatively more brittle fracture mode in this zone. Finally, Figure 4- 13 (d) presents melt zone, which shows a mixed behavior with both ductile and brittle features. The surface reveals dimples, suggesting some plastic deformation and a ductile fracture mode, along with areas of cleavage steps indicating brittle fracture. Overall, the fractured surface of sample 3 demonstrates a complex combination of ductile and brittle features in different zones. The predominance of ductile dimples in the melt zone contrasts with the relatively more brittle characteristics observed in the hardened zone and some areas of the heat-affected zone. These observations provide valuable insights into the fracture behavior of the laser-treated H13 tool steel and may guide further improvements in the laser surface treatment process to optimize the material's mechanical properties.

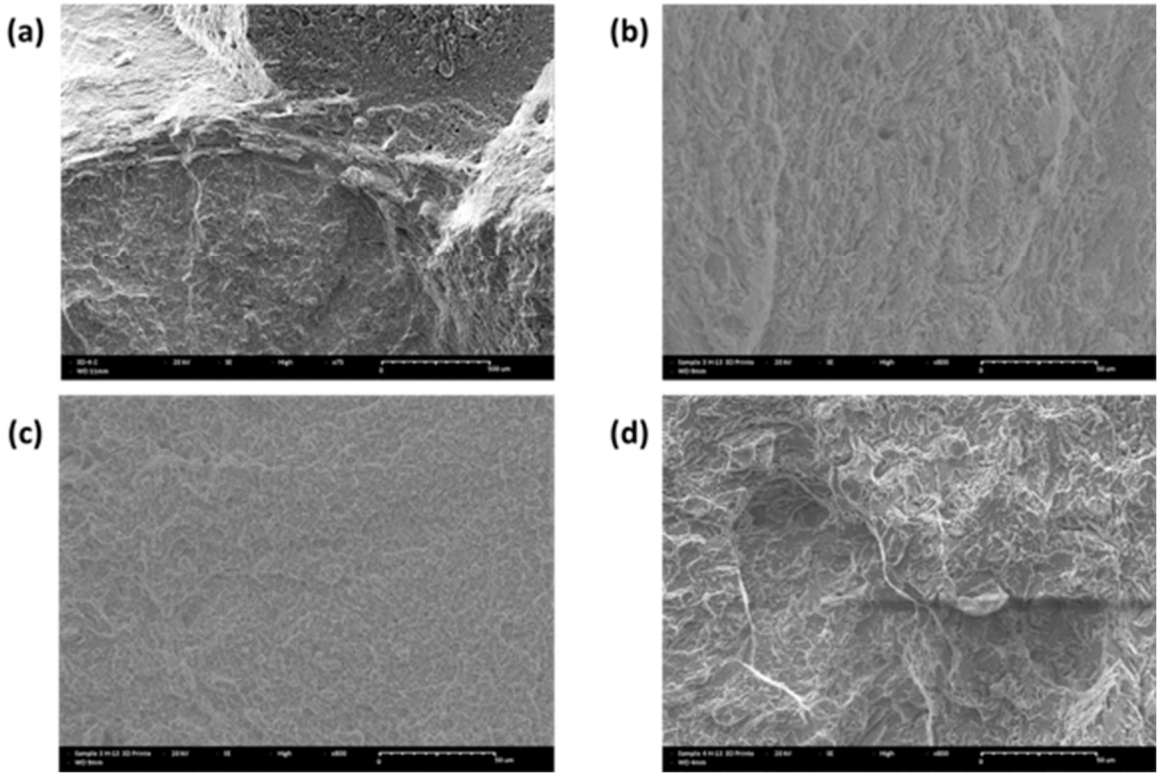

Figure 4- 13: (a) Fractured surface of sample 3 (b) Base region (c) Hardened zone (d) Melt zone

Figure 4- 14 (a) presents the overall fractured surface, including the base material. The fractured surface exhibits a combination of ductile and brittle features. Notable plastic deformation, elongation, and the presence of dimples indicate a predominantly ductile fracture behavior. However, areas with a clean appearance suggest regions of brittle fracture. In Figure 4- 14 (b), the base region is observed. The fractured surface displays a mixed behavior with both ductile and brittle features. Some areas reveal dimples, indicating plastic deformation and a ductile fracture mode, while other regions show cleavage steps, indicating brittle fracture. Moving to Figure 4- 14 (c), the hardened zone shows a predominantly brittle appearance compared to other zones. The fractured surface exhibits cleavage steps and fewer dimples, indicating a relatively more brittle fracture mode in this zone. Finally, Figure 4-14(d) showcases the melt zone, which predominantly displays a ductile appearance. The

surface reveals a significant number of dimples, suggesting substantial plastic deformation and a predominantly ductile fracture mode in this zone. The fractured surface of sample 4 demonstrates a complex combination of ductile and brittle features in different zones. The predominance of ductile dimples in the melt zone contrasts with the relatively more brittle characteristics observed in the hardened zone and some areas of the base region. These observations provide valuable insights into the fracture behavior of the laser-treated H13 tool steel and may guide further improvements in the laser surface treatment process to optimize the material's mechanical properties.

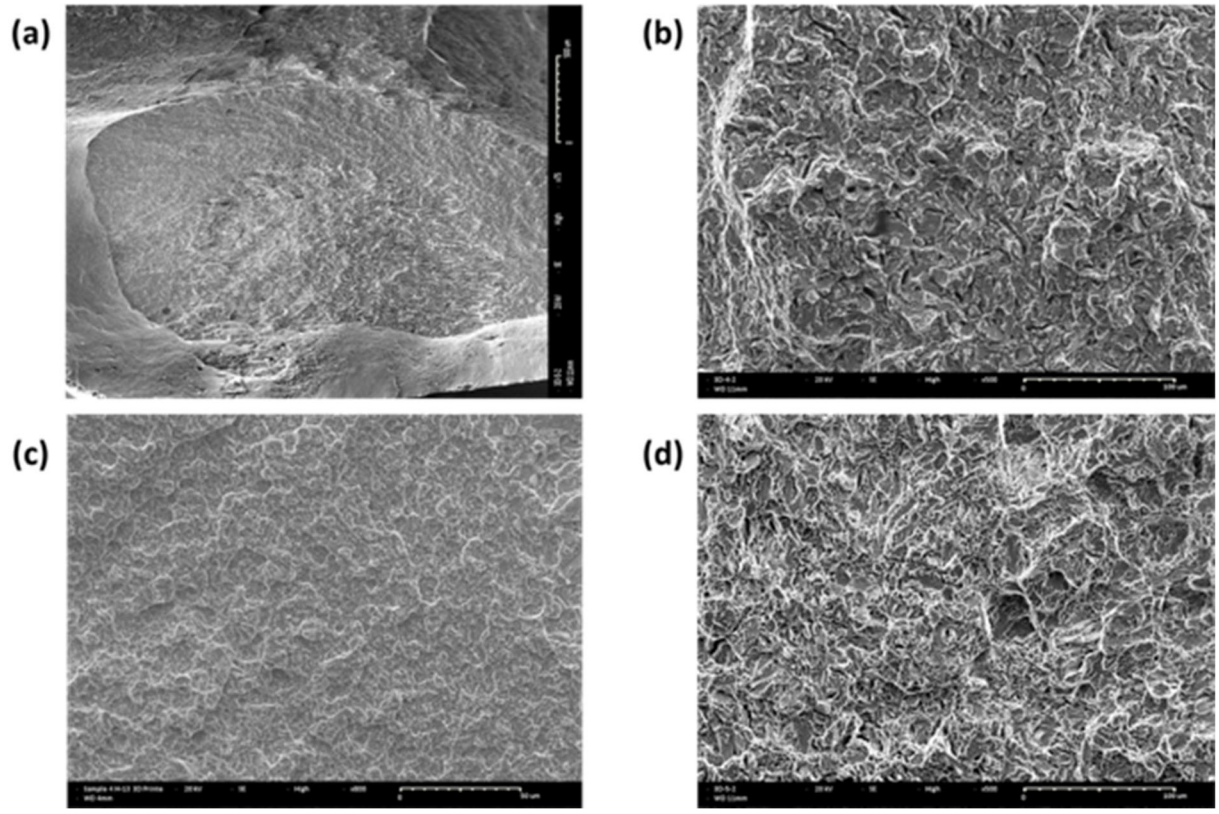

Figure 4- 14: (a) Fractured surface of sample 4 (b) Base region (c) Hardened zone (d) Melt zone

Figure 4- 15 (a) presents the overall fractured surface, including the base material. The fractured surface showcases a combination of ductile and brittle features. Extensive plastic deformation, elongation, and a number of dimples indicate a predominantly ductile fracture behavior. However, areas with a clean appearance suggest regions of brittle fracture. In Figure 4- 15 (b), the base region is observed. The fractured surface displays a mixed behavior with both ductile and brittle features. Some areas reveal dimples, indicating plastic deformation and a ductile fracture mode, while other regions show cleavage steps, indicating brittle fracture. Moving to Figure 4- 15Figure 4- 14Figure 4- 20 (c), the hardened zone exhibits a predominantly brittle appearance compared to other zones. The fractured surface exhibits cleavage steps and fewer dimples, indicating a relatively more brittle fracture mode in this zone. Figure 4- 15 (d) showcases the melt zone, which predominantly displays a ductile appearance. The surface reveals a significant number of dimples, suggesting substantial plastic deformation and a predominantly ductile fracture mode in this zone. The increased occurrence of ductile features in the melt zone is notable. The fractured surface of sample 5 demonstrates a complex combination of ductile and brittle features in different zones. The predominance of ductile dimples in the melt zone contrasts with the relatively more brittle characteristics observed in the hardened zone and some areas of the base region. These observations provide valuable insights into the fracture behavior of the laser-treated H13 tool steel and may guide further improvements in the laser surface treatment process to optimize the material's mechanical properties.

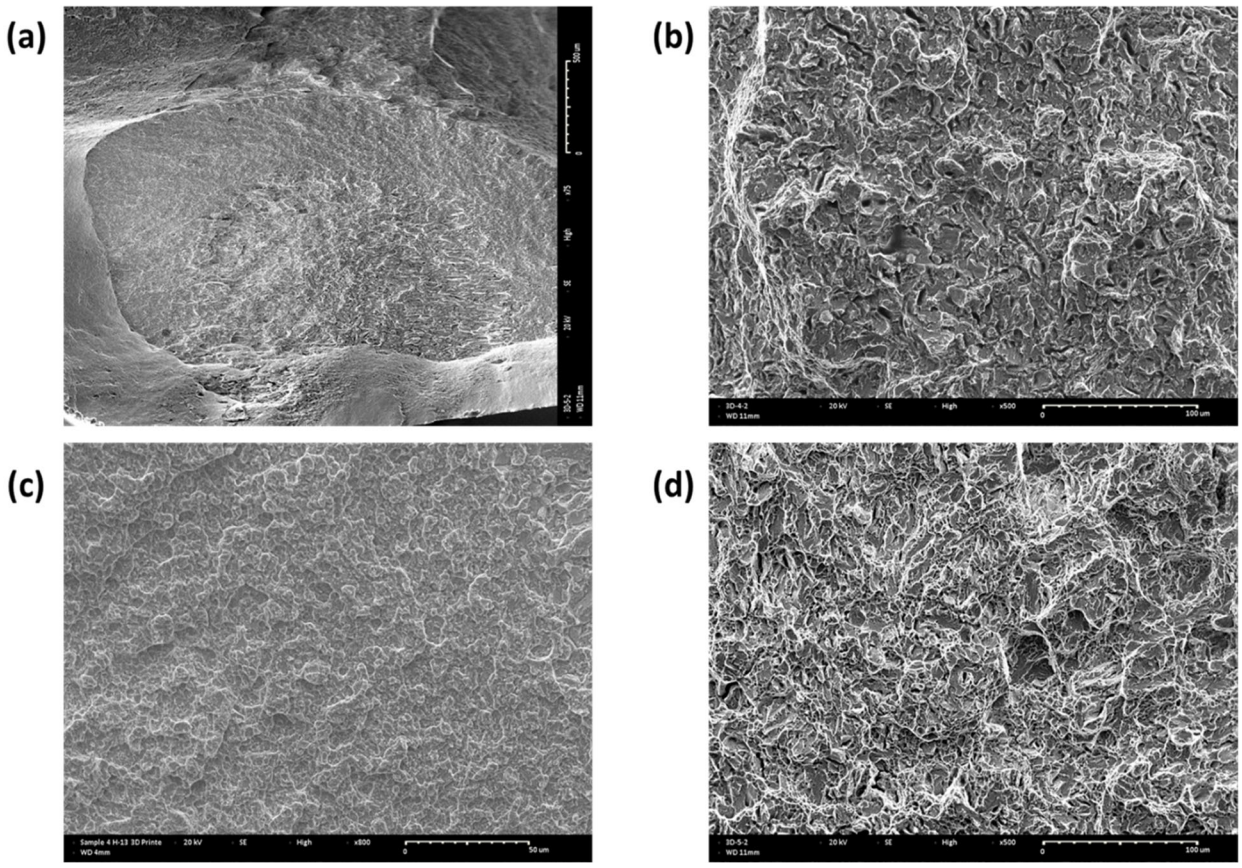

Figure 4- 15: (a) Fractured surface of sample 5 (b) Base region (c) Hardened zone (d) Melt zone

Figure 4- 16 (a) presents the overall fractured surface, including the base material. The fractured surface displays a combination of ductile and brittle features. Extensive plastic deformation, elongation, and a number of dimples indicate a predominantly ductile fracture behavior. However, there are also areas with a clean appearance, suggesting regions of brittle fracture. In Figure 4- 16 (b), the melt zone is observed. The fractured surface predominantly exhibits a ductile appearance in this zone. The surface reveals a significant number of dimples, indicating substantial plastic deformation and a predominantly ductile fracture mode. The fractured surface of sample 6 demonstrates a complex combination of ductile and brittle features. The predominance of ductile dimples in the melt zone indicates its relatively

higher ductility compared to other zones. These observations provide valuable insights into the fracture behavior of the laser-treated H13 tool steel and may guide further improvements in the laser surface treatment process to optimize the material's mechanical properties.

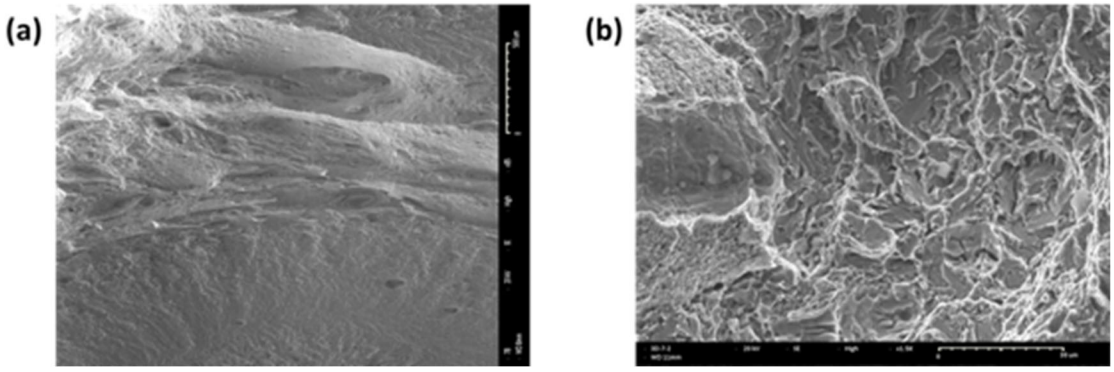

Figure 4- 16: (a) Fractured surface of sample 6 (b) Base region (c) Hardened zone (d) Melt zone

Figure 4- 17 (a) displays the overall fractured surface, including the base material. The fractured surface reveals a combination of ductile and brittle features. While extensive plastic deformation, elongation, and dimples indicate a predominantly ductile fracture behavior, there are also notable areas with a clean appearance, suggesting regions of brittle fracture. Moving to Figure 4- 17 (b), the base region is observed. The fractured surface displays a mixed behavior with both ductile and brittle features. Some areas reveal dimples, indicating plastic deformation and a ductile fracture mode, while other regions show cleavage steps, indicating brittle fracture. In Figure 4- 17 (c), the hardened zone exhibits a predominantly brittle appearance compared to other zones. The fractured surface exhibits cleavage steps and fewer dimples, indicating a relatively more brittle fracture mode in this zone. Finally, Figure 4- 17 (d) showcases the melt zone. The fractured surface in this zone also displays predominantly brittle features, with areas of cleavage steps indicating brittle fracture. The fractured surface of sample 7 demonstrates a complex combination of ductile and brittle features in different zones, with all zones showing a higher degree of brittleness. These observations provide valuable insights into the fracture behavior of the laser-treated H13 tool

steel and may guide further improvements in the laser surface treatment process to optimize the material's mechanical properties.

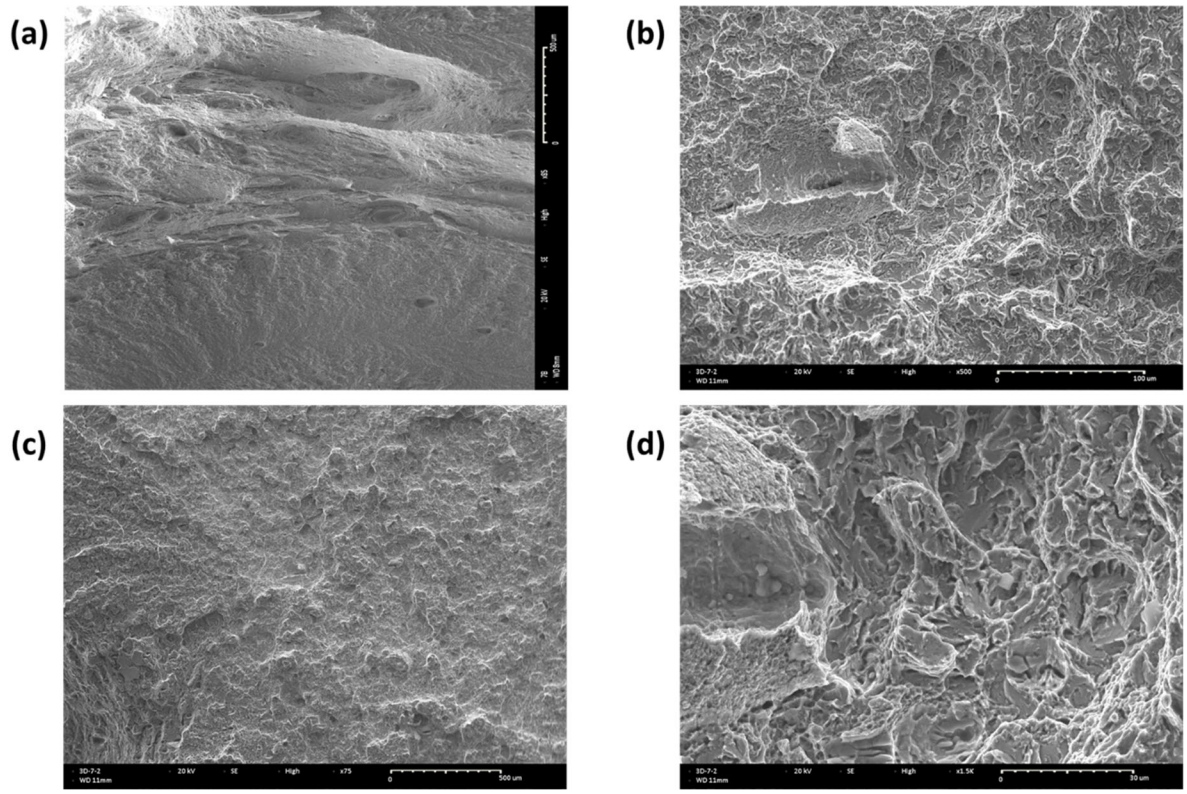

Figure 4- 17: (a) Fractured surface of sample 7 (b) Base region (c) Hardened zone (d) Melt zone

Figure 4- 18 (a) depicts the overall fractured surface, including the base material. The fractured surface showcases a combination of ductile and brittle features, with a presence of both plastic deformation and dimples indicating a predominantly ductile fracture behavior. Additionally, the surface displays areas with cleavage steps, suggesting regions of brittle fracture. In Figure 4- 18 (b), the base region is observed. The fractured surface exhibits a mixed behavior with both ductile and brittle features. Some areas reveal dimples, indicating plastic deformation and a ductile fracture mode, while other regions show cleavage steps, indicating brittle fracture. Moving to Figure 4- 18 (c), the hardened zone shows a

predominantly brittle appearance compared to other zones. The fractured surface displays cleavage steps and fewer dimples, indicating a relatively more brittle fracture mode in this zone. Finally, Figure 4- 18 (d) showcases the melt zone. The fractured surface in this zone exhibits a combination of ductile and brittle features, with the presence of dimples indicating some plastic deformation and a predominantly ductile fracture mode. However, there are also areas with cleavage steps suggesting brittle fracture. The fractured surface of sample 8 demonstrates a complex combination of ductile and brittle features in different zones, with some areas showing leges and steps. These observations provide valuable insights into the fracture behavior of the laser-treated H13 tool steel and may guide further improvements in the laser surface treatment process to optimize the material's mechanical properties.

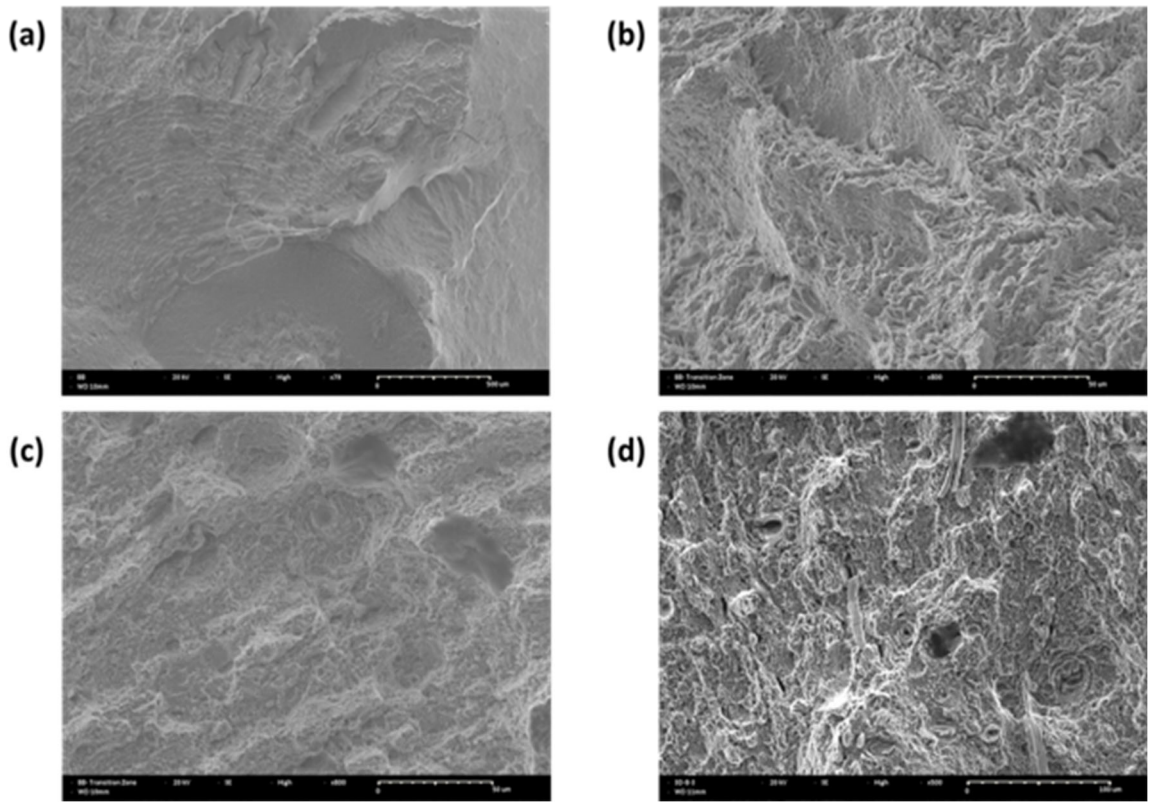

Figure 4- 18: (a) Fractured surface of sample 8 (b) Base region (c) Hardened zone (d) Melt zone

Figure 4- 19 (a) presents the overall fractured surface, including the base material. The fractured surface exhibits a combination of ductile and brittle features, with more surface features and less depth. The presence of plastic deformation, elongation, and dimples suggests a predominantly ductile fracture behavior. Additionally, the surface displays areas with cleavage steps, indicating regions of brittle fracture. In Figure 4- 19 (b), the base region is observed. The fractured surface displays a mixed behavior with both ductile and brittle features. Some areas reveal dimples, indicating plastic deformation and a ductile fracture mode, while other regions show cleavage steps, indicating brittle fracture. The surface features are more pronounced in this zone. Moving to Figure 4- 19 (c), the hardened zone shows a predominantly brittle appearance compared to other zones. The fractured surface exhibits cleavage steps and fewer dimples, indicating a relatively more brittle fracture mode in this zone. Finally, Figure 4- 19 (d) showcases the melt zone. The fractured surface in this zone exhibits a combination of ductile and brittle features, with the presence of dimples indicating some plastic deformation and a predominantly ductile fracture mode. The surface features are more pronounced in this zone as well. The fractured surface of sample 9 demonstrates a complex combination of ductile and brittle features in different zones, with more surface features and less depth. These observations provide valuable insights into the fracture behavior of the laser-treated H13 tool steel and may guide further improvements in the laser surface treatment process to optimize the material's mechanical properties.

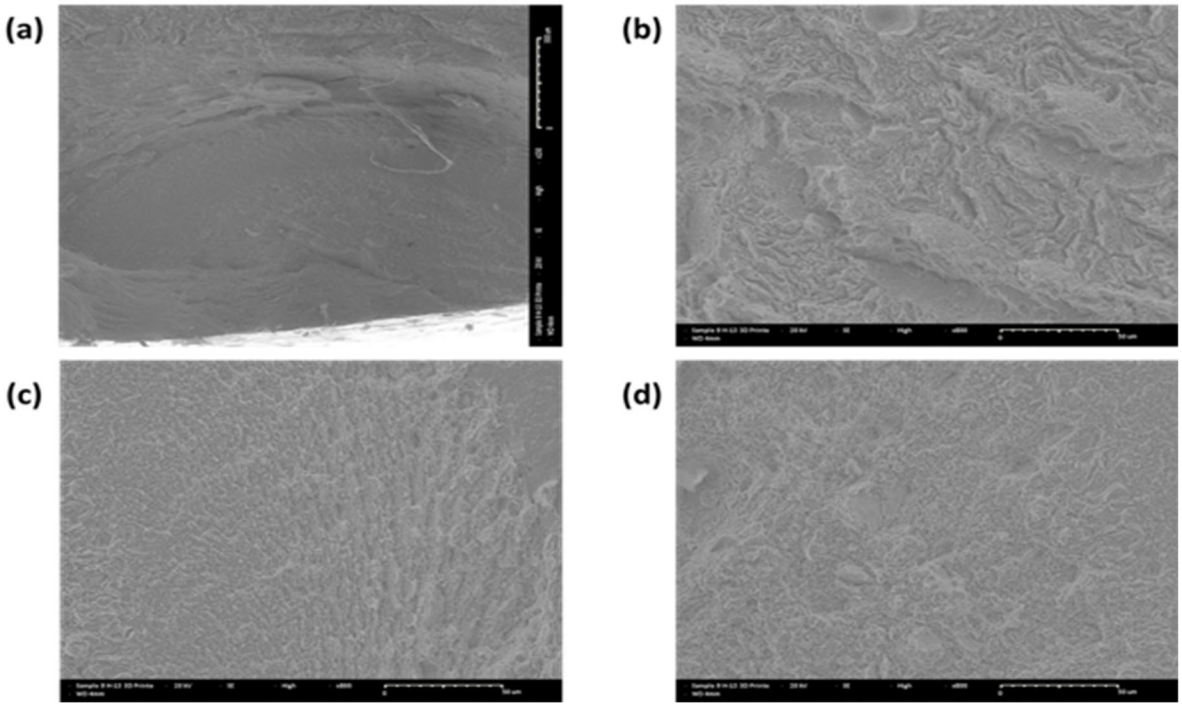

Figure 4- 19: (a) Fractured surface of sample 9 (b) Base region (c) Hardened zone (d) Melt zone

The enhancement of mechanical properties of H13 tool steel is primarily achieved through a conventional heat treatment process involving instantizing, quenching, and multiple tempering steps, each contributing to the material's improved characteristics. This study focuses on applying a conventional heat treatment to H13 tool steel fabricated using additive manufacturing methods, aiming to explore its effects on the mechanical properties and compare it with conventionally produced AISI H13 steel. The microstructural analysis reveals that the heat-treated H13 tool steel exhibits a homogenous microstructure similar to the conventional one, indicating a successful heat treatment process. Furthermore, the dendritic cellular structure, typically present in selective laser melting (SLM) processed materials, is eliminated due to the high thermal gradient during the additive manufacturing process. Regarding hardness, the heat-treated H13 samples achieve a hardness level of 42-44 HRC, which is comparable to the hardness obtained in quenched and tempered conventional H13 steel. This indicates that the conventional heat treatment process effectively enhances

the hardness of the 3D printed H13 tool steel. In terms of mechanical properties, both the quenched and tempered conventional H13 and 3D printed H13 exhibit excellent elongation values, with approximately 14% for the conventional H13 and 12% for the additive manufactured H13. Additionally, both materials show acceptable strength levels, showcasing their suitability for practical applications. The second objective of this essay is to examine the surface treatment of the material. The applied laser surface treatment shows significant positive effects on the material's strength, achieving a maximum improvement of 27.05% compared to the substrate. This improvement allows the material to withstand higher tensile forces, enhancing its overall mechanical performance. Overall, the study demonstrates the effectiveness of conventional heat treatment in improving the mechanical properties of additive manufactured H13 tool steel, making it comparable to conventionally produced counterparts. Furthermore, the laser surface treatment contributes to further strengthening the material, making it a promising candidate for various industrial applications.

4.8 STATISTICAL ANALYSIS

In this essay an L9 orthogonal Taguchi array id adopted to efficiently conduct experiments and minimize the number of trials. The use of Analysis of Variance (ANOVA), a powerful statistical analysis tool, allowed us to quantitatively analyze the data obtained from the experiments. ANOVA helped us determine the impact and contribution of each laser process parameter, including laser power, scanning speed, and defocusing distance, on the resulting material properties, specifically ultimate strength and elongation. The main objective of ANOVA was to identify the factors that had the most significant influence on the strength and elongation of the material. By understanding the contributions of each parameter, we aimed to optimize the laser processing parameters to enhance the mechanical properties according to the specific requirements of the desired application.

To facilitate the analysis, a statistical software Minitab is utilized, which provided valuable information, including the ANOVA table. The ANOVA table presented essential metrics such as the sum of squares (SS), degrees of freedom (Dof), F-statistic, and P-value.

The SS represented the total sum of squared deviations from the mean, while the Dof indicated the number of observations. The P-value served as an indicator of the statistical significance of the F-statistic, determining the probability of obtaining similar or more extreme results if the null hypothesis of no effect were true. A low P-value (less than 0.05) indicated a significant influence of the factors on the response variable. In addition to the ANOVA table, we utilized contour plots to gain further insights into the combined impacts of the input parameters on the responses. These contour plots helped us visualize the optimal combinations of laser parameters that led to the highest quality mechanical properties. By integrating the ANOVA analysis and the contour plots on the results mentioned in Table 4-6, we were able to understand the effects of laser process parameters on the material properties, ultimately guiding us in optimizing the laser processing techniques to achieve enhanced mechanical properties aligned with the specific needs of the intended application.

Table 4- 6: Summary of laser surface treatment parameters and tensile behavior of the substrate and laser treated SLM H13 tool steel

	Parameters and their levels Input			**Tensile test Results**	
Ex. No	**Defocusing(mm)**	**Speed (mm/s)**	**Power (W)**	**UTS(MPa)**	**Elongation (%)**
1	8	2	400	1349,258091	7,21
2	8	3	500	1367,303059	7,75
3	8	4	600	1395,075241	7,13
4	12	2	500	1468,402854	5,70
5	12	3	600	1459,18866	6,36
6	12	4	400	1253,751589	9,59
7	16	2	600	1567,047308	4,55
8	16	3	400	1353,566029	7,63
9	16	4	500	1318,940391	7,20
10	NT	NT	NT	1233,284703	12,81

4.8.1 The effect of laser parameters on the ultimate tensile strength

The ANOVA Table 4- 7, presents the results of statistical analysis, indicating that the P-values for laser power, scanning speed, and defocus distance are all less than 0,05. This signifies that the model is statistically significant and accurate for further analysis. Table 4-8 provides valuable information on the percentage contribution of each laser process parameter to the variation in the response variable. Among the parameters, laser power exhibits the highest contribution of 51,89%, indicating that it has the most significant impact on the resulting material properties. Following closely is the scanning speed, with a contribution of 41,77%. In contrast, the defocus distance has a relatively minor influence, contributing only 3,93% to the overall variation. These findings provide essential insights into the dominant factors affecting the mechanical properties of the material. The high contribution of laser power and scanning speed suggests that carefully controlling these parameters can lead to substantial improvements in the material's strength and elongation. On the other hand, the relatively low contribution of defocus distance implies that variations in this parameter may have a lesser impact on the material properties. By understanding the significance of each laser process parameter and their respective contributions, we can effectively optimize the laser processing conditions to achieve the desired mechanical properties for specific applications. This knowledge helps in guiding the manufacturing process to produce materials with enhanced strength and elongation, meeting the requirements of various engineering applications.

Table 4- 7: ANOVA table for Ultimate strength

Characteristic	Sum of squares	Dof	F-Value	P-value
Defocus distance	2727	1	8,18	0,035
Scanning Speed	28973	1	86,86	0,000
Power	35997	1	107,92	0,000
Error	1668	5		
Total	69365	8		

Table 4- 8: The contribution of laser parameters on the ultimate strength

Characteristic	Defocus distance	Scanning speed	Power	Error
Contribution (%)	3,93	41,77	51,89	2,40

Figure 4- 20 is a main effects plot for the SN ratios, it shows behavior of the ultimate strength according to the laser parameters, the UTS increases with the increase of both scanning speed and laser power, meanwhile it deceases with the increase of scanning speed.

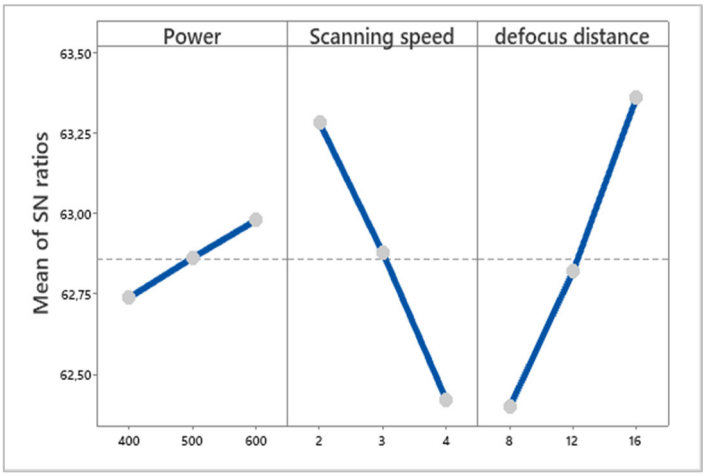

Figure 4- 20: Main effect plots for laser process parameters on the ultimate strength (P in W, S in mm/s and D in mm)

4.8.1.1 Regression equation

The regression equation provided by ANOVA analysis is mentioned below (4. 1), it can only used in the range of parameters used in the experiments. Where Laser power [400 W; 600 W], Scanning speed [2 mm/s; 4 mm/s], and defocus distance [8mm; 16 mm].

$$UTS = 1149{,}7 + 5{,}33\ Defocus - 69{,}49\ Speed + 0{,}7746\ Power \quad (4.\ 1)$$

According to the Figure 4- 21, there's a high correspondence between the predicted and measured data of the ultimate strength.

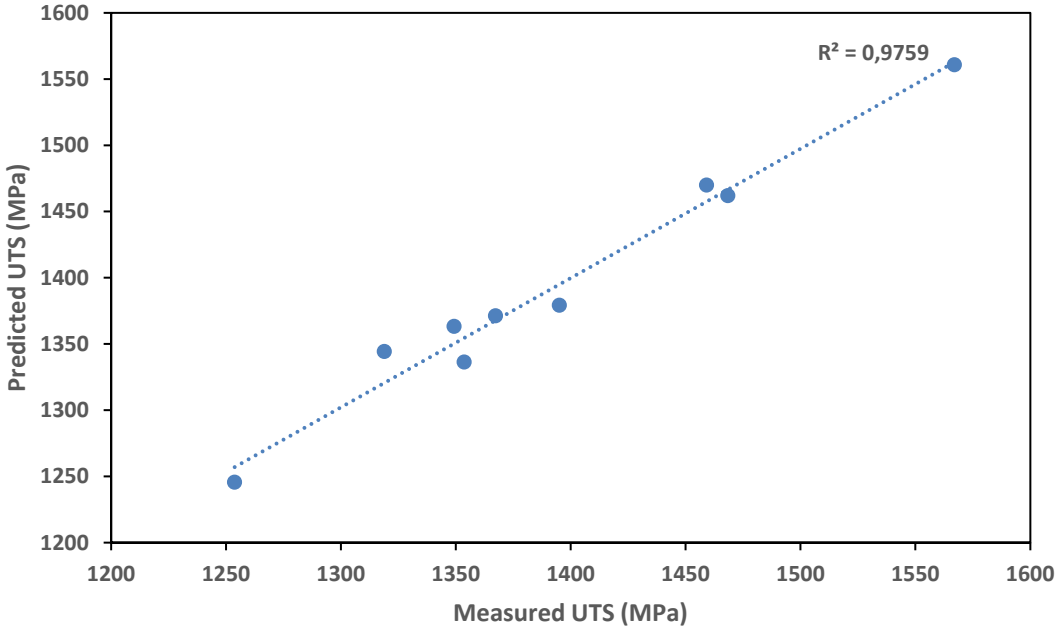

Figure 4- 21: Predicted vs measured values of UTS

4.8.1.2 Response surface method

The contour plots presented in Figure 4- 22, offer a comprehensive visualization of the response surface created using the ANOVA model. They depict how each factor, namely laser power, scanning speed, and defocus distance, influences the ultimate strength (UTS) of the material. At a constant laser power of 500 W, the contour plot reveals that the highest UTS values are obtained at high defocus distances of approximately 16 mm and lower scanning speeds of 2 mm/s. This indicates that adjusting the defocus distance to a higher value while keeping the scanning speed low can lead to enhanced ultimate strength in this scenario. Similarly, when the scanning speed is maintained at a constant value of 3 mm/s, the

contour plot illustrates that the highest UTS values are achieved at high laser power values and high defocus distances. This suggests that optimizing the laser power and defocus distance to higher values can result in improved ultimate strength when the scanning speed is fixed at 3 mm/s. Furthermore, when the defocus distance is held constant at 12 mm, the contour plot demonstrates that the highest UTS values are achieved at high laser power values and the lowest scanning speed values. This implies that maximizing the laser power and minimizing the scanning speed at a fixed defocus distance of 12 mm can lead to the highest ultimate strength. By analyzing these contour plots, we can identify the optimal combinations of laser process parameters that yield the highest ultimate strength for the material. This knowledge helps in fine-tuning the laser processing conditions to achieve superior mechanical properties, which is crucial for various engineering applications requiring materials with enhanced strength and performance.

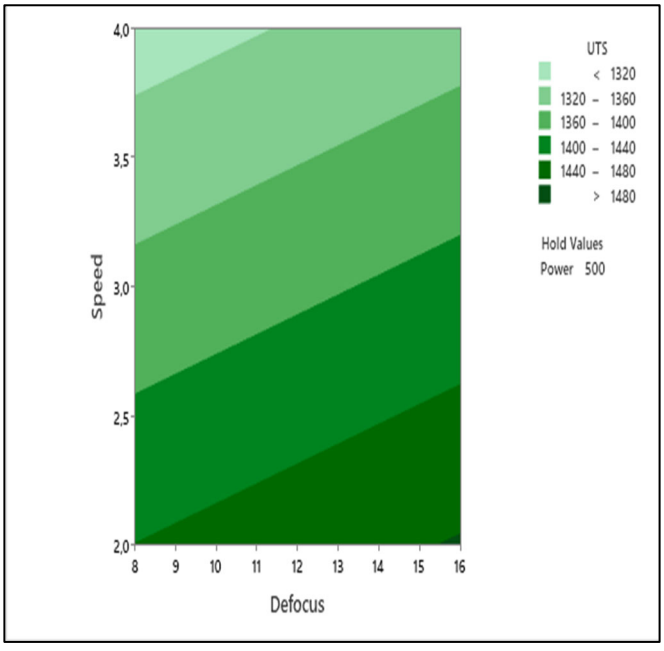

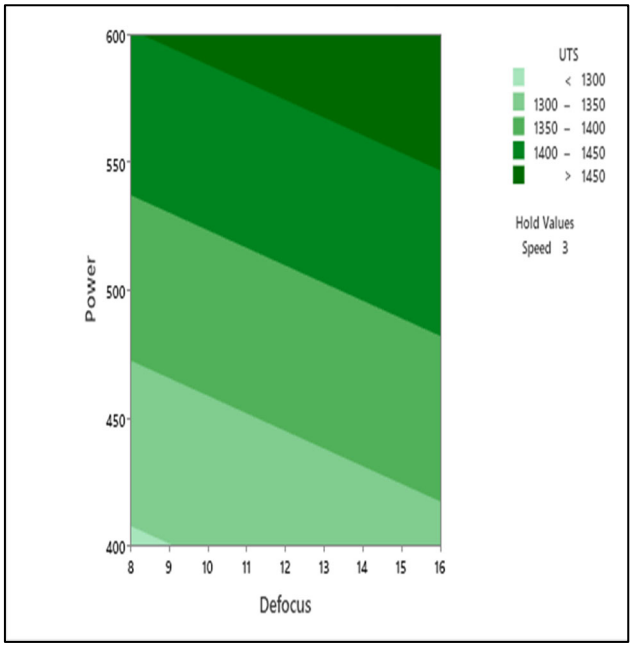

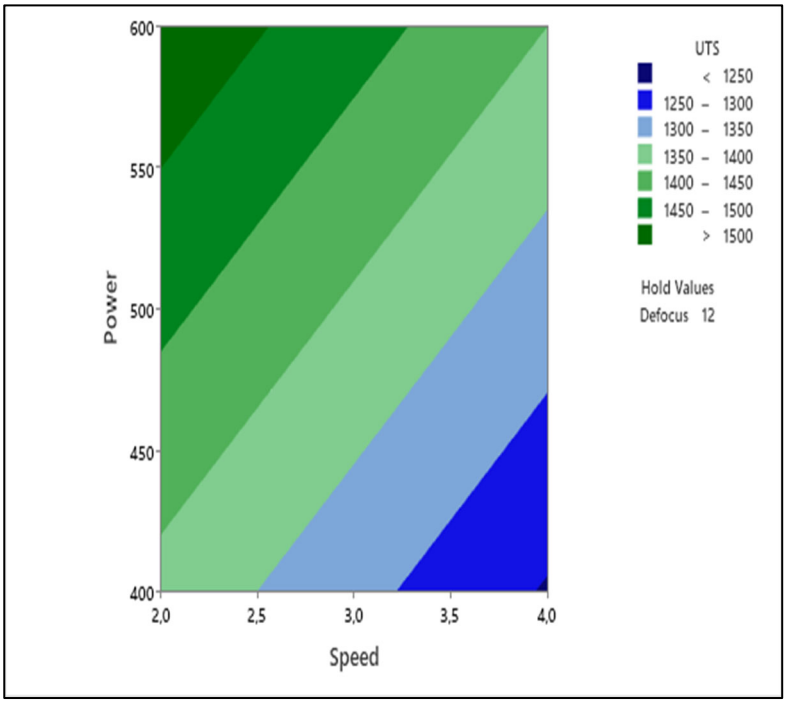

Figure 4- 22: RSM for ultimate strength (P in W, S in mm/s and D in mm)

4.8.2 Effect of laser parameters on the elongation

Table 4- 9 presents the gathered data from the ANOVA analysis, and the P-values for all three laser parameters (laser power, scanning speed, and defocus distance) are found to be less than 0,05. This indicates that the predicted model is reliable, and all three laser parameters significantly affect the elongation of the material. Table 4- 10 further elucidates the contribution of each factor on the elongation values. The results show that the scanning speed has the highest contribution, accounting for 43,87%, followed closely by the laser power with a contribution of 42,84%. On the other hand, the defocus distance does not have a substantial impact on the elongation, as it contributes only 7,70%. Moreover, it is important to note that the error of the model is relatively low, representing only 5,59% of the variation in the elongation values. This suggests that the model's predictions are quite accurate and reliable. In conclusion, the ANOVA analysis provides valuable insights into the impact of

laser process parameters on the elongation of the material. By understanding the significant contributions of each parameter, it becomes possible to optimize the laser processing conditions to achieve the desired elongation values for specific applications. This knowledge plays a crucial role in tailoring the material's properties to meet the specific requirements of different engineering and manufacturing processes.

Table 4- 9: ANOVA table for elongation

Characteristic	Sum of squares	Dof	F-Value	P-value
Defocus distance	1,2252	1	6,89	0,047
Scanning Speed	6,9772	1	39,23	0,002
Power	6,8142	1	38,31	0,002
Error	0,8893	5		
Total	1,2252	8		

Table 4- 10: The contribution of laser parameters on elongation

Characteristic	Defocus distance	Scanning speed	Power	Error
Contribution (%)	7,70	43,87	42,84	5,59

Figure 4- 23 is the main effects plots for SN ratios, it shows that elongation increases with the increases of scanning speed, and the decreases of both laser power and defocus distance.

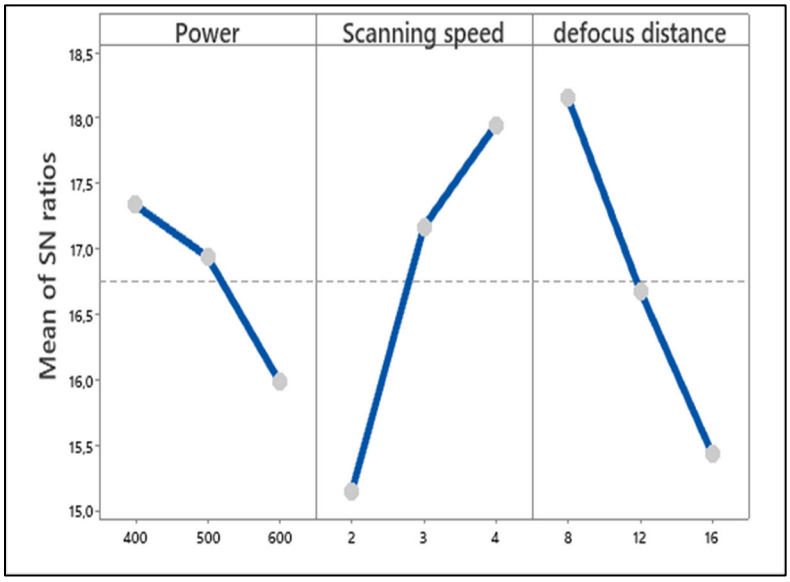

Figure 4- 23: Main effect plots for laser process parameters on the elongation

4.8.2.1 Regression equation

The mathematical equation mentioned bellow (4. 2) is given by ANOVA analysis, it can predict values of the elongation in the range of parameters used in the experiments.

Where Laser power [400 W; 600 W], Scanning speed [2 mm/s; 4 mm/s], and defocus distance [8mm; 16 mm].

$$Elongation = 10{,}46 - 0{,}1130\ Defocus + 1{,}078\ Speed\ \ - 0{,}01066\ Power \qquad (4.\ 2)$$

The values of predicted and measured values of elongation are so close as shown in Figure 4- 24 which means that the predicted model is consistent.

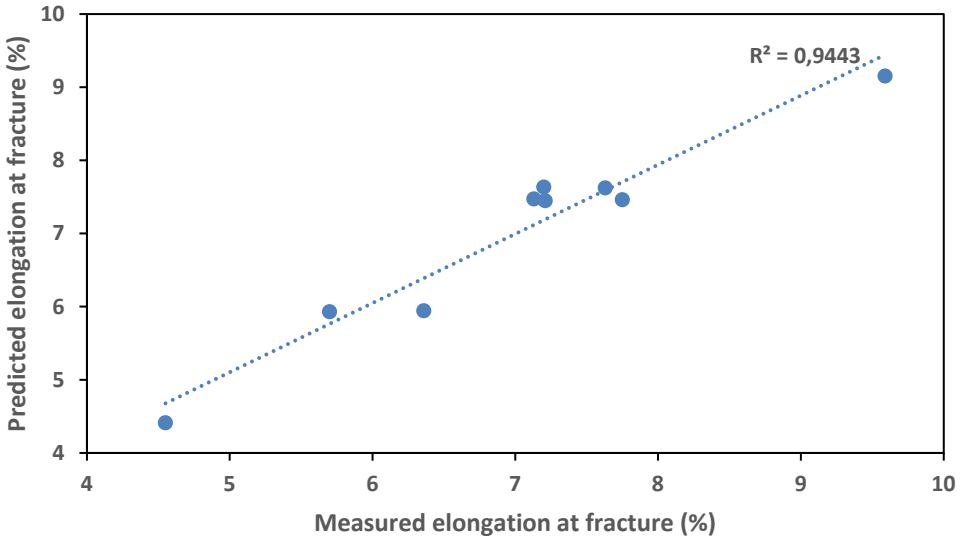

Figure 4- 24: Predicted VS measured values of elongation

4.8.2.2 Response surface method

The contour plots of elongation are visualized in Figure 4- 25, offer a visual representation of how the laser process parameters influence the elongation of the material. When the laser power is fixed at 500W, the elongation reaches its highest values at the highest scanning speed and the lowest defocus distance. On the other hand, when the defocus distance is maintained at 12 mm, the highest elongation values are achieved at the highest scanning speed and the lowest laser power settings. Furthermore, in the case where the scanning speed is fixed at 3 mm/s, the elongation reaches its peak values at the lowest laser power and defocus distance settings. These contour plots provide valuable insights into the optimal combinations of laser parameters to maximize the elongation of the material. By strategically adjusting the laser power, scanning speed, and defocus distance, it becomes possible to enhance the elongation properties, allowing for greater ductility and flexibility of the material. This information is crucial for tailoring the material's properties to suit specific engineering applications, where elongation is a critical factor in determining the material's performance and suitability for use in various components and structures.

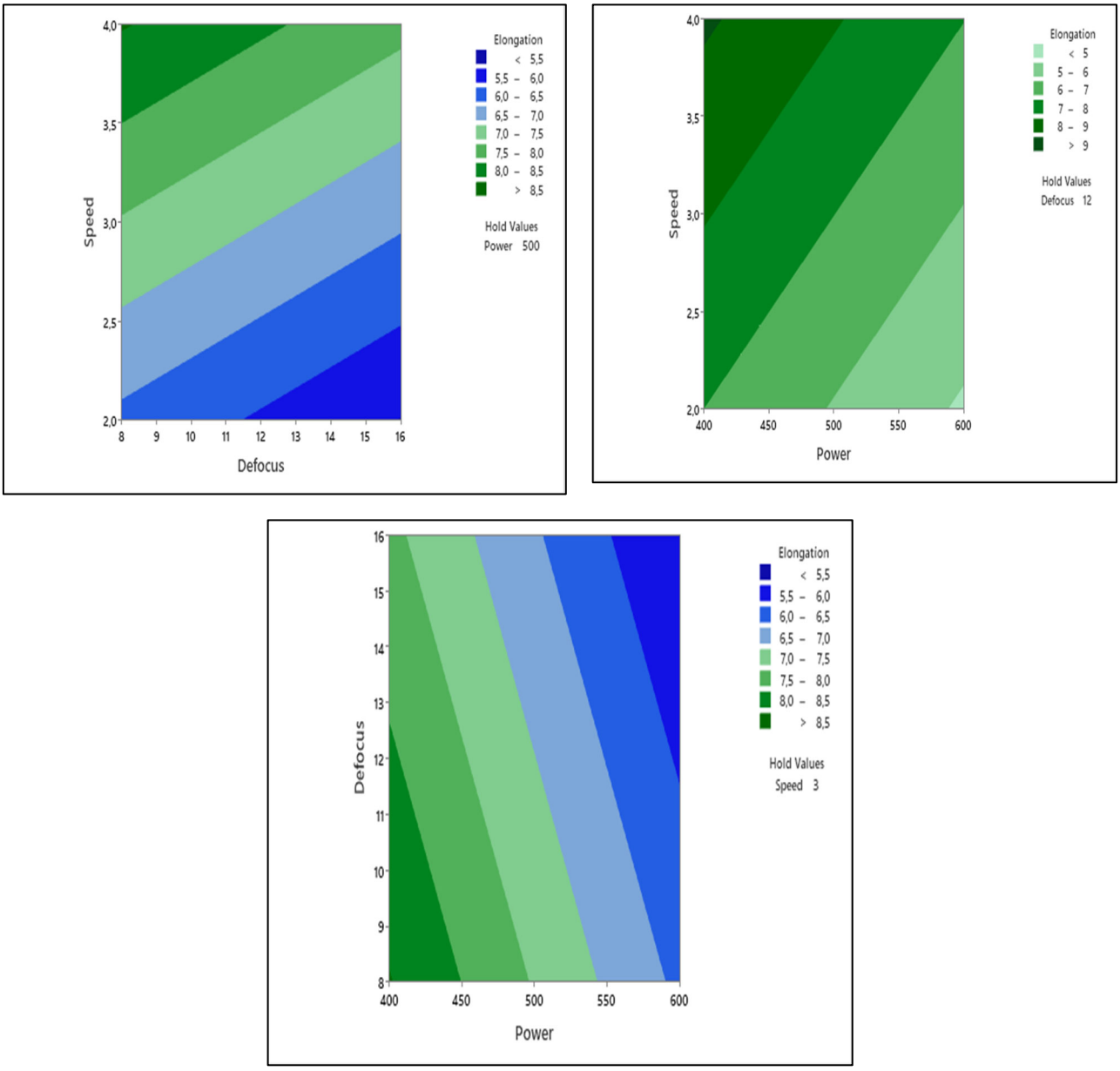

Figure 4- 25: RSM for the elongation (P in W, S in mm/s and D in mm)

4.9 CONCLUSION

This objective of this is to enhance the mechanical properties of SLM H13 tool steel by employing a specific laser treatment in the form of lines, while investigating the influence

of laser parameters on ultimate tensile strength (UTS) and elongation at the fracture. The conclusions drawn from this research are as follows:

- Tensile tests on laser-treated and heat-treated samples, with the latter serving as the reference, showed that the laser-treated samples exhibited higher UTS values and lower elongation at the fracture.

- The effectiveness of bionic units in the form of lines was demonstrated in improving the mold surface.

- The laser process parameters significantly affected the ultimate strength of the samples. However, it was observed that the laser treatment generally resulted in reduced elongation at fracture.

- Sample 7, treated with the highest laser power (600 W), the lowest speed (2 mm/s), and the highest defocus distance (16 mm), achieved the highest UTS of 1567 MPa, representing a 27% improvement. However, its elongation was the lowest at 4.5%.

- The fractography analysis of laser-treated samples reveals a diverse range of fracture behaviors in different zones. A combination of ductile and brittle features indicates the complexity of material response to laser parameters, providing valuable insights for optimization.

- The ANOVA analysis revealed the contributions of each laser process parameter on UTS response, with laser power and scanning speed being the most influential factors, and defocus distance having a less significant impact.

- Similarly, for elongation, scanning speed and laser power were the main contributing factors, while the defocus distance had a comparatively smaller effect.

4.10 REFERENCES

1. Mesquita, R.A., *Tool steels: properties and performance*. 2016: CRC press.
2. International, A.S.M., *ASM handbook. Volume 1, Properties and selection: irons, steels, and high-performance alloys*. 1990, ASM International: Materials Park, OH.
3. Bidare, P., A. Jiménez, H. Hassanin, and K. Essa, *Porosity, cracks, and mechanical properties of additively manufactured tooling alloys: a review.* Advances in Manufacturing, 2022. **10**(2): p. 175-204.
4. Gotlih, J., T. Karner, R. Belšak, M. Ficko, L. Berus, T. Brajlih, S. Pal, and M. Brezočnik. *Design and Manufacturing of Conformal Cooling Channels for Injection Molding: A Review*. in *New Technologies, Development and Application VI*. 2023. Cham: Springer Nature Switzerland.
5. Kanbur, B.B., Y. Zhou, S. Shen, K.H. Wong, C. Chen, A. Shocket, and F. Duan, *Metal Additive Manufacturing of Plastic Injection Molds with Conformal Cooling Channels.* Polymers, 2022. **14**(3): p. 424.
6. Srivastava, M. and S. Rathee, *Additive manufacturing: recent trends, applications and future outlooks.* Progress in Additive Manufacturing, 2022. **7**(2): p. 261-287.
7. Bandyopadhyay, A., K.D. Traxel, M. Lang, M. Juhasz, N. Eliaz, and S. Bose, *Alloy design via additive manufacturing: Advantages, challenges, applications and perspectives.* Materials Today, 2022. **52**: p. 207-224.
8. Zhang, Y., L. Wu, X. Guo, S. Kane, Y. Deng, Y.-G. Jung, J.-H. Lee, and J. Zhang, *Additive Manufacturing of Metallic Materials: A Review.* Journal of Materials Engineering and Performance, 2018. **27**(1): p. 1-13.
9. Ackermann, M., J. Šafka, L. Voleský, J. Bobek, and J.R. Kondapally. *Impact testing of H13 tool steel processed with use of selective laser melting technology*. in *Materials Science Forum*. 2018. Trans Tech Publ.
10. Holzweissig, M.J., A. Taube, F. Brenne, M. Schaper, and T. Niendorf, *Microstructural Characterization and Mechanical Performance of Hot Work Tool Steel Processed by Selective Laser Melting.* Metallurgical and Materials Transactions B, 2015. **46**(2): p. 545-549.
11. Lei, F., T. Wen, F. Yang, J. Wang, J. Fu, H. Yang, J. Wang, J. Ruan, and S. Ji, *Microstructures and Mechanical Properties of H13 Tool Steel Fabricated by Selective Laser Melting.* Materials, 2022. **15**(7): p. 2686.
12. Oliveira, A.P., L.H.Q.R. Lima, B.C.A. Felipe, C. Bolfarini, R.T. Coelho, and P. Gargarella, *Effect of microstructure and defect formation on the bending properties of additive manufactured H13 tool steel.* Journal of Materials Research and Technology, 2021. **15**: p. 3598-3609.
13. Zanni, M., F. Berto, P.E. Vullum, L. Tonelli, A. Morri, and L. Ceschini, *Effect of heat treatment and defects on the tensile behavior of a hot work tool steel manufactured by laser powder bed fusion.* Fatigue and Fracture of Engineering Materials and Structures, 2023.

14. Spears, T.G. and S.A. Gold, *In-process sensing in selective laser melting (SLM) additive manufacturing.* Integrating Materials and Manufacturing Innovation, 2016. **5**(1): p. 16-40.
15. Narvan, M., K.S. Al-Rubaie, and M. Elbestawi, *Process-structure-property relationships of AISI H13 tool steel processed with selective laser melting.* Materials, 2019. **12**(14).
16. Wu, L., S. Das, W. Gridin, S. Leuders, M. Kahlert, M. Vollmer, and T. Niendorf, *Hot Work Tool Steel Processed by Laser Powder Bed Fusion: A Review on Most Relevant Influencing Factors.* Advanced Engineering Materials, 2021. **23**(7).
17. Sun, Y., J. Wang, M. Li, Y. Wang, C. Li, T. Dai, M. Hao, and H. Ding, *Thermal and mechanical properties of selective laser melted and heat treated H13 hot work tool steel.* Materials & Design, 2022. **224**: p. 111295.
18. Deirmina, F., N. Peghini, B. AlMangour, D. Grzesiak, and M. Pellizzari, *Heat treatment and properties of a hot work tool steel fabricated by additive manufacturing.* Materials Science and Engineering: A, 2019. **753**: p. 109-121.
19. Wang, J., S. Liu, Y. Fang, and Z. He, *A short review on selective laser melting of H13 steel.* The International Journal of Advanced Manufacturing Technology, 2020. **108**: p. 2453-2466.
20. Bajaj, P., A. Hariharan, A. Kini, P. Kürnsteiner, D. Raabe, and E.A. Jägle, *Steels in additive manufacturing: A review of their microstructure and properties.* Materials Science and Engineering: A, 2020. **772**: p. 138633.
21. Yan, J.J., D.L. Zheng, H.X. Li, X. Jia, J.F. Sun, Y.L. Li, M. Qian, and M. Yan, *Selective laser melting of H13: microstructure and residual stress.* Journal of Materials Science, 2017. **52**(20): p. 12476-12485.
22. Wang, M., W. Li, Y. Wu, S. Li, C. Cai, S. Wen, Q. Wei, Y. Shi, F. Ye, and Z. Chen, *High-Temperature Properties and Microstructural Stability of the AISI H13 Hot-Work Tool Steel Processed by Selective Laser Melting.* Metallurgical and Materials Transactions B, 2019. **50**(1): p. 531-542.
23. Åsberg, M., G. Fredriksson, S. Hatami, W. Fredriksson, and P. Krakhmalev, *Influence of post treatment on microstructure, porosity and mechanical properties of additive manufactured H13 tool steel.* Materials Science and Engineering: A, 2019. **742**: p. 584-589.
24. Yan, J., H. Song, Y. Dong, W.-M. Quach, and M. Yan, *High strength (~2000 MPa) or highly ductile (~11%) additively manufactured H13 by tempering at different conditions.* Materials Science and Engineering: A, 2020. **773**: p. 138845.
25. Lee, J., J. Choe, J. Park, J.-H. Yu, S. Kim, and H. Sung, *Microstructural effects on the tensile and fracture behavior of selective laser melted H13 tool steel under varying conditions.* Materials Characterization, 2019. **155**: p. 109817.
26. Ren, B., D. Lu, R. Zhou, Z. Li, and J. Guan, *Preparation and mechanical properties of selective laser melted H13 steel.* Journal of Materials Research, 2019. **34**(8): p. 1415-1425.
27. Mazur, M., P. Brincat, M. Leary, and M. Brandt, *Numerical and experimental evaluation of a conformally cooled H13 steel injection mould manufactured with*

selective laser melting. The International Journal of Advanced Manufacturing Technology, 2017. **93**: p. 881-900.
28. Klobčar, D., L. Kosec, B. Kosec, and J. Tušek, *Thermo fatigue cracking of die casting dies.* Engineering Failure Analysis, 2012. **20**: p. 43-53.
29. Zang, C., T. Zhou, H. Zhou, Y. Yuan, P. Zhang, C. Meng, and Z. Zhang, *Effects of substrate microstructure on biomimetic unit properties and wear resistance of H13 steel processed by laser remelting.* Optics and Laser Technology, 2018. **106**: p. 299-310.
30. Zhang, P., H. Zhou, C.-t. Wang, Y. Liu, and L.-q. Ren, *Wear properties of H13 with micron scale and nano scale grains bionic units processed by laser remelting.* Optics & Laser Technology, 2013. **54**: p. 219-224.
31. Meng, C., H. Zhou, H. Zhang, X. Tong, D. Cong, C. Wang, and L. Ren, *The comparative study of thermal fatigue behavior of H13 die steel with biomimetic non-smooth surface processed by laser surface melting and laser cladding.* Materials & Design, 2013. **51**: p. 886-893.
32. Telasang, G., J. Dutta Majumdar, G. Padmanabham, and I. Manna, *Structure–property correlation in laser surface treated AISI H13 tool steel for improved mechanical properties.* Materials Science and Engineering: A, 2014. **599**: p. 255-267.
33. Li, C., Z. Liu, X. Fang, and Y. Guo, *Residual stress in metal additive manufacturing.* Procedia Cirp, 2018. **71**: p. 348-353.
34. Chen, C., K. Yan, L. Qin, M. Zhang, X. Wang, T. Zou, and Z. Hu, *Effect of Heat Treatment on Microstructure and Mechanical Properties of Laser Additively Manufactured AISI H13 Tool Steel.* Journal of Materials Engineering and Performance, 2017. **26**(11): p. 5577-5589.
35. International, A.S.M., *ASM handbook. Volume 4, Heat treatment*. 1991, [Materials Park, Ohio]: ASM International.
36. Kasman, Ş. and I.E. Saklakoglu, *Determination of process parameters in the laser micromilling application using Taguchi method: A case study for AISI H13 tool steel.* The International Journal of Advanced Manufacturing Technology, 2012. **58**: p. 201-209.
37. Astm, I., *Standard Test Methods For Tension Testing Of Metallic Materials Designation: E8/E8m-09.* Universidad Del Valle, Pennsylvania, 2010.
38. Masood Arif Bukhari, S., N. Husnain, F. Arsalan Siddiqui, M. Tuoqeer Anwar, A. Abbas Khosa, M. Imran, T. Hassan Qureshi, and R. Ahmad, *Effect of laser surface remelting on Microstructure, mechanical properties and tribological properties of metals and alloys: A review.* Optics & Laser Technology, 2023. **165**: p. 109588.
39. Krell, J., A. Röttger, K. Geenen, and W. Theisen, *General investigations on processing tool steel X40CrMoV5-1 with selective laser melting.* Journal of Materials Processing Technology, 2018. **255**: p. 679-688.
40. Telasang, G., J.D. Majumdar, G. Padmanabham, M. Tak, and I. Manna, *Effect of laser parameters on microstructure and hardness of laser clad and tempered AISI H13 tool steel.* Surface and Coatings Technology, 2014. **258**: p. 1108-1118.

41. Ning, A., Y. Liu, R. Gao, S. Yue, M. Wang, and H. Guo, *Effect of Tempering Condition on Microstructure, Mechanical Properties and Precipitates in AISI H13 Steel.* JOM, 2021. **73**(7): p. 2194-2202.
42. Zhu, J., Z. Zhang, and J. Xie, *Improving strength and ductility of H13 die steel by pre-tempering treatment and its mechanism.* Materials Science and Engineering: A, 2019. **752**: p. 101-114.

CONCLUSION GÉNÉRALE

En somme, cette étude a démontré de manière concluante que le traitement surfacique au laser constitue une approche efficace et prometteuse pour l'amélioration des performances et de la durabilité des moules en acier à outils H13, indépendamment de leur méthode de fabrication, qu'elle soit basée sur le forgeage traditionnel ou la fabrication additive. L'optimisation minutieuse des paramètres du processus a révélé être le pilier central de cette démarche, avec un accent particulier sur la durée et l'intensité de l'énergie laser, ainsi que la vitesse de refroidissement. Le contrôle précis de ces variables a abouti à des améliorations notables en termes de résistance, de microstructure et de dureté de l'acier H13, des qualités incontournables pour satisfaire les exigences industrielles.

La première phase de ce projet vise à améliorer la microstructure et la dureté de la surface de l'acier à outils H13 conventionnel par un traitement surfacique au laser. Pour ce faire, une démarche expérimentale et statistique est adoptée pour évaluer l'impact des paramètres laser sur l'acier à outils H13 conventionnel. L'approche expérimentale repose sur la méthodologie de planification expérimentale Taguchi, avec trois facteurs à trois niveaux, à savoir la puissance laser (500, 600 et 700 W), la vitesse de balayage (2, 3 et 4 mm/s) et la distance de dé-focalisation (8, 12 et 16 mm). L'analyse de la microstructure et de la micro-dureté de la partie affectée par le traitement thermique au laser a révélé l'existence de trois zones distinctes pour les neuf jeux de paramètres :

- Une zone fondue et rapidement solidifiée, principalement composée de cellules dendritiques résultant de la transformation de la martensite. Cette zone contient de la martensite non trempée et des régions inter-dendritiques enrichies en particules de carbures. Cette partie a connu une augmentation significative de la micro-dureté par rapport au substrat.

- Une zone durcie qui contient de la martensite non revenue et des carbures non dissous. Cette zone affiche la micro-dureté maximale au niveau de la partie traitée au laser. En ce qui concerne la profondeur, la micro-dureté varie de 65,7 à 61,4 HRC, tandis qu'en largeur, la dureté maximale varie de 64,3 à 59,5 HRC.

- Une zone affectée thermiquement (ZAT), soumise à un revenu, car la température diminue progressivement avec la profondeur, réduisant ainsi la quantité d'énergie absorbée par la surface. La température se situe probablement autour de la température de transformation Ac1, ce qui implique la précipitation de carbures à partir de martensite sursaturée. Cette troisième zone est sur-revenue et est identifiée par une réduction significative de la dureté avant de retrouver sa dureté initiale.

Une analyse statistique de variance ANOVA a été utilisée pour mettre en évidence l'impact des paramètres laser sur la largeur et la profondeur de la zone traitée au laser. Les résultats ont démontré que la puissance laser et la vitesse de balayage sont les principaux facteurs affectant la zone traitée, avec des contributions significatives de 84,29 % pour la puissance (P) et seulement 9,91 % pour la vitesse de balayage (S). En ce qui concerne la profondeur, elle augmente avec l'augmentation de la puissance laser et la diminution de la vitesse. Quant à la largeur, la puissance laser a l'impact prépondérant avec une contribution de 57,15 %, suivie de la vitesse de balayage (26,85 %), tandis que la distance de défocalisation contribue de manière relativement mineure, avec seulement 9,34 %. De plus, la largeur augmente avec l'augmentation de la puissance laser et de la distance de défocalisation, et diminue avec l'augmentation de la vitesse de balayage.

La deuxième partie de cette étude constitue un complément du premier chapitre, en utilisant le même plan d'expérience pour analyser les propriétés mécaniques des pièces traitées avec deux lignes parallèles sur les deux surfaces des éprouvettes. Il est apparu que le traitement au laser a amélioré la résistance ultime à la traction, mais a réduit l'élongation à la rupture. En particulier, le traitement au laser a entraîné une augmentation de la résistance ultime à la traction de 20 % par rapport au substrat pour l'échantillon numéro 7, qui a été

traité avec les paramètres spécifiques suivants : une distance de dé-focalisation de 16 mm, une vitesse de 2 mm/s et une puissance laser de 700 W.

L'analyse des modes de fracture à l'échelle microscopique a révélé une combinaison de modes de rupture fragiles et ductiles. La méthode ANOVA a été utilisée pour identifier les effets des paramètres laser sur les deux propriétés mécaniques suivantes : la résistance ultime à la traction et l'élongation à la rupture. Les résultats ont montré que la puissance du laser et la vitesse de balayage étaient les deux principaux facteurs influençant la résistance ultime à la traction (UTS) des échantillons traités au laser, avec des contributions respectives de 40,58 % pour la puissance et 25,34 % pour la vitesse de balayage. Il est à noter que la puissance laser a un impact positif sur la résistance ultime, tandis qu'une augmentation de la vitesse de balayage entraîne une diminution de la résistance ultime.

En ce qui concerne l'élongation à la rupture, l'analyse de variance a montré que la puissance du laser avait l'impact le plus significatif, avec une contribution de 68,11 %, suivie de près par la distance de dé-focalisation, qui a contribué à hauteur de 24,78 %.

La troisième phase a établi la même démarche sur l’acier à outils fabriqué par la fusion laser sélective (SLM), qui est un procédé de fabrication additive (AM) à base de poudre qui utilise une énergie laser élevée pour faire fondre les poudres et les solidifier en pièces solides. L'objectif de cette étude était d'explorer les possibilités offertes par la fabrication additive, qui présente de nombreux avantages par rapport aux méthodes conventionnelles, notamment la liberté de conception, la réduction des assemblages et la personnalisation, tout en conservant des propriétés mécaniques et thermiques comparables à l'acier outil conventionnel.

Les résultats ont confirmé la faisabilité et l'efficacité du traitement laser de surface en utilisant les paramètres appropriés en fonction des dimensions des échantillons. Ces paramètres incluaient la puissance laser (400, 500 et 600 W), la vitesse de balayage (2, 3 et 4 mm/s) et la distance de dé-focalisation (8, 12 et 16 mm). En conséquence, la dureté de la

zone traitée a considérablement augmenté, créant ainsi une couche protectrice plus résistante à l'usure et aux contraintes mécaniques.

L'analyse de la microstructure de l'acier H13 imprimé a révélé une microstructure hétérogène, caractérisée par une combinaison de structure cellulaire et colonnaire fine. Cette hétérogénéité est principalement due au gradient thermique élevé pendant le processus SLM. Cependant, cette microstructure a été homogénéisée grâce à un traitement thermique, comprenant un soulagement des contraintes résiduelles, une trempe et un revenu.

Le traitement au laser de la surface de l'acier H13 fabriqué par fabrication additive a également mis en évidence trois zones distinctes :

- Une zone fondue qui se solidifie rapidement, atteignant la température maximale en raison de l'absorption élevée d'énergie. Cette zone se caractérise par des cellules dendritiques, contenant de la martensite et des régions inter-dendritiques riches en particules de carbure. La micro-dureté de cette région est supérieure à celle du substrat.

- Une zone durcie qui est surchauffée, atteignant la température d'austénitisation Ac3. Cela conduit à la formation de martensite non revenue et de carbures non dissous. La micro-dureté atteint son maximum dans cette zone, avec des valeurs variant de 61,6 à 57,5 HRC pour les neuf échantillons, comparées à des valeurs de 42-44 HRC pour le substrat.

- La troisième zone représente une région atteinte par une température de transformation (Ac1), où les carbures précipitent à partir de la martensite sursaturée, entraînant une dureté de 38 HRC inférieure à celle du substrat.

Les profondeurs de la zone traitée au laser varient entre 1,3 et 1,8 mm, tandis que les largeurs varient de 1,26 à 2,4 mm. Une analyse statistique ANOVA a été appliquée aux valeurs de la profondeur et de la largeur. Les résultats ont montré que la puissance laser contribue à 53,30 % des variations de la profondeur, tandis que la vitesse de balayage

contribue à 28,94 %, et la distance de dé-focalisation a une contribution relativement faible de seulement 9,45 %. En ce qui concerne la largeur, l'analyse ANOVA a révélé que la puissance laser a la plus grande influence, avec une contribution de 54,76 %, suivie de la vitesse de balayage avec 32,11 %, tandis que la distance de dé-focalisation présente une contribution légèrement inférieure de 12,35 %.

La quatrième phase de cette étude vient en complément de la troisième partie et a pour objectif d'analyser les performances mécaniques statiques de l'acier H13 fabriqué par SLM, qui a été soumis à un traitement au laser avec deux lignes parallèles sur ses deux surfaces. Les échantillons ont été traités en suivant le même plan. Les essais de traction ont révélé que les échantillons traités au laser présentaient des valeurs de résistance ultime plus élevées et une rupture avec un allongement moins important par rapport au substrat d'origine. L'échantillon 7, qui a été traité avec la puissance laser la plus élevée (600 W), la vitesse de balayage la plus basse (2 mm/s) et la distance de dé-focalisation la plus élevée (16 mm), a atteint la résistance la plus élevée, mesurant 1 567 MPa, soit une amélioration de 27 %. Cependant, son allongement était le plus faible, à seulement 4,5 %. Les résultats de l'analyse statistique ANOVA concernant la résistance ultime à la traction ont mis en évidence que la puissance laser a la plus grande contribution, représentant 51,89 %, suivie de la vitesse de balayage avec une contribution de 41,77 %, tandis que la distance de dé-focalisation a eu un impact relativement mineur, ne contribuant qu'à hauteur de 3,93 %. En somme, la résistance ultime à la traction augmente avec l'augmentation de la vitesse de balayage et de la puissance du laser, tandis qu'elle diminue avec l'augmentation de la vitesse de balayage.

L'analyse de variance des effets des paramètres laser sur l'élongation à la fracture a montré que la vitesse de balayage avait la contribution la plus élevée, représentant 43,87 %, suivie de près par la puissance du laser avec une contribution de 42,84 %. En revanche, la distance de dé-focalisation n'a eu qu'un impact limité sur l'allongement, contribuant seulement à hauteur de 7,70 %. Il convient de noter que l'élongation augmente avec l'augmentation de la vitesse de balayage et diminue à la fois avec l'augmentation de la puissance du laser et de la distance de dé-focalisation.

PERSPECTIVES

Ce projet de recherche a mis en évidence l'efficacité Cette partie présentes d'autres perspectives à traiter pour les prochains travaux.

- Une étude des effets de paramètres laser sur d'autres propriétés du matériau H13 conventionnel et imprimé, en termes de de la résistance à la fatigue, et l'usure à haute températures.

- Analyse de la corrosion : Étant donné que l'acier H13 est souvent utilisé dans des environnements exigeants, une étude sur la résistance à la corrosion des pièces traitées au laser serait pertinente. Cela aiderait à déterminer la capacité des moules à résister à la corrosion lorsqu'ils sont exposés à des matériaux et à des conditions corrosives.

- L'étude de l'effet des morphologies de traitement au laser sur les propriétés mécaniques de l'acier à outils.

- L'exploration d'autres méthodes de post-traitement de l'acier à outils H13.

- Modélisation numérique : Utiliser des modèles de simulation numérique pour prédire le comportement des pièces traitées au laser en fonction des paramètres et des conditions d'opération. Une telle modélisation permettrait d'économiser du temps et des ressources en optimisant virtuellement les designs et les processus.

- La modélisation et la conception d'un moule équipé d'un canal de refroidissement conforme, et l'étude de l'efficacité de refroidissement.

RÉFÉRENCES BIBLIOGRAPHIQUES

1. Kale, P., P. Darade, and A. Sahu. *A literature review on injection moulding process based on runner system and process variables*. in *IOP Conference Series: Materials Science and Engineering*. 2021. IOP Publishing.
2. Maharjan, N., N. Wu, and W. Zhou, *Hardening Efficiency and Microstructural Changes during Laser Surface Hardening of 50CrMo4 Steel.* Metals, 2021. **11**(12): p. 2015.
3. Frizelle, W.G., *10 - Injection Molding Technology*, in *Applied Plastics Engineering Handbook (Second Edition)*, M. Kutz, Editor. 2017, William Andrew Publishing. p. 191-202.
4. Bryce, D.M., *Plastic Injection Molding... material selection and product design fundamentals, Jul. 1, 1997.* vol. II: Fundamentals of Injection Molding Series, Society of Manufacturing Engineers: p. 258-261.
5. Yang, Y., X. Chen, N. Lu, and F. Gao, *Injection molding process control, monitoring, and optimization*. 2016: Carl Hanser Verlag GmbH Co KG.
6. Kazmer, D., *27 - Design of Plastic Parts*, in *Applied Plastics Engineering Handbook (Second Edition)*, M. Kutz, Editor. 2017, William Andrew Publishing. p. 593-615.
7. Jhavar, S., C.P. Paul, and N.K. Jain, *Causes of failure and repairing options for dies and molds: A review.* Engineering Failure Analysis, 2013. **34**: p. 519-535.
8. Mesquita, R.A., *Tool steels: properties and performance*. 2016: CRC press.
9. Szumera, J.A., *The tool steel guide*. 2003: Industrial Press Inc.
10. Totten, G.E., *Steel heat treatment: metallurgy and technologies*. 2006: CRC press.
11. Davis, J.R., *Surface hardening of steels: understanding the basics*. 2002: ASM international.
12. Jeyaprakash, N., C.-H. Yang, and D.R. Kumar, *Laser Surface Modification of Materials*, in *Practical Applications of Laser Ablation*. 2020, IntechOpen London, UK.
13. Meijer, J. and I. van Sprang, *Optimization of Laser Beam Transformation Hardening by One Single Parameter.* CIRP Annals, 1991. **40**(1): p. 183-186.
14. Nath, A.K. and S. Sarkar, *Chapter 11 - Laser Transformation Hardening of Steel*, in *Advances in Laser Materials Processing (Second Edition)*, J. Lawrence, Editor. 2018, Woodhead Publishing. p. 257-298.
15. P, D., B. K R, and B.G. Naidu, *Laser surface hardening: A review.* Int. J. of Surface Science and Engineering, 2011. **5**: p. 131-151.
16. Gu, D., *Laser additive manufacturing of high-performance materials*. 2015: Springer.

17. Chandra, M., K. Vimal, and S. Rajak, *In situ process monitoring and control in metal additive manufacturing.* Additive Manufacturing: Advanced Materials and Design Techniques, 2023: p. 57.
18. Liu, J., V. Nguyen-Van, B. Panda, K. Fox, A. du Plessis, and P. Tran, *Additive manufacturing of sustainable construction materials and form-finding structures: a review on recent progresses.* 3D Printing and Additive Manufacturing, 2022. **9**(1): p. 12-34.
19. Peng, T., K. Kellens, R. Tang, C. Chen, and G. Chen, *Sustainability of additive manufacturing: An overview on its energy demand and environmental impact.* Additive Manufacturing, 2018. **21**: p. 694-704.
20. Kumar, R., M. Kumar, and J.S. Chohan, *The role of additive manufacturing for biomedical applications: A critical review.* Journal of Manufacturing Processes, 2021. **64**: p. 828-850.
21. Najmon, J.C., S. Raeisi, and A. Tovar, *Review of additive manufacturing technologies and applications in the aerospace industry.* Additive manufacturing for the aerospace industry, 2019: p. 7-31.
22. Craveiroa, F., J.P. Duartec, H. Bartoloa, and P.J. Bartolod, *Additive manufacturing as an enabling technology for digital construction: A perspective on Construction 4.0.* Sustain. Dev, 2019. **4**(6): p. 251-267.
23. Srivastava, M. and S. Rathee, *Additive manufacturing: Recent trends, applications and future outlooks.* Progress in Additive Manufacturing, 2022. **7**(2): p. 261-287.
24. Sarvankar, S.G. and S.N. Yewale, *Additive manufacturing in automobile industry.* Int. J. Res. Aeronaut. Mech. Eng, 2019. **7**(4): p. 1-10.
25. Mehrpouya, M., A. Dehghanghadikolaei, B. Fotovvati, A. Vosooghnia, S.S. Emamian, and A. Gisario, *The potential of additive manufacturing in the smart factory industrial 4.0: A review.* Applied Sciences, 2019. **9**(18): p. 3865.
26. Dilberoglu, U.M., B. Gharehpapagh, U. Yaman, and M. Dolen, *The role of additive manufacturing in the era of industry 4.0.* Procedia manufacturing, 2017. **11**: p. 545-554.
27. Hernandez Korner, M.E., M.P. Lambán, J.A. Albajez, J. Santolaria, L.d.C. Ng Corrales, and J. Royo, *Systematic literature review: integration of additive manufacturing and industry 4.0.* Metals, 2020. **10**(8): p. 1061.
28. Srivatsan, T. and T. Sudarshan, *Additive manufacturing: innovations, advances, and applications.* 2015.
29. Standard, A., *F2792-12a: standard terminology for additive manufacturing technologies (ASTM International, West Conshohocken, PA, 2012).* Procedia Eng, 2013. **63**: p. 4-11.
30. Zhou, K. and C. Han, *Metal Powder-Based Additive Manufacturing*. 2023: John Wiley & Sons.
31. Galy, C., *Etude des interactions matériau/procédé en vue d'une optimisation des conditions opératoires du procédé de fabrication additive SLM sur des alliages d'aluminium pour des applications aéronautiques*. 2019, Bordeaux.

32. Tan, J.H.K., S.L. Sing, and W.Y. Yeong, *Microstructure modelling for metallic additive manufacturing: A review.* Virtual and Physical Prototyping, 2020. **15**(1): p. 87-105.
33. Gao, B., H. Zhao, L. Peng, and Z. Sun, *A review of research progress in selective laser melting (SLM).* Micromachines, 2022. **14**(1): p. 57.
34. Sefene, E.M., *State-of-the-art of selective laser melting process: A comprehensive review.* Journal of Manufacturing Systems, 2022. **63**: p. 250-274.
35. Zhang, B., Y. Li, and Q. Bai, *Defect Formation Mechanisms in Selective Laser Melting: A Review.* Chinese Journal of Mechanical Engineering, 2017. **30**(3): p. 515-527.
36. Lee, J., J. Choe, J. Park, J.-H. Yu, S. Kim, and H. Sung, *Microstructural effects on the tensile and fracture behavior of selective laser melted H13 tool steel under varying conditions.* Materials Characterization, 2019. **155**: p. 109817.
37. Tan, J.H., W.L.E. Wong, and K.W. Dalgarno, *An overview of powder granulometry on feedstock and part performance in the selective laser melting process.* Additive Manufacturing, 2017. **18**: p. 228-255.
38. Mostafaei, A., A.M. Elliott, J.E. Barnes, F. Li, W. Tan, C.L. Cramer, P. Nandwana, and M. Chmielus, *Binder jet 3D printing—Process parameters, materials, properties, modeling, and challenges.* Progress in Materials Science, 2021. **119**: p. 100707.
39. DebRoy, T., H.L. Wei, J.S. Zuback, T. Mukherjee, J.W. Elmer, J.O. Milewski, A.M. Beese, A. Wilson-Heid, A. De, and W. Zhang, *Additive manufacturing of metallic components – Process, structure and properties.* Progress in Materials Science, 2018. **92**: p. 112-224.
40. Li, C., Z. Liu, X. Fang, and Y. Guo, *Residual stress in metal additive manufacturing.* Procedia Cirp, 2018. **71**: p. 348-353.
41. Singh, R. and J.P. Davim, *Additive manufacturing: applications and innovations*. 2018: CRC Press.
42. Peng, X., L. Kong, J.Y.H. Fuh, and H. Wang, *A Review of Post-Processing Technologies in Additive Manufacturing.* Journal of Manufacturing and Materials Processing, 2021. **5**(2): p. 38.
43. Mahmood, M.A., D. Chioibasu, A. Ur Rehman, S. Mihai, and A.C. Popescu, *Post-Processing Techniques to Enhance the Quality of Metallic Parts Produced by Additive Manufacturing.* Metals, 2022. **12**(1): p. 77.
44. Laleh, M., E. Sadeghi, R.I. Revilla, Q. Chao, N. Haghdadi, A.E. Hughes, W. Xu, I. De Graeve, M. Qian, I. Gibson, and M.Y. Tan, *Heat treatment for metal additive manufacturing.* Progress in Materials Science, 2023. **133**: p. 101051.
45. Malakizadi, A., D. Mallipeddi, S. Dadbakhsh, R. M'Saoubi, and P. Krajnik, *Post-processing of additively manufactured metallic alloys–A review.* International Journal of Machine Tools and Manufacture, 2022. **179**: p. 103908.
46. Feng, S., A.M. Kamat, and Y. Pei, *Design and fabrication of conformal cooling channels in molds: Review and progress updates.* International Journal of Heat and Mass Transfer, 2021. **171**: p. 121082.
47. Gotlih, J., T. Karner, R. Belšak, M. Ficko, L. Berus, T. Brajlih, S. Pal, and M. Brezočnik. *Design and Manufacturing of Conformal Cooling Channels for Injection*

Molding: A Review. in *New Technologies, Development and Application VI*. 2023. Cham: Springer Nature Switzerland.
48. Kanbur, B.B., Y. Zhou, S. Shen, K.H. Wong, C. Chen, A. Shocket, and F. Duan, *Metal Additive Manufacturing of Plastic Injection Molds with Conformal Cooling Channels.* Polymers, 2022. **14**(3): p. 424.
49. Arman, S. and I. Lazoglu, *A comprehensive review of injection mold cooling by using conformal cooling channels and thermally enhanced molds.* The International Journal of Advanced Manufacturing Technology, 2023: p. 1-72.
50. He, H., Y. Xing, R. Wang, Y. Lu, L. Zhang, and F. Li, *Optimization design of cooling system for injection molding mold of non-pneumatic tire.* Thermal Science and Engineering Progress, 2023. **42**: p. 101866.
51. Nguyen, V.-T., P.S. Minh, T.M.T. Uyen, T.T. Do, N.C. Ha, and V.T.T. Nguyen, *Conformal Cooling Channel Design for Improving Temperature Distribution on the Cavity Surface in the Injection Molding Process.* Polymers, 2023. **15**(13): p. 2793.
52. Tomasoni, D., S. Colosio, L. Giorleo, and E. Ceretti, *Design for additive manufacturing: thermoforming mold optimization via conformal cooling channel technology.* Procedia Manufacturing, 2020. **47**: p. 1117-1122.
53. Mazur, M., P. Brincat, M. Leary, and M. Brandt, *Numerical and experimental evaluation of a conformally cooled H13 steel injection mould manufactured with selective laser melting.* The International Journal of Advanced Manufacturing Technology, 2017. **93**: p. 881-900.
54. Ferreira, D.F.S., J.S. Vieira, S.P. Rodrigues, G. Miranda, F.J. Oliveira, and J.M. Oliveira, *Dry sliding wear and mechanical behaviour of selective laser melting processed 18Ni300 and H13 steels for moulds.* Wear, 2022. **488-489**: p. 204179.
55. Park, H.-S. and X.-P. Dang, *Development of a Smart Plastic Injection Mold with Conformal Cooling Channels.* Procedia Manufacturing, 2017. **10**: p. 48-59.
56. Tan, C., D. Wang, W. Ma, Y. Chen, S. Chen, Y. Yang, and K. Zhou, *Design and additive manufacturing of novel conformal cooling molds.* Materials & Design, 2020. **196**: p. 109147.
57. Tan, Q., Y. Yin, F. Wang, H. Chang, S. Liu, G. Liang, T. Wu, and M.-X. Zhang, *Rationalization of brittleness and anisotropic mechanical properties of H13 steel fabricated by selective laser melting.* Scripta Materialia, 2022. **214**: p. 114645.
58. Zhao, M., C. Duan, and X. Luo, *Heat Transfer, Laser Remelting/Premelting Behavior and Metallurgical Bonding During Selective Laser Melting of Metal Powder.* Metals and Materials International, 2022. **28**(9): p. 2225-2238.
59. Yan, J.J., D.L. Zheng, H.X. Li, X. Jia, J.F. Sun, Y.L. Li, M. Qian, and M. Yan, *Selective laser melting of H13: microstructure and residual stress.* Journal of Materials Science, 2017. **52**(20): p. 12476-12485.
60. Katancik, M., S. Mirzababaei, M. Ghayoor, and S. Pasebani, *Selective laser melting and tempering of H13 tool steel for rapid tooling applications.* Journal of Alloys and Compounds, 2020. **849**.
61. Wu, L., S. Das, W. Gridin, S. Leuders, M. Kahlert, M. Vollmer, and T. Niendorf, *Hot Work Tool Steel Processed by Laser Powder Bed Fusion: A Review on Most Relevant Influencing Factors.* Advanced Engineering Materials, 2021. **23**(7).

62. Bajaj, P., A. Hariharan, A. Kini, P. Kürnsteiner, D. Raabe, and E.A. Jägle, *Steels in additive manufacturing: A review of their microstructure and properties.* Materials Science and Engineering: A, 2020. **772**: p. 138633.
63. Lei, F., T. Wen, F. Yang, J. Wang, J. Fu, H. Yang, J. Wang, J. Ruan, and S. Ji, *Microstructures and Mechanical Properties of H13 Tool Steel Fabricated by Selective Laser Melting.* Materials, 2022. **15**(7): p. 2686.
64. Meng, C., H. Zhou, Y. Zhou, M. Gao, X. Tong, D. Cong, C. Wang, F. Chang, and L. Ren, *Influence of different temperatures on the thermal fatigue behavior and thermal stability of hot-work tool steel processed by a biomimetic couple laser technique.* Optics & Laser Technology, 2014. **57**: p. 57-65.
65. Wang, C., H. Zhou, Z. Zhang, Y. Zhao, P. Zhang, D. Cong, C. Meng, and F. Tan, *Tensile property of a hot work tool steel prepared by biomimetic coupled laser remelting process with different laser input energies.* Applied Surface Science, 2012. **258**(22): p. 8732-8738.